Climate Data Record (CDR) Program

Climate Algorithm Theoretical Basis Document (C-ATBD)

International Satellite Cloud Climatology Project (ISCCP)

Cloud Properties - ISCCP

(H-Series Product)

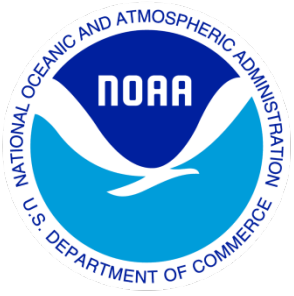

CDR Program Document Number: CDRP-ATBD-0872
Configuration Item Number: 01B-29
Revision 1 / June 1, 2022

REVISION HISTORY

Rev.	Author	DSR No.	Description	Date
0	William B. Rossow Cooperative Remote Sensing Science and Technology Center (CREST) at The City College of New York and NASA Goddard Institute for Space Studies (GISS)	DSR-1109	Initial Submission to CDR Program	04/03/2017
1	William B. Rossow Cooperative Remote Sensing Science and Technology Center (CREST) at The City College of New York and NASA Goddard Institute for Space Studies (GISS)	DSR-1626	Revisions to clarify the changes made in HGG for nighttime and to fill in missing data	06/01/2022

TABLE of CONTENTS

LIST of FIGURES

LIST of TABLES

Search Word online help for "Add or delete captions" for assistance with this table.

1. Introduction

1.1 Purpose

The purpose of the International Satellite Cloud Climatology Project (ISCCP) (Schiffer and Rossow 1983) was to: (1) produce a global, reduced resolution, calibrated infrared and visible radiance dataset, along with basic information on the radiative properties of the atmosphere and surface, from which cloud properties can be derived, (2) coordinate basic research on techniques for inferring physical cloud properties from satellite radiance data and to derive and evaluate a global cloud climatology, (3) promote research using ISCCP data to improve understanding of the earth's radiation budget and the hydrological cycle and the parameterization of cloud processes in climate models. Since 1983, these objectives, while still ongoing, have largely been accomplished. The first purpose was met by the production of a calibrated radiance datasets (Schiffer and Rossow 1985). These data have now been replaced by higher resolution versions with improved calibrations (see Sections 2.2 and 6.2). The second purpose was met by producing and evaluating two versions of a cloud climatology (Rossow and Schiffer 1991, 1999).

The purpose of this document is to describe the ISCCP cloud algorithm and satellite data processing system, submitted to the NOAA NCEI by William B. Rossow (CREST at City College of New York and NASA GISS), that will be used to create the ISCCP H-Series Version Climate Data Record (third version) based upon imaged data from international constellation of weather satellites. The ISCCP H-Series Version products are modifications and improvements of the previous C-Series and (Rossow and Schiffer 1991) and D-Series Versions (Rossow and Schiffer 1999) of the ISCCP. More information about the earlier products can be found on a NASA-maintained website (Rossow and Duenas 2004) at http://isccp.giss.nasa.gov. The actual algorithm is defined by the computer programs that accompany this document so the intent here is to provide a guide to understanding that algorithm from both a scientific perspective, as well as documenting the processing details, to assist a software engineer or end-user in performing an evaluation of the code and/or running the processing system and developing ISCCP cloud products.

1.2 Definitions

Following is a summary of the definitions and symbols used to define the algorithm.

Satellite Radiances: The satellite radiances used in ISCCP processing are measured at two wavelengths (approximately). (1) Visible (VIS or V) radiances at H 0.65 ⌈m, are defined as "scaled" radiances, which are the measured radiances divided by the instrument "solar constant". The instrument solar constant (SOLCON) is the wavelength integral of the product of the normalized spectral response function of the instrument and the solar spectrum at the top of the atmosphere (Neckel and Labs 1984). The visible reflectance, R (as a fraction), is VIS divided by the cosine of the solar zenith angle at the satellite pixel, ⌈$_0$.

(2) The infrared (IR) radiance at H 10.5 ⌠m, is represented in energy units by a brightness temperature, TB (in Kelvins), which is the temperature of a blackbody emitting the same amount of energy. The value of TB corrected to a nadir view is TN. TB is converted to energy units, BT, using the instrument wavelength bandwidth (BANDWIDTH). The bandwidth is calculated from the wavelength integral of the normalized instrument spectral response function (see Section 3.3.1.2 and Appendix B). The two formats of satellite data are the NOAA Global Area Coverage (GAC) format for polar orbiter imager (AVHRR) data and a special version of the various geostationary imager data, called B1U, that can be read by a single program. The location of each image pixel is specified by the latitude (lat) and longitude (lon). The solar illumination and satellite viewing geometry are specified by three angles, the cosine of the solar zenith angle, ⌠0, the cosine of the satellite view zenith angle, ⌠, and the relative azimuth angle, ⟩0. Here ⟩0 = 0 represents forward scattering of sunlight and ⟩0 = 180° represents backscatter.

Clear Sky Composite: The cloud detection algorithm begins by examining the space-time variations of the radiances to estimate clear sky conditions for each pixel at each time associated with ISCCP processing (i.e., 00Z, 03Z, 06Z, … 21Z) regardless of whether clouds are present. These "clear" radiance values are referred to as the clear sky composite radiances (see Section 3.4.1.1).

Cloud Detection Thresholds: Cloud detection thresholds are the magnitudes of the VIS and IR radiance **differences** between observed values from satellite imagery and the clear sky composite values required to label a pixel as cloudy (see Sections 3.4.1.1.3 and 3.4.1.1.4). These quantities are scene dependent. For VIS the thresholds are reflectance differences (⊗R, although ⊗V is also used inside the algorithm); for IR the thresholds are brightness temperature differences (⊗TB).

Cloud Amount: Cloud amount, CA, represents the number of cloudy pixels in a map grid cell divided by the total number of pixels available. At a given time, this quantity represents cloud cover fraction; when averaged over time it represents the product of cloud cover fraction and the frequency of occurrence. This quantity is only determined in the gridded products in a 1-degree-equivalent equal-area map; at pixel level the value of CA is either 0 or 1, representing a cloud mask. Marginal CA refers to the fraction of the total number of pixels in a map grid cell that have R or TB differences from the clear sky composite values that are larger than the cloud detection thresholds but less than twice the detection thresholds.

Cloud Properties: There are four basic retrieved cloud properties, cloud top temperature, TC (in Kelvins), cloud top pressure, PC (in mb), visible optical thickness, TAU (or ⌡, unitless), and water path, WP (in g/m^2). TC is determined directly from the cloudy pixel TB values, corrected for the effects of water vapor and aerosol absorption. At night when there are no VIS data available, TC is the value for an IR-opaque (blackbody) cloud layer; this value of TC is also reported during daytime. During daytime TAU is used to correct for both IR cloud scattering and transmission of IR radiation from below the cloud layer. PC is the atmospheric pressure where the air temperature corresponds to TC based on the Ancillary atmospheric temperature profile dataset. TAU is the visible optical thickness retrieved

directly from R values, corrected for the radiative effects of ozone absorption, Rayleigh scattering, scattering/absorption by stratospheric and tropospheric aerosols, and the surface reflectance. Averages of TAU values are performed in a radiatively-weighted fashion that preserves the cloud visible albedo. WP is calculated from the linearly-averaged TAU values assuming four microphysical models, two for liquid clouds with different droplet sizes for ocean and land and two for ice clouds with different particle sizes for different ranges of TAU. Cloud phase is determined from TC where TC ε 253 K is liquid and TC < 253 K is ice.

Surface Properties: There are two basic retrieved surface properties. These include surface physical skin temperature, TS (in Kelvins), and surface visible reflectance, RS (as a fraction). TS is retrieved directly from both the clear sky composite and clear pixel values of TB, corrected for the effects of atmospheric water vapor and aerosol absorption and accounting for variable surface emissivity at 10.5 ⌈m specified by surface type. RS at 0.65 ⌈m wavelength is retrieved directly from the clear sky composite and clear pixel values of R, corrected for the effects of atmospheric ozone absorption, Rayleigh scattering, and scattering/absorption by stratospheric and tropospheric aerosols. RS is retrieved for all surface types assuming they are isotropic reflectors; however, the values reported over water are replaced in the cloud retrieval by a detailed angle-dependent water reflectance model. An additional value, RS0, is retrieved over all surface types, except open water, by ignoring the effects of aerosol to be used in the cloud retrieval over these surfaces.

Cloud Types: In addition to the values of TC, PC, TAU and WP averaged over all clouds, the ISCCP products also report the averages of these quantities for 18 cloud types during daytime defined by two phases (liquid for TC ε 253 K and ice for TC < 253 K), three PC categories (PS ε PC > 680 mb, 680 ε PC > 440 mb and 440 ε PC) and three TAU categories (0.02 δ TAU < 3.55, 3.55 δ TAU < 22.63 and 22.63 δ TAU δ 450). The nine combinations of PC and TAU define cloud types (increasing TAU for each PC interval) called Cumulus, Stratocumulus, Stratus (low-level), Altocumulus, Altostratus, Nimbostratus (middle-level) and Cirrus, Cirrostratus and Deep Convection (high-level). In addition there are three cloud types (Low, Middle, High) defined only by the (blackbody) PC categories reported day and night. There are also histograms giving the number of cloudy pixels in 7 PC intervals, day and night based on the blackbody value of TC, and for 7 PC and 6 TAU intervals (42 total intervals) during daytime.

Atmospheric Pressure: Atmospheric pressure, P (in mb), is the vertical coordinate of the temperature-humidity profile Ancillary data product (NNHIRS). The pressure levels are fixed, except that levels with P > PS, the surface pressure, are not included (fill values reported). The fixed levels are 900, 800, 740, 680, 620, 560, 500, 440, 380, 320, 260, 200, 150, 100, 50 and 10 mb. In addition to the surface pressure, the tropopause pressure, PT, and the pressure at which the profile-maximum temperature occurs, PMAX, are reported. For most profiles, PMAX = PS.

Atmospheric Temperature: Atmospheric temperature, T (in Kelvins), is reported from NNHIRS at all pressure levels, except those with P > PS, including a near-surface air

temperature, TA at PS, the profile-maximum T, TMAX at PMAX, and the tropopause temperature, TT at PT (see Appendix D.1).

Relative Humidity: Atmospheric water vapor amount from NNHIRS is reported as relative humidity, RH (in percent), at all pressure levels, except those with P > PS, including near-surface relative humidity, RHA at PS, relative humidity at the maximum temperature level, RHMAX at PMAX and the relative humidity at the tropopause, RHT at PT. RH is used to provide the same precision at all levels, but it is determined from the specific humidity, Q, and temperature, T, at each level with respect to liquid water for $T \geq T_0$ (T_0 = 273.15 K) and with respect to ice for $T < T_0$ (see Appendix D.1 for the formulae used).

Ozone Abundance: Total column ozone abundance, O3 (in Dobson units), is assumed to represent stratospheric ozone abundances (see Appendix D.2).

Aerosol Optical Depth: Aerosol optical depths, AOD (unitless), are reported for the stratosphere and troposphere for both VIS and IR wavelengths in the Ancillary AEROSOL data product (see Appendix D.3). Stratospheric aerosols are assumed to be sulfuric acid droplets with effective radius of 0.5 ⌈m and tropospheric aerosols are assumed to be a mixture of "fine" sulfate aerosols with an effective radius of 0.5 ⌈m and "coarse" mineral dust aerosols with an effective radius of 1.0 ⌈m. The amount of each aerosol type in the tropospheric mixture is reported as the fine fraction.

Cloud Algorithm Parameters: Three types of parameters are used in the Cloud Detection Algorithm: NMIN, DEL and Detection Thresholds (⊗TB for IR and ⊗R, as well as ⊗V, for VIS). NMIN refers to the minimum number of samples required for the statistical tests of radiance distributions to be reliable. DEL values are radiance differences that refer to the shape of the radiance distributions on the "clear side" in terms of the difference between the average and extremum values. Detection Thresholds refer to the differences between the observed radiances and the clear sky composite estimate of clear sky radiances: the magnitude of the Thresholds represents the estimated uncertainty in the clear sky radiances, so the differences are required to be larger to detect the presence of clouds. The Threshold values are scene dependent.

Other details on symbols referenced in equations presented within the C-ATBD are given below. See Appendix A for complete list of symbols, acronyms and abbreviations.

$\Delta\lambda$ = *bandwidth (μm)* *(1.01)*

λ = *wavelength (μm)* *(1.02)*

SOLCON = band solar constant $(Wm^{-2}\mu m^{-1})$ *(1.03)*

ϑ, ϑ_o = *satellite view angle, solar zenith angle (°)* *(1.04)*

$\mu = \cos(\vartheta)$ *cosine of the satellite view zenith angle* *(1.05)*

$\mu_o = \cos(\vartheta_o)$ *cosine of the solar zenith angle at the satellite pixel* *(1.06)*

$\rangle_0$ = *relative azimuth angle, backscatter is 180°* *(1.07)*

TB = IR Brightness Temperature (K) *(1.08)*

RH = Relative Humidity *(1.09)*

TA = Surface Air Temperature (K) *(1.10)*

TN = angle-corrected IR brightness temperatures (K) *(1.11)*

TS = Surface Skin Temperature (K) *(1.12)*

V = Visible (VIS) Scaled Radiances *(1.13)*

BT_{dn} *= Downwelling radiation at the surface* *(1.14)*

BTA = upwelling emission by the atmosphere at the top of the atmosphere *(1.15)*

BTCLR = Clear sky IR Radiance from clear sky composite *(1.16)*

BTS = upwelling radiation at surface equivalent to TS *(1.17)*

RS = Surface Reflectance *(1.18)*

RS0 = Surface Reflectance retrieved with aerosol effects neglected *(1.19)*

AOD = Aerosol Optical Depth *(1.20)*

⊗TB = IR Brightness temperature differences *(1.21)*

TAU = VIS cloud optical depth *(1.22)*

TC = Cloud Top Temperature (K) *(1.23)*

PC = Cloud Top Pressure (mb) *(1.24)*

TS = surface skin temperature (K) *(1.25)*

PS = surface pressure (mb) *(1.26)*

Z = surface elevation (km) *(1.26)*

WP = Water Path (g/m²) *(1.27)*

p = pressure (mb) *(1.28)*

T = temperature (K) *(1.29)*

TT = tropopause temperature (K) *(1.30)*

PT = tropopause pressure (K) *(1.31)*

$e_{s,l}$ *= saturation vapor pressure over liquid water* *(1.32)*

$e_{s,l}$ *= saturation vapor pressure over ice* *(1.33)*

ext = atmospheric extinction in the upwelling direction *(1.34)*

ε = *surface emissivity* *(1.35)*

Q = specific humidity *(1.36)*

QS = specific humidity at saturation *(1.37)*

$/_L$ *= Optical thickness of Water Vapor line absorption* *(1.38)*

$/_S$ *= Optical thickness of Water Vapor Self-broadening Absorption* *(1.39)*

$/_f$ *= Optical thickness of Water Vapor Foreing-broadening Absorption* *(1.40)*

1.3 Referencing this Document

This document should be referenced as follows:

ISCCP H-Version – Climate Algorithm Theoretical Basis Document, NOAA Climate Data Record Program (CDRP-ATBD-0872) Rev 0 (2017). Available at https://www1.ncdc.noaa.gov/pub/data/sds/cdr/CDRs/Cloud_Properties-ISCCP/AlgorithmDescription_01B-29.pdf

1.4 Document Maintenance

This document describes the submission, version 1.0 and revision 0.0, of the processing algorithm and resulting data. The version and revision number will be incremented for any subsequent enhancements or revisions and these changes will be coordinated with the CDR Program office.

2. Observing System Overview

2.1 Products Generated

Although the satellite imager radiances are not generated by ISCCP, the version of these data used to produce the cloud products is accompanied by complete Quality Checking results, as well as removal of individual bad images from the collection. Moreover, all the radiances have been calibrated to the same absolute standard. The geostationary images have been sampled to a spatial interval of about 10 km and slightly re-formatted so that a common program reads and navigates all of them (B1U format). The polar orbiter data are input in the standard NOAA GAC format and sampled to 10 km intervals during processing. READ codes for both formats are part of the ISCCP processing system software. The radiance calibrations are provided in HBT tables. The previous version of all radiances, sampled to 30 km intervals, in one readable format (called B3 Data) included the initial calibration tables; updates were available in a separate dataset. Thus, the particular version of the radiance images used by ISCCP is considered to be an ISCCP product (see Section 3.3.1).

The basic analysis has four main steps: cloud detection, surface property retrieval, cloud property retrieval and statistics (the changes from the previous C-Version and D-Version processing are summarized in Section 6). Cloud detection is the process by which each image pixel is labeled as cloudy or clear; at pixel level, cloud fraction is either zero or one (see Section 3.4.1.1). As part of the cloud detection algorithm, clear sky radiances are estimated for each pixel at each time (clear sky composite): a sufficient difference between the observed and estimated clear sky radiances indicates the presence of clouds. Two basic surface properties, skin temperature (TS) and visible reflectance (RS), are retrieved from the clear sky radiances (see Section 3.4.1.2). Then two basic cloud properties, top temperature (TC) and visible optical thickness (TAU), are retrieved. Cloud top pressure (PC) is determined from the atmospheric temperature that corresponds to TC and cloud water path (WP) is calculated from TAU and assumed cloud microphysical properties (see Section 3.4.1.3). Finally, several products are produced that report the cloud and surface information at different space-time scales. There are two Level 2 (pixel-level) products and four Level 3 (gridded) products. The products on the 1-degree-equivalent equal-area grid include the Ancillary data and report cloud amount (CA, cloud cover for a single image pixel is 0 or 1), cloud properties, cloud type information and cloud property distributions.

The analysis of the satellite image VIS and IR radiances, employing the Ancillary Data Products, produces six Cloud Data Products (see Appendix C for details): Level 2 products are HXS and HXG, Level 3 products are HGS, HGG, HGH, and HGM. The HXS Product provides the basic results – cloud and surface properties retrieved or used in the retrieval -- for each individual satellite image in nearly the original projection for geostationary satellites and for groupings of orbit swaths in six midlatitude (ascending and descending swaths in 120° longitude sectors) and two polar sectors. Also provided are the calibrated VIS and IR radiances used for retrieval and up to nine extra spectral channel radiances (not calibrated) measured by the particular satellite. The time sampling interval is 3 hr and the approximate spatial sampling interval is 10 km. The HXG Product is a global merger of the

information from HXS common to all satellites every 3 hr on a 0.10-degree equal-angle grid. The HGS Product reduces the HXS Product to the 1-degree-equivalent equal-area grid, determines additional statistical and cloud type information, and merges these results with the Ancillary Data Products. The HGG Product is the global merger of the HGS Products from all available satellites, where overlapping coverage is resolved in favor of the satellite with the best viewing geometry with a preference for geostationary results at lower latitudes and polar orbiter results in the polar regions. The time interval is 3 hr and the map grid is 1-degree-equivalent equal-area. This is the main ISCCP Cloud Product. The HGH Product provides the monthly average of the HGG Product at each of eight times-of-day UTC. The HGM Product is the average of the eight HGH Products for each month.

The ISCCP Cloud Products are produced using six Ancillary Data Products that are produced from available sources but slightly modified to provide missing or more complete information and to make them compatible with the time sampling intervals and map grids used for the ISCCP Cloud Products. These products are NNHIRS, OZONE, AEROSOL, SNOWICE, TOPO, and SURFACETYPE (see Section 3.3.2 and Appendix D). NNHIRS is a time varying data product reporting the global variations of the vertical distributions of atmospheric temperature and relative humidity from the surface to 10 mb level every 3 hours. OZONE is a time varying data product reporting the daily variations of the global distribution of total column ozone abundance. AEROSOL is a time varying data product reporting monthly average global distributions of aerosol optical properties. The aerosol properties reported are optical depth at 0.65 μm and 10.5 μm wavelengths, together with the fine fraction for tropospheric aerosols, and optical depths at the same wavelengths for stratospheric aerosols. SNOWICE is a time varying data product reporting the daily variations of snow and sea ice cover over the whole globe, including permanent sea ice shelves and land glaciers. TOPO is a fixed data product providing a land-water mask together with topographic height information (mean, standard deviation) over land including at lake surfaces. SURFACETYPE is a fixed data product that characterizes the Earth's surface at each map location as water or permanent ice shelf or as land in terms of sixteen vegetation types or permanent glaciers. All of these products are available in the same ISCCP 1-degree-equivalent equal-area grid and are included in the gridded Cloud Products except for AEROSOL. A 0.1-degree-equivalent equal-area version of TOPO and 0.25-degree-equivalent equal-area versions of SNOWICE and SURFACETYPE are used in the pixel-level processing of the Cloud Products and reported along with those results.

All H-Version ISCCP products, except HXS, are in the NetCDF-4 format and currently cover the time period from 1982 through 2015 but will be extended operationally into the future.

2.2 Instrument Characteristics

The primary instruments providing input to the ISCCP analysis are the imaging radiometers on operational weather satellites, AVHRR on the polar orbiting satellites and a variety of imagers on the geostationary satellites (see Appendix B for a list of satellites, satellite agencies and instrument characteristics). Although many of these radiometers make measurements at other wavelengths, the primary radiance data come from the visible (VIS H 0.65⌈m wavelength) and "window" infrared (IR H 10.5 ⌈m wavelength)

channels. The normalized spectral response functions for these instruments/channels are represented in Appendix B by the peak-response wavelength and SOLCON for VIS and BANDWIDTH for IR (the normalized spectral response functions for the GOES can be obtained from http://www.ospo.noaa.gov/Operations/GOES/goes-imager-srfs.html, AVHRR can be obtained from, http://noaasis.noaa.gov/NOAASIS/ml/calibration.html, and METEOSAT can be obtained from, http://www.eumetsat.int/website/home/Data/Products/Calibration/Instrumentstatusandcalibration/index.html#met1mviri . The pixel sizes in the original images ranges from 1 km to 7 km, varying with spectral channel and satellite; higher resolution VIS data are averaged to match the IR pixel sizes ("average" size about 5 km). The version of these images used for the ISCCP analysis are sampled at approximately 10-km intervals. All orbits of the polar orbiting data are used but the geostationary images are sampled at 3-hr intervals.

The Ancillary Data Products used in the ISCCP analysis are also determined (mostly) from a variety of satellite measurements as follows: (1) the NNHIRS atmospheric temperature-humidity product is based on HIRS infrared sounder measurements in the troposphere and a combination of SAGE and MLS water vapor measurements in the stratosphere, (2) the OZONE product is based on several UV instruments, mainly the TOMS and OMI supplemented by SBUV and TOVS (IR) measurements, (3) land snow cover in SNOWICE is obtained from a combination of VIS imagery and SSMI/SSMIS microwave measurements, and sea ice cover in SNOWICE is obtained from SSMI/SSMIS microwave measurements. Appendix D provides more information on these instruments and data products.

3. Algorithm Description

3.1 Algorithm Overview

The ISCCP processing algorithm has three major components: cloud detection, cloud and surface property retrieval, and classification and statistics. Figure 1 shows the main steps for the first two parts and Figure 2 shows the processing structure leading to the third part. The cloud detection procedure is composed of four parts: (1) a set of space and time radiance comparisons to identify possibly clear radiance values for each image pixel location and time using the TOPO Ancillary Product (B4PROD output = B4), (2) the logical combination of all the space-time test results to obtain composite clear sky radiances for each image pixel location and time using the TOPO, SURFACETYPE and SNOWICE Ancillary Products (CLRSKY output = CLRSKY), (3) application of detection threshold tests that identify image pixels with radiances sufficiently different from the clear sky values to be labeled as cloudy using the Ancillary Products (BXPROD output = BB, BX), and (4) a revision of the composite clear sky radiances based on the prior detection threshold results and application of revised threshold tests of each image pixels against the revised composite clear sky radiance values using the Ancillary Products (CYPROD output = CY). The cloud and surface retrieval step (DXPROD output = HXS) uses the NNHIRS, OZONE, AEROSOL and SNOWICE Ancillary products and has three parts: (1) retrieval of surface properties (skin temperature at all times of day, visible reflectance during daytime) from the composite clear sky radiances, (2) retrieval of cloud properties for cloudy pixels (top temperature/pressure at all times of day, visible optical thickness during daytime) using the results from the first step assuming optically thick clouds (also retrieval of surface properties for clear pixels), (3) revision of cloud top temperature/pressure for optically thinner clouds during daytime. The Level 2 output is the HXS product for each satellite. A global Level 2 product, HXG, is also produced by merging all of the HXS products; some interpolation/replication is performed to fill missing values (see Appendix C).

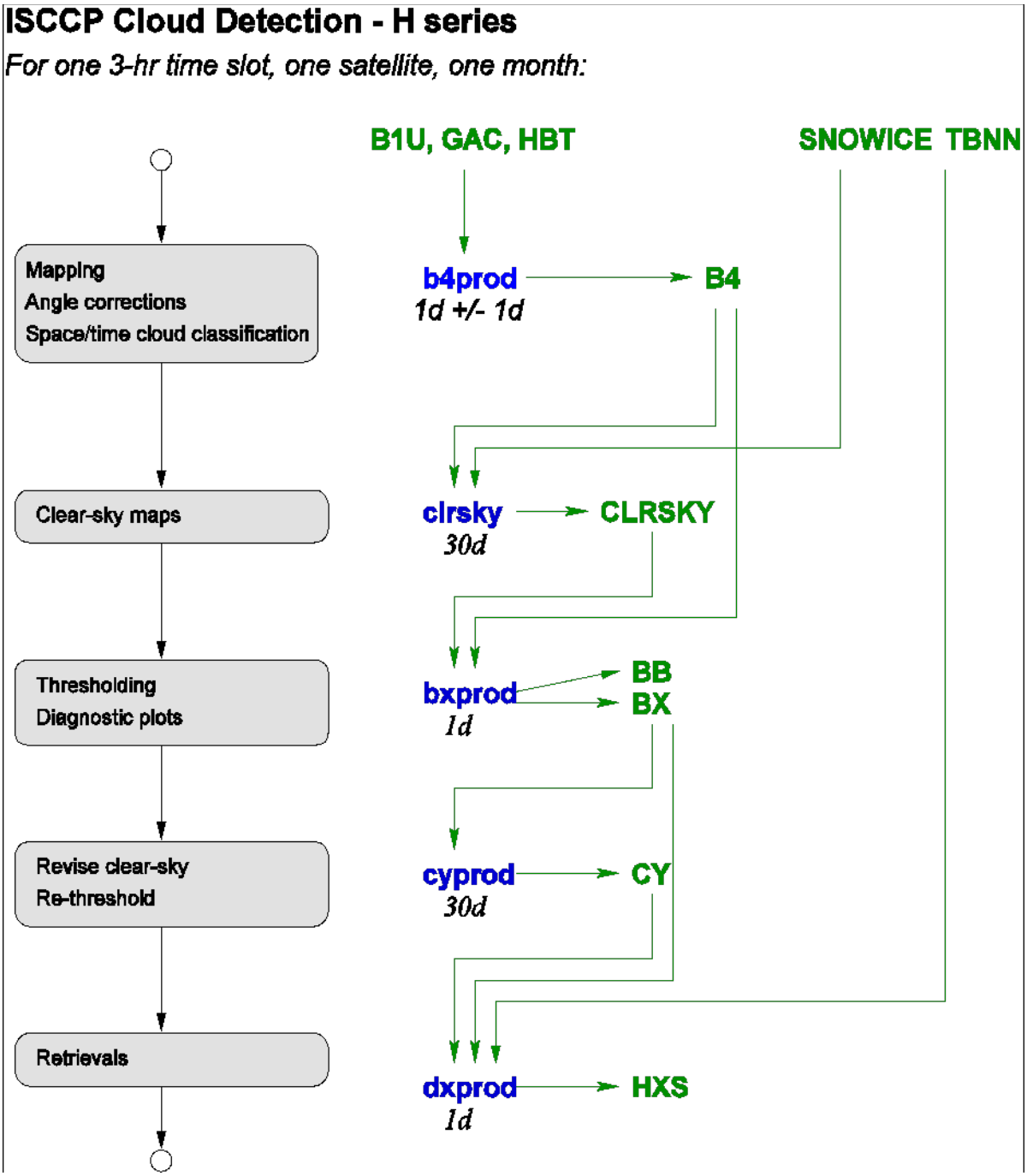

Figure 1: Cloud detection steps

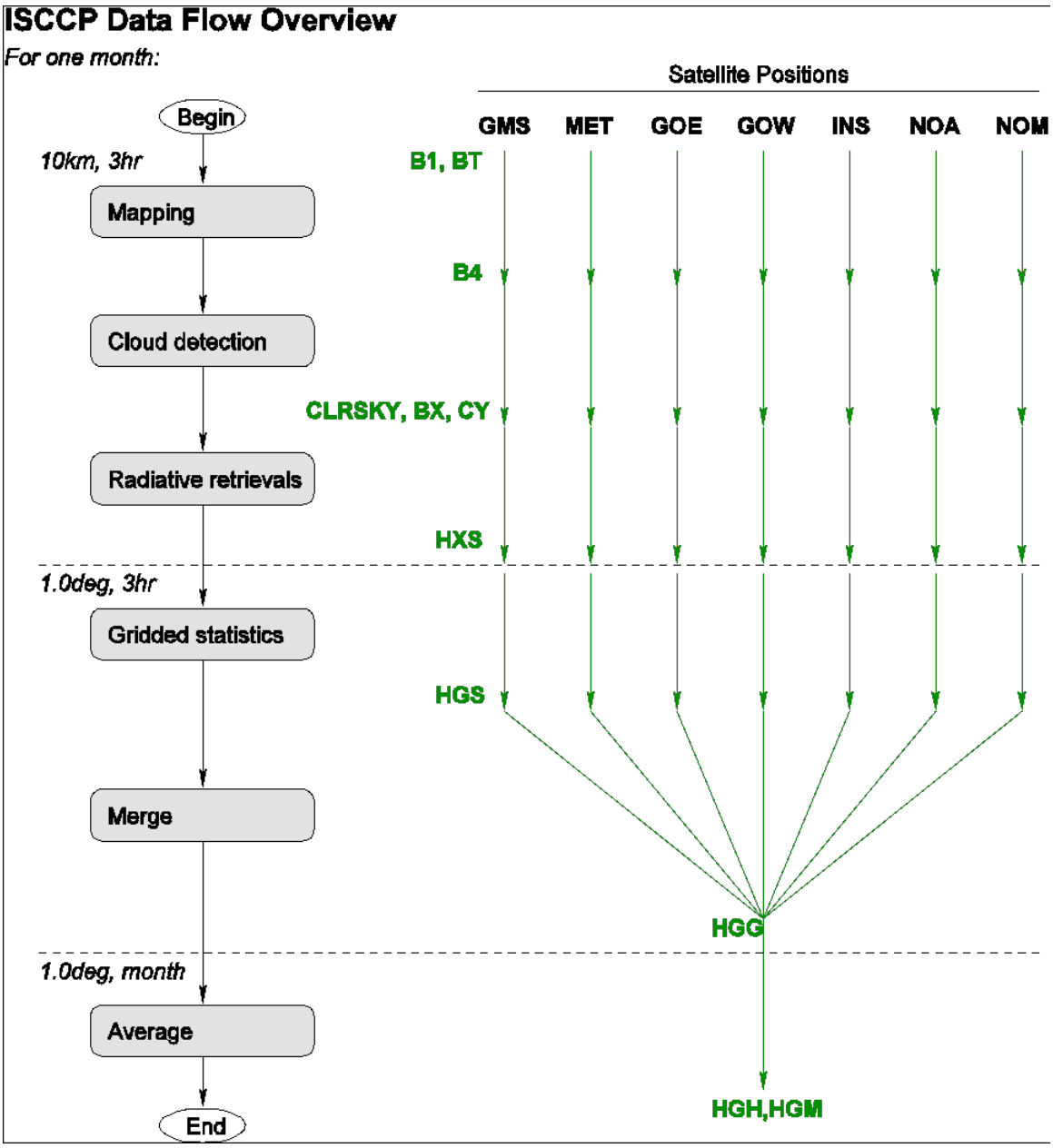

Figure 2: Data Flow Overview

Figure 2 shows that each month of data for each satellite is processed separately but in parallel. The Level 2 results (HXS) are then reduced in spatial resolution to the Level 3 1-degree-equivalent equal-area map grid and combined with the Ancillary Products to produce the HGS product. This step includes determination of total cloud amount and classification of clouds by phase based on cloud top temperature and by three ranges of cloud top pressure and three ranges of optical thickness. The results from the separate HGS products are then merged to form the global HGG product. The merger procedure for each map grid chooses the single result from those available using a hierarchical order that prefers the geostationary satellite with the best viewing geometry at latitudes δ 55° and the polar orbiter satellite with the best viewing geometry at higher latitudes. The merging

hierarchy is illustrated for one case in Figure 3. A multi-part procedure is applied to HGG to fill missing values. Finally, HGG is averaged first over each month at constant time of day UTC to produce HGH product and then the eight HGH products for each month are averaged to product HGM (see Appendix C). Note that some quantities are averaged in a non-linear, radiatively-weighted fashion.

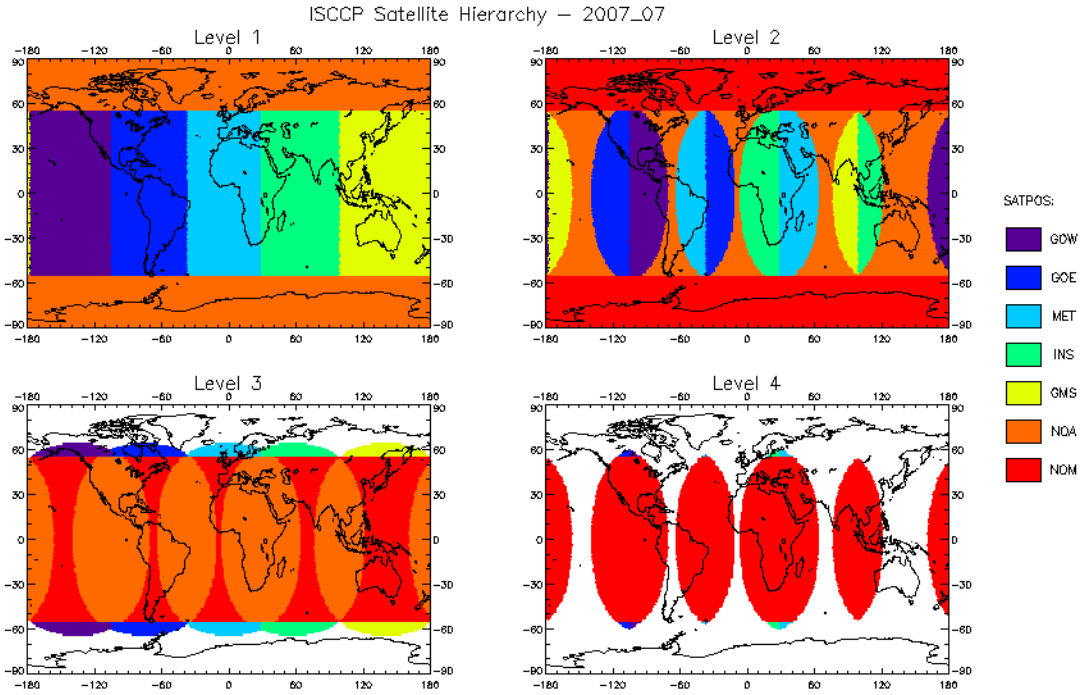

Figure 3: July 2007 satellite hierarchy plot for the 1 degree grid

3.2 Processing Outline

Figure 4 illustrates the complete processing flow, showing all inputs (including some metadata files that record satellite-specific information), processing steps and outputs. Complete OPS Guides for the main processing and the Ancillary data processing are available (see Appendix F). The first process inputs the radiance images for a month (GAC, B1U formats), calibrates the radiances using the calibration tables (HBT), performs radiance comparisons over two spatial sub-domains aided by land-water information (TOPO), maps the images to a common projection for the month (slightly different for each satellite, possibly different in different months if the satellite location changes), performs radiance comparisons over daily time intervals and outputs B4 (see Section 3.4.1.1.1). TOPO, SURFACETYPE and REFGEO information are combined to define scene types output in AUX, which in turn is combined with SNOWICE0.25 and B4 in the second process to produce the first clear sky radiance composites for each image pixel and time (CLRSKY, see Section 3.4.1.1.2). Application of detection thresholds produces BX, the first cloud decision

(see Section 3.4.1.1.3). The processing continues by using the BX results to refine the clear sky radiance composites and then applies revised thresholds to produce the final cloud-clear decision, CY (see Section 3.4.1.1.4).

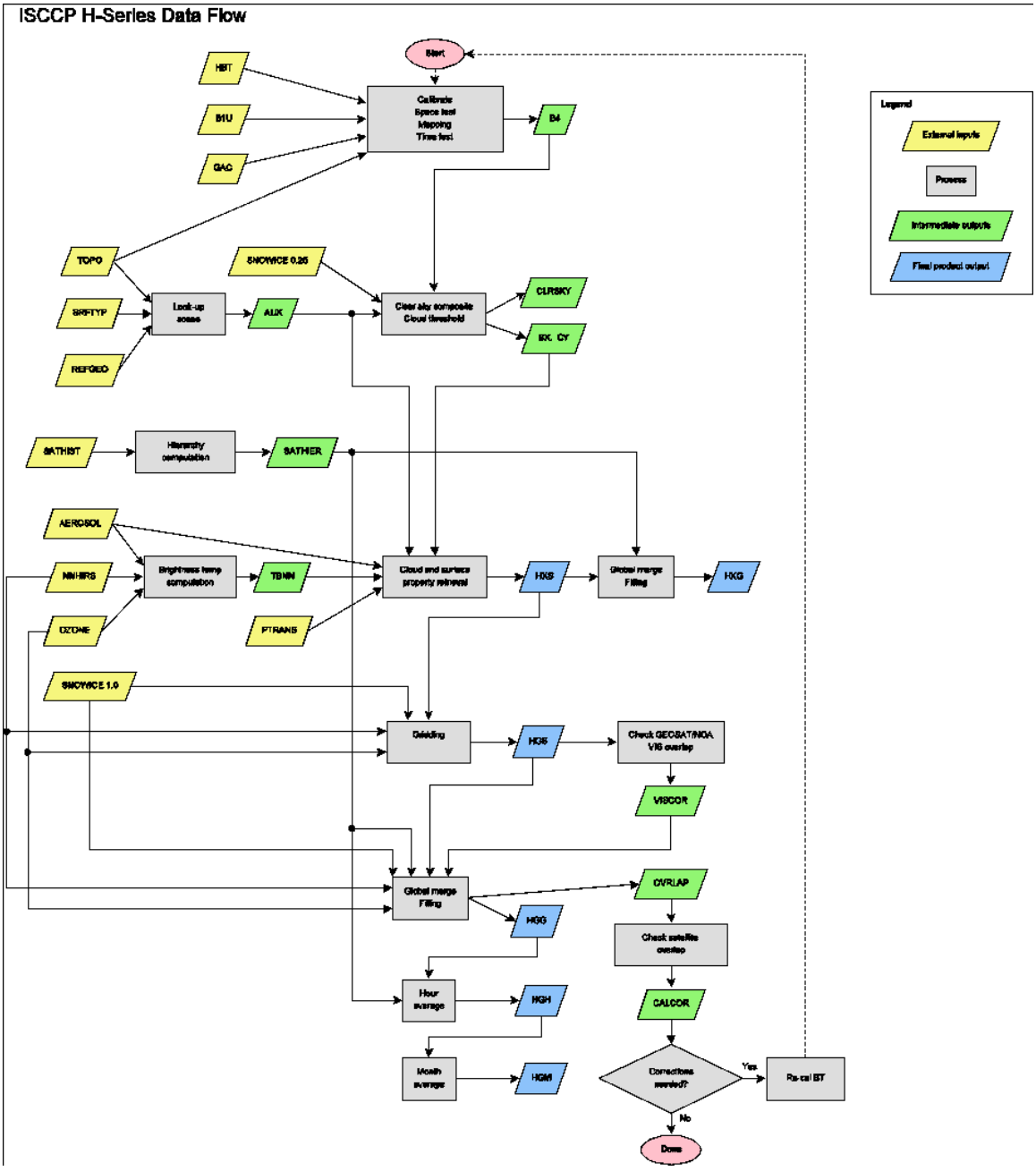

Figure 4: Data flow diagram

To prepare for the third process, cloud and surface property retrieval, a separate procedure uses the NNHIRS, OZONE and AEROSOL data products to calculate brightness temperature profiles for each location and time, output as TBNN. Then the third process combines BX, CY, AUX, TBNN and PTRANS to retrieve cloud and surface properties for each image pixel, output as the first cloud data product HXS (see Section 3.4.1.2 and 3.4.1.3).

The HXS products for all available satellites are used to produce a globally merged Level 2 product, HXG, using the SATHIST sub-system to prepare SATHIER (see Section 3.4.2). HXS is also reduced to the main 1-degree-equivalemt equal-area map grid to produce HGS, which also includes total cloud amount, cloud type classification, additional statistics and the Ancillary Data products (NNHIRS, OZONE, SNOWICE). Because some radiometers have broader VIS channels than most, a small correction procedure, VISCOR, is applied to surface reflectances by comparing the geostationary result in HGS to the afternoon polar orbiter result.

The HGS results from all satellites are then merged (see Section 3.4.2) using SATHIER to produce HGG and a filling procedure is applied to account for any missing HGS (the Ancillary Data Products are written into HGG separately so that they are present even if some HGS files are missing because of missing satellite images). This step also interpolates daytime results over the nighttime. Overlapping observations from the reference polar orbiter and the geostationary satellites are compared as a final check of the radiance calibration consistency in the CALCOR procedure; if unacceptable differences are found for any satellite/channel, the HBT tables are modified for that satellite/channel and the processing repeated (this iteration continues until the CALCOR output indicates acceptable calibration agreement). The HGG product is averaged over the month at each of eight times of day UTC to produce HGH; the eight HGH files are then averaged to produce the monthly mean product, HGM.

There are additional procedures outside the basic Processing Flow that must be performed before beginning processing, as well as during and after the processing to monitor the product quality. Figures 5 and 6 show two versions of the procedure flow, one followed to Re-Process the ISCCP products for the period July 1983 through December 2009 (Figure 5), where comparison to the D-Version of the products is possible, and one followed for New-Processing for time periods outside this date range and into the future (Figure 6). These additional procedures are Ingest, Radiance Calibration and QC Analysis, as well as Ancillary Data Ingest or Production, prior to Cloud Production, and Wrap-Up (see OPS Guides together with Add-On, Appendix F).

The Ingest procedures include staging the satellite radiance data (GAC, B1U) to the system, reviewing the satellite operator reports for any problems or changes (updating SATEVENTS.TXT) and, if a new satellite, setting up the metadata files (SAT.PM, PTRANS, REFGEO, see Section 3.4.5.1) that provide satellite-specific information. For New-Processing, this step also requires initializing the calibration tables with the nominal radiance calibration to run the Radiance QC procedures. During the re-processing time period, the Ancillary Data Products were provided so these also need to be staged; otherwise, the source data for the Ancillary Data Products needs to be staged and processed to produce the ISCCP versions (see Appendix F for information about the Ancillary OPS Guide).

The Radiance Calibration step during Re-Processing only requires creation of new HBT files if images are added that were not in the previous processing cycle. During New-Processing, the H-Version of ISCCP calibration procedures should be employed (see Appendix F, ADD-ON document). These procedures include the polar orbiter MONITOR and

the geostationary NORM that are run to generate the coefficients used to produce the radiance calibration tables (HBT). The Radiance QC procedure is crucial to the quality of the final products – quality is also checked during and after Cloud Production. The Ancillary Data Production also includes QC procedures. The Radiance QC procedures (B1QC) are automated checks of image statistics that flags images that appear to have multiple problems but also plots image and radiance statistics for the whole month. These results have to be manually inspected and individual flagged images examined to determine whether they should be retained or can be fixed.

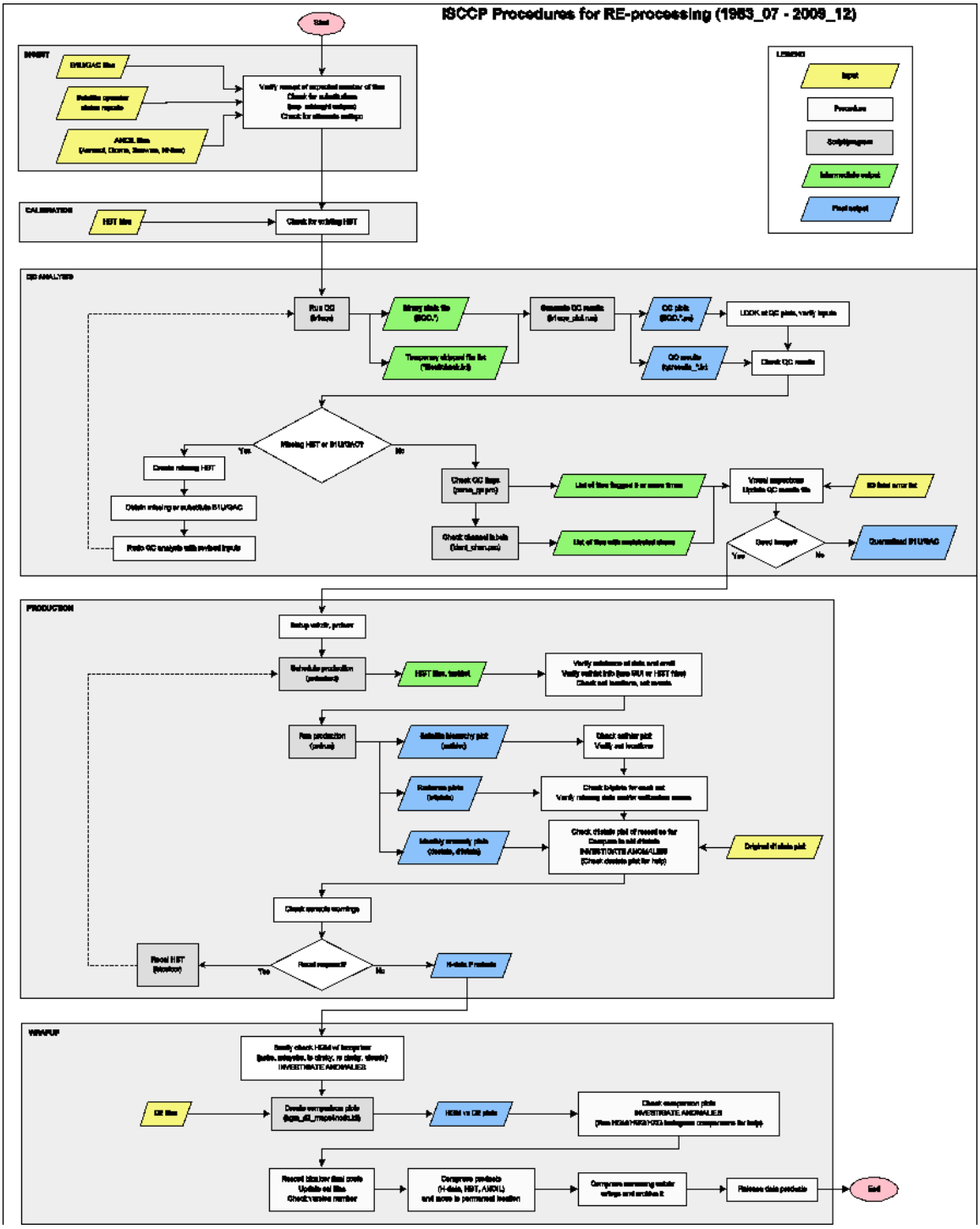

Figure 5: Procedures for RE-processing

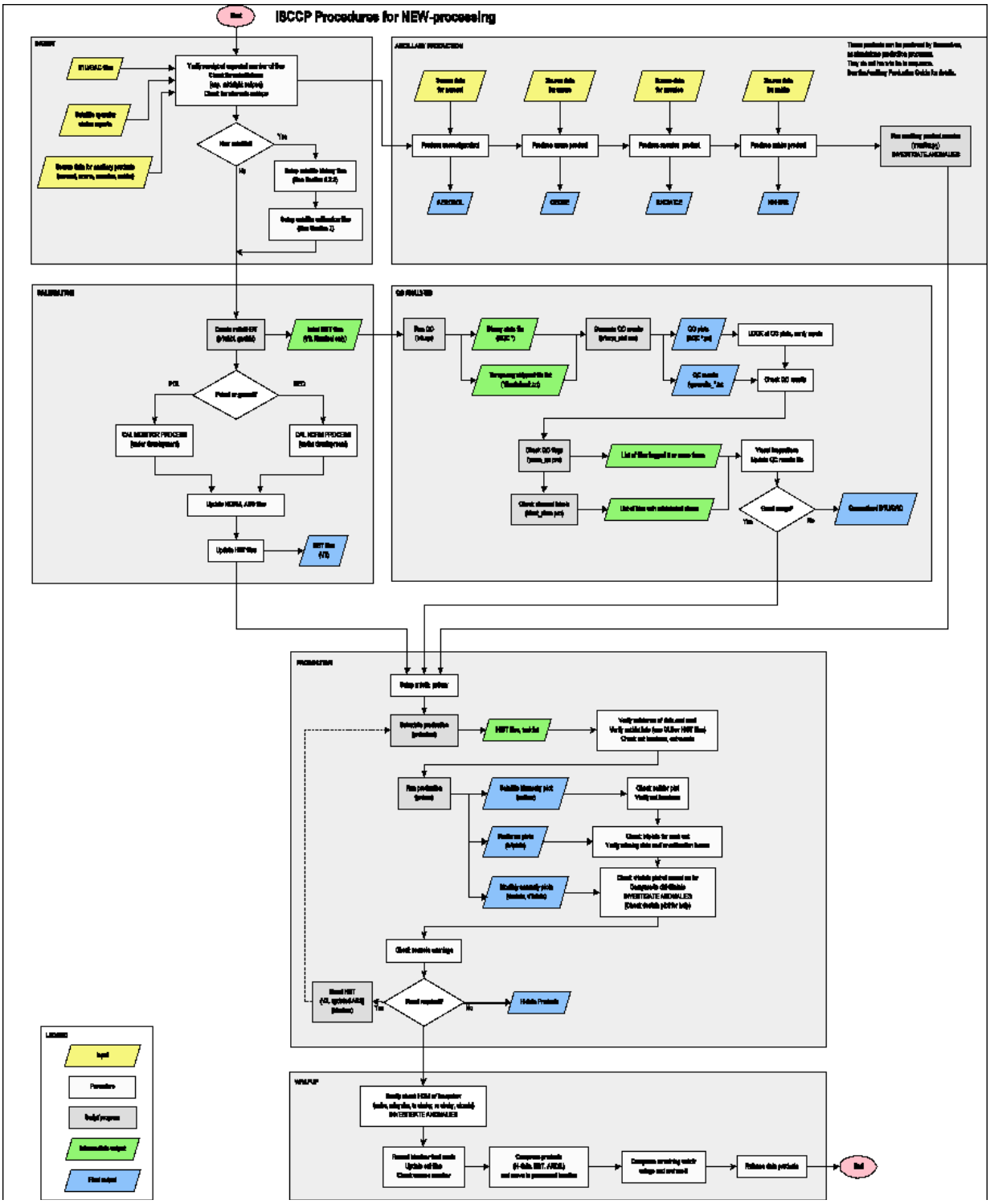

Figure 6: Procedures for NEW processing

3.3 Algorithm Input

3.3.1 Primary Sensor Data

3.3.1.1 Polar Orbiter and Geostationary Data

The primary sensor inputs to the ISCCP analysis are the VIS (H 0.65 ± 0.05-0.20 ⌈m) and IR (H 10.5 ± 0.5-0.75 ⌈m) radiances from the operational weather satellite imaging radiometers. The list of satellites with imaging radiometers included in the ISCCP analysis are provided in Table 1 and Table 2 where the tables respectively represent polar orbiter and geostationary satellite descriptions. The pixel sizes in the original geostationary images range from ~1 km to 7 km, varying with spectral channel and satellite; higher resolution VIS data are averaged to match the IR pixel sizes ("average" size is ~5 km).

Table 1: Historical and currently operational AVHRR instrument informationTable. This table combines information from the NOAA KLM User's Guide, with NOAA-N, -N' supplement (February 2009) and **http://www.star.nesdis.noaa.gov/smcd/emb/vci/VH/vh_avhrr_ect.php**, and Ignatov et al. (2004).

Satellite Name	Launch Date	Service Start	Service End	Approximate Daytime Equatorial Crossing Time at Satellite Launch	GAC Filename Satellite ID String
NOAA-7	23 Jun 1981	24 Aug 1981	7 Jun 1986	0230 PM	NC
NOAA-8	28 Mar 1983	3 May 1983	31 Oct 1985	0730 AM	NE
NOAA-9	12 Dec 1984	25 Feb 1985	11 May 1994	0230 PM	NF
NOAA-10	17 Sep 1986	17 Nov 1986	17 Sep 1991	0730 AM	NG
NOAA-11	24 Sep 1988	8 Nov 1988	13 Sep 1994	0200 PM	NH
NOAA-12	13 May 1991	14 May 1991	15 Dec 1994	0730 AM	NI
NOAA-14	30 Dec 1994	30 Dec 1994	23 May 2007	0130 PM	NJ
NOAA-15	13 May 1998	13 May 1998	Present	0730 AM	NK
NOAA-16	21 Sep 2000	21 Sep 2000	9 June 2014	0200 PM	NL
NOAA-17	24 Jun 2002	24 Jun 2002	10 Apr 2013	1000 AM	NM
NOAA-18	20 May 2005	30 Aug 2005	Present	0200 PM	NN
NOAA-19	6 Feb 2009	2 Jun 2009	Present	0200 PM	NP
MetOp-A	19 Oct 2006	20 Jun 2007	Present	0930 AM	M2
MetOp-B			Present		M1

Table 2: Historical and currently operation geostationary satellite, instrument name, launch dates, service start/end dates, spatial resolution, and Primary Satellite Processing Stream

Satellite Name	Instrument	Launch Date	Service Start	Service End	Spatial Resolution VIS/IR (km)	Primary Satellite Processing Stream (Satpos)
GMS-1	VISSR	Jul. 14, 1977	1982-01	1984-06	1.25/5.0	GMS
GMS-2	VISSR	Aug. 11, 1981	1982-01	1984-09	1.25/5.0	GMS
GMS-3	VISSR	Aug. 3, 1984	1984-10	1989-11	1.25/5.0	GMS
GMS-4	VISSR	Sep. 6, 1989	1989-12	1995-05	1.25/5.0	GMS
GMS-5	VISSR	Mar. 18, 1995	1995-06	2003-04	1.25/5.0	GMS
GOE-4	VAS	Sep. 09, 1980	1982-01	1983-06	0.9/6.9	GOW
GOE-5	VAS	May 22, 1981	1982-01	1984-07	0.9/6.9	GOE
GOE-6	VAS	Apr. 28, 1983	1983-07	1989-01	0.9/6.9	GOW
GOE-7	VAS	Feb. 26, 1987	1987-04	1995-12	0.9/6.9	GOW
GOE-8	IMAGER	Apr. 13, 1994	1995-05	2003-03	1.0/4.0	GOE
GOE-9	IMAGER	May 23, 1995	1996-01	1998-07	1.0/4.0	GOW
GOE-10	IMAGER	Apr. 25, 1997	1998-08	2006-06	1.0/4.0	GOW
GOE-11	IMAGER	May 3, 2000	2006-07	2011-11	1.0/4.0	GOW
GOE-12	IMAGER	Jul. 23, 2001	2003-04	2010-03	1.0/4.0	GOE
GOE-13	IMAGER	May 24, 2006	2010-04	9999-99	1.0/4.0	GOE
GOE-15	IMAGER	Mar. 04, 2010	2011-12	9999-99	1.0/4.0	GOW
MTS-1	AMI	Feb. 26, 2005	2005-11	9999-99	1.0/4.0	GMS
MTS-2	IMAGER	Feb. 18, 2006	2010-07	2015-06	1.0/4.0	GMS
HMW8	AHI	Oct. 7, 2014	2015-07	9999-99	0.5/2.0	GMS
MET-2	MVIRI	Jun. 19, 1981	1983-07	1988-07	2.5/5.0	MET
MET-3	MVIRI	Jun. 15, 1988	1988-08	1990-04	2.5/5.0	MET
MET-4	MVIRI	Mar. 6, 1989	1990-05	1994-01	2.5/5.0	MET
MET-5	MVIRI	Mar. 2, 1991	1994-02	2006-12	2.5/5.0	MET/INS
MET-6	MVIRI	Nov. 20, 1993	1997-03	1998-05	2.5/5.0	MET
MET-7	MVIRI	Sep. 2, 1997	1998-06	9999-99	2.5/5.0	MET
MSG-1	SEVIRI	Aug. 28, 2002	2006-07	2007-04	1.0/3.0	MET
MSG-2	SEVIRI	Dec. 21, 2005	2007-05	2013-01	1.0/3.0	MET
MSG-3	SEVIRI	Jul. 05, 2012	2013-02	9999-99	1.0/3.0	MET

The geostationary data are slightly re-formatted so that a common program reads and navigates all of them; this is the B1U format. For the polar orbiters, the standard is the

NOAA GAC data format. All images are sampled to ~10 km intervals during processing. READ codes for B1U and GAC are part of the ISCCP processing system software.

The HBT tables homogenize calibration across all the radiances observed from geostationary and polar orbiter instruments. Further details on each instruments spectral response functions and instrument characteristics are outlined below and in Appendix B.

3.3.1.2 ISCCP HBT Tables

The following section provides a description of the calibration approach that is used to compute the VIS scaled radiance and IR brightness temperatures and provides a description of the HBT Tables themselves.

3.3.1.2.1 Scaled Radiances and Brightness Temperatures

The ISCCP HBT Tables and are used to convert raw image count[1] values obtained from the satellite operator to VIS scaled radiance and IR brightness temperatures. As previously described, imager data used in ISCCP have been quality checked by ISCCP procedures. To reduce sensitivity to the small differences in spectral responses, the VIS radiances used in ISCCP H-Series processing are normalized by the "solar constant" of each instrument (SOLCON). The SOLCON is defined as the wavelength integral of the product of the normalized instrument spectral response function and the solar spectrum at the top of the atmosphere (Neckel and Labs 1984). The IR radiances used in ISCCP H-Series processing are represented as brightness temperatures, defined by a blackbody temperature that represents the same amount of energy as measured by the instrument at its central wavelength over a bandwidth (BANDWIDTH) given by the wavelength integral of the normalized instrument spectral response function. See Appendix B for the specific values of SOLCON and BANDWIDTH for each satellite. Given the narrow wavelength range for most satellite channels, the spectral dependence is weak for most Earth scenes in individual image pixels (about 5 km across), especially for clouds, ice, snow, open water and soil and rock. Vegetation can exhibit some dependence but only for much broader channels on a few satellites (METEOSAT-2 through METEOSAT-7, GMS-5, MTSAT-1 and 2). All radiances are then "calibrated" to the same standard channels (a combination of the AVHRR VIS and IR channels on NOAA-9 and NOAA-18) as if they are all the same (however, the ozone absorption treatment accounts for instrument differences).

3.3.1.2.2 ISCCP Calibration Procedures

The ISCCP calibration procedure concerns only the IR and VIS radiances common to all polar orbiting and geostationary satellites. To produce a globally uniform radiance dataset, the calibrations of all the imaging radiometers have to be normalized to a common standard (Schiffer and Rossow 1985, Brest and Rossow 1992, Desormeaux *et al.* 1993, Brest *et al.* 1997, Rossow and Ferrier 2015). This is important since the spectral responses of the various satellite radiometers differ somewhat. Furthermore, raw image counts can change from image-to-image, month-to-month, and satellite-to-satellite due to slow and

[1]In cases where the radiometric resolution of the satellite data exceeds 8 bits or count values of 0-255, the resolution is reduced to fit within these guidelines to provide a homogeneous data record.

abrupt changes in the instrument's calibration that are caused by satellite drift, changes in telemetry, etc.

Because the NOAA polar-orbiting satellites underfly all the geostationary satellites, the ''afternoon'' polar orbiters are used as the normalization standard while the reference calibration is AVHRR on NOAA-9 (cf. Whitlock et al. 1990; Rao et al. 1993a; Rao et al. 1993b) for the portion of the time series that extends through Dec. 31, 2009 and NOAA-18 after this time. The radiometer calibrations of NOAA-9 are anchored on ER-2 aircraft under-flights with a laboratory-calibrated spectrometer while NOAA-18 calibrations are anchored on comparisons to Aqua and Terra MODIS with on-board calibration.

Each HBT file contains three different calibration tables for IR and VIS channels. These refer to the nominal, normalized and absolute calibrations. The systematic approach used to produce and manage the HBT calibration products employ several steps that are fully outlined in the ISCCP Calibration document found in Appendix F. These steps are briefly described here so that the user has some knowledge of how these steps work.

1. HBT tables are initially created using the nominal calibration information provided by the Satellite Processing Centers (usually the satellite operator) that provides the radiance data and are based on pre-launch, on-board or other estimates of the calibration.
2. Calibration stability and consistency are realized through analysis of AVHRR radiance measurements found in the ISCCP data set using a variety of targets. In this process the AVHRR VIS Monitor (the AVHRR IR Monitor is described next) procedure reads the GAC files, applies the HBT nominal calibration, retrieves the reflectance for each pixel after correcting for absorption by ozone and makes a global map of clear sky reflectance and total reflectance including clouds. These maps are generated using specific surface types to define a set of targets on Earth. The resulting map for clear sky reflectances is averaged over the globe for each month. The global monthly mean AVHRR reflectances for each satellite are then differenced from the NOAA-9 climatology (if for data prior to Jan. 1, 2010). A linear fit is made to the time series of the reflectance differences and multiplied by a variable factor (K) until the offset of the linear fit is ~0. The K-factor becomes the NORM coefficient for the current afternoon polar orbiter satellite. The ABS coefficient equals 1.0 + S/K, where S is the slope of the linear fit to the reflectance differences.
3. For the AVHRR IR Monitor, the procedure calculates the record mean for 25^{th} and 90^{th} water percentile for the current AVHRR and fits a line through the regression plot against the NOAA-9 record. The slope and intercept of the fitted line are the NORM slope and intercept calibration coefficients for IR AVHRR. The IR AVHRR ABS slope and intercept 1.0 and 0.0, respectively, for all AVHRRs through NOAA-14 and are 0.977 and 5.667, respectively for all later AVHRRs.
4. After the polar orbiter results are determined, all geostationary satellite radiances are normalized each month to the contemporaneous primary "afternoon" polar orbiter radiances by matching monthly histogram statistics of collocated (within 50 km) and coincident (within 1.25 hr) observations over oceans with cosine of the

satellite zenith angle > 0.5 (this is the NORM procedure). The number of matches found will vary and there may not be matches found every day. Only the GAC images whose starting times are within 30 minutes of the geosat nominal time are searched. For each set of matching pixels, a histogram is made for nominally calibrated reflectance (VIS channel) and brightness temperature (IR channel). Nine percentiles are calculated 1st, 5th, 10th, 25th, 50th, 75th, 90th, 95th and 99th. A linear fit is done using the two extreme percentile values (i.e., 1st and 99th) for each set of polar and geostationary histograms. The resulting gain and offset are used as NORM calibration coefficients for the geostationary satellites.

5. The geostationary satellites ABS coefficients are a combination of the AVHRR NORM and ABS.

For a full description, again please see ISCCP Calibration document found in Appendix F. It should also be noted that during the retrieval of cloud and surface properties, the calibrations of the geostationary satellites may undergo a further adjustment (CALCOR procedure) to maintain consistency of the retrieved cloud and surface properties with the polar orbiter results. This is outlined in the RECAL procedure in the Build 5 Operations Guide. Also, taking the uncertainties of these steps together, ISCCP has determined that the VIS calibration relative uncertainty is no larger than ±3%–5% over the entire radiance data set (Rossow and Ferrier 2015). The estimated IR radiance calibration uncertainty is ± 1.5 K over the entire data record.

3.3.1.2.3 **Final Calibration Adjustment**

The CALCOR routine tries to fine-tune the normalization of geostationary satellite VIS and IR radiance calibrations to the (contemporaneous afternoon) AVHRR calibration by calculating the average difference of the retrieved values of TAU (expressed as a reflectance) and RS for VIS and TC and TS for IR for matched grid cells every 3 hr over a month. This procedure is meant to detect small residual offsets of the calibration but is insensitive to very small differences because it compromises between the radiance differences at the smaller and larger end of the range. Therefore, one final check is made by visual inspection of the monthly mean maps (and the plot of latitude-averages at each longitude) of these four variables, as well as Cirrus cloud amount. If there is a visually obvious discontinuity in any of these variables at the boundary between the regions covered by each geostationary satellite – which appears as a vertical line at the boundary-longitude in the map at lower latitudes and is confirmed by the latitude-average plots – then the "radiance pairs" (TAU and RS for VIS, TC AND TS for IR) are checked to see if they both exhibit a discontinuity of the same sign and show similar differences at both longitude boundaries for a particular geostationary satellite. This situation occurs most often for IR. If there is no such discontinuity or no consistency of the sign or of an effect at both boundaries, no further action is required. If TC shows a feature but TS does not, then the needed adjustment is usually for VIS, which can usually be verified by a the existence of a discontinuity of Cirrus cloud amount. If discontinuities are present, then the calibration of the particular geostationary satellite that appears to differ from its neighbors is adjusted so as to reduce the discontinuity. Discontinuities in TC/TS imply a needed change in IR calibration; discontinuities in TAU/RS imply a needed change in VIS calibration. This adjustment should be in increments of 0.01 for VIS and 0.5 K for IR and should not

generally exceed 0.03 for VIS and 1.5 K for IR. When the radiances for the adjusted satellite are re-processed, CALCOR may request another change of calibration. If so, this change should be implemented and the data processed again. No further changes of calibration should be made afterwards.

3.3.1.2.4 ISCCP HBT Table Format

There is one HBT file for each 3-hour time slot for each satellite. For geo-stationary satellites, each file contains tables for one image. For polar orbiters, each file contains multiple sets of tables, for as many orbits as occur in the 3-hour time slot.

Each HBT file, has a series of table sets, each consisting of a one- line header followed by the 6 calibration tables. Table sets are repeated for each channel that was in the B3 data file. For files with multiple orbits, the whole series (header+tables are repeated for each channel) is then repeated for each orbit in the 3-hour time slot.

Each header line contains the following text fields in the format (A8,I9,2I2,2I7,6I2):

After the header line, there are 256 lines of 6 columns each. The lines correspond to the count values 0-255 (count 255 is reserved to indicate “undefined”), and the 6 columns are the calibration tables in the format (6F8.3):

- Column 1 = Nominal physical radiance
- Column 2 = Normalized physical radiance
- Column 3 = Absolute physical radiance
- Column 4 = Nominal scaled radiance or temperature, depending on channel
- Column 5 = Normalized scaled radiance or temperature, depending on channel
- Column 6 = Absolute scaled radiance or temperature, depending on channel

3.3.2 Ancillary Data

To isolate the cloud effects on the VIS and IR radiances, the effects of the atmosphere and surface must be accounted for. Moreover, use of the retrieved cloud properties to determine radiative fluxes and to study the role of clouds in the hydrological cycle is facilitated by combining them with consistent atmosphere and surface properties that have compatible space-time sampling and coverage. To achieve both these goals, ISCCP also obtains data products quantifying atmospheric temperature-humidity profiles (NNHIRS), total column ozone abundance (OZONE), tropospheric and stratospheric aerosol optical properties (AEROSOL), land snow cover and ocean sea ice cover (SNOWICE), land surface type (SURFACETYPE) and topographic height information (TOPO also provides a land-water mask) (see Appendix D and also the Ancillary OPS Guide, Appendix E). These products are pre-processed into the form used by the ISCCP analysis in one or more ways: (1) some changes of variable and/or removal of out-of-range values, (2) merger of more than one product and reconciliation of systematic differences, if needed, and (3) space-time interpolations to obtain compatible space-time sampling and/or to fill missing values for complete coverage. The three types of alterations are summarized briefly below with the details, links to sources, and references provided in Appendix D.

3.3.2.1 NNHIRS

The ISCCP atmospheric temperature-humidity profile product (see Section D.1 for details) is produced by combining a new analysis of the operational HIRS sounder measurements (Shi *et al.* 2016) with a product that is a combination of SAGE and MLS stratospheric water vapor products, called SWOOSH (Davis and Rosenlof 2016). NNHIRS provides 3-hourly global coverage on a 1-degree-equivalent equal-area grid for the period 1980 to present. The main alterations performed in the pre-processing are: (1) some profiles are removed that were excessively "hot" or "cold" at the surface based on local space-time comparisons – the latter caused by cloud contamination, (2) slight changes to the surface pressure are made and the profiles adjusted accordingly, (3) the tropopause (usually minimum temperature) level and the presence of surface temperature inversions are identified and recorded, (4) specific humidities are changed to relative humidities to preserve numerical precision over the whole range, where the daily minimum near-surface specific humidity is used over land and the daily average near-surface specific humidity is used over oceans, (5) small systematic biases in the surface humidities over oceans are corrected based on the SEAFLUX microwave-based determinations (Clayson and Bogdanoff 2013) and small biases in surface air temperatures over land are corrected based on the global collection of surface weather station measurements (ISD, Smith *et al.* 2011), (6) the lower resolution SWOOSH data are replicated to the standard 1-degree-equivalent equal-area grid, (7) the specific humidity profiles from HIRS and SWOOSH are joined by interpolation between the 100 mb to 320 mb levels and reconciled so that the lower level specific humidity always equals or exceeds the upper level value, and (8) since the original HIRS product provides about 30% global coverage at four times of day when two satellites are operating (the usual situation), global coverage at eight times of day is obtained by simple linear time (and some spatial) interpolations over oceans and by a diurnal variation model over land up to the 500 mb level (linear interpolation above that level). Surface pressure is fixed at 1013 mb over water and is calculated from topographic height (Z from TOPO), using the zonal, monthly mean surface air temperature, TA, (from NNHIRS):

$$PS\,(Z) = 1013.25\,(\,(TA - 6.5 \times Z) / TA)^{5.25} \qquad (1)$$

up to a maximum of maximum = 1019 mb.

3.3.2.2 Ozone

The ISCCP total ozone abundance product (see Section D.2 for details and links to data sources) is produced by merging the TOMS and OMI time records and filling missing values, especially at the winter poles using values from the TOVS operational product (*cf.* Reale *et al.* 2008) before 2005 and the NOAA SMOBA product afterwards, where the latter product is a combination of TOVS and SBUV measurements. OZONE provides daily, global coverage on a 1-degree-equivalent equal-area map grid for the period 1979 to present. The main alterations performed in the pre-processing are: (1) some excessively small and large values were removed from the separate products based on overall climatology, (2) all products were mapped to the standard 1-degree-equivalent equal-area map grid each day, (3) the TOMS and OMI records were combined into one record with a small adjustment of the OMI data based on a regression of OMI and TOMS results in an overlapping period, (4) some missing data were filled by space-time interpolations of TOMS/OMI data, and (5) the

remaining missing data, particularly the un-illuminated polar regions, were filled using TOVS results before 2005 and SMOBA results afterwards – these two products were compared with TOMS and OMI to develop correction factors so that they covered the same dynamic range.

3.3.2.3 Aerosol

The ISCCP tropospheric and stratospheric aerosol optical properties product (see Section D.3 for details) is adapted from the MACv.1 product (Kinne *et al.* 2013) to provide tropospheric aerosol optical depth, tropospheric fine mode fraction, and stratospheric aerosol optical depth (all fine mode), all at 0.65 ⌈m and 10.5 ⌈m wavelengths. AEROSOL provides monthly global coverage on a 1-degree-equivalent equal-area map grid for the period 1979 to present. The main alterations performed in the pre-processing are: (1) using the optical characteristics of the aerosols (accounting for variable fine fraction for tropospheric aerosols) and a radiative transfer model calculation of visible and infrared scattering and absorption, the optical depths are adjusted to 0.65 ⌈m and 10.5 ⌈m reference wavelengths (see next section), (2) zero values of fine fraction are filled with minimum values of 0.01, (3) as the volcanic aerosol decays, the AOD in the stratosphere falls below detectable limits, so minimum values for the visible and infrared values (0.0005 and 0.00005, respectively) are set whenever the reported AOD is smaller, (4) aerosol properties are re-mapped to the standard 1-degree-equivalent equal-area map grid, (5) maps for years prior to 1980 are produced by replicating the nearest year results for each month of year, and (6) all stratospheric AOD values for 2000 and beyond are the minimum value.

3.3.2.4 SNOWICE

The ISCCP land snow cover and sea ice cover product (see Section D.4 for details and links to data sources) combines two NOAA operational snow cover products, Northern Hemisphere EASE-Grid Weekly Snow Cover and Sea Ice Extent (Version3), and the NOAA NSIDC IMS Daily Northern Hemisphere Snow and Ice Analysis (*cf*. Brown and Robinson 2011), with the OSI-SAF Global Sea Ice Concentration Reprocessing Dataset. Also added from the SURFACETYPE product are the GLIMS permanent glacier cover product (Amstrong *et al.* 2005) and a permanent ice shelf cover product derived from the combination of two topographic height products. SNOWICE provides daily global coverage on 0.25-degree-equivalent and 1-degree-equivalent equal-area map grids (replicating from lower resolution products where needed) for the period 1979 to present. The main alterations performed in the pre-processing are: (1) the original products are re-mapped to the standard 0.25-degree-equivalent equal-area map grid (the 1.0-degree version is produced from this version), (2) the snow cover and sea ice products land-water masks are reconciled to the ISCCP land-water mask, (3) permanent glaciers and ice shelves are added, over-writing snow and sea ice, respectively, where they overlap, and (4) a small amount of time interpolation is performed to complete coverage.

3.3.2.5 TOPO

The ISCCP topographic height (mean and standard deviation) product (see Section D.5 for details and links to data sources), which also provides the land-water mask used in

processing, is based primarily on the USGS EROS GTOPO30 product reconciled with the USGS Global Land 1-KM AVHRR Project land-water mask. The product provides the mean and standard deviation of topographic height in meters (only land points are included in the statistics in mixed land-water grid cells). “Shore” distance is calculated as the distance to the center of the nearest land-dominated (land fraction >65%) or mixed land-water (coast) grid cell if the map grid cell is water-dominated (land fraction < 35%) or to the nearest water-dominated or coast grid cell if the map grid cell is land-dominated. The shore distance is 0 km for coast map grid cells. TOPO is used directly in two forms, one on a 0.10-degree-equivalent equal-area map grid and one a 1.0-degree-equivalent equal-area map grid. Another form on a 0.25-degree-equivalent equal-area map grid is reconciled with the SURFACETYPE information on water cover fraction. The latter two forms are derived directly from the 0.10-degree form. The main alterations performed in the pre-processing are: (1) the products are mapped to a 0.10-degree-equivalent equal-area map grid and the standard deviation of topographic height added, and (2) the land-water masks for GTOPO30 and AVHRR 1-KM are reconciled in favor of GTOPO30, except for two systematic differences that indicate large inland lakes and permanent ice shelves.

3.3.2.6 SURFACETYPE

The ISCCP surface type information (see Section D.6 for details and links to data sources) is based primarily on the MODIS IGBP surface type classification (Loveland *et al.* 2009), changed to be consistent with the TOPO land-water mask and with the GLIMS permanent glacier cover and permanent ice shelf cover products. SURFACETYPE provides global coverage on a 0.25-degree-equivalent equal-area map grid. The main alterations performed in the pre-processing are: (1) the separate products are re-mapped to a 0.25-degree-equivalent equal-area map grid, (2) the water fraction reported is reconciled with the TOPO land-water mask for consistency, and (3) permanent glaciers from GLIMS product and ice shelves are added and the fractional coverage adjusted for consistency. The surface types that result include the following:

Table 3: Surface type code values and definitions. The IR emissivity specified for each surface type is also listed in the last column.

Surface Type Code	Description	IRemiss
0	Water	0.99
1	Evergreen Needleleaf Forest	0.985
2	Evergreen Broadleaf Forest	0.98
3	Deciduous Needleleaf Forest	0.985
4	Deciduous Broadleaf Forest	0.98
5	Mixed Forest	0.985
6	Closed Shrubland	0.98
7	Open Shrubland	0.975
8	Woody Savanna	0.98
9	Savanna	0.98
10	Grassland	0.98
11	Permanent Wetland	0.98
12	Cropland	0.98
13	Urban and Built-up	0.98
14	Cropland/Natural Vegetation Mosaic	0.98
15	Permanent Snow and Ice (Glaciers)	0.99
16	Barren or Sparsely Vegetated	0.965
17	Unclassified	0.98
18	Permanent Ice Shelf	0.99

Also shown in the above table are the values of the IR (approximately 10.5 ⌈m wavelength) surface emissivity assigned to each surface type.

3.3.3 Derived Data

The calibrated VIS and IR radiances are represented by scaled radiances and brightness temperatures to minimize the instrument spectral dependence when viewing different Earth scenes. The ISCCP Calibration Product, HBT, provides conversion tables from counts to scaled radiances or brightness temperature in Kelvins for each individual satellite image. Alternative conversion tables provide the actual energy measured by the instruments in watts/m^2/sr/⌈m. The relationship between these two sets of radiance units is determined by two instrument-specific constants, SOLCON for VIS and BANDWIDTH for IR. SOLCON is given by the integral over wavelength of the product of the instrument spectral response function (normalized to a maximum value of unity) and the spectrum of the sun at the top of the atmosphere (Neckels and Labs 1984, more modern compilations do not differ significanty at wavelengths 0.5-0.7 ⌈m). For IR the brightness temperature can be used to determine the energy emitted by a blackbody at the wavelength of peak instrument sensitivity, which can then be converted to energy units using a BANDWIDTH that represents the wavelength-averaged spectral response of each instrument.

To preserve precision over the whole range of specific humidity values, Q, they are converted to relative humidity, RH = Q/QS at each location and local hour using the contemporaneous temperature values in formulae for e_s from Murphy and Koop (2005).

$$e_{s,l} = e_0 \exp [(\langle - 1) e_6 + d_2 (T_0 - T) / TT_0 + d_3 \ln (T/T_0) + d_4 (T - T_0)] \quad (2)$$

where $e_{s,l}$ is the saturation vapor pressure over liquid water for $T \geq T_0$, T_0 = 273.15 K, e_0 = exp (e_1 + e_6) = 6.091888 mb, $\langle$ = tanh [e_5 (T − 218.8 K)], d_i = (e_i + $\langle$ e_{i+5}) and the values of e_i are:

e_i	
e1	6.564725
e2	−6763.22 K
e3	−4.21
e4	0.000367 K−1
e5	0.0415 K−1
e6	−0.1525967
e7	−1331.22 K
e8	−9.44523
e9	0.014025 K−1

and

$$e_{s,i} = B \exp [b_1 (T_0 - T) / T_0T + b_2 \ln (T/T_0) + b_3 (T - T_0)] \quad (3)$$

where $e_{s,i}$ is the saturation vapor pressure over ice for $T < T_0$, b_0 = 9.550426, b_1 = −5723.265 K, b_2 = 3.53068, b_3 = −0.00728332 K^{-1} and

$$B = (10^5) \exp [b_0 + b_1/T_0 + b_2 \ln (T_0) + b_3T_0] = 6.111536 \text{ mb} \quad (4)$$

The vapor pressures are converted to saturation specific humidity using:

$$QS = 0.622 e_s / (P - 0.378 e_s) \quad (5)$$

Thus RH is determined with respect to liquid phase at and above freezing temperature (273.15 K) and with respect to ice phase below freezing. If the NNHIRS value of RH = Q/QS < 0.5% at any temperature, it is reset to 0.5%. If RH > 110% at T ε 273.15 K, then it is re-set to 110%. If RH > 150% at T < 273.15 K, it is reset to 150%. The larger upper limit at lower temperatures is consistent with upper air humidity measurements indicating very large vapor supersaturations are required to initiate ice condensation (Jensen et al. 2001).

3.3.4 Forward Models

The ISCCP cloud and surface property retrievals employ two radiative transfer models (RTM), one for "window" IR (wavelength about 10.5 ⎧m) and one for VIS (wavelength about 0.65 ⎧m). The cloud physical parameters in these models are mutually consistent.

IR RTM: The IR RTM is based on the k-distribution representation of gaseous absorption in a vertically inhomogeneous atmosphere, including the effects of multiple scattering (Lacis and Oinas 1991). The k-distribution method re-arranges the spectral dependence of atmospheric absorption into k intervals that provide a monotonically ordered set of absorption coefficient magnitudes. The original model has been refined in a number of ways, including increasing the number of k intervals to more accurately represent overlapping absorption by different gases, using more modern absorption coefficient information (spectral line atlases) and improving treatment of scattering by clouds and aerosols (Oinas 2015). The particular version used for ISCCP calculates narrowband IR radiances (one particular k interval, equivalent to the spectral coverage of the NOAA-9 AVHRR channel at an approximate wavelength of 10.5 ⎧m to which all other radiometers are normalized), neglects scattering effects (which are treated separately for clouds), includes aerosol absorption, and employs a revised water vapor emission-absorption treatment based on quantum calculations that determine the absorption coefficient as a function of temperature and pressure (*cf.* Ma *et al.* 2013).

Water vapor absorption is produced by continuum and line absorption. The optical thickness of the continuum absorption in a gas layer of pressure thickness, dP (in mb), following Ma and Tipping (1991, 1992, 1994) and including the temperature dependence of self-broadening and foreign-broadening, is

$$/_S = a\ (1.607\ AS)\ dP\ /\ (\log AS_b - \log AS_t) \qquad (6)$$

$$/_S = a\ (1.607\ AS)\ dP\ /\ (\log AF_b - \log AF_t) \qquad (7)$$

where a is Loschmidt's number times molar volume divided by the molecular weight of water and by the acceleration of gravity = 3.41539×10^{19} (cgs units). The factor 1.607 is the ratio of atmospheric and water molecular weights. The subscripts indicate the top and bottom of the gas layer. The quantities AS_B, AS_T, AF_B, and AF_T are functions of layer top and bottom temperatures from the model of Ma and Tipping and

$$AS = AS_T\ P_T - AS_B\ P_B - (AS_B - AS_T)\ dP\ /\ (\log AS_B - \log AS_T) \qquad (8)$$

$$AF = AF_T\ P_T - AF_B\ P_B - (AF_B - AF_T)\ dP\ /\ (\log AF_B - \log AF_T) \qquad (9)$$

If the variation of AS and AF over a layer is too small (difference < 0.001), AS / (log AS_B – log AS_T) is replaced by AS_T ($P_T^2 - P_B^2$) / 2 and AF / (log AF_B – AF_T) is replaced by AF_T ($P_T^2 - P_B^2$) /2.

The optical thickness of the line absorption (much weaker than the continuum absorption at 10.5 ⎧m) is based on a fit with a Malkmus model for very narrow spectral intervals,

weighted by the response of the NOAA-9 AVHRR 10.5 ⌈m channel, and using the line strengths given by Rothman *et al.* (1983, but see updated results in Rothman *et al.* 2003):

$$/_L = U\,(0.000067 + 0.0065\,U) / (1 + 115\,U + 1.3\,U^{1.6}) \qquad (10)$$

Other notable features of the model are: (1) instead of treating each atmospheric layer as isothermal or with a linear temperature gradient, this model assumes a within-layer temperature profile such that the Planck function is linear, and (2) an explicit treatment of satellite view angle dependence is achieved by a three-point numerical quadrature.

The (gas only) model is used directly to associate with the NNHIRS temperature-humidity profiles corresponding brightness temperature profiles at three satellite view zenith angles, but accounting for stratospheric aerosol absorption in the 50-100 mb layer and tropospheric aerosol absorption in the first two atmospheric layers at the surface (model code is available in the TOVIRT subroutine of the NNHIRSPAC program). The model determines the top-of-atmosphere radiances from the edge of each atmospheric layer assuming a blackbody emitter at that edge and using the edge temperatures and the layer-integrated water vapor (precipitable water amount above the edge), determined by interpolating the edge relative humidities (RH), converted to specific humidities (Q), into 2 mb intervals using lnQ/lnP, and summing over the layer. The atmosphere has sixteen standard pressure levels: 900, 800, 740, 680, 620, 560, 500, 440, 380, 320, 260, 200, 150, 100, 50, and 10 mb. There are three additional pressure levels: the surface, the tropopause and the level of the maximum temperature point, which may not always be at the surface. Surface pressure is determined by,

$$PS\,(Z) = 1013.25\,((TA - 6.5 \times Z) / TA)^{5.25}T_0) \qquad (11)$$

where PS is in millibars, Z height in kilometers and TA in Kelvins is the zonal, monthly mean near-surface air temperature over land (maximum PS = 1019 mb). The atmospheric profiles are terminated at the PS level. The calculated downward radiances at the surface are also saved for use in the retrieval of surface skin temperatures with non-unit emissivity.

Cloud visible optical thicknesses (see below) are converted to IR optical thicknesses by multiplying them by 0.391 for liquid water clouds and by 0.376 for ice clouds. The latter value is an adjustment of an earlier empirical estimate (Minnis *et al.* 1993a,b) that is made to reduce conflicts of the liquid and ice cloud retrieval results: if larger values are used, some values of TC for liquid clouds are colder than for ice clouds or vice versa for the same radiance values. Additional offline calculations (*cf.* Oinas 2015) are used to pre-calculate two look up tables (LUT), one for liquid water clouds and one for ice clouds, that provide a scattering correction to cloud top temperatures (IR emission) as a function of cloud optical thickness, cloud and clear sky temperatures, and satellite view zenith angle.

VIS RTM: The VIS RTM is used to pre-calculate eleven LUTs, all as functions of solar illumination (Neckel and Labs 1984) and satellite view geometry (cosine of solar and satellite zenith angles, ⌈0, ⌈, respectively, and the relative azimuth angle, ⟩0) in addition to other parameters. The model is the scalar version of a full vector code used, for example, in

the analysis of ground-based and aircraft polarized radiance measurements at multiple solar wavelengths (Cairns *et al.* 1997, 1999, Alexandrov *et al.* 2012). This code is a modified doubling/adding code that is essentially the same as presented by Hansen and Travis (1974) with modifications based on the work of de Haan *et al.* (1987). The doubling/adding approach allows for building up any atmospheric vertical structure out of simpler (homogeneous) layers and determining the effects of multiple scattering (and absorption) on reflected and transmitted radiation. In particular, the treatment of particle scattering depends on the total optical thickness of a layer, the single-scattering albedo and phase function of the particles, which depends on the particle size distribution and shape. The optical constants of liquid water are taken from Hale and Querry (1973) and Downing and Williams (1975) and of ice from Warren 1984. With these properties of clouds and aerosols (as well as gas molecules) specified for each thin layer, the complete scattering effects of the whole atmosphere or any portion of it can be calculated (Martin *et al.* 2014). The specific optical constants used are equivalent to spectral coverage of the NOAA-9 AVHRR channel at an approximate wavelength of 0.65 ⌈m to which all other radiometers are normalized.

Two of the LUTs are used to correct VIS radiances to remove the effects of stratospheric ozone absorption (PTRANS, coefficients from Inn and Tanaka 1953) as a function of its total column abundance (and the viewing/illumination geometry) and of stratospheric aerosol scattering/absorption (INTEN3) as a function of its optical depth (and the viewing/illumination geometry): ozone is assumed to be in the 50-100 mb layer but above the stratospheric aerosol layer. Ozone absorption coefficients are pre-calculated for the specific VIS-channel spectral responses of each satellite. Stratospheric aerosols are assumed to be composed of sulfuric acid with an effective radius of 0.5 ⌈m.

Application of these two LUTs produces **corrected** VIS radiances that are then used for the subsequent cloud and surface property retrievals. A third and fourth LUT (INTEN1 for "coarse" aerosols and INTEN2 for "fine" aerosols) are used for clear atmospheric conditions and return the surface VIS reflectance (RS) as function of **corrected** VIS radiance, the viewing/illumination geometry, surface pressure (accounting for Rayleigh scattering) and tropospheric aerosol optical depth and fine fraction, where the aerosol is assumed to be in the two lowest atmospheric layers at the surface. Tropospheric aerosol scattering and absorption properties are represented by specifying a fine fraction that affects both the effective size and the single scattering albedo: fine fraction determines a mixture of sulfate (fine) and mineral dust (coarse) aerosol with effective radii of 0.5 and 1.0 ⌈m, respectively. The results from the two LUTs are averaged using the fine fraction as the weight. A special "zero aerosol" value of surface reflectance (RS0) is also returned from a fifth LUT (INTEN) for use in the cloud optical thickness retrievals over land and ice surfaces.

The sixth and seventh LUTs return a cloud optical thickness (TAU) over water surfaces for either a liquid water (TC ε 253.1 K, OTAUHIW) or ice (TC < 253.1 K, OTAUHII) cloud as a function of **corrected** VIS radiance, the viewing/illumination geometry, cloud top pressure, and tropospheric aerosol optical depth and fine fraction. The cloud phase is decided by cloud top temperature based on Riedi *et al.* (2010). In the L2 products retrievals for both phases are reported at all temperatures; the choice of one phase is made in the L3 products

(see Section 3.4.2). This LUT employs a bi-directional visible reflectance model of the water surface, assuming a surface wind speed of 2 m/s and bulk scattering by suspended particles of 1% (Chowdhury *et al.* 2012). This model also includes a direct treatment of sunglint. The eighth and ninth LUTs return a cloud optical thickness of either a liquid water (TAUHIW) or ice (TAUHII) cloud as a function of **corrected** VIS radiance, the viewing/illumination geometry, cloud top pressure, and surface visible reflectance. This LUT is used for clouds over land and ice surfaces where the surface reflectance used is the special "zero aerosol" value (RS0) that accounts for aerosol scattering below the cloud. Over snow and ice surfaces, it is possible in some viewing/illumination geometries for the cloudy scene VIS radiance to be smaller than the clear scene VIS radiance (cloud detected only by IR tests). In this special case, two other LUTs (TAULOW for liquid water clouds, TAULOI for ice clouds) are used to retrieve TAU.

Two cloud-layer microphysical models are used for the IR and VIS radiance modeling, one composed of spherical liquid water droplets and one composed of ice crystals. The liquid droplet cloud has a distribution of spherical particles with a refractive index of liquid water and an effective size variance of 0.10. Two different effective radii are used: 13 ⌈m for clouds over land (including snow and ice) and 15 ⌈m for clouds over ocean. These values of effective radius lead to conversion factors from linearly-averaged TAU to Water Path of 8.18 and 9.44, respectively. The ratio of IR TAU to VIS TAU is 0.391. The ice particle cloud uses an empirical scattering phase function (called the Inhomogeneous Hexagonal Monocrystal model), developed from polarization measurements of cloud-reflected sunlight by the POLDER satellite instrument, to account for the variety of ice crystal sizes and shapes that occur in clouds (Descloitres *et al.* 1998, Baran and Labonnote 2006, 2007, Zhang *et al.* 2009, *cf.* Baran and Francis 2004). Particle size and shape are not explicit in this case, but the effective radius used to determine ice water path is assumed to be 20 μm for VIS TAU < 3.55 and 34 μm for VIS TAU ε 3.55. These values of effective radius lead to conversion factors from linearly-averaged TAU to Water Path of 7.00 and 11.9. The IR/VIS TAU ratio is 0.376 to reduce the frequency of ambiguous retrievals (see phase decision logic in Section 3.4.2).

The atmospheric vertical structures used to represent the range of TAU dependence on cloud top pressure in the sixth and seventh LUTs are as follows (Figure 5).

For low liquid clouds over ocean, the structure is:

Layer 1: Surface (PS = 1013 mb) to 950 mb – gas and aerosol
Layer 2: P = 950 mb to 850 mb – liquid cloud layer and gas
Layer 3: P = 850 mb to 0 mb – gas

For high liquid clouds over ocean, the structure is:

Layer 1: Surface (PS = 1013 mb) to 950 mb – gas and aerosol
Layer 2: P = 950 mb to 500 mb – gas

Layer 3: P = 500 mb to 440 mb – liquid cloud layer and gas
Layer 4: P = 440 mb to 0 mb – gas

For low ice clouds over ocean, the structure is:

Layer 1: Surface (PS = 1013 mb) to 950 mb – gas and aerosol
Layer 2: P = 950 mb to 850 mb – ice cloud layer and gas
Layer 3: P = 850 mb to 0 mb – gas

For high ice clouds over ocean, the structure is:

Layer 1: Surface (PS = 1013 mb) to 950 mb – gas and aerosol
Layer 2: P = 950mb to 350 mb – gas
Layer 3: P = 350 mb to 150 mb – ice cloud layer and gas
Layer 4: P = 150 mb to 0 mb – gas

For low liquid clouds over land, the structure is:

Layer 1: Surface (PS = 950 mb) to 850 mb – gas (aerosol for clear sky)
Layer 2: P = 850 mb to 750 mb – liquid cloud layer and gas
Layer 3: P = 750 mb to 0 mb – gas

For high liquid clouds over land, the structure is:

Layer 1: Surface (PS = 950 mb) to 800 mb – gas (aerosol for clear sky)
Layer 2: P = 800mb to 500 mb – gas
Layer 3: P = 500 mb to 440 mb – liquid cloud layer and gas
Layer 4: P = 440 mb to 0 mb – gas

For low ice clouds over land, the structure is:

Layer 1: Surface (PS = 950 mb) to 850 mb – gas (aerosol for clear sky)
Layer 2: P = 850 mb to 750 mb – ice cloud layer and gas
Layer 3: P = 750 mb to 0 mb – gas

For high ice clouds over land, the structure is:

Layer 1: Surface (PS = 950 mb) to 800 mb – gas (aerosol for clear sky)
Layer 2: P = 800 mb to 350 mb – gas
Layer 3: P = 350 mb to 150 mb – ice cloud layer and gas
Layer 4: P = 150 mb to 0 mb – gas

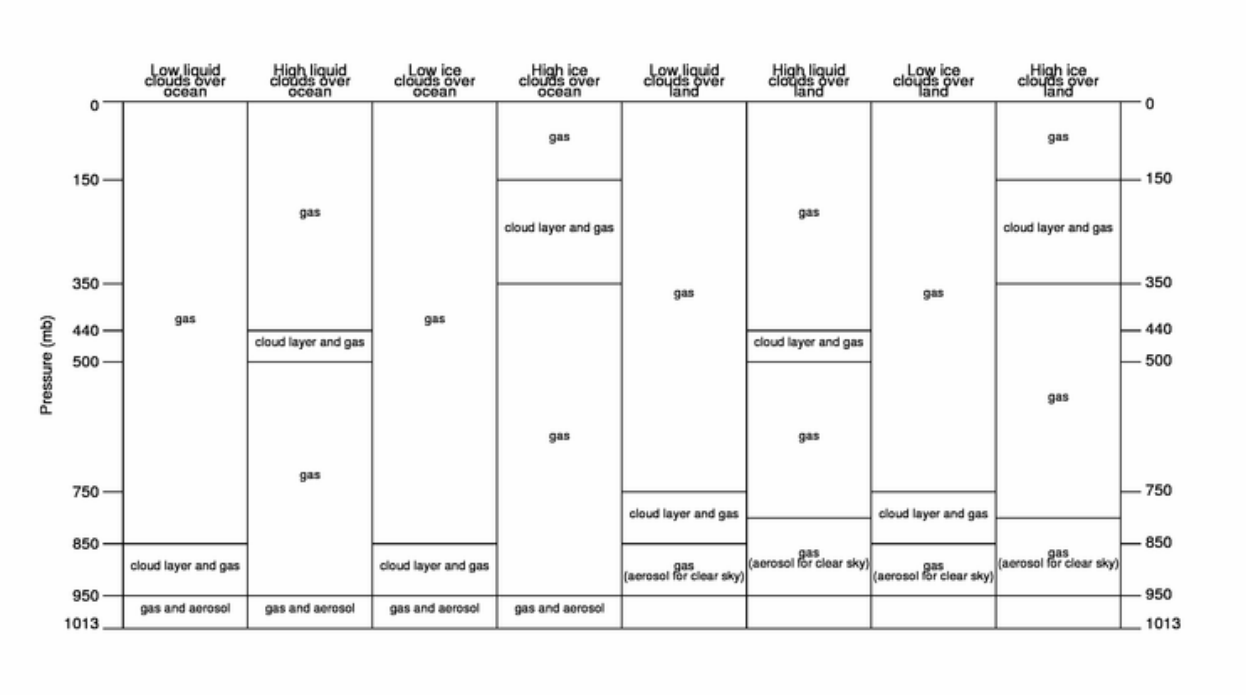

Figure 7: Schematic of atmospheric layers in VIS RTM

Note that cloud top pressure can be < 100 mb or > 950 mb by extrapolating between the two extremes in these LUTs. Also note that stratospheric aerosol and ozone effects are removed before using these LUTs. The layer thicknesses used here are based on Wang and Rossow (1995), which compare well with CloudSat-Calipso results (*cf*. Mace *et al.* 2009).

3.4 Theoretical Description

The basic ISCCP analysis tasks are to separate the satellite image pixels into two categories, cloudy and clear, and to retrieve cloud and surface properties. At pixel-level scale (about 5 km), cloud cover fraction is taken to be 0 or 1; cloud amounts are estimated only in the gridded products from multi-pixel results. Thus the analysis has four logical steps: (1) cloud detection, (2) surface property retrieval, (3) cloud property retrieval assuming all clouds are optically thick, and (4) cloud retrieval adjustment for optically thinner clouds (see Figure 4). The cloud detection step analyzes the space-time variability of the IR and VIS radiances, separately, at several scales (see Sections 3.4.1.1.1), aided by Ancillary data products that identify different surface types, to estimate clear sky radiances for all locations and times (each pixel). The resulting clear sky composite values of IR and VIS radiance are then compared to the actually observed values: differences of the correct sign and larger than the estimated uncertainty in the clear sky values (threshold values) indicate the presence of clouds. Clouds are assumed to have smaller IR and larger VIS radiances (except for wintertime conditions over snow and ice where clouds can have larger IR radiances). Clouds are taken to be present if **either** radiance differs from its clear sky value by more than the scene-type-dependent threshold value. Daytime cloud detection is based on the combined results of the separate IR and VIS radiance threshold tests;

nighttime cloud detection is based solely on IR radiance threshold tests, but the results of the same IR radiance threshold tests are also reported in daytime.

For physical consistency, the surface properties used to retrieve cloud properties are obtained from estimates of the clear sky radiances for all locations and times in the clear sky composites (although surface properties are also retrieved for clear pixels). The two surface properties that most strongly affect the IR and VIS radiances are skin temperature (TS) and VIS reflectance (RS), respectively (see Section 3.4.2). Other properties of the surface are of secondary importance in the magnitude of their effects on these two radiances. These additional quantities are specified explicitly to form the radiative transfer model of surfaces used for the retrievals (see Section 3.3.4).

The two cloud properties that most strongly affect the IR and VIS radiances are cloud top temperature (TC) and optical thickness (TAU) (see Section 3.4.3). For optically thicker clouds, these two properties affect the two radiances (nearly) independently, but for optically thinner clouds, the two properties affect both radiances. For optically thicker clouds, the two radiances are (nearly) independent of the properties of the underlying surface, but for optically thinner clouds, the two radiances depend on both the cloud and surface properties. Other properties of clouds are of secondary importance in the magnitude of their effects on these two radiances. These additional quantities are specified explicitly to form the radiative transfer model of clouds surfaces used for the retrievals (see Section 3.3.4). The values of these parameters are chosen to minimize bias error by estimating the statistical center of the distributions of their values. Other properties of the atmosphere and surface that affect the detection of clouds and these two radiances are specified from Ancillary data products to better separate the cloud and surface effects.

The initial cloud top temperature retrieval at all times of day assumes that all clouds are optically thick (blackbody). During daytime, optical thickness is retrieved and the initial cloud top temperature is adjusted to account for IR radiation transmitted from below through optically thinner clouds and for scattering by all clouds. Cloud top pressure (PC) is determined by the level in the atmosphere from the NNHIRS product with the same physical temperature as cloud top temperature. Cloud water path (WP) is determined from TAU using coefficients based on the microphysical model. To preserve the original satellite sampling, all pixels are processed. Because of limited radiance precision (generally equivalent to 8 bits of information), retrieval sensitivity can be degraded at both extremes of the cloud and surface property distributions so the retrieval code is modified in these circumstances to preserve distribution shapes.

3.4.1 Physical and Mathematical Description

The ISCCP analysis is illustrated in Figure 1 and discussed in the sub-sections below.

3.4.1.1 Cloud Detections

The first step in the ISCCP analysis is cloud detection – deciding whether an individual image pixel contains cloud or not. This decision cannot be precisely binary (yes, no) because the cloud effect on the measured radiances depends on its optical thickness, which can have a wide range of values including arbitrarily close to zero, and because the cloud

can cover all or a fraction of the typical satellite image pixel area (about 5km across typically), including arbitrarily close to zero. Moreover, at the smallest spatial scales below about 1-3 km (depending on wavelength), the radiation field is three-dimensional so that the cloud radiative effect is not limited strictly to the area actually occupied by cloud mass (Rossow 1989). Hence, the detection decision reduces to a division of the pixels into a group called "clear" that contains less than a certain "amount" of cloud – determined by the combined optical thickness and fractional area coverage -- and a group called "cloudy" that contains more than this minimum "amount" of cloud. Note that this situation makes the detectability of clouds, consequently, dependent on spatial scale and pixel area.

The only information available in a single pixel is spectral radiances, generally only a few wavelengths from the higher resolution imaging radiometers. Although many wavelengths have been investigated for cloud detection purposes, sensitivity to the presence of cloud in the pixel is maximized at wavelengths where the typical radiances from Earth are largest and the gaseous atmosphere has the smallest effects, namely VIS (wavelengths 0.5-0.7 ⌈m) and "window" IR (wavelengths 10-11 ⌈m). Although the atmosphere is most transparent at these wavelengths, the radiances coming from some surface types can be large enough to reduce cloud detection sensitivity: deserts and snow-ice can be more reflective at VIS wavelengths than low optical thickness clouds and thin, low-level clouds embedded in humid marine boundary layers can emit almost the same amount of IR as clear locations (Rossow and Garder 1993b). Moreover, in the polar regions the usual radiance contrast between clear and cloudy scenes (cloudy VIS > clear VIS and cloudy IR < clear IR) can be reversed. Hence, the usual situation is that the presence of clouds in a satellite image pixel does not have a unique spectral radiance signature and the sensitivity to the presence of cloud is situation-dependent, *i.e.*, dependent on the surface type.

The ISCCP cloud detection relies on differences of the characteristic spatial and temporal variability of the IR and VIS radiances related to the presence of clouds (Rossow and Garder 1993a), where research results show that temporal radiance variability is generally a better indicator of cloudiness. As with spectral radiance signals, the contrast between cloudy and clear situations is both scale and surface-type-dependent, but generally the appearance of clouds increases the temporal and spatial variability of the radiances. The surface-type-dependence necessitates the use of Ancillary data products to identify these surface types by location.

The main principles of the ISCCP cloud detection are to employ tests of the radiance variability at various time and space scales to estimate the radiance values corresponding to clear scenes for all pixels, because these values are generally less variable (hence more accurately estimated from a sample), and to label pixels with radiances that differ from these clear sky values by more than their estimated uncertainty (called the threshold amount). This definition of the detection threshold is "cloud conservative" in that a pixel is called cloudy only when the cloud effect on the radiances is larger than the uncertainty in the clear radiance values. The implication is that clouds will not be detected when their radiative effects are too small – very low optical thicknesses and/or small temperature contrasts with the surface – or when the surface variability is large enough to be confused with cloud effects (Rossow and Garder 1993a,b. Since the range of optical thicknesses of

clouds and aerosols can overlap, increasing the detection algorithm sensitivity to the presence of clouds will include optically thicker aerosol events as well. This cloud conservative choice of detection threshold magnitudes also makes the error in cloud area, obtained by counting finite-sized cloudy pixels, more nearly random by underestimating smaller areas (missed detections) while overestimating partial areal coverage (Wielicki 1992, Rossow *et al.* 1993).

There are three additional algorithm design principles. First, the various tests of the radiance variability in time and space are performed independently and all results passed to the end where the final decision is made. This allows for making a choice among the different results both as a cross-check and to account for different situations by giving different weights to different tests. Second, evaluations of the algorithm performance subsequent to the first design revealed a second type of situation dependence where the radiance variability tests could be misleading: situations where the cloud amount is either very close to zero or one for a whole month tend to produce over- or under-estimates of the actual cloud cover. To account for this, the clear sky radiance estimation is done twice with different criteria; the cloud detection from the first cycle is used to adjust the clear sky radiances in situations with very small or very large average cloud cover. Third, to allow for an unbiased diurnal sample, the IR and VIS wavelength tests are performed independently. The IR-only results are reported at all times of day to produce uniform results over the whole day. During daytime the combined IR and VIS results are also reported. Because of the different detection capabilities of the IR and VIS, the daytime result is a combination where a pixel is labeled as cloudy if **either** channel detects cloud. To provide an estimate of uncertainty at pixel-level, marginal cloud detections are indicated (see Figure 16 and discussion in Section 3.4.1.1.4).

These principles can be summarized in terms of five premises: (1) clear pixels exhibit less spatial and/or temporal radiance variability than cloudy pixels, (2) clear pixels exhibit larger/smaller IR/VIS radiances than cloudy pixels, (3) the first two premises vary with surface type and/or climate regime, (4) no single test is reliable under all conditions for all cloud types and (5) cloud presence is only reliably indicated by radiance differences from the clear sky larger than their uncertainty (threshold values).

The current H-Version of the ISCCP cloud detection algorithm is a minor modification of the D-Version, which was a modification of the C-Version. Hence, all publications regarding the first two versions are relevant to the current version as explained next. The first (C) version is described in Rossow and Garder (1993a) and evaluated in Rossow and Garder (1993b) and Rossow *et al.* (1993). The C-Version algorithm estimated clear sky IR radiances for each image pixel based on a spatial contrast test, a time contrast test, the average clear radiance from these tests and the maximum radiance, the latter two collected over two time scales (different for land and water). The clear sky VIS radiances are based on the minimum values over two time scales. Cloud detection is then performed by comparing each pixel IR and VIS radiance to the estimated clear sky values; if either radiance differs from its corresponding clear sky value by more than the (scene dependent) threshold amount (IR radiance < clear IR radiance, VIS radiance > clear VIS radiance), the pixel is labeled as cloudy. Subsequent evaluations, summarized in Rossow and Schiffer

(1999), led to minor revisions of the C-Version (mostly changes of test parameters) and to the addition of two steps. The first added step revisits the clear sky radiance estimates to make adjustments for situations where the C-Version cloud fractions are either nearly zero or one. The second added step repeats the threshold test with slightly modified criteria – generally reduced thresholds for certain situations that were found to be too conservative in the C-Version. The H-Version algorithm is the same as the D-Version with some modifications of test criteria and threshold magnitudes and with one logical change in the polar cloud treatment (see Section 3.4.1.1.4). Figure 4 and Page 26 of the Operations Guide show the overall structure of the ISCCP analysis: the cloud detection part of the analysis involves the programs b4prod, clrsky, bxprod and cyprod. The detailed flow charts for these four programs are discussed next and shown on pages 31-37 of the Operations Guide (Appendix E).

The test parameters in the clear sky estimation procedure are surface-type-dependent, where the surface types are determined from the Ancillary Products. TOPO provides a land/water mask and topographic height information (mean, standard deviation) at 10 km and 100 km scales. SURFACETYPE provides further classification of the surface by water, permanent ice shelf, land vegetation type and permanent glacier at 25 km scale. SNOWICE provides daily fractional cover of land snow cover and sea ice cover at 25 km scale.

3.4.1.1.1 **B4Prod**

Space Contrast Test: In B4PROD (Figure 9), the radiances are first approximately corrected to reduce view/illumination geometry dependence. The IR brightness temperatures as a function of cosine satellite view zenith angle, T (⌠), are corrected approximately to nadir view as follows:

$$T(1) = T(⌠) + C_0(⌠) + C_1(⌠)[T(⌠) - 250] \quad (12)$$

$$C_0(⌠) = □(1.93 + 2.520 ⌠)(1/⌠□⌠) / 4.8 \quad (13)$$

$$C_1(⌠) = □(0.267 + 0.053 ⌠)(1/⌠□⌠) / 4.8 \quad (14)$$

This correction is based on a simple best fit to radiative transfer calculations over a global distribution of atmospheric temperature-humidity profiles. The formula fits these results to within about 2 K. However, this correction is only needed for the time test for polar orbiting data, which have time-varying view zenith angles over a month for a given location; but since ⌠ ε 0.45 for polar orbiter data, the fit error is actually δ 1 K. Although the view zenith angles for geostationary images vary with location, they do not vary with time over a month, so this correction has no effect. For clarity below, the IR brightness temperatures, T (⌠), are called T and the angle-corrected values are called TN.

The VIS scaled radiances as a function of cosine solar zenith angle, V (⌠$_0$), are also corrected approximately to nadir-sun conditions as follows:

$$R(1) = V(⌠, ⌠_0) / ⌠_0 \quad (15)$$

The value of ⌠0 is determined for each image pixel at its observation time and location. This formula neglects the relatively weak anisotropy of land surface reflectances and the ⌠ and ⌠0 dependence of Rayleigh scattering and ozone absorption that partially offset each other. Aerosol effects also reduce the angle dependence of the land surface reflectances somewhat. These values are not true reflectances because we neglect the variations of solar illumination over the year; however, this correction is only used for short time scale (one month) comparisons. Tests of this approach show errors are generally δ 0.02 absolute. The anisotropy of VIS reflectance for open water is much stronger, but the clear sky VIS radiances for open water are constrained by a model of water reflectivity. For clarity below, the VIS scaled radiances, V (⌠, ⌠0), are called V and the angle-corrected values are called reflectances, R.

The space (radiance) contrast test (Figure 10) uses three surface types: for individual pixels these are land, water or coast (a pixel that contains both land and water mixture based on the 10-km land-water mask from TOPO) and for multi-pixel domains these are land, water and mixed. For geostationary satellite images, sampled to about 10 km intervals, the test labels as CLOUDY all pixels within small domains (about 90 km in size, 9x9 pixels if the pixel is over land, and about 450 km in size, 45x45 pixels if the pixel is over water) that have IR brightness temperatures colder than the locally warmest pixel (by 6.0 K over land, 3.5 K over water); all other pixels, including the warmest are labeled UNDECIDED. In the C-Version and D-Version of the algorithm, this test was done without regard to whether the domain had a mixture of land and water pixels, but in the H-Version, if the domain contains both land and water, the same test is performed at a smaller scale (about 30 km in size, 3x3 pixels if the pixel is over land, and about 150 km in size, 15x15 pixels if the pixel is over water). If the smaller region is all one surface type, then the test values are 4.0 K over land and 3.0 K over water; if the smaller region is a mixture of land-water, then the test values are 6.0 K if the pixel is over land and 3.5 K if the pixel is over water. In the H-Version the space tests are applied to full resolution (4 km) polar orbiter data (the low-resolution domains are 18x18 pixels over land and 30x30 pixels over water, the high-resolution domains are 6x6 pixels over land and 10x10 pixels over water).

Re-Mapping: All images in a month for each geostationary satellite are re-mapped (Figure 10) to a common 10-km grid (a general perspective projection that is similar to the original image). The polar orbiter data are sampled to about 10 km intervals and mapped to a simple latitude-longitude grid in midlatitudes and to a polar projection at high-latitudes (> 50° in each hemisphere). This re-mapping approximately aligns image pixels from all images to facilitate comparisons of radiances from individual pixels and small regions from image to image over time.

Time Contrast Test: The value of TN at each location and time are compared to the values on the previous and next days at the same time of day. The time (radiance) contrast test (Figure 11) labels as CLOUDY-PREVIOUS all pixels with TN values that are colder (3.5 K over water, 8.0 K over land or coast) on the current day (same time UTC) than on the previous day and labels as CLEAR-PREVIOUS all pixels with TN values that are similar (within 1.0 K over water, 2.0 K over land or coast) on the current day to the previous day values. Similarly, the test labels as CLOUDY-NEXT all pixels with TN values that are colder

than the next day (same time UTC) value and labels as CLEAR-NEXT all pixels with TN values that are similar to the next day value.

Preliminary Cloud Classes: The four flags from the time test are combined with the CLOUDY flag from the space test to label each pixel as CLEAR, CLOUD, MIXED or UNDECIDED (Figure 11). The label is CLEAR if none of the CLOUDY flags are set and the time test indicated either CLEAR-PREVIOUS or CLEAR-NEXT. The label is CLOUD if any of the CLOUDY flags are set and none of the CLEAR flags are set. The label is MIXED if any of the CLOUDY flags are set and one or more CLEAR flags are set (disagreement). The label is UNDECIDED if none of the flags were set. This logic is illustrated in Figure 11.

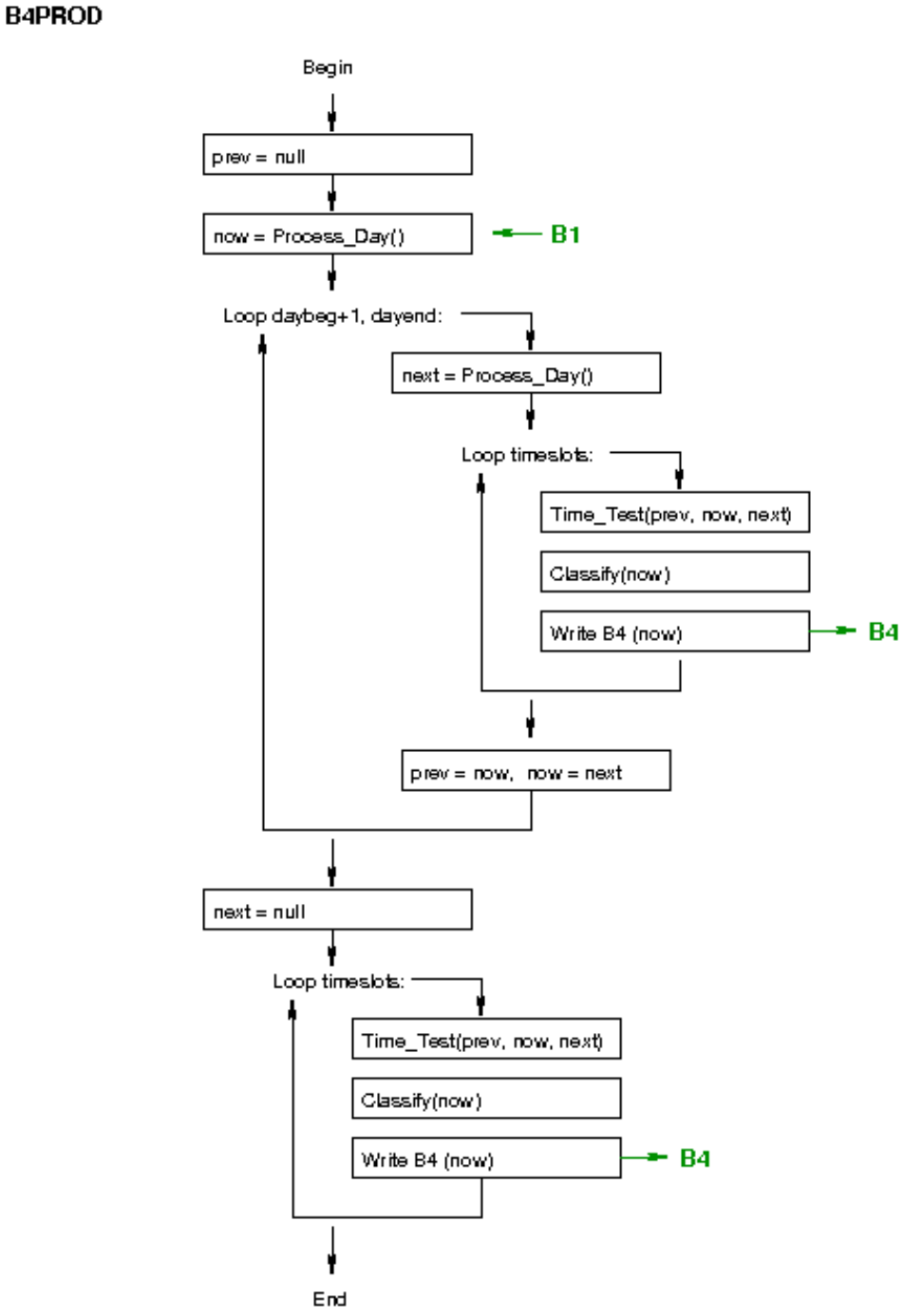

Figure 8: B4PROD Main Program

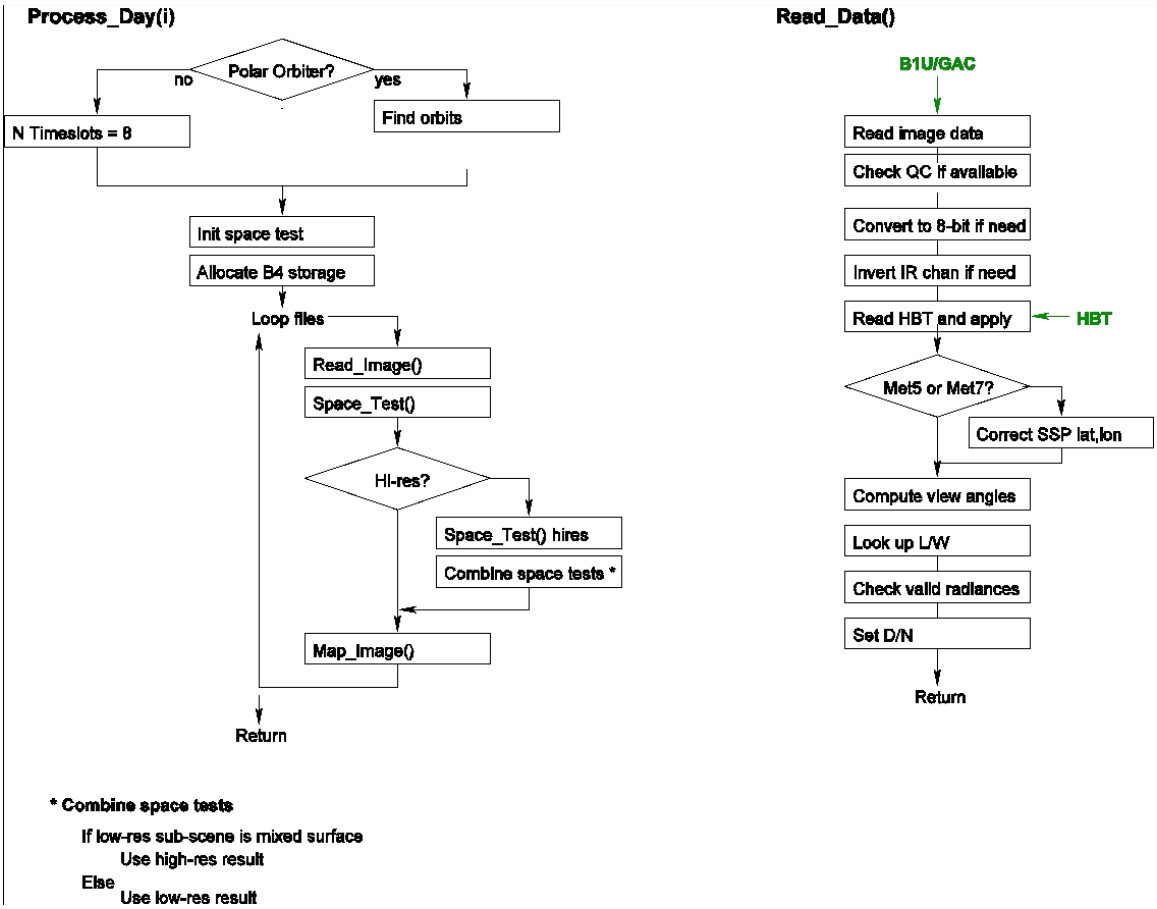

Figure 9: B4PROD subroutines *process_dat* and *read_data*

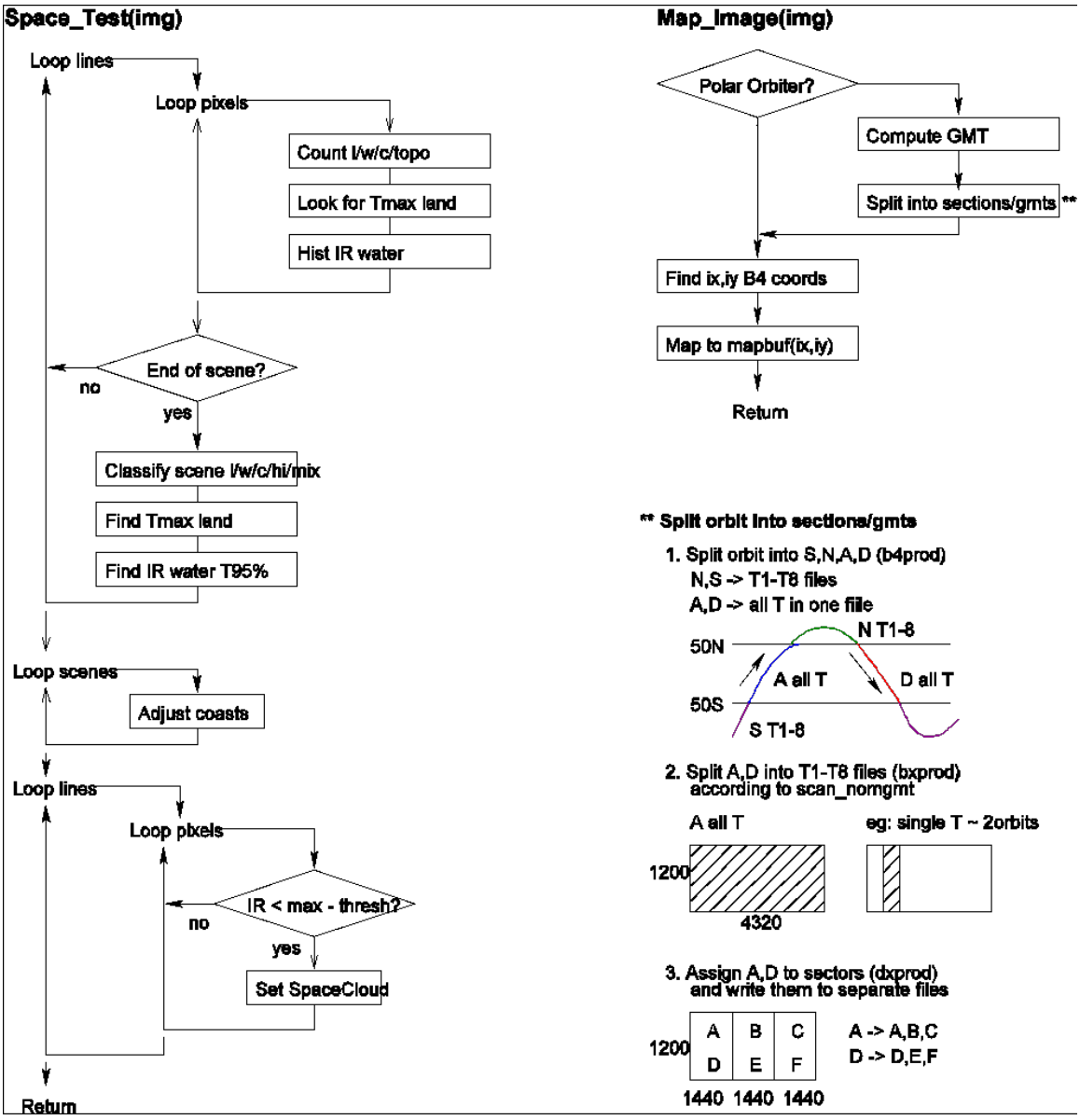

Figure 10: B4PROD subroutines *time_test* and *classify*

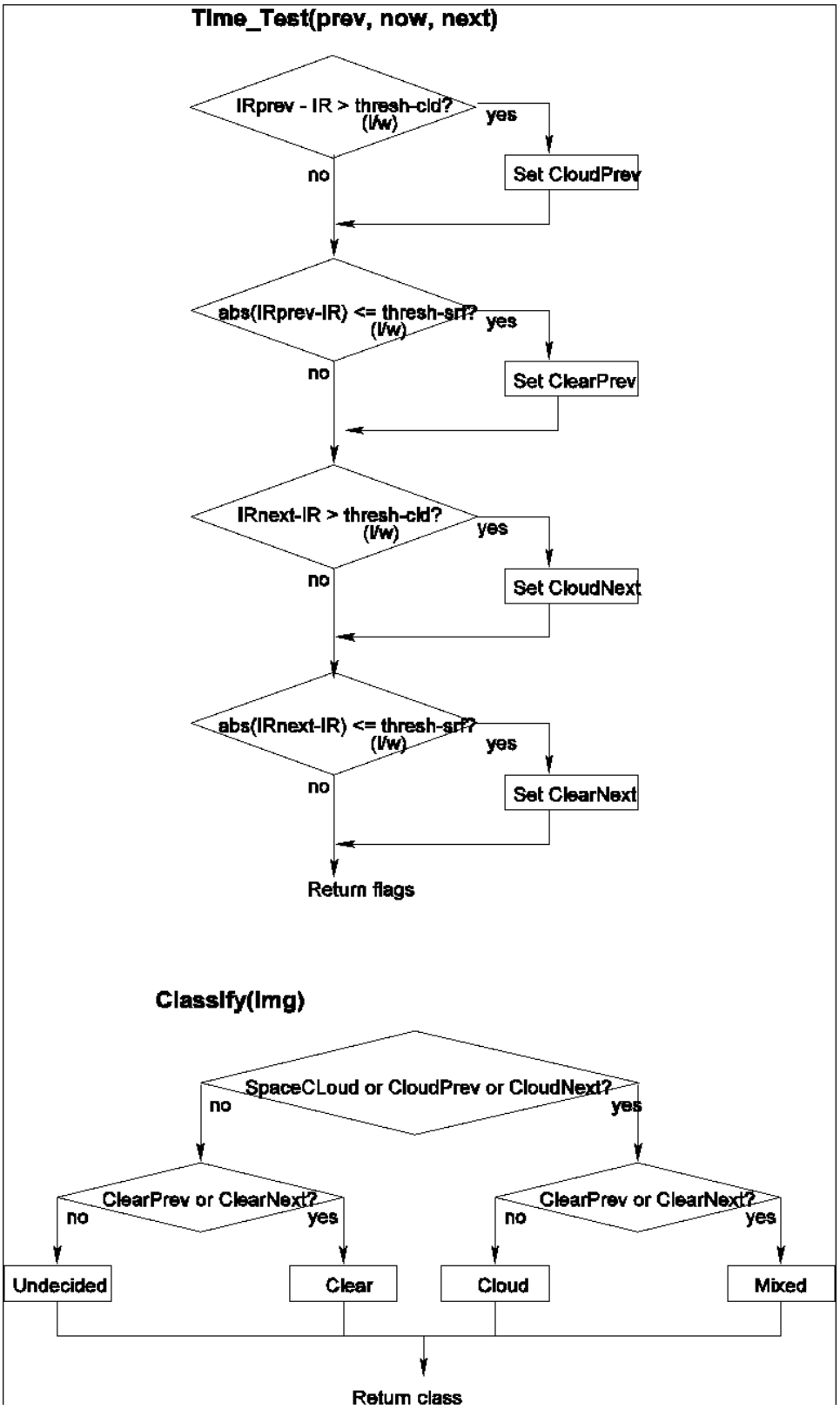

Figure 11: B4PROD subroutines *time_test* and *classify*

3.4.1.1.2 IR Clear Sky Composite

IR Clear Sky Composite: The CLRSKY program collects IR statistics from re-mapped images to produce composite clear sky TN maps for 5-day intervals at each time of day UTC over the whole month for each satellite containing: (1) the number of CLEAR pixels, NCLEAR-ST (ST = short-term, defined below), in a small (9x9 pixels) domain centered on each pixel, (2) the average IR brightness temperature of CLEAR pixels in this domain, TAVG-ST, and (3) the five largest TN values in this domain over 5 days (called TMAX1 through TMAX5 in descending order). A dynamic search of the five largest values checks for any differences > 12 K; if such a difference is found the lower value (below the large difference) is used for TMAX-ST. This procedure is necessary to protect against spuriously large values (bad data). The values of NCLEAR-LT (LT = long-term, defined below), TAVG-LT and TMAX-LT are calculated from the ST values.

In this step pixels are classified into four surface type groups based on TOPO and SNOWICE for selection of test parameters and thresholds: (1) open water (not shore, not sea ice), (2) near-coastal (shore) water (δ 115 km to nearest land), sea ice or permanent ice shelf margin (δ 115 km to nearest ice), sea ice or permanent ice shelf (cover fraction > 0), (3) open land (not high or rough topography, including snow-covered land, and (4) high or rough topography (height > 1750 m or height standard deviation in 1-degree equal-area grid > 250 m). For all IR Surface Types, except Type 1 (open water), ST = 5 days and LT = 15 days; for Surface Type 1, ST = 15 days and LT = 30 days. If the total number of observations in a 5-day interval is δ 20, no clear sky analysis is performed. Because of slow seasonal variation, TMAX-ST is adjusted based on the median values of the zonal distributions of differences of 15-day TMAX-ST values: a linear trend correction is applied to each 5-day interval (15-day for Surface Type 1). This correction is performed only if the number of observations for each surface type is ε 300 and the number of TMAX differences available is ε 65% of the total land/water pixels in the zone.

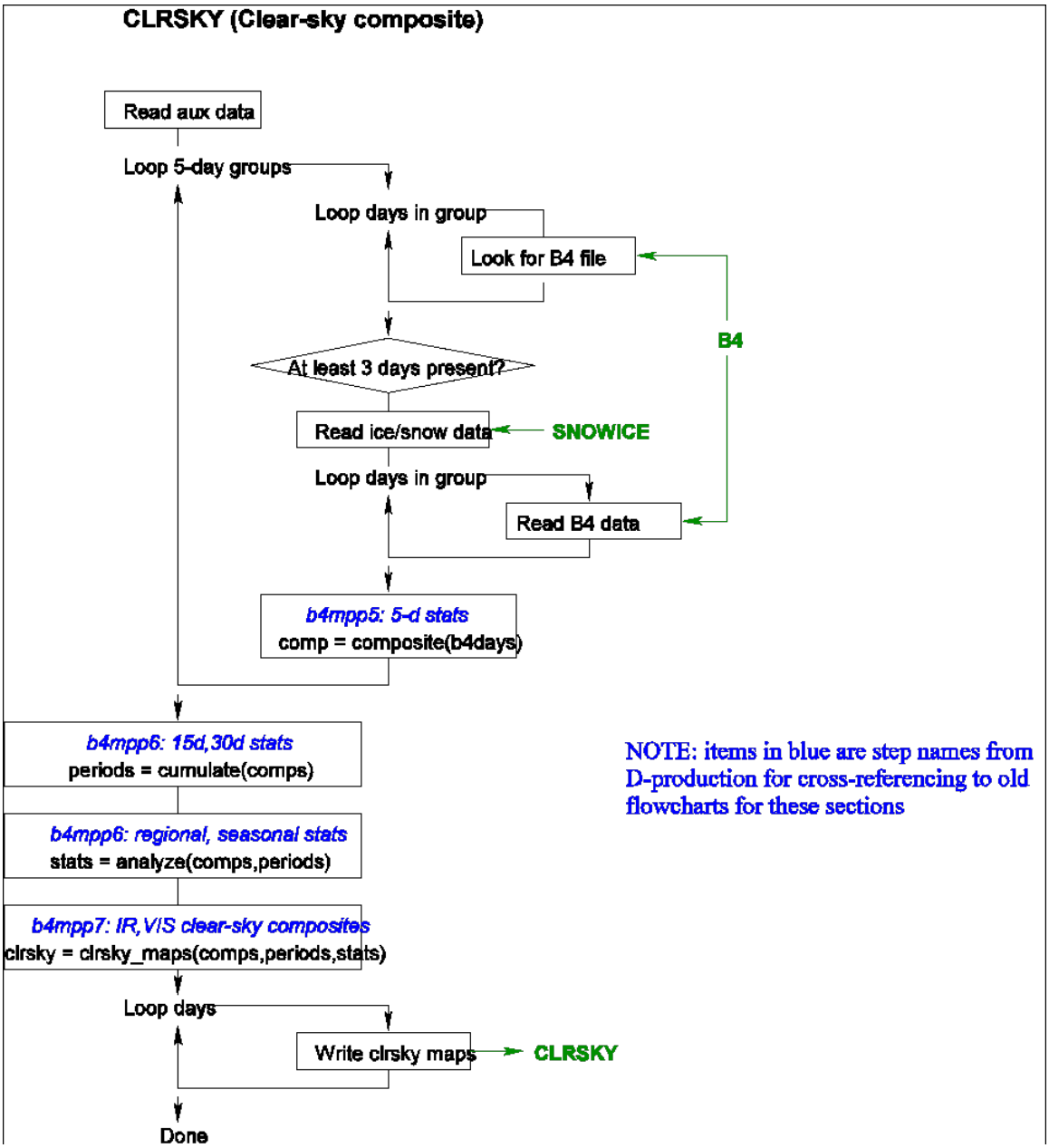

Figure 12: *CLRSKY* main program

The values of NCLEAR-ST, TAVG-ST, TMAX-ST, NCLEAR-LT, TAVG-LT and TMAX-LT (one set of values for each time of day UTC) are used to estimate the clear sky IR brightness temperature using the logic shown in Figure 13. This logic assumes that the relatively small time variations of clear sky brightness temperatures (at constant diurnal phase) and their (almost global) tendency to be larger than cloudy brightness temperatures produce a characteristic shape of the warmest part of brightness temperature distribution that varies only with surface type. The compositing logic tests the shape of the brightness temperature distribution using the average and maximum values: larger differences than expected (set

by the DEL parameters) are interpreted to indicate cloud contamination. Cloud contamination is assumed to decrease over larger time intervals. The characteristic shape also provides the estimated difference between the maximum and average values in the absence of clouds.

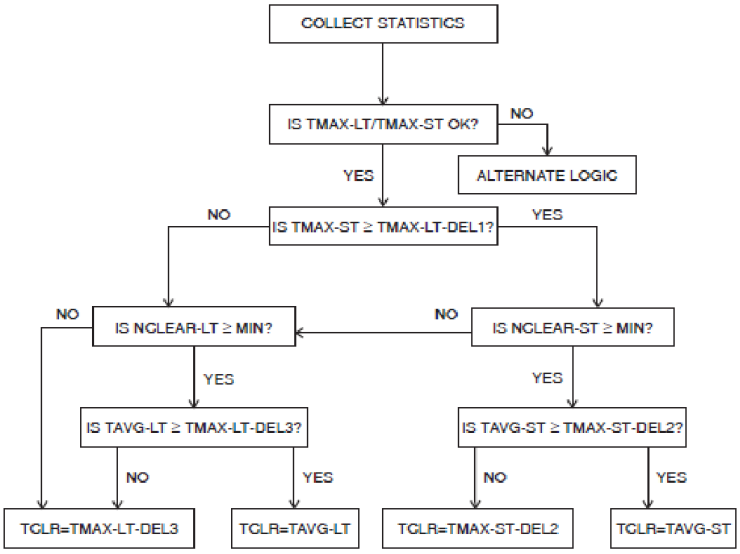

Figure 13: IR clear sky composite logic

There are five situations that can occur.

1) A pixel is partially cloudy but the cloud-clear brightness temperature difference is very small or the cloud cover is complete but the cloudy brightness temperatures exhibit very little space and time variability.
2) The pixel is mostly cloudy and the cloud-clear brightness temperature difference is small but larger than the variability of clear brightness temperatures or cloud persistence and extent are large but not total.
3) The pixel is mostly cloudy but the cloudy brightness temperatures exhibit relatively large variability in space and/or time.
4) The pixel is partly cloudy (spatially) or almost totally cloud covered occasionally and the cloud-clear difference is relatively large.
5) The pixel is relatively clear.

The first and last cases resemble each other in that the magnitude of the cloud brightness temperature variability is similar or the cloud cover is complete for the whole month with small variations. If this resemblance is strong enough, any clouds representing case 1 will not be detected.

In case 2 either the brightness temperature variations caused by clouds are relatively small or there are almost no clear sky observations. This case is indicated by TMAX-LT > TAVG-LT + DEL3 and TAVG-ST + DEL1 in which case the best estimate of clear sky brightness

temperature is TCLR = TMAX-LT – DEL3. (See Table 4 for DEL values.) This test is less effective over land than water so the test parameter values shift the result towards shorter-term values over land.

In case 3, the clouds produce large enough brightness temperature variations that the space/time tests detect the clouds; that the location is mostly cloudy is indicated by a small value of NCLEAR. If this situation persists for the whole month (NCLEAR-LT < 18), then the best estimate is TCLR = TAVG-LT. To maintain consistency for case 2 and 3, the value of TCLR is required to be ε TMAX-ST – DEL2. This test is more effective over land than water.

In case 4, while NCLEAR-ST is large enough (ε 18), there is still enough cloud contamination such that TMAX-ST > TAVG-ST + DEL2, so TCLR = TMAX-ST – DEL2. In case 5, the best estimate is TCLR = TAVG-ST.

Because of the sensitivity of the detection algorithm to the values of TMAX, extra protection against spuriously large values (bad data) is provided by comparing TMAX-LT – DEL4 against the mode of a regional distribution of TMAX-LT values: if the test fails, the particular value of TMAX-LT (and the corresponding TMAX-ST) are replaced by the regional mode value.

Table 4: Test parameter (DEL) values (in Kelvins) used in IR clear sky compositing logic.

IR Surface Type	DEL1	DEL2	DEL3	DEL4
1	2.0	2.0	2.5	4.0
2	4.0	3.0	4.0	6.0
3	6.0	5.0	8.0	8.0
4	9.0	7.0	11.0	10.0

VIS Clear Sky Composite: The CLRSKY program also collects VIS statistics from the re-mapped images to produce composite clear sky R maps for 5-day intervals at each time of day UTC over the whole month for each satellite containing: (1) the minimum VIS reflectance for each 5-day interval, RMIN-ST, and (2) the minimum VIS reflectance for the month, RMIN-LT. RMIN-LT is calculated for 15-day instead of 30-day periods poleward of 50° latitude. If any nighttime ($\int_0$ < 0.15) data are found within the monthly period for a particular pixel, no RMIN values are reported and all pixels at that location are declared to be nighttime. The VIS compositing logic assumes that the small variations of clear sky VIS reflectances and their (almost global) tendency to be smaller than cloudy reflectances produce a characteristic shape of the darker part of the VIS reflectance distributions. Since time variations of surface reflectances are generally very small, except for the effects of variable snow and sea ice cover, the compositing procedure for VIS is much simpler (Figure 14). Identification of the minimum reflectance over a sufficiently long time scale usually eliminates cloud effects; however, the small variations of the surface reflectance over time cause the minimum value (RMIN) to be biased, so the distribution shape assumption is used to increase RMIN to provide a better estimate of the average clear sky reflectivity.

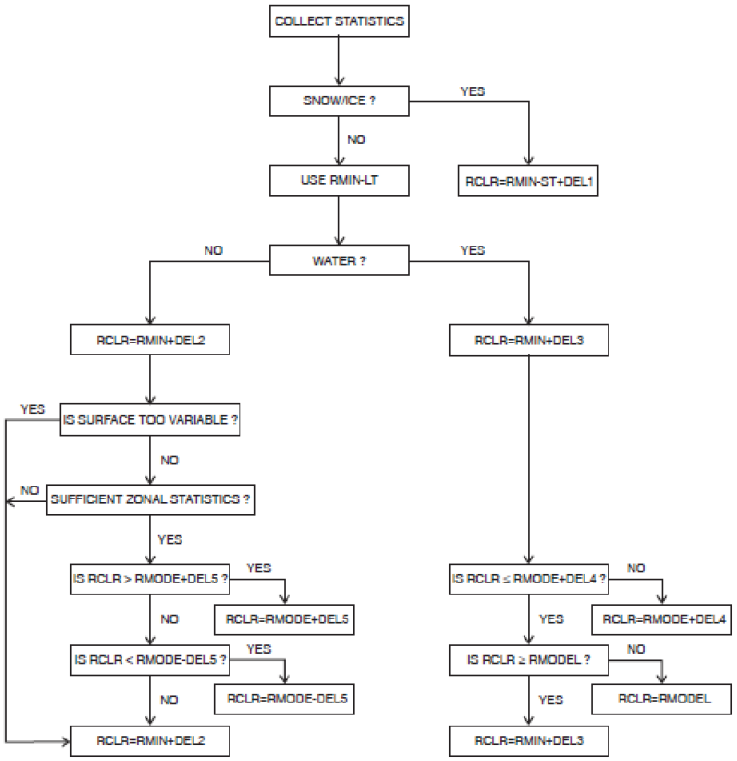

Figure 14: VIS clear sky composite logic

In this step, six surface type groups are considered based on TOPO, SNOWICE and SURFACETYPE:

1) Open water (Surface Type 0) that is not covered by sea ice during the time period (either ST or LT).
2) Sea ice or permanent ice shelf cover fraction > 0 or ice margin (δ 115 km to nearest ice) during the period.
3) Evergreen needle leaf and broadleaf forests (Surface Types 1 and 2)
4) Deciduous needle leaf and broadleaf forests, mixed forests (Surface Types 3, 4, and 5)
5) Closed and open shrublands, woody savannahs (Surface Types 6, 7, and 8)
6) Savannas, grasslands, croplands, cropland/natural vegetation mosaic (Surface Types 9, 10, 12, 14)

All other land types (Surface Types 11, 13, 15, 16, 17, 18), as well as snow-covered or snow-margin (δ 115 km to nearest snow/glacier) locations are excluded.

1) Open water generally exhibits constant reflectance in space and time for the same viewing/illumination geometry. However, the geometry dependence can be strong, so RCLR = RMIN-LT + DEL3, where DEL3 = 0.015. This value of RCLR is constrained by a model of water reflectivity so that RMODEL + DEL2 ε RCLR (where model refers here to the water surface reflectance model described in Section 3.3.4).

2) All vegetated land is temporally as well as spatially homogeneous, so RCLR = RMIN-LT + DEL2. However, the individual values are compared to the distribution of values for the same surface group (3, 4, 5, 6, defined above) in 10° latitude zones but, if the standard deviation is > 0.08, the zonal values are replaced by global statistics for that surface group.
3) Variable water and rapidly varying land caused by the presence of sea ice and snow cover (permanent ice shelves and glaciers are treated in the same way). These two cases have both low reflectance contrast between clear and cloudy conditions as well as higher clear reflectance variability, so the best estimate is RCLR = RMIN-ST + DEL1, where DEL1 = 0.050.
4) Rough topography, wetlands, urban and desert locations, which exhibit relatively large spatial variations (shadowing in the first case) but small time variations, so RCLR = RMIN-LT + DEL2, where DEL2 = 0.035.

3.4.1.1.3 Preliminary Cloud Detection Threshold Tests: BXPROD

The status of each image pixel is decided by comparison of the observed IR and VIS radiances, independently, to their respective clear sky values without regard to the labels from previous tests (Figure 15). For this comparison the clear sky composite radiances are corrected back to the particular view/illumination geometry of each pixel by reversing the angle correction applied in B4PROD, *i.e.*, TN TB and R V. Note that "threshold" here refers to the magnitude of the radiance difference between the pixel value and the clear sky composite value for that pixel; when this difference exceeds a "threshold value", the presence of cloud is indicated. These threshold values are scene-dependent as described below. Since the IR channel is relatively insensitive to low clouds, especially if they are small optical thickness or broken clouds, and the VIS channel is relatively insensitive to optically thin cirrus clouds, a pixel is called CLOUDY if **either** threshold test indicates cloudiness: if IR brightness temperature, TB, is < TBCLR – ΔTB **or** VIS scaled radiance (not reflectance), V, is > VCLR + ΔV. The values of the thresholds used at this stage represent the earlier C-Version estimates of the uncertainty of the clear sky composite radiances.

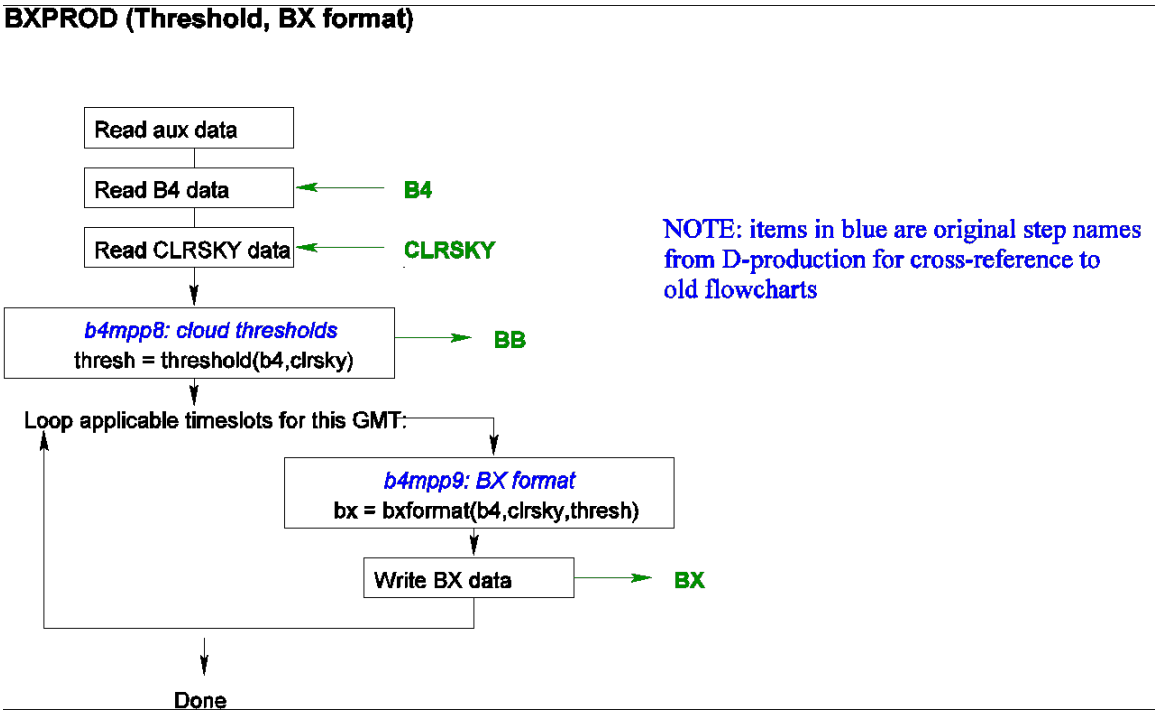

Figure 15: BXPROD Main Program

The same four surface type categories are used as in the preliminary IR clear sky compositing step (CLRSKY). The VIS thresholds use only three categories (Type 1 = open water that is not sea ice or permanent ice shelf, Type 2 = open land that is not snow or glacier, and Type 3 = sea ice or snow indicated by fractional coverage > 0 or margin). Table 5 gives the values of ΔTB and ΔV for these surface types.

Table 5: Values of the IR brightness temperature thresholds (in Kelvins) and the VIS thresholds (scaled radiance) for the four surface variability types.

	Surface Type			
Radiance	1	2	3	4
ΔTB (K)	2.5	4.0	6.0	8.0
ΔV (scaled radiance)	0.03	0.06	0.06	

The threshold values define five categories relative to the clear sky radiance value that are recorded by flags in the output (Figure 16): for IR, (IR flag 1) TB ε TCLR + ΔTB, (IR flag 2) TCLR + ΔTB > TB ε TCLR, (IR flag 3) TCLR > TB ε TCLR – ΔTB, (IR flag 4) TCLR – ΔTB > TB ε TCLR – 2 ΔTB, and (IR flag 5) TCLR – 2 ΔTB > TB, and for VIS, (VIS flag 1) V δ VCLR – ΔV, (VIS flag 2) VCLR – ΔV < V δ VCLR, (VIS flag 3) VCLR < V δ VCLR + ΔV, (VIS flag 4) VCLR + ΔV < V δ VCLR + 2 ΔV, and (VIS flag 5) VCLR + 2 ΔV < V. Cloud is indicated by **either** threshold flag = 4 or 5.

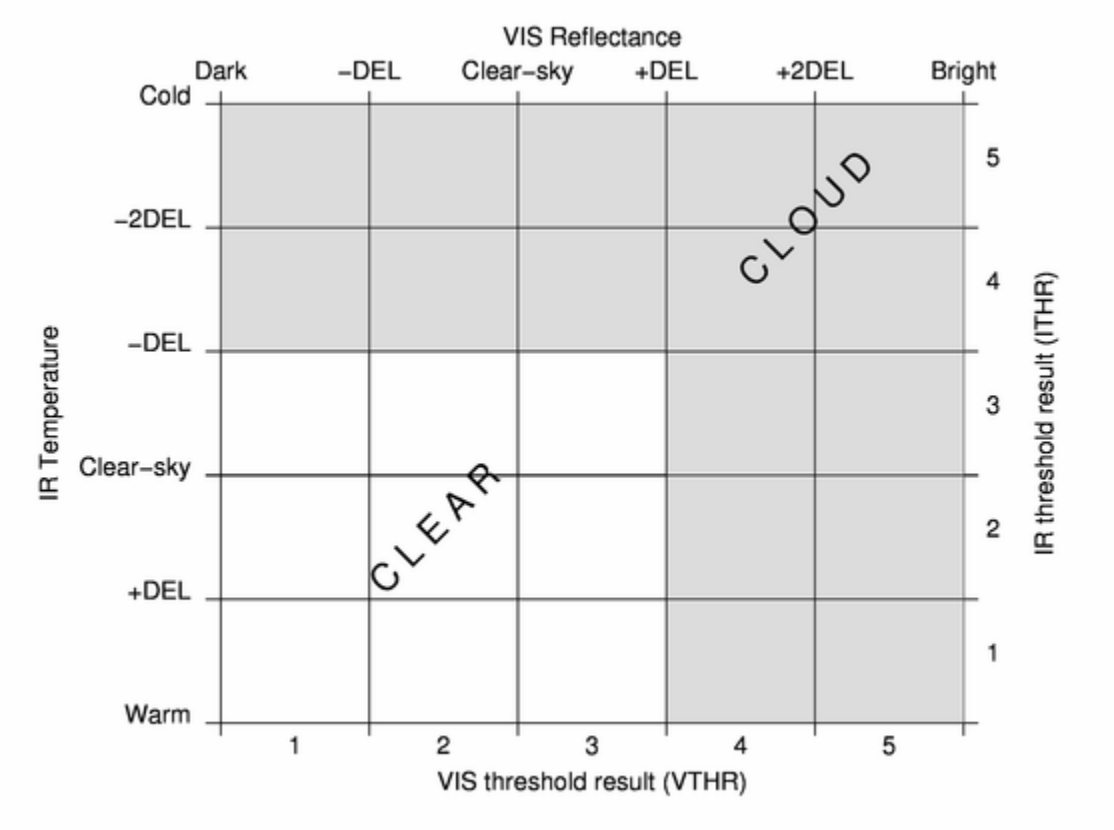

Figure 16: Threshold flag schematic

3.4.1.1.4 **CYPROD**

In the evaluation of the original C-Version cloud detection algorithm (composed of B4PROD, CLRSKY, BXPROD), it was found that some extreme situations occurred (nearly complete absence or complete cover of clouds for a whole month) and that some detection errors occurred because image navigation errors misplaced the coastlines. Also further evaluation of the C-Version products indicated that some of the uncertainty estimates for clear sky composite radiances were too conservative – *i.e.*, the uncertainties were overestimated. Hence, in the D-Version two algorithm steps were added in CYPROD (Figure 17): the clear sky composite maps for each location and time step are reconstituted (the output from BXPROD gives clear sky composite values of T and V for each pixel so these are angle-corrected back to TN and R) and adjusted and then revised detection thresholds applied.

IR Clear Sky Composite Adjustment: IR (and VIS) pixels are classified into four categories using TOPO and SNOWICE. These categories are used for matching pixels with those of the same type in order to make adjustments to the clear-sky maps. Shore pixels (δ 115km to opposite land-water type) or pixels with high or rough topography (pixel height > 1750m or height standard deviation in a 1-degree equal-area cell > 250 m) that are not land ice (glacier cover δ 65%) are skipped. The categories are (1) water that is not sea ice covered over the whole period (ST or LT), (2) full sea ice cover, including permanent ice shelf cover,

over the whole period, (3) land that is not snow covered over the whole period and (4) any snow cover, including glacier, over the whole period.

The whole month of IR clear sky composites is examined in four steps (Fig. 15) that look for unusually large TCLR values that can distort the cloud detection for the whole month. The first step identifies the three largest TCLR values (called TMX1, TMX2, TMX3) in the time record for each pixel of each type. The second step sets a HOT flag for any pixel where TMX1 – TMX2 > 10 K. The third step examines the 15x15 domain around each HOT pixel; if there is any unflagged pixel in the same category with its TMX1 greater than the flagged value, the HOT flag is turned off. The fourth step reconstitutes the 5-day composite clear sky brightness temperature maps setting flags to indicate which statistic (TAVG-ST, TMAX-ST, TAVG-LT, TMAX-LT) was used. Prior evaluation showed that the values of DEL2 and DEL3 used in CLRSKY were too large over snow-covered land, so the TCLR values for Type 3 are increased by 1.0 K when TMAX-ST was used and by 2.0 K when TMAX-LT was used and there is any snow/ice.

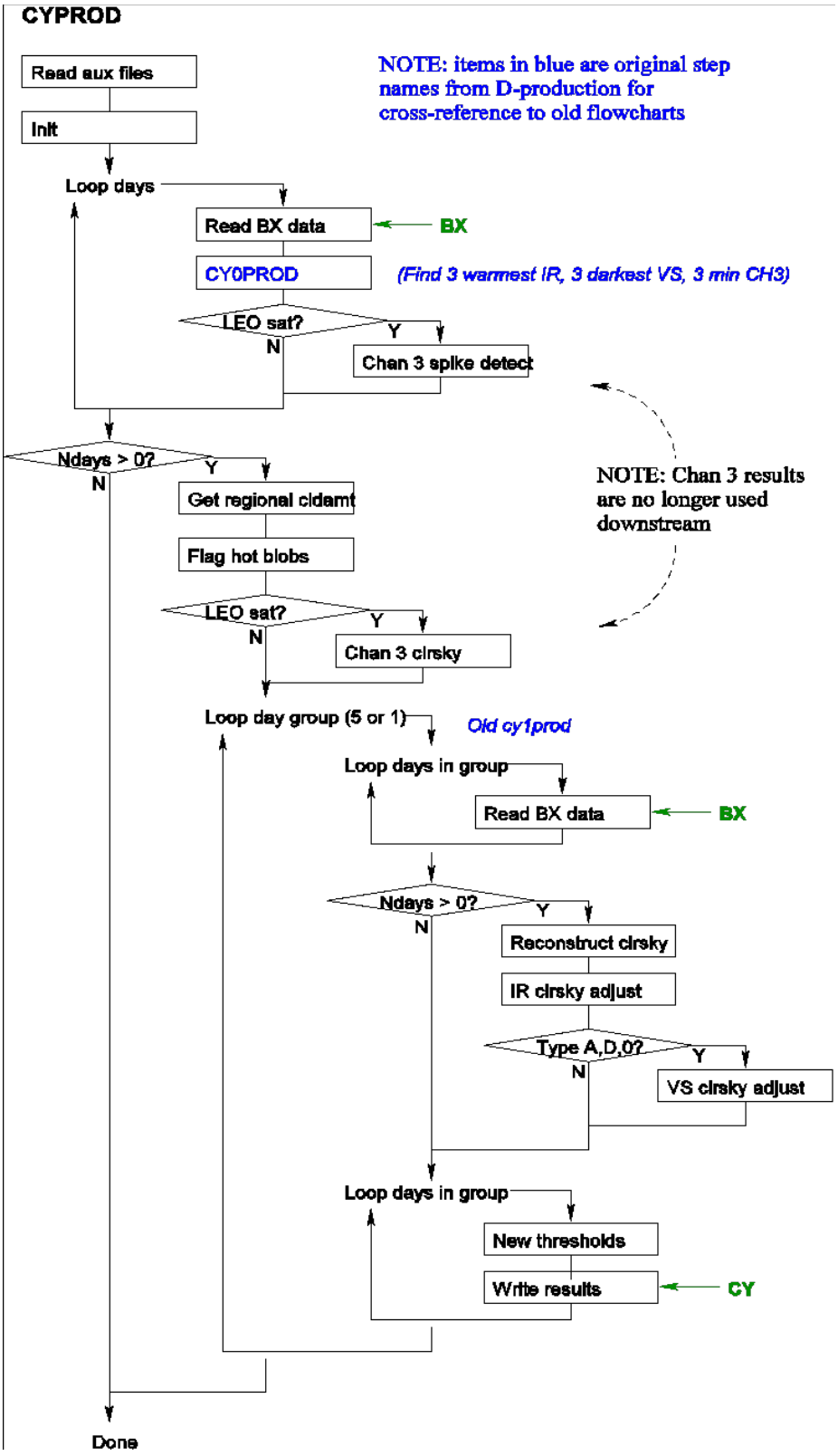

Figure 17: CYPROD Main Program

Next, three procedures are applied to correct for any spuriously large TCLR values, to reduce the effects of navigation errors, and to correct for some residual cloud contamination. The first procedure checks all pixels that do not have the HOT flag set; if TCLR > TMX1 + 1.0 K, the HOT flag is set. If TCLR > (TMX1 + TMX2)/2, the surrounding 15x15 domain containing a HOT flag is searched and if at least two neighboring pixels in the same category and with no HOT flag are found, the flagged value of TCLR is replaced by the average TCLR of all un-flagged neighboring pixels of the same surface class and the HOT flagged turned off. If insufficient neighboring pixels are found, no change is made.

The second procedure is applied only to Type 1 pixels: a 21x21 pixel domain around each target is examined to determine if it includes a mixture of land and water pixels. If sea ice is present in the domain, this procedure is skipped. The average value of TCLR (TSAME) for all unflagged pixels (minimum of two) of the same type, land or water, and for all unflagged pixels (minimum of two) of the "opposite" type (TOPP) are calculated. If TOPP – TSAME > 4.0 K and TOPP – TCLR < 2.5 K, a flag is set. If insufficient pixels are available, the procedure is skipped for that particular pixel. Once all pixels have been examined, the flagged values of TCLR are replaced by TSAME (re-calculated to exclude flagged pixels) and the flag turned off. These two procedures are needed because occasional navigation errors (coastline location errors) or errors in the snow/sea ice location can cause mixing of values of TCLR from two different surface types that causes spurious or missed cloud detections.

The third procedure examines 9x9 pixel domain around each pixel. If < 5 pixels are found, then an 11x11 pixel domain is searched. If < 9 pixels are found, the procedure is skipped. If any neighboring pixel is a different land/water category or a different snow/ice category than the target, this procedure is also skipped. For domains with at least three neighbors, the spatial variance of TCLR is calculated; if it exceeds 0.6 K over water or 7.6 K over land, the smallest TCLR value is flagged COLD. Once all pixels have been examined, flagged TCLR values are replaced by the average TCLR (from the 9x9 domain) of unflagged neighbors. If insufficient neighbors are available, the procedure is skipped. This procedure removes residual cloud contamination in cases where the monthly cloud cover fraction approaches 1.0.

VIS Clear Sky Composite Adjustment: VIS pixels are classified into four categories using TOPO and SNOWICE. These categories are used for matching pixels with those of the same type in order to make adjustments to the clear-sky maps. Shore pixels (δ 115km to opposite land-water type), or pixels with high or rough topography (pixel height > 1750m or height standard deviation in a 1-degree cell > 250 m) that are not land ice (glacier cover δ 65%) are skipped. The categories are (1) water that is not sea ice covered over the whole period (ST or LT), (2) full sea ice cover, including permanent ice shelf cover, over the whole period, (3) land that is not snow covered over the whole period and (4) any snow cover, including glacier, over the whole period.

The whole month of VIS clear sky composites is examined in two steps with the night criterion changed to $\lceil_0$ < 0.20. The first step collects the two smallest RCLR values for each pixel for each time of day, called RMN1 and RMN2. The second step reconstitutes the 5-day VIS clear sky radiance maps. The adjustment procedure compares the original RCLR values to the RMN1 and RMN2 values in different ways depending on the cloud fraction in a fixed

grid of 15x15 pixels determined in CYPROD. In the case of cloud amounts < 0.80, disagreement among these values is interpreted to be caused by cloud shadows causing an underestimate of the clear sky VIS radiance. In the case of cloud amounts ε 0.80, disagreements are interpreted as cloud contamination. This comparison is not performed over snow/ice-covered locations. For cloud fraction < 0.80 and RMN2 – RMN1 > 0.05, if RCLR < RMN2, RCLR is replaced by RMN2. If this is not done, but the pixel is land and (RCLR – RMN1) ε 0.03, then RCLR is replaced by RMN1 – 0.015. For cloud fraction ε 0.80 over water, if RCLR – (RMN1 + RMN2)/2 ε 0.03, RCLR is replaced by (RMN1 + RMN2)/2 + 0.03. For cloud fraction ε 0.80 over land, if RCLR ε RMN1 + 0.03, RCLR is replaced by RMN1.

Final Cloud Detection Threshold Tests: In CYPROD the final IR threshold test magnitudes depend on combinations of factors: high or rough topography, snow-ice cover, shore or land-water. A matrix assigns the threshold values representing all possible combinations, resulting in the table given below.

Based on detailed comparisons of the performance of the ISCCP D-Version cloud detection algorithm with other proposed methods that were evaluated by a whole year of collocated, coincident surface cloud radar and lidar observations from the SHEBA experiment in the Arctic (Intrierie *et al.* 2002) and global observations by the Calipso (lidar, Winker *et al.* 2010), the ISCCP algorithm was modified in two ways. In daytime (summertime) over snow and ice-covered locations, the IR and VIS threshold magnitudes are reduced. In nighttime over snow and ice-covered locations, the IR threshold flag classes are changed as follows: originally threshold classes 1, 2 and 3 were called clear and 4 and 5 were called cloudy but this is changed so that classes 1, 2 become class 5 (cloudy) and class 4 becomes class 3 (clear). In CYPROD the final VIS threshold tests are applied to pixel and clear sky reflectances by multiplying the scaled radiance threshold magnitudes by the pixel value of $\lceil_0$ (but constrained to minimum values of 0.025 for open water, 0.030 for ice/margin, 0.035 for open land, and 0.040 for snow/margin/rftopo), unlike the threshold test in BXPROD which uses scaled radiances. The same threshold categories as in BXPROD are used (see Figure 16).

Table 6: H-Version final cloud detection thresholds compared to D-Version values (see Section 6 for more details).

Surface Type	H-Version IR Thresholds	D-Version IR Thresholds	H-Version VIS Thresholds	D-Version VIS Thresholds
Open Water	2.5	2.5	3.0	3.0
Open Water Shore	3	3.5	3.0	6.0
Marginal Sea Ice	3	4	4.5	6.0
Marginal Sea Ice Shore	3	4	4.5	3.0
Full Sea Ice	3	4	4.0	6.0
Full Sea Ice Shore	3	4	4.5	3.0
Open Land	4	4	5.0	6.0
Open Land Shore	4	4	5.0	9.0

Marginal Snow	4	4	6.5	9.0
Marginal Snow Shore	4	4	6.5	9.0
Full Snow	4	4	6.0	9.0
Full Snow Shore	4	4	6.0	9.0
High Topography	5	6	7.5	9.0
Rough Topography	5	6	7.5	9.0

3.4.1.2 Surface Property Retrieval

After each pixel is labeled as cloudy or clear, the ISCCP analysis next retrieves the surface and cloud properties (Figure 18). Because the cloud property retrieval depends on the surface properties, this analysis is first applied to the clear sky composite radiance values that are available for all pixels (see Figure 19); the two surface properties retrieved are skin temperature (TS) and visible reflectance (RS, also RS0). The same surface retrieval procedure is also used in the processing the observed radiances for clear pixels.

To retrieve surface skin temperature, TS, all surfaces are assumed to have an emissivity ($\sum_s$ at an effective wavelength 10.5 ⌈m) based on the SURFACETYPE and emissivity values in the corresponding table, IREMISS (see Table 4 in Section 3.3.2.6). If any snow or ice is present at pixel level, the value of $\sum_s$ for snow/ice is used. Atmospheric corrections are determined from quantities calculated from NNHIRS, including a correction for aerosols using AEROSOL. The calculated quantities (TBNN) include the difference between the near-surface air temperature and the calculated brightness temperature at the top of the atmosphere (DT in radiance units), the upwelling emission by the atmosphere at the top of atmosphere (BTA), the atmospheric extinction of the upwelling radiation (ext) from the surface, and the downwelling radiation at the surface (BT_{dn}), all as functions of the cosine of the satellite view zenith angle (⌈). This information, interpolated to the value of ⌈ for each pixel, is used in SRFRET to retrieve values of TS for all pixels from the clear sky composite IR radiances (all brightness temperatures, including the satellite observed value, T, are converted to physical radiances represented by BT):

$$BTS = (BT - BTA - ext * (1.0 - \sum_s) * BT_{dn}) / (ext * \sum_s) \quad (15)$$

where BTS is the upwelling radiance at surface equivalent to its physical temperature (TS), BT is the radiance seen by the satellite, BTA is the upwelling emission by the atmosphere, ext is atmospheric extinction in the upwelling direction, BT_{dn} is downwelling emission by the atmosphere and $\sum_s$ is surface emissivity. TS is obtained by converting BTS back to temperature using a table that assumes the NOAA-9 IR (10.5 ⌈m) spectral response function (all other radiometers are normalized to this standard).

Because there are errors in the TS retrieval (from errors in radiance calibration, estimates of clear sky value or cloud detection, ancillary data, radiative transfer model), there are very rare instances when the retrieved values of TS fall outside the expected range. This situation is controlled in part by encoding the retrieved values to COUNT values; the conversion table of counts to physical values for temperatures (see Appendix C.7) is constrained to a range of 160 to 350 K. Any retrieved value of TS outside this range is encoded as the smallest or largest COUNT value, so no values are reported out of range.

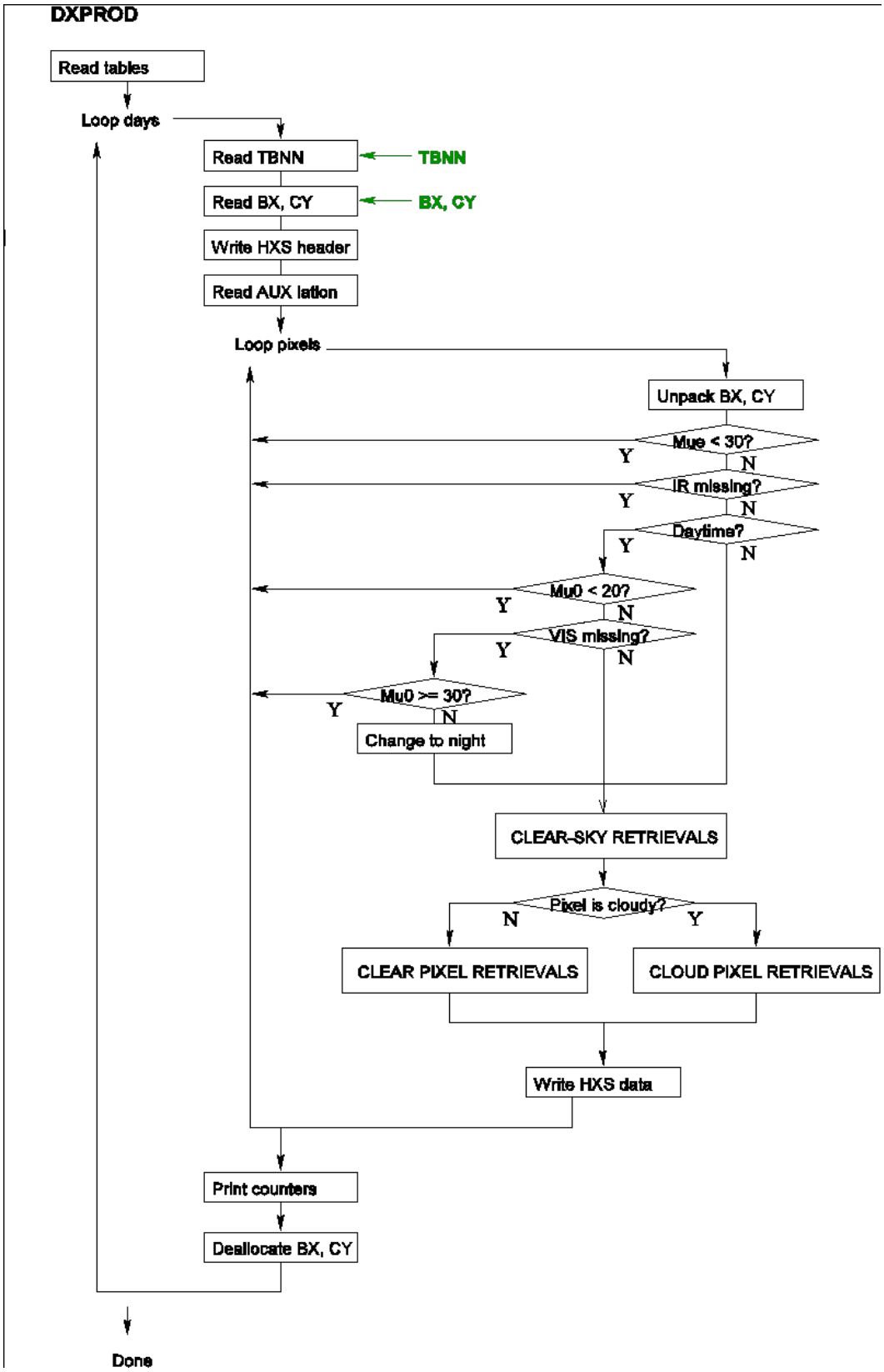

Figure 18: DXPROD main program

The largest TS values occur in extreme conditions: a combination of large satellite view zenith angle (low ⌠), large total column water vapor abundance and large atmospheric and surface temperatures. Under these conditions the retrieval becomes very sensitive to small uncertainties in water vapor abundance, because of the temperature dependence of water vapor absorption, and can produce very large values of TS. To mitigate this effect, an alternate retrieval is used whenever any one of three conditions obtains: (1) if the estimated clear sky radiance is equal to or less than the radiative transfer model calculated emission of the atmosphere with a black body surface with the same temperature as the surface air temperature, (2) the atmospheric transmission over the atmospheric path is too small (1/ext < 0.1) or (3) the retrieved value of TS > 350 K. The first two conditions can occur because the contribution to the observation actually coming from the surface is very small. In any of these cases, an alternate retrieval is used that subtracts from the observed clear sky radiance (BT) the radiative-model-calculated difference (DT) between the upward radiance at the surface, assuming a temperature equal to the surface air temperature, and the associated top-of-atmosphere radiance:

$$BTS = \quad (BT + DT - (1.0 - \sum_s) * BT_{dn}) / \sum \qquad (16)$$

This alternate is an approximation because it slightly underestimates the non-linear dependence of the full radiative transfer calculation, especially in conditions of large temperature and water vapor abundance.

To retrieve the surface visible reflectivity, RS (at an effective wavelength of 0.65 ⌠m), all surfaces including water are assumed to be isotropic reflectors. Although the value of RS is reported for water surfaces, it is replaced by a more accurate ocean surface reflectivity model (Chowdhury *et al*. 2012) in the cloud retrieval. Atmospheric corrections are made for ozone absorption (Inn and Tanaka 1953), using OZONE and a table of effective transmissions unique to each satellite (PTRANS), and for scattering/absorption by stratospheric and tropospheric aerosols using AEROSOL. The subroutine CORRAD adjusts the VIS radiances to the sun-earth distance appropriate to the specific date and corrects the clear sky visible radiances to remove the effects of ozone absorption and stratospheric aerosol scattering, the latter using a pre-calculated table as function of viewing geometry and AOD. The **corrected** VIS radiances are then input to QAGRD1 (a LUT for clear conditions) that returns a value of RS as a function of surface pressure (PS), viewing geometry (⌡, ⌡$_0$, cosine of solar zenith angle, and ⌝$_0$, relative azimuth angle) and tropospheric AOD and fine fraction. This routine also returns another value, RS0, of surface reflectivity assuming zero tropospheric AOD that is used in the cloud retrieval over land/ice surfaces.

Because there are errors in the RS retrieval (from errors in radiance calibration, cloud detection, ancillary data, radiative transfer model), there very rare instances when the retrieved values of RS fall outside the expected range. This situation is controlled by encoding the retrieved values to COUNT values; the conversion table of COUNTS to physical values for reflectances (see Appendix C.7) is constrained to a range of 0.002 to 1.120. Any value of RS outside this range is encoded as the smallest or largest COUNT value, so no values are reported out of range. The values of RS over vegetated land obtained from some radiometers with much broader spectral responses are used in the cloud retrieval for consistency but are adjusted in the final output by regression against the narrow AHVRR-channel results (VISCOR); land areas with snow-ice fraction > 0.35 are excluded. This correction is done only for the 1-degree gridded products, not the pixel-level products.

3.4.1.3 Cloud Property Retrieval

Using the surface properties retrieved from the clear sky composite radiances and Ancillary data, the cloudy pixels are processed to retrieve cloud top temperature/pressure

(TC/PC) and visible optical thickness (TAU) and water path (WP) by the procedure illustrated in the Figure 17 and 19. First, cloud top temperature (TC) and the corresponding pressure (PC) at the same level in the atmosphere that has the same physical temperature are determined from the observed IR brightness temperature assuming all clouds are blackbodies and correcting for emission/absorption by the atmosphere above the cloud level (CLDRET). There are three special cases for determining PC that are handled explicitly: the value of TC is colder than the tropospause temperature (TT, usually the coldest point on the temperature profile), the value of TC is warmer than the warmest temperature on the temperature profile when a near-surface temperature inversion is present, and the value of TC is warmer than the warmest temperature on the temperature profile in the absence of a temperature inversion (this case uses the surface retrieval, SRFRET, to place the cloud top at the surface). If nighttime (no VIS radiances), this is the end of the cloud retrieval. If daytime, cloud optical thickness (TAU) is retrieved as a function of PC and VIS radiances (corrected for stratospheric aerosol and ozone effects, CORRAD) assuming all clouds are composed of liquid water (TAUF2, TAUVF, TAUVFP). If TAU is small enough that some IR radiation is transmitted through the cloud, the values of TC/PC are adjusted to account for this effect (TAUCOR). Then the values of TC for all clouds are adjusted as a function of TAU to account for IR scattering (SCACOR). The TAU retrieval and TC/PC-retrieval correction are then repeated assuming all clouds are composed of ice (scattering correction in SCAICE). Thus, for each cloudy pixel three values of TC/PC are reported, for blackbody clouds (all day), for liquid **and** for ice clouds (daytime only), and two values of TAU are reported, for liquid **and** for ice clouds (daytime only).

Prior to the cloud analysis, the atmospheric temperature-humidity profile (NNHIRS) and IR aerosol optical depth (AEROSOL) for the specific time and location are used to pre-calculate the brightness temperatures viewed at the top of the atmosphere as a function of pressure (P) and cosine satellite view angle ($\sec\theta$) by placing a blackbody at each pressure level in the atmospheric profile. These pre-calculated brightness temperatures are matched with the corresponding physical temperature at each pressure level. Comparison of the observed cloudy pixel brightness temperatures (TB) to the pre-calculated values (interpolated to the specific value of $\sec\theta$) determines a physical cloud top temperature (TC) and the corresponding pressure (PC) for blackbody clouds in CLDRET. If TB is less than or equal to the brightness temperature corresponding to the tropopause temperature (TT), TC = TB because there is so little water vapor above the tropopause that the brightness and physical temperatures are essentially identical. For a blackbody cloud, the pressure corresponding to TC < TT is calculated by assuming a dry adiabatic profile above the tropopause under the assumption that such a cloud top temperature is produced by penetrating convection. For values of TB warmer than the tropopause value, the pre-calculated brightness temperature profile is searched downward (increasing pressure) until a value in the profile exceeds TB. PC is then determined by interpolation. The maximum brightness temperature of a profile occurs either at the surface or above the surface if a near-surface temperature inversion is present. In the latter case, the value of TC is set to a value larger than the maximum physical temperature (corrected for atmospheric effects) to preserve the observation and PC is set to the pressure at the peak of the inversion. In the former case, the surface retrieval subroutine (SRFRET) is used to set TC

equal to a temperature retrieved like surface skin temperature, but using unit emissivity, and PC = PS.

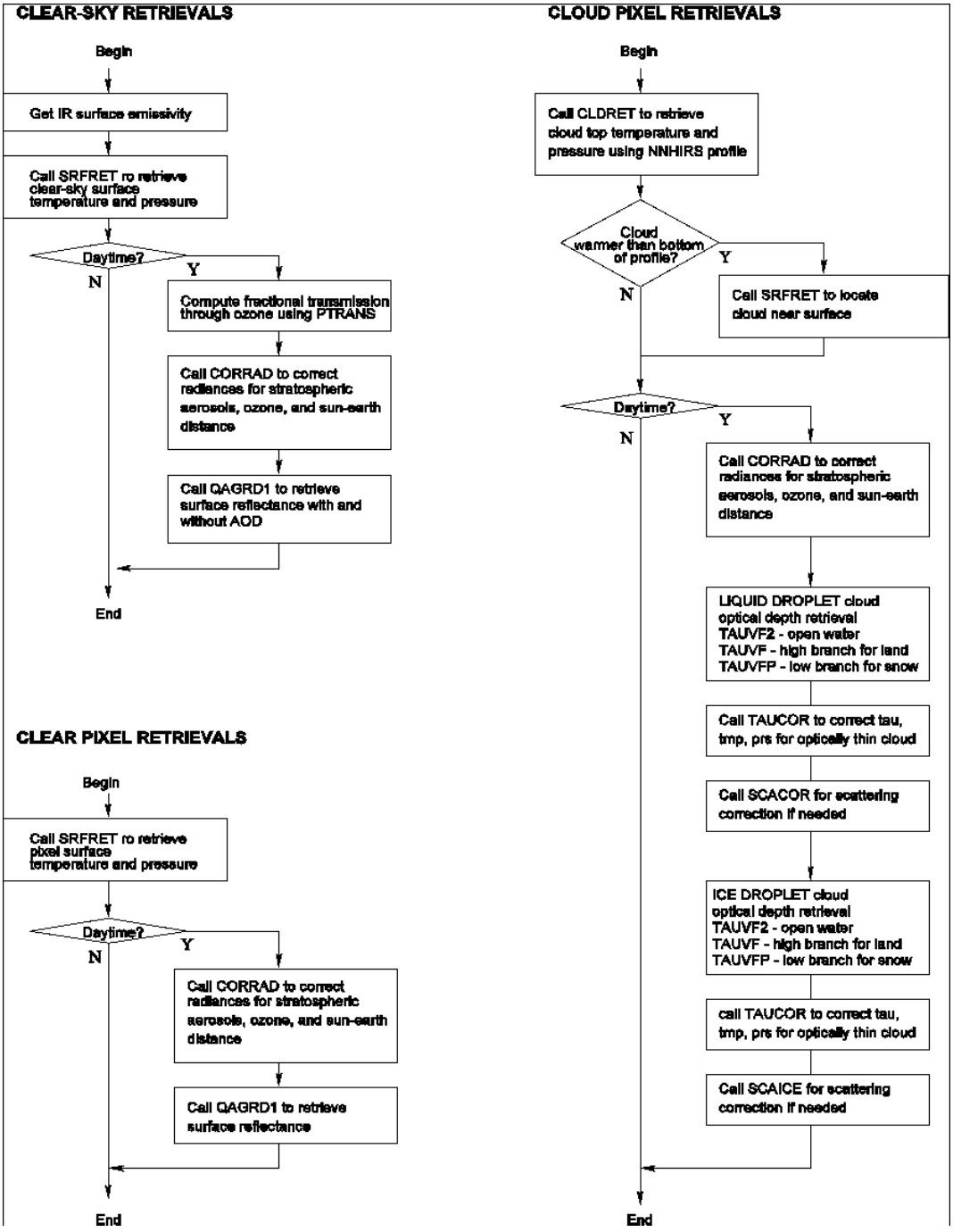

Figure 19: DXPROD Subroutines

During daytime, when the VIS radiances are available, they are used to retrieve cloud optical thickness (TAU) assuming both a liquid water and ice cloud model at all temperatures and to make any needed corrections to the blackbody values of TC and PC.

The observed VIS radiances are first adjusted to remove the effects of stratospheric ozone absorption and aerosol scattering (CORRAD), as described for the surface retrievals. These **corrected** VIS radiances are then entered into the pre-calculated LUTs that return values of TAU for a liquid water cloud as a function of illumination-viewing geometry (, ,) and other parameters. The LUTs used over open water (in TAUF2) are based on an explicit model of water surface reflectance as a function of geometry and accounts for variations of tropospheric aerosol properties (AOD and fine fraction). Over all other surfaces, except for certain cases over snow and ice, the LUTs that are used (in TAUVF) account for the combined variations of aerosols and surface reflectivity (RS) by using a special value, RS0, retrieved from the clear sky composite assuming AOD = 0. Since the angle dependence of scattering by clouds is very different from that of snow-ice surfaces (assumed to be isotropic), the reflectivity of a cloudy scene can be smaller than for clear sky over these surfaces. This situation is accounted for by special LUTs (in TAUVFP) that are used over snow-ice surfaces for clouds that are detected in the IR but not in the VIS, as is the case when the cloudy reflectivity is less than the clear sky reflectivity. If the cloudy scene VIS radiances are larger than or equal to the clear sky value, then TAUVF is used for the retrieval.

Since there can be errors (from errors in radiance calibration, cloud detection, ancillary data, radiative transfer model), retrieval of TAU values near zero is very sensitive to small inconsistencies that can lead to non-physical results (negative values) if linear interpolation is used. Because the cloud reflectivity (VIS radiances) is more nearly linear in the logarithm of optical thickness, the LUT interpolation is performed in lnTAU. This has the effect of preventing negative values, but does allow for arbitrarily small values of TAU. Encoding of the results into COUNTS limits the precision so that the smallest possible TAU value to 0.01. At the high end of the TAU range, the cloud reflectivity becomes insensitive to large variations of TAU. Interpolation in lnTAU controls this behavior and the encoding of the results into COUNTS limits largest possible value to 450 (see Appendix C.7).

The value of TAU for liquid water clouds ( ) is converted to an IR optical thickness by $_{IR}$ = 0.391 . If $_{IR}$ 5.5 , the values of TC and PC are corrected for the effects of IR radiation transmitted through the cloud (TAUCOR). The revised cloud top temperature emission, BTCLD, is given by:

$$BTCLD = [BTOBS - BTCLR \exp(-\ _{IR}/\ )] / [1 - \exp(-\ _{IR}/\ )] \qquad (17)$$

where BTOBS is the observed IR radiance and BTCLR is the clear sky IR radiance from the clear sky composite. In some cases, usually a marginal VIS-only cloud detection that may be a dust storm or very thick aerosol event, BTOBS can be ε BTCLR so no correction is made to TC and PC. In some cases, $<$ $_{min}$, where to $_{min}$ is the smallest value consistent with the coldest possible value of TC = TT for an optically thin cloud. In this case, = $_{min}$, TC = TT and PC = PT, the tropopause pressure. If $_{min}$ / is too small, exp (-- $_{min}$/) < 0.001, then BTOBS is nearly equal to or less than the minimum possible value of BTCLD; this is interpreted to be an optically thick cloud (TC and PC are set to the same values as for a blackbody cloud). The revised value of TC determined from BTCLD is used to determine a new value of PC and then (visible) TAU is re-calculated with the new PC value. This whole

procedure is iterated until the change in PC < 50 mb and the change in TAU < 0.02. The iteration can also stop if the revised value of TAU, when converted to τ_{IR}/τ is > 5.5, which means that the cloud is too thick for further correction of TC and PC. The iteration also stops if the procedure is repeated more than 10 times, indicating no convergence to a solution. In this very rare situation no correction to TC and PC is made (blackbody values retained).

Finally, very small adjustments to TC and PC (but not TAU) are made for all clouds to account for IR scattering (SCACOR for liquid water clouds), but the smallest correction allowed is 0.2 K.

The above sequence of subroutines is then called again to produce values of TAU, TC and PC for ice clouds; in this case the conversion to $\tau_{IR} = 0.376\ \tau$ and SCAICE is called instead of SCACOR to correct for IR scattering.

The pixel-level output of the cloud detection, surface and cloud retrievals for each satellite forms the HXS product, which also includes radiances values from up to nine extra spectral channels, if available for a particular satellite. Cloud top temperature and pressure for blackbody clouds are reported for all times of day; daytime retrievals of cloud optical thickness and corrected cloud top temperatures/pressures are reported for retrievals assuming both liquid water **and** ice clouds. There is additional detailed information about the cloud detection and retrieval procedures that gives some indication of quality. This product does not report any of the Ancillary information except for flag values indicating categories of surface types, topography and the presence of snow or ice. Because of occasional image navigation errors (misplaced coastlines) that can produce erroneous clear sky radiances and spurious or missed cloud detections, all pixels within ±20 km of the coastline are removed in HXS. These are the only discarded pixels. The HXS products are globally merged to form the HXG product that contains only the information common to all satellites. See Section 3.4.7 and Appendix C for listings of the contents of HXS and HXG.

3.4.2 Data Merging Strategy

The original satellite images are space-time samples (at a variety of intervals) of the distribution of cloud and surface properties over the earth and over time. The images used for the ISCCP processing are further sampled to common 10-km (approximately) and 3-hr intervals (except for polar orbiters where all orbits are used). To preserve the statistics of pixel-level radiance values, which are good statistical representations of the full resolution satellite images (Seze and Rossow 1991b), all pixels are processed in a consistent fashion: a pixel is either cloudy or clear. To provide a nearly uniform sampling over the whole globe, an equal-area mapping is used for the reduced-resolution products (Rossow and Garder 1984).

Cloud amount (cloud cover fraction at one instant of time) is only estimated in the ISCCP products at larger spatial scales (in this case, at about 100-km scale) as the ratio of the number of cloudy pixels to the total pixel number in the larger domain. Because the pixels have a finite size (about 5-km across) the accuracy of cloud amount is reduced, but the cloud detection thresholds have been tuned so that the error in cloud amount is

approximately random (*cf.* Rossow *et al.* 1993). The precision of the cloud amount is dependent on the total number of pixels, which is limited to ε 25.

The retrieved quantities at pixel-level are encoded in (unsigned byte) COUNT values (0-255) that are designed to be linear in the measurements used to determine them (see Appendix C.7). In particular, the cloud and surface properties determined from satellite-measured radiances are encoded approximately in linear intervals of measured energy. When averaging these properties over space or time, the COUNT values are averaged to preserve proper radiative weighting. When averaging over time, the best statistical practice is to average first over the quasi-random part of the signal, in this case, the synoptic (day-to-day) variations at constant times-of-day, and then to average over time-of-day as diurnal variations are the regular part of the signal.

To provide different kinds of information about clouds, several different products are produced. The pixel-level results for individual satellites (HXS), which view overlapping spatial domains, are reduced in volume by mapping them to a 1-degree-equivalent equal-area grid: this process involves determination of cloud cover fraction, spatial averaging of cloud and surface properties, and determination of some additional sub-grid information (see below, also see Appendix C for details) to produce the HGS product, which is still separate by satellite and at 3-hr intervals. In addition, this product includes the Ancillary atmospheric and surface data.

The ISCCP processing stream for a month of data analyzes in parallel all of the satellites in the seven standard sectors (see Figures 2 and 3): afternoon and morning polar orbiters, Africa-Europe, Indian Ocean, West Pacific, East Pacific, Americas. The HXS and HGS products for these sectors are merged into two global products, HXG and HGG, respectively, at 3-hr intervals. The former is mapped in a 0.1-degree equal-angle grid, preserving the approximate spatial sampling of the pixel-level data, and the latter is mapped in a 1-degree-equivalent equal-area grid. The merger process is designed to compromise between the best available view of each location (largest value of ⌈) and the most uniform time sampling. This compromise establishes a preference hierarchy of satellites for each Earth-location depending on the set of satellites available in a given month (Figure 3). At lower latitudes (cell center latitude < |55°|), results from geostationary satellites are the first preference; if more than one geostationary satellite is available, the results from the geostationary satellite with the larger value of ⌈ are preferred. If no geostationary results are available, then the afternoon polar orbiter results are used. If no geostationary or afternoon polar orbiter data are available, results from the morning polar orbiter are used. At higher latitudes (cell center latitude ε |55°|) results from the afternoon polar orbiter are first preference; second preference is the morning polar orbiter. If results are not available from either polar orbiter, then geostationary results are used if available. Map locations in the HXG and HGG products are thus filled by searching for results in the HXS and HGS products in descending hierarchy order.

As part of the reduction of spatial sampling to produce HGS from HXS (approximately 100-km from 10-km), various statistics are calculated from the available pixels (limited in number to ε 25). In addition to cloud cover fraction (ratio of cloudy to total pixel number),

the average properties (and spatial standard deviation) of all clouds (from cloudy pixels) and the surface (from clear sky composite for all pixels and from clear pixels, if available) are determined, where the averaging is “radiatively weighted” for some quantities. More “sub-grid” information is provided in terms of cloud type information and 1-D and 2-D histograms of cloud properties. IR radiances are available at all times of day, so results solely from IR cloud detection and blackbody cloud retrieval are reported in form of a 1-D histogram of cloud top pressures (number of pixels in each of seven pressure intervals) and in terms of the amount and mean top temperature/pressure of low, middle and high cloud types, defined by PS ε PC > 680 mb, 680 ε PC > 440 mb and 440 ε PC. During daytime results from the combined IR and VIS analysis are also reported in the form of a 2-D histogram of cloud top pressures and optical thicknesses (number of pixels in the joint seven pressure – six optical thickness intervals). The pressure and optical thickness intervals in the 1-D and 2-D histograms are as follows: PS-800, 800-680, 680-560, 560-440, 440-310, 310-180, 180-10 mb and 0.02-1.27, 1.27-3.55, 3.55-9.38, 9.38-22.63, 22.63-60.36 and 60.36-450.

In addition the amount, mean cloud top temperature/pressure, mean optical thickness and mean water path of 18 cloud types defined by two phases (liquid for TC ε 253.1 K, ice for TC < 253.1 K) and by nine combinations of cloud top pressure intervals (PS ε PC > 680 mb, 680 ε PC > 440 mb and 440 ε PC), optical thickness intervals (0.02 δ TAU < 3.55, 3.55 δ TAU < 22.63 and 22.63 δ TAU δ 450) (Figure 20). Note that the cloud types are defined by the values of PC and TAU but that the phase (and the PC and TAU values used) are determined by TC. In some rare instances, the pixel-level TC for the ice cloud retrieval can be ε 253.1 K while TC for the liquid cloud retrieval is < 253.1 K. Thus, for consistency, the phase decision logic is: (1) if TC (liq) ε 253.1 K, the phase is liquid, (2) else if TC (ice) < 253.1 K, the phase is ice, (3) else the cloud is counted as ice but the liquid cloud retrieval values of PC and TAU are used.

An additional cloud property, called Water Path (WP), is determined from the **linear** average of TAU values using conversion factors given in Section 3.3.4. Note that TAU averages are performed in COUNTS, linear in energy.

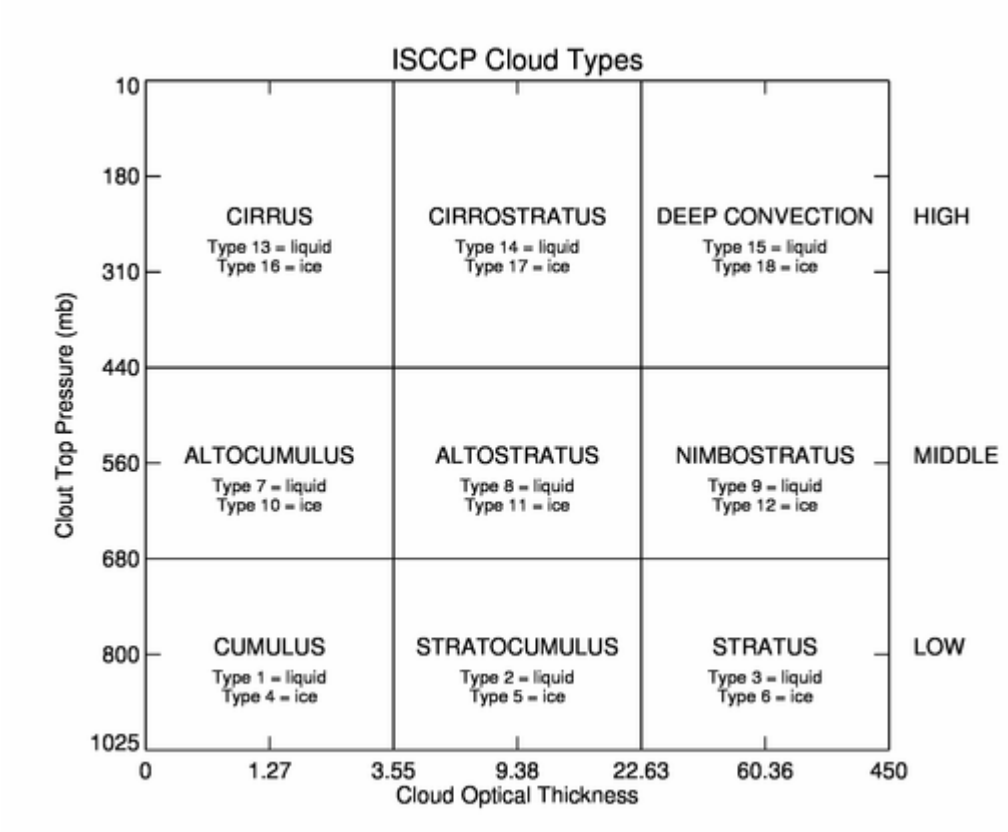

Figure 20: *Cloud types defined by PC-TAU ranges*

Nighttime Adjustments: Two changes to the nighttime grid-average cloud properties are made in the HGG product. The nighttime values of the grid cell values of CA, PC and TC are originally equal to the IR values, but are adjusted based on interpolation between the nearest daytime difference between these quantities (21 hr), which can only increase CA (capped at 1.0) and decrease PC/TC (capped by the tropopause values). In addition the daytime values of TAU, WP and the number of VIS/IR cloud types, which were originally set to 255, are interpolated from adjacent daytime values. Flag values indicate these changes. Given these changes, the grid-averaged cloud properties and the weighted-average of the cloud type properties in monthly averaged products (HGH, HGM) are no longer consistent. Consistency can be restored by scaling the time-averaged cloud type properties by the ratio in Counts of the grid-averages and the cloud type-weighted-averages.

Fill Procedure: Several procedures are performed to attempt to fill in missing satellite data (as indicated by flag values); missing values that remain are set to 255. In the HXG product, a simple and limited replication in space or interpolation in time is performed as indicated by a flag and described in the summary at the end of the nc_dump-h output: replication from the nearest longitude within 3, or replication from the nearest latitude within 3, or interpolation in time by 3 hr. In the HGG product the included Ancillary data have their own Fill procedures so they are always present in every map grid cell. First, interpolation from adjacent time slots (3 hr) at each location is attempted. If unsuccessful, interpolation from nearest day (within 5 days) at the same time of day at each location is attempted. A special polar procedure replicates results from nearby (3) equal-area cells, first in

longitude, then in latitude. Finally, if needed, interpolation from nearest week (within 2 weeks) is attempted. Some cells may remain empty: in particular, since the near-coastal image pixels are deleted to avoid problems of earth-location errors, there are 10 map cells (mostly in the Maritime Continent area) that never have satellite data because there are not enough pixels available. The HGG Fill Procedure is described at the end of the nc_dump output and documented by flag values. Any still missing quantities are reported as COUNT = 255.

Two time-averaged gridded products are produced from the filled HGG product. To reduce the dependence of average values on the sampling for a time signal that contains both quasi-random and quasi-regular components, the averages should be made first over the random component at constant phase of the regular component. In this case, the HGH product is the monthly average of the HGG results at each time of day UTC. This approach averages over the synoptic (day to day) variations at constant diurnal phase. The full monthly average, HGM, is the average of the eight HGH products for each month.

Since most earth targets are radiometrically constant across the spectral interval of these narrow channels, the radiance calibration approach to combine data from all seven satellite processing streams used by ISCCP reduces the sensitivity of the results to the small differences in spectral response by representing the VIS radiances as a value scaled by the instrument "solar constant" and the IR radiances as brightness temperatures. The instrument "solar constant" given in Appendix B is the wavelength integral of the product of the normalized spectral response function and the solar spectrum at the top of the atmosphere and the brightness temperature is the wavelength integral of the normalized spectral response function (see Appendix B for the satellite-specific values of the "solar constants" and the IR bandwidths).

3.4.3 Numerical Strategy

The main numerical strategies used in each processing step are as follows:

- **Mapping step** – double precision computation of General Vertical Perspective and Lambert Azimuthal Equal Area map projection equations
- **Cloud detection algorithm step**s - common statistical methods (histograms, medians, means) and nearest neighbor regional search windows in (i,j) coordinate space (image coordinates), thresholding against parameterized limits based on surface types
- **Cloud and Surface property retrieval step** – radiative transfer formulas, look-up tables, atmospheric profile searches, interpolation and extrapolation
- **Gridding step** - geographic binning, accumulation of integer counters, averaging of property values within grid cells
- **Global merging step** - hierarchical selection of preferred satellite based on viewing geometry, linear interpolation to fill missing values
- **Temporal averaging steps** - accumulation of integer counters, averaging of property values over time. Time averaging is done by first averaging over day-to-day variations at each time of day – the quasi-random part of the signal, and then averaging over time of day – the regular part of the signal.

Two specific features of the data processing are designed to preserve the original image radiance sampling in the output quantities. The physical quantities retrieved from the radiances are reported with 8-bit precision, similar to the original radiance precision, and with non-uniform intervals that are approximately linear in radiometer energy. Quality checking and control of the input radiances is crucial to product quality because the processing does not discard any pixels (except for near-coastal ones) – all pixels are processed so that the resulting sampling is the same as in the original images.

3.4.4 Calculations

All calculations are described in previous sections.

3.4.5 Look-Up Table Description

3.4.5.1 Tables in the code

There are Look-Up-Tables in the analysis codes that are used at various stages of the analysis (see also Ops Guide Section 4.12).

AVEAB9.TAB42 and AVEABN9.TAB4 (used in NNHIRS to TBNN) contain water vapor absorption coefficients.

NOA9CH4.RADTMP (used in NNHIRS and DXPROD) is a table used to convert IR brightness temperatures to physical radiance units and back; the physical radiances are used in retrievals of surface and cloud temperatures. The relationships in this table assume the spectral response function of NOAA-9, to which all other radiometers are normalized, and blackbody spectral distribution (Planck function).

ANGCOR4.DATA (used in B4PROD, CLRSKY, BXPROD, CYPROD) is used to correct IR radiances viewed at any angle (μ = cosine satellite view angle) to nadir (μ = 1) and back. The correction to nadir allows for comparison of views at different angles to produce the clear sky composite; the reverse relationship adjusts the clear sky composite values to the view of a particular pixel. The relationships are only meant to be approximate and are based on the NOAA-9 spectral response and global, annual mean temperature and water vapor profiles for the whole depth of the atmosphere. Although applied to all satellites for consistency, only the polar orbiter data actually requires this treatment.

GLNTAB.DATA (used in BXPROD) contains the open water glint model used in the Version C/D parts of the cloud detection algorithm but replaced by a more accurate model in the H-Version cloud retrieval.

LNDOCN.TABLES (used in BXPROD and CYPROD) contains the land and ocean visible reflectance models.

MYCLR_SKY_AODFINE_OCN.DAT (used in CYPROD) contains the new ocean visible reflectance model.

IREMISS (in DXPROD code) is a small table that assigns a value of surface IR emissivity as a function of SURFACETYPE.

PTRANS_sssnn.DATA (for each satellite sssnn, used in DXPROD) is used to correct VIS radiances for stratospheric ozone absorption using ozone abundance from OZONE and the results of PTRANS, which calculates the absorption coefficients for each individual satellite spectral response.

ISCACO2.DATA (used in DXPROD) contains the IR scattering correction.

RADDIF_STRTAOD_NOSRF.DAT (used in DXPROD) is used to correct VIS radiances for scattering and absorption by stratospheric aerosols using stratospheric AOD from AEROSOL. This pre-calculated table assumes that stratospheric aerosols are composed on sulfuric acid and have an effective radius of 0.5 ⌈m.

A LUT for VIS radiances (corrected for specific sun-earth distance, ozone and stratospheric aerosol effects) under clear sky conditions (computed in QAGRD1 from two input LUT files MYCLR_SKY_AODCOARSE.DAT and MYCLR_SKY_AODFINE.DAT) returns two values of surface reflectance, one dependent on tropospheric AOD from AEROSOL and one assuming AOD = 0. The reflectance is also a function of surface pressure and illumination and viewing geometry. This table is applied to all surfaces, but the retrieved reflectances over oceans are replaced by a more accurate model of surface reflectance for cloud retrievals.

Six LUTs for VIS radiances (corrected for specific sun-earth distance, ozone and stratospheric aerosol effects) are used for cloud-covered conditions to return cloud optical thickness values over three different surface types. Two LUTs are for clouds over water (M_WTRTAUHIBRCH_AODOCN.DAT for liquid, M_ICETAUHIBRCH_AODOCN.DAT for ice, used in TAUVF2), two are for clouds over land (M_WTRTAUHIBRCH.DAT for liquid, M_ICETAUHIBRCH.DAT for ice, used in TAUVF), and a special two for clouds over snow-ice that are darker than the surface (M_WTRTAULOBRCH.DAT for liquid, M_ICETAULOBRCH.DAT for ice, used in TAUVFP). The LUTs in TAUVF2 employ a detailed water surface reflectance model (including glint effects) and corrects for tropospheric aerosols using AOD and fine fraction from AEROSOL. The LUTs in TAUVF account for tropospheric aerosol by using the special value of surface reflectance that combined aerosol and surface effects. The LUTs in TAUVFP account for situations where a cloud is darker than a bright surface (snow-ice-covered). All of these LUTs return cloud TAU values for either liquid or ice clouds and are functions of cloud top pressure and illumination and viewing geometry.

TABCNT4.DATA (used in all steps) that converts the retrieved cloud and surface properties (cloud top temperature/pressure, cloud optical thickness, surface temperature and reflectance), as well as the atmospheric ozone abundance and temperature and relative humidity profiles, into COUNT values that control the range and precision of the results. The COUNT values for retrieved variables are linear in measured energy.

CNTTAB4.DATA (used in all steps) converts the COUNT-coded quantities back to physical values (see Appendix C.7).

3.4.5.2 Tables in the Data Products

The COUNT-CONVERSION tables from CNTTAB4.DATA (see Appendix C.7) are included in the netCDF formatted data products and are used to convert the COUNT-coded quantities to physical values. Tables are provided for temperatures and temperature spatial variance (in Kelvins), pressures (in mb), reflectivities (unitless), cloud optical thicknesses (unitless), ozone abundance (in Dobson units), relative humidity (in percent) and cloud water path (in g/m^2). There are two key inter-relationships in these tables: the reflectivity values corresponding to each cloud optical thickness value give the spherical albedo of the cloud (scene albedo if there is no gas and the surface is black) and the water path values corresponding to each cloud optical thickness value give the linearly-averaged values of optical thickness in contrast to the radiatively-averaged value that is obtained by averaging COUNT values.

3.4.6 Parameterization

The radiative model calculations underlying the cloud and surface property retrieval procedures are very accurate as discussed above, so the accuracy of the results depends more on the assumed properties of the clouds, atmosphere and surface. Since very specific fixed properties are assumed, this constitutes a parameterization of the satellite radiances. The advantage of this approach is that these assumptions can be easily changed given better (climatological) information. Indeed, this version of the ISCCP products, the third, differs from the previous two versions almost entirely in terms of small changes in the assumed cloud properties. The main new fixed features of clouds are: finite layer thickness ranging from 100 (lower-level clouds) to 200 mb (upper-level clouds) composed of gas and either spherical droplets for liquid water clouds (effective radii are 13 ⌈m over land and 15 ⌈m over ocean and an effective variance of 0.1) or a mixture of crystal shapes producing an empirical scattering phase function for ice clouds (effective radii are 20 ⌈m for TAU < 3.55 and 34 ⌈m for TAU ε 3.55). Aerosol properties are as follows: stratospheric aerosols are assumed to be composed of sulfuric acid with an effective radius of 0.5 ⌈m and tropospheric aerosols are assumed to be a mixture (controlled by the fine fraction) of sulfuric acid with an effective radius of 0.5 ⌈m and mineral dust with an effective radius of 1.0 ⌈m. All surfaces have an assigned IR emissivity by type and are assumed to isotropic reflectors except for open water, which is represented by a detailed reflectivity model.

3.4.7 Algorithm Output

The basic retrieved or calculated quantities reported at pixel-level (Level 2, HXS and HXG products) are as follows: (1) cloud-clear threshold flags, (2) cloud top temperatures (and corresponding atmospheric pressures) for a blackbody cloud (all day), for a liquid water cloud and for an ice cloud (daytime only), (3) cloud optical thickness and cloud water path for a liquid water and ice cloud (daytime only), (4) surface skin temperature from the clear sky composite and for clear pixels and (5) surface reflectivity from the clear sky composite and for clear pixels. The cloud-clear threshold flags show which radiance channel test indicated cloud or clear conditions by classifying the relationship of the pixel-observed radiances relative to the clear sky composite radiances (see Figure 16). Flag values are also reported to indicate the quality of the retrievals.

When the pixel-level product (HXS) is mapped to the gridded products, HGS and HGG, one additional cloud property is determined: cloud amount (CA) is determined by the ratio of cloudy pixel number to total pixel number. At one instant of time (HGS and HGG), this quantity is cloud cover fraction. When averaged over time (HGH, HGM), this quantity is cloud cover fraction times frequency of occurrence. To preserve nearly uniform precision of CA, the gridded products are mapped into an equal-area map (Rossow and Garder 1984), defined by equal latitude increments and variable longitude increments that preserve the area. The gridded products also report cloud type statistics where a phase decision is made, separating liquid water (TC ε 253 K) from ice clouds (TC < 253 K), and reporting average cloud top pressure (PC) and optical thicknesses (TAU) for nine combinations of three pressure intervals, PS ε PC > 680 mb, 680 ε PC > 440 mb and 440 ε PC), and three optical thickness intervals, 0.02 δ TAU < 3.55, 3.55 δ TAU < 22.63 and 22.63 δ TAU δ 450 (see Figure 18).

See Appendix C for a complete list of quantities in the Cloud Products and Appendix D for a complete list of quantities in the Ancillary Products.

4. Test Datasets and Outputs

This version of the ISCCP products is a small refinement of the previous version, so the published literature on the evaluations of the previous versions is relevant to quality assessment. Discussion of evaluations of the overall quality of the ISCCP products is presented in Section 6; below some of the datasets used for these evaluations are listed. Here we also describe the Test Package delivered with the complete ISCCP processing system code that is used to confirm the implementation of these codes on different computer systems

4.1 Test Input Datasets

Three specific tests of the ISCCP processing system have been performed: (1) a test to establish the sensitivity of the total cloud amount (CA) and cloud type amounts to changes in radiance calibration, (2) a test of the sensitivity of the monthly total cloud amount to variations in the space-time coverage, and (3) a test of the angle dependence of the retrieved cloud and surface properties at pixel-level and in the gridded products.

Figure 21 directly demonstrates the effect on total CA, as well as the CA of four cloud types, caused by artificially changing the radiance calibrations separately for visible and infrared radiances and re-processing the data with all other factors being identical. The estimated uncertainties of the calibrations (see Section 6.2.2) are about 3% for VIS and 2% for IR. These test results show that the ISCCP values of total CA are not dependent on radiance calibration: the estimated calibration uncertainty translates into uncertainties of CA < 0.5% and < 1.0% for the cloud types.

Over the whole ISCCP record to date (1983-2009), space-time coverage was on average 93%, but varied from a low of 70% to a high of 98%. Note that the monthly mean products actually cover the whole globe; the lower coverage fractions represent missing time samples during the month over some portions of the globe. To test the effect of the missing

data on the determination of global mean CA, the monthly global mean CA was re-calculated for the month with maximum coverage, August 1998, after removing the same locations and times missing in the month with minimum coverage, August 1984. Although the standard deviation of geographical differences in CA is ±0.02, the global mean difference in CA is < 0.01. The missing data is apparently sufficiently randomly distributed that the global mean CA is not significantly affected.

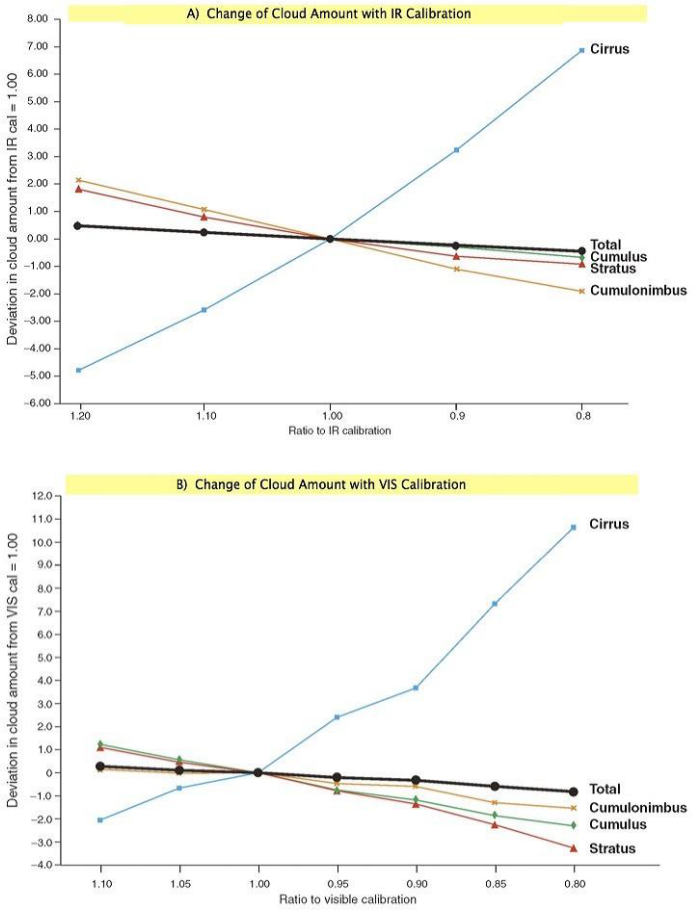

Figure 21: *Change of global, monthly mean cloud amounts in percent produced by artificial changes of (A) IR radiance calibration and (B) VIS radiance calibration*

Because the ISCCP cloud detection procedure uses constant radiance thresholds, the detection sensitivity varies with satellite viewing zenith angle in the presence of optically thin clouds. Several studies show the presence of pervasive very thin cirrus, especially at lower latitudes: comparison of ISCCP to the limb-viewing SAGE cloud detections (Liao *et al.* 1995a), comparison of ISCCP and HIRS cloud amounts (Jin *et al.* 1996, Wylie and Menzel 1999, Stubenrauch *et al.* 1999), comparison of HIRS-Wisconsin and SAGE (Wylie and Wang 1997), comparison of ISCCP to CALIPSO lidar (Mace *et al.* 2009), and comparison of all of these instruments to ISCCP and MODIS-based cloud amounts (Stubenrauch *et al.* 2012, 2013). Figure 22 demonstrates this dependence by showing for April 2009 the systematic

difference of total CA between pairs of geostationary satellites viewing the same locations at the same time but from different angles: the difference in CA with difference in cosine satellite zenith angle, ⌈ (the sign of ΔCA is negative and the sign of Δμ is positive for the satellite to the west in each pair). The varying regression slopes (with satellite pair, season and year) are related to the amount of cirrus cloud present in each region in each month as is demonstrated by the last panel in Figure 22 that shows the relation of the monthly mean cirrus cloud amount in the overlapping regions with the regression slope values for all the months in 2009 (both values are the anomalies normalized by their standard deviations): more negative regression slope values are associated with larger cirrus cloud amounts.

Similar satellite-pair plots for pixel-level retrieved cloud and surface properties show much smaller angle dependencies compared to that of the original radiances (*cf*. Rossow 1989). This supports the conclusion that the angle dependence of the gridded quantities, shown in Figure 22, is dominated by the detection sensitivity variation with view angle.

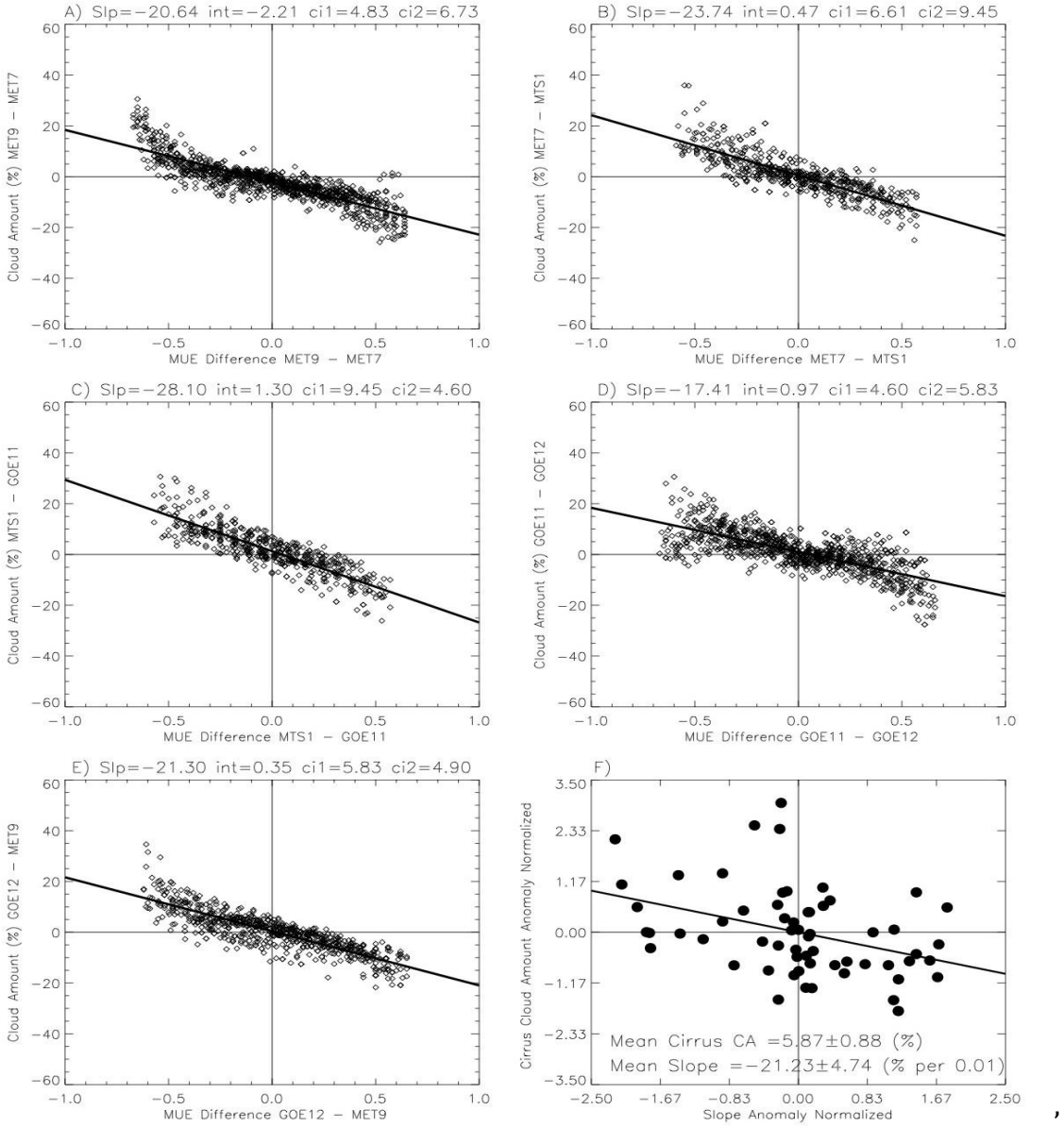

Figure 22: Difference of total cloud amount between pairs of geostationary satellites viewing the same locations at the same time but from different angles. Lower right panel shows relation of fit slopes in other panels to average cirrus cloud amount

The global, multi-year datasets used for evaluations of the ISCCP products (discussed in more detail in Section 6) included the collection of cloud amount estimates from surface weather station observers (Warren *et al.* 1986, 1988, Hahn *et al*. 2001), observations by the limb-sounding instrument, SAGE (Liao *et al.* 1995a,b), two different analyses of infrared sounder (HIRS) data (Wylie and Menzel 1999, Stubenrauch *et al.* 1999), cloud products produced by MODIS and MISR (*cf.* Marchand *et al*. 2010), the merged CloudSat and CALIPSO data (Mace *et al.* 2009) and eleven other global cloud products in the GEWEX Assessment (Stubenrauch *et al.* 2012, 2013).

The final delivery of code was called Build 5. Together with all the software for the complete ISCCP processing system, all of the required calibration tables and ancillary datasets for July 2007 are also included in the package. These datasets are (1) HBT (calibration) for all satellites, (2) NNHIRS atmospheric temperature-humidity profiles, (3) OZONE abundance, (4) AEROSOL optical properties, and (5) SNOWICE cover fraction, as well as other fixed datasets (TOPO, SURFACETYPE). To run the system all that is needed is to input the GAC and B1U radiance images from the NOAA archive for all satellites (in this case, NOAA-17, NOAA-18, METEOSAT-7, METEOSAT-9, MTSAT-1, GOES-11 and GOES-12).

A slightly modified version of the code, together with this document and the test input data (except the radiances) is available to the public from https://www.ncdc.noaa.gov/cdr/atmospheric.

4.2 Test Output Analysis

The comparison of the previous D-Version of the ISCCP products to eleven other global cloud products is documented by a GEWEX database that contains the versions of all of the products that were compared (http://climserv.ipsl.polytechnique.fr/gewexca/). A summary of the comparison results is published in Stubenrauch *et al.* (2013).

The test output dataset is all of the cloud products (HXS, HXG, HGS, HGG, HGH and HGM) for July 2007 (see samples in Figure 23) produced at NASA GISS by the processing code development team. Included in the package are a set of plotting routines to check data quality; in this case they are used to confirm implementation of the processing system: B4PLOTS, HXS-HIST, HGG-HIST and HGM-HGM.

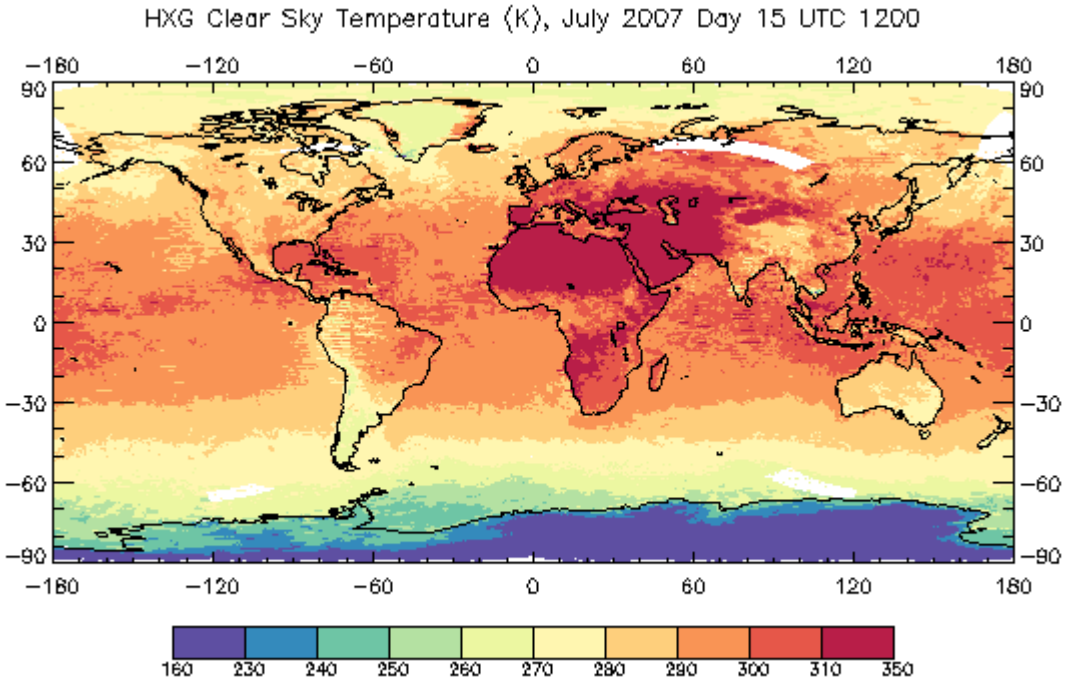

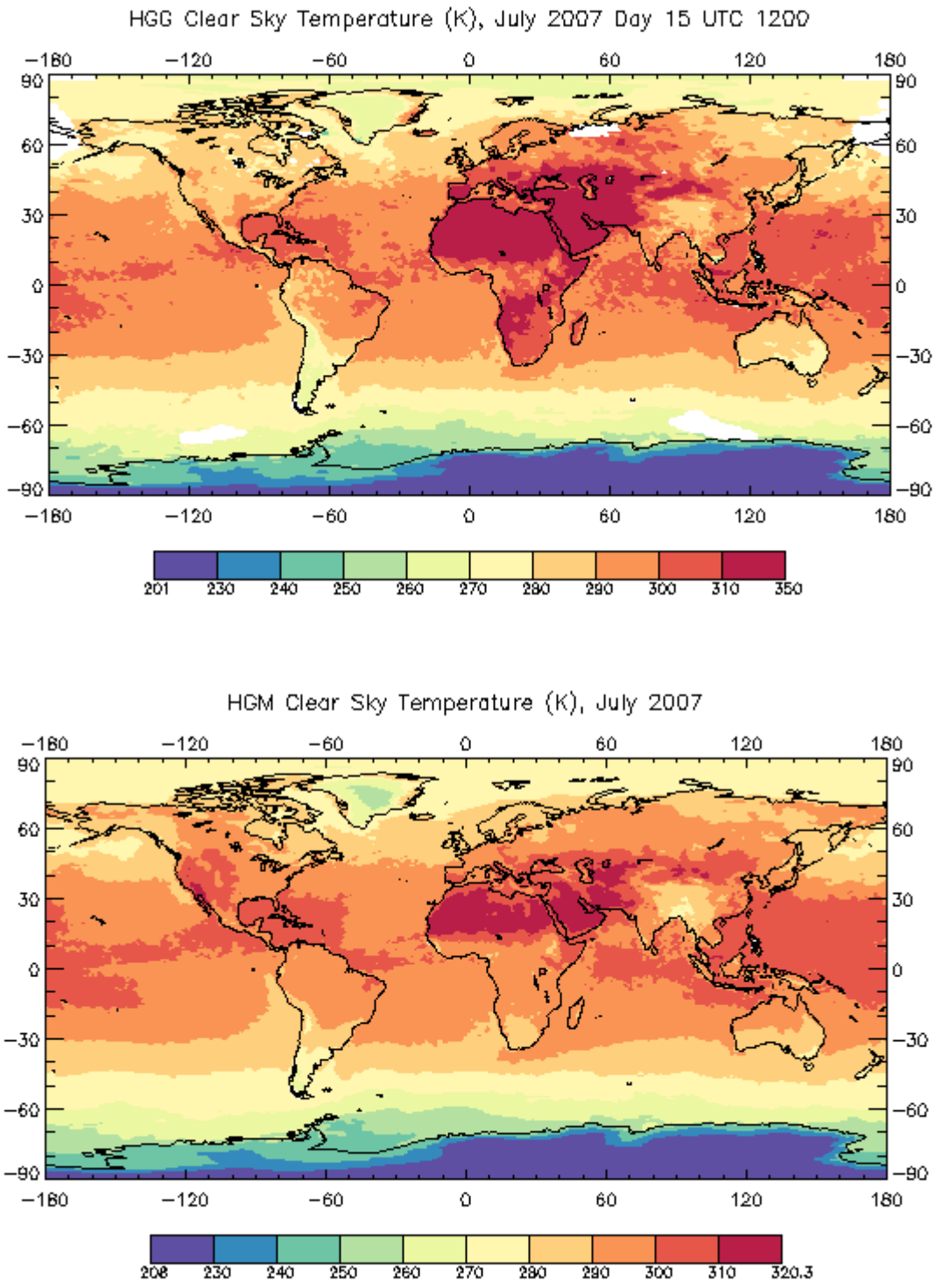

Figure 23: *Sample HXG, HGG and HGM maps of TS for July 2007*

4.2.1 Reproducibility

Reproducibility is tested in two ways. The Build 5 code delivery package contains all of the inputs to produce the main cloud products for one month, with the exception of the GAC and B1U image data files that are available from the NOAA archive. The output produced on another computing system should be nearly identical to the version produced by the developers: some small (<< 1%) differences will occur because of differences in computer system precision. The second test of reproducibility is that during the re-processing of the base data period (July 1983 – December 2009), the period covered by the previous version of the products, each month of H-Version products will be compared to the corresponding D-Version. There will be differences because of refined algorithm and retrieval procedures and changes of input datasets, but these differences should also be small (generally a few percent).

4.2.2 Precision and Accuracy

Most internal computations are integer or single-precision (R*4). The satellite navigation (latitude, longitude, viewing geometry) is double-precision (R*8). The ISCCP product variables are encoded as integer COUNT values, which controls the precision of the output quantities to approximately that of the original radiance measurements. Round-off errors from internal computations are within the precision of the output products. The precision of the output quantities is equivalent to 8-bit values.

4.2.3 Error Budget

See Section 6.

5. Practical Considerations

5.1 Numerical Computation Considerations

Results are not dependent on “endian-ness” of internal representation. The system runs on both “big-endian” or “little-endian” machines and output products are either integer values or NetCDF internal representation. Most internal computations are integer or single-precision (R*4). The satellite navigation (latitude, longitude, viewing geometry) is double-precision (R*8). The ISCCP product variables are encoded as integer COUNT values. Look-up tables are provided to convert the integer values to physical values. Round-off errors from internal computations are within the precision of the output products.

Each month of data processed is a single processing stream, composed of many individual executable steps with a controlling script. Each satellite sector (see Figures 2 and 3) is processed in parallel. Parallelization can be achieved through multiple processing streams, each processing a different month. The satellite navigation and mapping in the first processing step is the most computationally intensive part of the process.

5.2 Programming and Procedural Considerations

Quality control (QC) and instrument calibration of the input data are necessary and essential to ensure quality product results. The automated production system is designed to process whatever input data is available, in whatever condition it is found, so the raw satellite input data must be carefully checked and calibrated before beginning production in order to avoid "garbage-in -- garbage-out" situations. There are quality assurance procedures that are used during and after the production to ensure product quality.

The production system configuration is controlled via Unix shell environment variables, including specification of locations of input data directories. Satellite characteristics and relevant parameters are specified in a satellite history sub-system. Production is initiated by using a scheduling GUI to generate a task list for a particular time period, usually one calendar month. A single Perl script is then initiated to sequentially identify and run individual processing steps until the task list has been completed. Production takes place as a series of executable steps, each of which reads the output from the previous step and writes output for the next step. Each step is a Fortran 90 code unit with an associated Perl script to set parameters and manage the input/output files. The top-level run script initiates steps, checks return codes and error messages, and determines the next step to run.

Run-time may be decreased by running multiple production streams in parallel. As long as they are processing different time periods there is no conflict. Required disk space may be reduced by activating the automatic clean-up function whereby intermediate files are removed as soon as they are no longer needed. This version of the ISCCP processing has options to run in alternative modes: in "calendar" mode the radiance statistics used for cloud detection are collected from fixed time intervals in each month, in "real-time" mode the radiance statistics are collected from the time interval preceding the given image date, in "climate" mode, the time intervals slide in time to center approximately on a given day. Normal production mode is calendar mode.

The system architecture and production procedures are described in detail in the ISCCP Operations Guide (see Appendix F).

5.3 Quality Assessment and Diagnostics

There are QC procedures that are run pre-production, during production and post-production to ensure data product quality. See description in Section 3.2 and OPS Guide in Appendix F. Quality assessment and diagnostics occur in various parts of ISCCP H-Series architecture:

Pre-production: (1) Examination of automatically generated QC results for the satellite images and Ancillary processing, (2) Visual inspection of questionable input images, (3) Repair or quarantine (remove from production) bad images

During production: Examination of radiance and cloud algorithm result plots (B4PLOT) that are automatically generated to identify anomalies for investigation

Post-production: (1) Examination of log warnings, (2) Examination of monthly mean maps (either HGM_D2 plots or HGM_HGM plots), (3) Examination of global monthly mean anomaly plots to evaluate long-term trends (D1STATS)

Problem Investigation: Other plot programs available show summary statistics (histograms) from HGG and from HXS.

These QC procedures and diagnostic plots are described in detail in the ISCCP Operations Guide (see Appendix F).

5.4 Exception Handling

Expected exceptions include bad or missing inputs, invalid data values encountered during processing and errors creating output files. All exceptions are handled by a single error function that generates informative messages that are printed in text log files. After each executable step finishes, the text log files are automatically scanned for any messages. These are of two types: non-fatal "warnings" and fatal "errors". Any non-fatal warnings found in the log files are summarized and echoed to the operator console and production continues to the next step. These should be investigated. Any fatal errors found in the log files cause production to halt until the operator takes corrective action and then re-starts the system. Histograms of the output quantities can be monitored for excessive frequency of occurrence of the limiting values.

5.5 Algorithm Validation

The re-engineered modernized code was validated by running it on the B3 data input, producing previous D1/D2 products and doing a byte-by-byte comparison to the original D1/D2 products, before any code enhancements were done. The subsequent code enhancements (new higher-resolution inputs, algorithm changes, H-product formats) were then evaluated by statistical comparisons to the original D1/D2 products. The transfer of code to NCEI for operational use was validated by using the July 2007 test package with fixed inputs and known expected outputs to compare results produced at NASA GISS with those produced at NCEI.

The scientific evaluation of the whole ISCCP analysis is founded on the work for the previous two versions of the product since the H-Version is only a small modification. The Uncertainty discussion given in Section 6 is based on all of the prior research (see cited references). Many of the changes from the D-Version to the H-Version are based on the results of a comprehensive comparison of the ISCCP D-Version products to eleven other global cloud products (Stubenrauch *et al.* 2012, 2013). However, assessment of the products is an on-going research task.

5.6 Processing Environment and Resources

The ISCCP production system is portable and has been built and run successfully on a variety of Linux and Mac OS X operating systems. It may be built on both 32-bit and 64-bit hardware, using Gnu "make" utility to automatically select appropriate compiler options. "Endian-ness" is handled by configuration parameters allowing the system to run on either "big-endian" or "little-endian" machines without code changes. Software is written in Fortran 90, Perl 5 and IDL 8. The Fortran 90 program units have been successfully compiled with GNU, Intel and Lahey compilers.

Test production runs at NASA GISS on a shared Mac OS X machine (x86_64, Darwin 11.4.2, 1.6G memory) required 19.5 CPU hours to run one calendar month and used 580G of disk space when not erasing any intermediate files. The ISCCP processing is I/O intensive and benefits more from increased memory than from increased CPU. Currently products are produced at NCEI on significantly faster blade server hardware with CPU time under 10 hours per month, and the ability to run many months in parallel.

Additional 3rd party software that is required:

- Tk.pm Perl module, available from www.cpan.org
- NetCDF4, which requires also HDF5
- NCO NetCDF Operators, available from nco.sourceforge.net

6. Assumptions and Limitations

The current version of the ISCCP analysis represents relatively minor adjustments to the cloud detection algorithm, some changes to radiative transfer model used for retrievals and more detail in the statistics reported. Small refinements of the radiance calibrations and improvements of the radiance image quality checking have also been made, but the largest changes are improvements of the Ancillary data. All of these changes are summarized below. Some assumptions and limitations have already been discussed in Section 3.1. The following discussion and quantitative estimates of uncertainty are based on many years of research as documented in the publications listed at the beginning of each sub-section below.

CHANGES from C-Version to D-Version to H-Version

Radiance Calibrations from C-Version to D-Version: (1) Revised VIS and IR calibrations to remove spurious changes between different polar orbiters. (2) Revised geostationary satellite normalization to remove occasional short-term deviations.

Radiance Calibrations from D-Version to H-Version: (1) Anchor for VIS calibration extended to combined results for NOAA-9 and NOAA-18, spanning most of the time record. (2) Overall IR calibration for the newer AVHRRs (NOAA-15 *et seq.*) adjusted for small gain error in AVHRR calibrations compared to MODIS. (3) Geostationary normalization

procedure changed to use all of the radiance data directly instead of a small number of special samples – manual procedures eliminated.

Cloud Detection Algorithm from C-Version to D-Version: (1) Improved cirrus detection with smaller IR thresholds over land. (2) Improved cloud detection over snow and ice with smaller VIS thresholds and added test at 3.7 ⌈m wavelength. (3) Improved low cloud detection at high latitudes by changing VIS threshold test to reflectance difference instead of radiance difference.

Cloud Detection Algorithm from D-Version to H-Version: (1) Added new radiance space contrast test inside original regions that are land-water mixtures. (2) Updated surface type categories for algorithm tests; in particular improved tests in rough topography. (3) Revised daytime cloud detection over snow and ice by eliminating 3.7 ⌈m tests (no longer available) and implementing simpler test for reversed VIS radiance contrast situations to improve homogeneity of record. (4) Improved summertime polar cloud detection by reducing VIS thresholds over snow and ice. (5) Improved wintertime polar cloud detection by changing marginally cloudy to clear and marginally clear to cloudy.

VIS and IR Radiative Models from C-Version to D-Version: (1) Improved treatment of cold (ice) clouds by introducing explicit ice microphysics with a polycrystal scattering phase function for TAU retrievals. (2) Improved TAU retrieval over snow and ice, when radiance contrast is reversed, using 3.7 ⌈m radiances. (3) Improved TC retrieval by accounting for IR scattering by clouds. (4) Improved cloud and surface temperature retrievals using more modern treatment of water vapor continuum IR absorption.

VIS and IR Radiative Models from D-Version to H-Version: (1) Replaced ocean VIS reflectance model with more accurate version with explicit glint treatment. (2) Calculated instrument-specific ozone absorption coefficients. (3) Added water vapor above 300 mb level in atmospheric ancillary data. (4) Added treatment of stratospheric and tropospheric aerosol scattering and absorption. (5) Improved surface temperature retrieval by accounting for variations of surface IR emissivity by surface type. (6) Introduced explicit atmospheric and cloud vertical structures for retrievals. (7) Revised specified liquid cloud droplet effective radius from 10 ⌈m everywhere to 13 and 15 ⌈m over land and ocean, respectively. (8) Changed TC value identifying ice phase clouds from 260 K to 253 K. (9) Updated ice cloud scattering phase function to empirically-based model and revised specified ice particle effective radius from 30 ⌈m for all clouds to 20 and 34 ⌈m for clouds with TAU < 3.55 and TAU ε 3.55, respectively. (10) Corrected placement of thin clouds from just above the tropopause to just at the tropopause. (11) Added treatment of cloud top location when surface temperature inversions are present. (12) Updated solar ephemeris to epoch 2000.

Gridded Product Contents from C-Version to D-Version: (1) Added sixth TAU category for histograms. (2) Added cloud water path parameter. (3) Added average properties of cloud types. (4) Added separate results for liquid and ice forms of each cloud type. (5) Provided conversion of PC to cloud top heights. (6) Added cloud amount frequency distribution to monthly products.

Gridded Product Contents from D-Version to H-Version: (1) Spatial sampling changed from 30 km to 10 km. (2) Revised the COUNTS-to-physical conversion tables to remove special values for underflow and overflow. (3) Increased uncertainty estimate information. (4) Filling of missing observations is performed in the global, 3-hr product instead of in the monthly product. (4) All products, except the satellite-specific Level 2 product, are formatted in netCDF-4.

New Product in D-Version: Pixel-level (Level 2, called DX) cloud product with resolution of 30 km and 3 hr.

New Products in H-Version: (1) All Ancillary Products replaced with more up-to-date versions – in particular the new atmospheric temperature-humidity profiles treat diurnal variations explicitly. (2) Globally merged version of the Level-2 product (HXG). (3) Gridded version of data for each satellite, prior to global merger, (HGS).

D-Version Product List: (1) B3 Data: Calibrated, navigated, reduced resolution (30 km, 3 hr) Radiances, (2) Cloud Products: DX, D1, D2. (3) Ancillary Products: TOVS including ozone), SI (snow-ice), Surface Types and Topography.

H-Version Product List: (1) Radiances: GAC format for AVHRR, B1U for geostationary, (2) Cloud Products: HXS, HXG, HGS, HGG, HGH, HGM. (3) Ancillary Products: NNHIRS, OZONE, AEROSOL, SNOWICE, TOPO, SURFACETYPE.

6.1 Algorithm Performance

The quality of the five main retrieved variables (cloud amount, top temperature, and optical thickness, surface temperature and reflectance), as well as the two main derived variables (cloud top pressure, water path), is firstly dependent on the quality of the input radiances and their calibrations (see next section). Total cloud amount does not depend on radiance calibration (see Figure 21). The quality of all the other variables is inter-related because all pixels are processed: every pixel is accounted for as either cloudy or clear and the radiances analyzed accordingly. Hence variable quality is secondly dependent on the "correctness" of the cloud-clear decision. The most important limitation of the cloud amount is a view-angle-dependent detection sensitivity caused by use of constant radiance thresholds and the presence of very thin, high-level clouds: some of these clouds are missed at nadir view and more are detected at slant views. Larger problems with cloud detection are specific to particular regions, most notably: (1) polar regions where radiance contrast is very low, or even reversed from the usual relationships, (2) desert (or heavily polluted) regions where unusually optically thick aerosol events occur, mainly dust storms, that can be detected as clouds, and (3) rainforest regions where persistent hazes or fog layers may be missed, especially at night.

Thirdly, the quality of these variables depends on the fidelity of their treatment in the radiative transfer model. The most important limitations of the representation of clouds in the radiative transfer model are: (1) fixed instead of variable microphysical properties that are cloud-top-temperature-dependent (phase decision), so incorrect phase identification

produces erroneous optical thickness retrievals that can also affect cloud top location if the optical thickness is small enough, (2) clouds are treated as plane parallel, which is more inaccurate for highly broken or scattered cloudiness, and (3) all clouds are treated as single layers. Differences between the assumed and actual cloud microphysical properties and small-scale (below about 5 km) inhomogeneities cause view-illumination-angle-dependent retrievals errors. Representing clouds as single layers only becomes a significant factor when the uppermost layer of a multi-layer situation is optically thin enough to transmit thermal radiation from below: in this case, the retrieved optical thickness represents the sum of the multi-layer optical thickness which, being assigned to the uppermost layer, overestimates cloud top temperature and pressure for that layer. Cloud top pressure is determined from cloud top temperature by finding the atmospheric level with the same temperature; however this is not the location of the literal top of the cloud mass because the IR radiance is emitted from deeper into a diffuse-topped cloud. The most important limitations of the retrieved surface properties are: (1) a seasonal-diurnal bias of clear sky composite temperatures as compared to actual surface temperatures in cloudy conditions (this bias does not affect cloud detection) and (2) view-illumination-angle-dependent errors of surface reflectance caused by treating all surfaces as isotropic reflectors and the uncertainty of aerosol optical depths. Aerosol optical depth errors can sometimes partially offset errors in surface reflectance. The most important limitations associated with Ancillary data are: (1) errors in cloud top pressure from errors in the temperature-humidity profile shapes from NNHIRS, particularly near the surface, and (2) cloud and surface reflectance errors from inaccurate aerosol information from AEROSOL. The aerosol-dependent cloud errors are only significant for optically thinner and broken boundary layer clouds.

Finally, some additional quality dependence arises from use of the filling procedures to estimate results for locations with missing observations.

6.1.1 Cloud Detection and Cloud Amount Uncertainty

Publications relevant for cloud detection algorithm and cloud amount uncertainty (in chronological order) are: Rossow *et al.* (1985), Rossow (1989), Schneider *et al.* (1989), Rossow *et al.* (1989b), Key and Barry (1989), Rossow and Lacis (1990), Rossow and Schiffer (1991), Wielicki and Parker (1992), Schweiger and Key (1992), Rossow and Garder (1993a, 1993b), Rossow *et al.* (1993), Mokhov and Schlesinger (1993, 1994), Kondragunta and Gruber (1994), Liao *et al.* (1995a), Cairns (1995), Curry *et al.* (1996), Jin *et al.* (1996), DiGirolamo and Davies (1997), Stubenrauch *et al.* (1999), Scott *et al.* (1999), Rossow and Schiffer (1999), Luo *et al.* (2002), Stordal *et al.* (2005), Marchand *et al.* (2010), Stubenrauch *et al.* (2012), Stubenrauch *et al.* (2013), Li *et al.* (2015).

Cloud amount in the ISCCP products is determined by counting cloudy pixels so it is only reported in the 1-degree gridded products. At a given time, this quantity represents area coverage fraction; when averaged over time, this quantity combines coverage fraction with frequency of occurrence. At the 1-degree-equivalent scale (about 100 km), the instantaneous coverage fraction is either nearly zero or nearly one about 55% of the time on average. There are three sources of error in cloud amount: (1) a precision limit that

depends on the total number of pixels, (2) an area error produced by treating all pixels as either completely cloudy or completely clear, and (3) cloud detection mistakes.

The precision limit of cloud cover fraction is caused by the finite number of pixels available in each map grid cell. There are about 100 pixels present on average but there is regional variability that depends on the portion of a satellite image projection mapped to that location. Precision ranges is better than 1% to 4% (the latter occurs rarely in HGG because the more extreme satellite views are usually eliminated).

Treating all cloudy pixels as completely cloud covered produces error in the area fraction estimate: this error is larger for broken cloudiness. For the size of the pixels used (about 5 km), the choice of detection thresholds (*i.e.*, the detection sensitivity) mitigates this source of error somewhat by making it more nearly random so that the average error from this source is small (*cf*. Wielicki and Parker 1992, Rossow *et al.* 1993, DiGirolamo and Davies 1997).

By far the largest source of error comes from detection mistakes, either missed clouds or falsely detected clouds. Detection errors depend on the instrument sensitivity and the accuracy of the clear sky radiances. The fact that the surface properties retrieved from the clear sky radiances may differ from the actual values **under** clouds, particularly for TS over land and sea ice, does not affect the cloud detection accuracy because the indication of the presence of clouds comes from the difference in radiances between cloudy and clear scenes at nearby locations or at different times at the same location. The accuracy of the retrieved surface properties (see below) provides an estimate of the uncertainty of the clear sky radiance estimate and thus, of the cloud detection. The detection thresholds (difference between clear sky and cloudy sky radiances) that are used are based on the estimated uncertainty of the clear sky radiances evaluated by comparing retrieved surface properties to other measurements.

Evaluations of the ISCCP cloud detections show that there is a systematic underestimate of cloud amount of about 0.05-0.10 because (mostly) of missed detections of very optically thin cirrus clouds. The more random component of the cloud amount uncertainty is documented in the dataset by reporting the amount of cloud in the radiance difference interval from one to two threshold amounts. This estimate of uncertainty is referred to as the "marginal" cloud amount – as in marginally detected – and is reported for VIS and IR separately as well as jointly. On average the IR marginal cloud amount is about 0.10, so this is interpreted as an instantaneous cloud amount uncertainty of ±0.05. The monthly average random uncertainty is estimated to be about ±0.01-0.02. Bias errors are regional in character and may be as large as 0.05-0.10, notably in the polar regions and in regions dominated by boundary layer cumulus. On average detection errors appear to be the largest source of (systematic) uncertainty.

6.1.2 Surface Property Uncertainty

Publications relevant for uncertainty in surface temperature retrievals (in chronological order) are: Rossow *et al.* (1989a), Rossow and Lacis (1990), Rossow and Garder (1993b),

Rossow and Schiffer (1999), Zhang *et al.* (2007), Moncet *et al.* (2011), Jimenez *et al.* (2012), Raschke *et al*. (2012).

Publications relevant for uncertainties in surface reflectance retrievals (in chronological order) are: Matthews and Rossow (1987), Rossow *et al.* (1989a), Rossow and Lacis (1990), Rossow and Garder (1993b), Rossow and Schiffer (1999), Zhang *et al.* (2007).

Before discussing the uncertainties of the cloud property retrievals, the surface property uncertainties are discussed because they provide another indication of the uncertainty of cloud detection and because they can affect cloud retrieval for certain types of clouds. The clear sky analysis procedure provides an estimate of the clear radiances for every satellite image pixel, treated as a scene of about 10 km size, every three hours, however the statistical nature of this estimate means that the effective spatial sampling interval attained for IR is about 75 km (land) and 150 km (ocean) and about 30 km for VIS; the effective time sampling interval for IR is about 5 days (land) and 15 days (ocean) and about 30 days for VIS. Systematic diurnal variations are resolved by conducting the whole analysis at eight diurnal phases over each month. Note that this estimate of clear sky radiances is interpreted to be the values that would obtain if clear conditions prevailed.

By design the cloud detection procedure does not detect clouds if the differences between the observed radiances and the estimated clear sky radiances are smaller than the uncertainty in the latter. Thus, the retrieved surface properties for clear pixels are slightly cloud contaminated: TS is too low and RS is too high. Experience comparing the surface properties obtained from the ISCCP analysis confirms these biases and shows that the clear sky composite values are generally more accurate (less biased) than the clear-pixel values. However, since the values of TS are determined from clear scenes and extrapolated to all times at each location, there are still biases in the surface temperature for cloudy conditions because cloud radiative effects alter the surface skin temperature, particularly over land. Hence, the clear sky composite values of TS are “clear-sky-biased” for cloudy locations: too large during daytime, especially in summer, and too small during nighttime, especially during winter.

When a particular satellite image is missing, values of surface properties are interpolated by the FILL procedure, primarily an interpolation in time. Consequently, the surface properties that are labeled as filled values are more uncertain.

The estimated clear sky radiance uncertainties for different scene types are represented by the threshold values shown in Section 3.4.1.1.4. These translate approximately into the following random uncertainties over land, snow-covered land, ocean and sea ice-covered ocean: TS (4.0, 4.0, 2.5, 3.0 K) and RS (0.05, 0.06, 0.03, 0.04). Some regions have larger uncertainties for RS because of larger (but uncertain) aerosol optical depths. Both TS and RS are more uncertain in rough topography and in the polar regions.

The ISCCP HGS and HGG products report not only the marginal cloud amounts, which can also be taken as estimates of the uncertainty of clear sky amount, but also report the average surface properties for this subset of the pixels to provide an additional estimate of uncertainties by indicating how much the surface properties would change if this subset were declared to be clear instead of cloudy:

$$Delta\ TS = | TS - [(1 - CA)\ TS + CA_{marg} - TS_{marg}] / (1 - CA + CA_{marg}) | \quad (18)$$

$$Delta\ RS = | TS - [(1 - CA)\ RS + CA_{marg} - RS_{marg}] / (1 - CA + CA_{marg}) | \quad (19)$$

6.1.3 Cloud Property Uncertainty

Publications relevant for uncertainties in cloud top temperature/pressure retrievals (in chronological order) are: Rossow *et al.* (1987), Rossow (1989), Rossow and Lacis (1990), Rossow and Schiffer (1991), Liao *et al.* (1995b), Curry *et al.* (1996), Jin *et al.* (1996), Jin and Rossow (1997), Stubenrauch *et al.* (1999), Wang *et al.* (1999), Rossow and Schiffer (1999), Chen and Rossow (2002), Zhang *et al.* (2004), Rossow *et al.* (2005), Marchand *et al.* (2010), Rossow and Zhang (2010), Stubenrauch *et al.* (2012), Stubenrauch *et al.* (2013).

Publications relevant for uncertainties in cloud phase determination and cloud type identification (in chronological order) are: Fu *et al.* (1990), Rossow and Schiffer (1991), Lin and Rossow (1994, 1996), Jin and Rossow (1997), Rossow and Schiffer (1999), Hahn *et al.* (2001), Luo *et al.* (2002), Waliser *et al.* (2009), Riedi *et al.* (2010), Stubenrauch *et al.* (2012), Stubenrauch *et al.* (2013).

Publications relevant for uncertainties in cloud optical thickness retrievals (in chronological order) are: Rossow *et al.* (1987), Rossow (1989), Rossow and Lacis (1990), Rossow and Schiffer (1991), Kobayashi (1993), Han *et al.* (1994), Lin and Rossow (1994), Han *et al.* (1995), Macke *et al.* (1996), Mishchenko *et al.* (1996), Curry *et al.* (1996), Chambers *et al.* (1997a, 1997b), Davis *et al.* (1997), Descloitres *et al.* (1998), Stubenrauch *et al.* (1999), Rossow and Schiffer (1999), Rossow *et al.* (2002), Zhang *et al.* (2004), Baran and Francis (2004), Baran and Labonnoite (2006, 2007), Zhang *et al.* (2009), Marchand *et al.* (2010), Stubenrauch *et al.* (2012), Stubenrauch *et al.* (2013).

Publications relevant for cloud variability statistics, such as characteristic variations, sampling, mapping, statistical representations, are (in chronological order): Rossow, W.B., and L. Garder (1984), Seze and Rossow (1987), Rossow and Lacis (1990), Rossow and Schiffer (1991), Seze and Rossow (1991a,b), Rossow *et al.* (1993), Rossow and Cairns (1995), Rossow (1996), Rossow and Schiffer (1999), Rossow *et al.* (2002), Stubenrauch *et al.* (2012), Li *et al.* (2015).

The uncertainties in cloud properties depend on the type of cloud. Since missed or false cloud detections cause larger random errors in cloud properties, an overall estimate of this source of uncertainty is provided in ISCCP HGS and HGG products by reporting the average cloud properties associated with the marginally detected clouds:

$$Delta\ RS\ TAU = | TAU - [CA - TAU - CA_{marg} - TAU_{marg}] / (CA - CA_{marg}) | \quad (20)$$

$$Delta\ TC\text{-}PC = | TC\text{-}PC - [CA - TC\text{-}PC - CA_{marg} - TC\text{-}PC_{marg}] / (CA - CA_{marg}) | \quad (21)$$

The random uncertainties of TC for clouds, which are optically thick in the IR ($|_{IR} > 5.5$), are relatively small, about ± 1-2K, associated with radiance calibration and the effects of "fuzzy" tops. The difference of the radiometric TC value and the temperature at the literal cloud top for "fuzzy-topped" high-level clouds is systematic and can be as large as +10 K;

however the consequent errors in the radiative effects of these clouds are much smaller because the retrieved TC is a radiatively effective value (*cf.* Chen and Rossow 2002). For low-level clouds, especially at night, detection errors can introduce more uncertainty in regions dominated by this cloud type. PC uncertainties, about ± 50 mb, arise from temperature profile shape uncertainties in the NNHIRS product, which are more important for low-level clouds and can be systematic, especially over oceans or high topography. TC uncertainties are larger for upper-level clouds that are not optically thick in the IR, caused by uncertainties in the TAU values (discussed next) used to correct for transmitted radiation and the fact that the apparent emission temperature applies to the whole cloud layer rather than its top. These are generally random uncertaintites; however, the most significant biases in TC for upper-level clouds arise in multi-layer situations, where the uppermost layer is optically thin with an optically thicker layer below, because the correction for transmitted IR radiation uses the TAU value, which is the column total. The magnitude of the high bias in TC depends on the IR optical thickness of the upper cloud layer and on the temperature difference between the upper and lower cloud layer: smaller upper-layer optical thickness and larger temperature difference cause larger overestimates of TC (*cf.* Jin and Rossow 1997). The consequent high bias in PC can be significant, about 100-200 mb, enough to change the cloud type identification from high- to middle-level. The underestimate of high cloud amount in the ISCCP results is about one third of the total high cloud amount (| > 0.1), equivalent to CA underestimate of about 0.05 compared with IR sounder-based cloud detections and < 0.10 compared to the CALIPSO lidar-based estimates. Since the ISCCP total cloud amount is similar to or slightly less than the IR sounder results and only about 0.10 lower than the lidar results, about half (*i.e.*, about 0.05) of this difference in high cloud amount appears as mislabeled middle-level clouds.

Uncertainties in TAU retrievals associated with cloud detection errors are most important for low-level clouds (difficult to detect in IR) that are optically thin (difficult to detect in VIS). The same type of clouds also has larger uncertainties associated with cloud amount estimates. For optically thicker clouds the main uncertainties arise from the assumed microphysical properties (particle size, phase) and VIS radiance calibration. The phase dependence, based on cloud top temperature, produces the most random uncertainty for middle-level clouds where the temperature criterion is too simple. An additional uncertainty for ice clouds is associated with the empirical scattering phase function used in the retrieval. Nevertheless, the estimated uncertainty in TAU values caused by errors in microphysics is about ± 15%: the choice of microphysical model parameters has been tuned to minimize the bias component of this uncertainty.

Water Path (WP) values are calculated from TAU values using the specified microphysics; hence the uncertainties are proportional to uncertainties in the assumed effective particle radius, which can be as large as 50% (or more in specific instances). This uncertainty is mostly random as the assumed effective radii are estimated from several satellite climatologies (*cf.* Stubenrauch *et al.* 2012, 2013).

Filled values of TC, PC, TAU and WP are more uncertain. The most important case is the interpolation of daytime TAU values over the nighttime.

6.2 Sensor Performance

6.2.1 Sensor Characteristics

The imaging radiometer channels used to produce the ISCCP products are the "window" IR and VIS channels with approximate wavelengths of 10.5 ⎧m and 0.65 ⎧m, respectively. Specific spectral responses differ in detail and are documented in Appendix B. The IR radiances are represented by brightness temperatures, calculated as the wavelength integral of the product of the instrument spectral response (BANDWIDTH in Appendix B). The VIS radiances are represented by "scaled radiances", calculated as the radiance divided by the instrument "solar constant" (SOLCON in Appendix B), which is the wavelength integral of the product of the instrument spectral response and the solar spectrum at the top of the atmosphere. This approach reduces the dependence on the differences of the spectral responses; the ISCCP calibration procedure then normalizes all satellite radiances to the reference standard, the equivalent channels on the NOAA-9 AVHRR.

The linearity of the response of these radiometers to energy received from earth targets has been monitored as part of the ISCCP calibration procedures and found to be generally very good. Known exceptions are for the GMS series VIS radiances, which exhibit some scan-angle dependence and the MTSAT IR radiances which exhibit a significant decrease in sensitivity for brightness temperatures < 200 K. Starting with AVHRR instruments on NOAA-15, the VIS channel is designed with two sensitivity ranges, being more sensitive at smaller radiances than at larger radiances (*cf.* Heidinger *et al.* 2010), and the IR channel has an explicit non-linear response (only partially) accounted for by a fixed quadratic correction.

The calibration stability of these imaging radiometers, based on the ISCCP calibration monitoring, is generally good, exhibiting degrading sensitivity at rates from about 1-3% per year. Notable exceptions are the IR channel on GOES-6, which experienced a failure of a heater that stabilizes the instrument temperature, and the VIS channel on GOES-8 that degraded at a much faster rate.

6.2.2 Radiance Calibration Uncertainty

The summary and quantitative estimates of calibration uncertainty below are based on the following publications (in chronological order): Schiffer and Rossow (1985), Whitlock *et al.* (1990), Brest and Rossow (1992), Desormeaux *et al.* (1993), Nagaraja Rao *et al.* (1993, 1995), Brest *et al.* (1997), Knapp (2008), Heidinger *et al.* (2010), Molling *et al.* (2010), Stone *et al.* (2013), Rossow and Ferrier (2015), Inamdar & Knapp (2015).

Since all satellites have on-board calibration for the IR channels, their calibrations have not been as extensively studied. The ISCCP procedures normalize all radiometers to the reference standard, NOAA-9, to remove small calibration differences that arise because of spectral response differences and differences in calibration procedures. The estimated uncertainty of ISCCP IR radiances is based on: (1) estimates of the uncertainty of the on-board calibrations for each individual radiometer (*cf.* references in Whitlock *et al.* 1990, Brest and Rossow 1992, Desormeaux *et al.* 1993, Nagaraja Rao *et al.* 1993, 1995, Brest *et al.*

1997), (2) the measured differences among the radiometers when collocated and coincident measurements are compared (including CALCOR results), (3) preliminary results from a comparison of geostationary IR calibration against collocated and coincident infrared spectrometer (IASI) measurements by the GSICS program, (4) comparison of collocated and coincident AVHRR and MODIS measurements (Cao and Heidinger 2002), and (5) the evaluation of surface temperatures retrieved from these radiances (Moncet *et al*. 2011, Jimenez *et al.* 2012). Unfortunately, many of these results focus on the "hot" end (large radiances) of the radiometer responses, except for (2) and (4). The studies (3) and (5) suggested a small systematic "gain" difference of the ISCCP IR calibration for the geostationary imagers in recent years (post 2001), where brightness temperatures < 200 K are a little low and brightness temperatures > 300 K are a little high. That these results are consistent across all the geostationary satellites suggests that this difference is actually caused by the AVHRR calibration to which all of the geostationary imagers are normalized by ISCCP. The direct comparison of AVHRR and MODIS confirmed this same difference (Cao and Heidinger 2002). In the D-Version products a sudden increase of TS values near the end of 2001 was noted (Zhang *et al.* 2007, Raschke *et al.* 2012). It was thought that the cause of this change was related to the change from ATOVS to RTOVS as the source of atmospheric temperature-humidity profiles; however, since this discontinuity is not present in the NNHIRS product but the same change in TS occurs in preliminary processing, it turns out to be caused by the change of IR channel in the newer AVHRRs (NOAA-15 *et seq.*). Knapp (2008) had also compared the IR calibration of the geostationary satellites to HIRS showing good agreement ($\pm$ 1 K, with a small 1-3 K cold bias at values below 220K) before October 2001 and a similar sudden increase afterwards. Therefore, the reference calibration for all IR imagers based on NOAA-16 (including NOAA-15) and following is modified as follows: TBnew = 0.9767 TBold + 5.667 K. This raises a 200 K brightness temperature to 201.0 K and lowers a 320 K brightness temperature to 318.2 K. After this correction the estimated absolute uncertainty of IR brightness temperatures is about $\pm$ 1 K over the whole range. Noise levels of these radiometers are generally smaller than the 8-bit precision used by ISCCP, but shorter-term calibration variations are still possible but within the estimated uncertainty.

The estimated uncertainty of the ISCCP VIS radiances is based on a number of direct comparisons to other standards as well as an indirect evaluation of radiative fluxes calculated using the ISCCP Cloud Products. The former involve: (1) comparison of several vicarious calibration method results for NOAA-7 and NOAA-9 (Whitlock *et al.* 1990, Nagaraja Rao *et al.* 1993, 1995), (2) comparison of the "standard" radiometer, the AVHRR on NOAA-9, with a spectrometer on six ER-2 under-flights that was calibrated in a laboratory by a calibrating sphere (*cf*. Abel *et al.* 1993 and references therein, Brest *et al.* 1997), (3) lunar-based determinations of the VIS calibration of several geostationary satellite radiometers (Stone *et al*. 2013), and (4) comparison of MODIS calibrations (Xiong and Barnes 2006, Xiong *et al.* 2007, 2010, Wu *et al.* 2013) with collocated and coincident AVHRR measurements on NOAA-16 and NOAA-18 (Heidinger *et al.* 2010, Molling *et al*. 2010) and adoption of NOAA-18 as a second "standard" radiometer (Rossow and Ferrier 2015). The Heidinger *et al.* (2010) results were applied to the whole AVHRR series independently; Rossow and Ferrier (2015) showed that these two calibrations of the AVHRR series agree within their mutual uncertainty (with the exception of a two morning

satellites for which the ISCCP analysis was lacking in information). In addition the normalization of the geostationary VIS calibrations to AVHRR was performed independently showing agreement with the ISCCP results to within mutual uncertainty (Inamdar and Knapp 2015). The VIS calibration has also been evaluated indirectly by comparing shortwave fluxes calculated from ISCCP products with direct measurements (Zhang *et al.* 2004). Based on all these results, the best estimate of the absolute VIS radiance calibration uncertainty is ±3% (in terms of scaled radiances) over the whole range. Noise levels of these radiometers are generally smaller than the 8-bit precision used by ISCCP, but shorter-term calibration variations are still possible but within the estimated uncertainty. This estimate of radiometer noise is true even for the 6-bit VIS data from earlier satellites because the ISCCP procedure of matching IR and VIS pixel sizes was done by averaging the smaller VIS pixels, which reduced noise somewhat. The notable exception is the five-month period, October 1994 – February 1995, where there was no afternoon polar orbiter data available to normalize the VIS calibrations; IR calibrations were normalized to the morning polar orbiter.

The ISCCP radiance calibration results are available for every individual satellite image in a data product called HBT that has tables that convert image 8-bit count values to physical radiances: these tables also show the Nominal (from the satellite operator), Normalized and Absolute calibrations. The tables convert radiance counts to two alternative sets of physical units: for VIS these are the scaled radiance (radiance divided by the instrument "solar constant"), ranging from 0.002 to 1.120, and "energy" units (watts/m^2/sr/$\lceil$m) and for IR these are brightness temperature in Kelvins, ranging from 160 to 350 K, and "energy" units (watts/m^2/sr/$\lceil$m).

7. Future Enhancements

The H-Version of the ISCCP processing code allows for processing any version of the same satellite image data with space-time sampling intervals the same or smaller than 30 km and 3 hr (assuming that ancillary products are also available). Thus, full resolution geostationary data can be processed with this code to obtain better time resolution for the study of cloud dynamics. This feature of the code has already been tested by French researchers. Another feature of this code is that it also allows for near-real time processing by collecting statistics for the clear sky radiance estimates from the time interval preceding the most recent image available. However, the radiance calibration and QC procedures might not be applied in this case. A slightly revised version of the code package with test input (except the radiances), test output and documentation is available from https://www.ncdc.noaa.gov/cdr/atmospheric.

8. References

Abel, P., B. Guenther, R.N. Galimore and J.W. Cooper, 1993: Calibration results for NOAA-11 AVHRR channels 1 and 2 from congruent path aircraft observations. *J. Atmos. Ocean Tech.*, **10**, 493-508.

Alexandrov, M.D., B. Cairns, C. Emde, A.S. Ackerman and B. van Diedenhoven, 2012: Accuracy assessments of cloud droplet size retrievals from polarized reflectance measurements by the research scanning polarimeter. *Remote Sens. Environ.*, **125**, 92-111, doi:10.1016/j.rse.2012.07.012.

Armstrong, R.L., and M.J. Brodzik, 2002: *Northern Hemisphere EASE-Grid Weekly Snow Cover and Sea Ice Extent Version 2*, Boulder, CO: National Snow and Ice Data Center, CD-ROM.

Armstrong, R., B. Raup, S.J.S. Khalsa, R. Barry, J. Kargel, C. Helm and H. Kieffer, 2005: *GLIMS glacier database*, Boulder, CO: National Snow and Ice Data Center Digital media: http:nsidc.org/data/nsidc-0272.html.

Baran, A.J., and P.N. Francis, 2004, On the radiative properties of cirrus cloud at solar and thermal wavelengths: A test of model consistency using high-resolution airborne radiance measurements. *Quart. J. Royal Meteor. Soc.*, **130**, 763-778, doi:10.1256/qj.03.151.

Baran, A.J., and L-C. Labonnote, 2006: On the reflection and polarisation properties of ice cloud. *J. Quant. Spectrosc. Radia. Trans.*, **100**, 41-54, doi:10.1016/j.jqsrt.2005.11.062.

Baran, A.J., and L-C. Labonnote, 2007: A self-consistent scattering model for cirrus. I: The solar region. *Quart. J. Roy. Meteor. Soc.*, **133**, 1899-1912, doi:10.1002/qj.164.

Baranov, Yu.I, W.J. Lafferty, Q. Ma and R.H. Tipping, 2008: Water-vapor continuum absorption in the 800-1250 cm^{-1} spectral region at temperatures from 311 to 363 K. *J. Quant. Spectrosc. Radia. Trans.*, **109**, 2291-2302, doi:10.1016/j.jqsrt.2008.03.004.

Brest, C.L., and W.B. Rossow, 1992: Radiometric calibration and monitoring of NOAA AVHRR data for ISCCP. *Int. J. Remote Sensing*, **13**, 235-273.

Brest, C.L., W.B. Rossow and M.D. Roiter, 1997: Update of radiance calibrations for ISCCP. *J. Atmos. Ocean Tech.*, **14**, 1091-1109.

Brown, R.D., and D.A. Robinson, 2011: Northern hemisphere spring snow cover variability and change over 1992-2010 including an assessment of uncertainty. *The Cryosphere*, **5**, 219-229, doi:10.5194/tc-5-219-2011.

Cairns, B., 1995: Diurnal variations of cloud from ISCCP data. *Atmos. Res.*, **37**, 135-146.

Cairns, B., B.E. Carlson, A.A. Lacis and E.E. Russell, 1997: An analysis of ground-based polarimetric sky radiance measurements. In D.H. Goldstein and R.H. Chipman (Eds.) *Polarization: Measurement, Analysis, and Remote Sensing Proc. SPIE*, **3121**, 382-393.

Cairns, B., E.E. Russell and L.D. Travis, 1999: Research scanning polarimeter: Calibration and ground-based measurements. In D.H. Goldstein and D.B. Chenault (Eds.) *Polarization: Measurement, Analysis, and Remote Sensing Proc. SPIE*, **3753**, 186-197.

Cao, C-Y., and A.K. Heidinger, 2002: Inter-comparison of the longwave infrared channels of MODIS and AVHRR/NOAA-16 using simultaneous nadir observations at orbit intersections. *Proc. SPIE*, **4814**, Earth Observing Systems VII, 306, doi:10.1117/12.451690.

Chahine, M.T., T.S. Pagano, H.H. Aumann, R. Atlas, C. Barnet, J. Blaisdell, L. Chen, M. Divakarla, E.J. Fetzer, M. Goldberg, C. Gautier, S. Granger, S. Hannon, F.W. Irion, M. Kakar, E. Kalnay, B.H. Lambrigsten, S-Y. Lee, J. Le Marshall, W.W. McMillan, L. McMillin, E.T. Olsen, H. Revercomb, P. Rosenkranz, W.L. Smith, D. Staelin, L. Larrabee Strow, J. Susskind, S. Tobin, W. Wolf and L. Zhou, 2006: AIRS: Improving weather forecasting and providing new data on greenhouse gases. *Bull. Amer. Meteor. Soc.*, **87**, 911-926, doi:10.1175/bams-87-7-911.

Chambers, L.H., B.A. Wielicki and J.F. Evans, 1997a: Accuracy of the independent pixel approximation for satellite estimates of oceanic boundary layer cloud optical depth. *J. Geophys. Res.*, **102**, 1779-1794.

Chambers, L.H., B.A. Wielicki and J.F. Evans, 1997b: Independent pixel and two dimensional estimates of Landsat-derived cloud field albedo. *J. Atmos. Sci*., **54**, 1525-1532.

Chen, T., and W.B. Rossow, 2002: Determination of top-of-atmosphere longwave radiative fluxes: A comparison between two approaches using ScaRab data. *J. Geophys. Res.*, **107**, doi 10.1029/2001JD000914 (1-14).

Chowdhury, J., B. Cairns, F. Waquet, K. Knobelspiesse, M. Ottaviani, J. Redemann, L. Travis and M. Mishchenko, 2012: Sensitivity of multiangle, multispectral polarimetric remote sensing over open oceans to water-leaving radiance: Analyses of RSP data acquired during the MILAGRO campaign. *Remote Sens. Environ.*, **118**, 284-308, doi:10.1016/j.rse.2011.11.003.

Clayson, C.A., J.B. Roberts and A.S. Bogdanoff, 2012: The SeaFlux Turbulent Flux dataset version 1.0 documentation. SeaFlux Project, 5pp. [available online at http://seaflux.org/seaflux_data/DOCUMENTATION/SeaFluxV1.0documentation.pdf]

Clayson, C.A., and A.S. Bogdanoff, 2013: The effect of diurnal sea surface temperature warming on climatological air-sea fluxes. *J. Climate*, **26**, 2546-2556, doi:10.1175/JCLI-D-12-00062.1.

Curry, J.A., W.B. Rossow, D. Randall and J.L. Schramm, 1996: Overview of Arctic cloud and radiation characteristics. *J. Climate*, **9**, 1731-1764.

Davis, A., A. Marshak, R. Cahalan and W. Wiscombe, 1997: The Landsat scale break in stratocumulus as a three-dimensional radiative transfer effect: Implications for cloud remote sensing. *J. Atmos. Sci.*, **54**, 241-260.

Davis, S., and K. Rosenlof, 2016: NOAA ESRL Stratospheric Water and OzOne Satellite Homogenized (SWOOSH), Version 2. NOAA National Centers for Environmental Information (NCEI). doi:10.7289/V5TD9VBX.

Descloitres, J.C., J.C. Buriez, F. Parol and Y. Fouquart, 1998: POLDER observations of cloud bidirectional reflectances compared to a plane-parallel model using the International Satellite Cloud Climatology Project cloud phase functions. *J. Geophys. Res.*, **103**, 11,411-11,418.

Desormeaux, Y., W.B. Rossow, C.L. Brest and G.G. Campbell, 1993: Normalization and calibration of geostationary satellite radiances for ISCCP. *J. Atmos. Ocean Tech*., **10**, 304-325.

DiGirolamo, L., and R. Davies, 1997: Cloud fraction errors caused by finite resolution measurements. *J. Geophys. Res.*, **102**, 1739-1756.

Downing, H.D., and D. Williams, 1975: Optical constants of water in the infrared. *J. Geophys. Res.*, **80**, 1656-1661.

Fu, R., A.D. Del Genio and W.B. Rossow, 1990: Behavior of deep convective clouds in the tropical Pacific deduced from ISCCP radiance data. *J. Climate*, **3**, 1129-1152.

de Haan, J.F., P.B. Bosna and J.W. Hovenier, 1987: The adding method for multiple scattering calculations of polarized light. *Astron. Astrophys.*, **183**, 371-382.

Hahn, C.J., W.B. Rossow and S.G. Warren, 2001: ISCCP cloud properties associated with standard cloud types identified in individual surface observations. *J. Climate*, **14**, 11-28.

Hale, G.M., and M.R. Querry, 1973: Optical constants of water in the 200-nm to 200-⌠m wavelength region. *Appl. Optics*, **12**, 555-563.

Han, Q-Y., W.B. Rossow and A.A. Lacis, 1994: Near-global survey of effective cloud droplet radii in liquid water clouds using ISCCP data. *J. Climate*, **7**, 465-497.

Han, Q., W.B. Rossow, R. Welch, A. White and J. Chou, 1995: Validation of satellite retrievals of cloud microphysics and liquid water path using observations from FIRE. *J. Atmos. Sci*., **52**, 4183-4195.

Hansen, J.E., and L.D. Travis, 1974: Light scattering in planetary atmospheres. *Space Sci. Rev.*, **16**, 527-610.

Hartmann, J.M., M.Y. Perrin, Q. Ma, and R.H. Tipping, 1993: The infrared continuum of pure water vapor: Calculations and high-temperature measurements. J. Quant. Spectrosc. Radiat. Transfer, 49, 675-691, doi:10.1016/0022-4073(93)90010-F.

Helfrich, S.R., M. Li and C. Kongoli, 2012: Interactive Multisensor Snow and Ice Mapping System Version 3 (IMS V3) Algorithm theoretical basis document version 2.1. NOAA NESDIS Center for Satellite Applications and Research (STAR), 61 pp.

Heidinger, A.K., W.C. Straka, C.C. Molling, J.T. Sullivan and X. Wu, 2010: Deriving an inter-sensor consistent calibration for the AVHRR solar reflectance data record. *Int. J. Remote Sens.*, **31**, 6493-6517, doi:10.1080/01431161.2010.496472.

Heidinger, A.K., M.J. Foster, A. Walther and X.Z. Zhao, 2014: The Pathfinder atmospheres-extended AVHRR climate dataset. *Bull. Amer. Meteor. Soc.*, **95**, 909-922, doi:10.1175/BAMS-D-12-00246.1.

Inamdar, A.K., and K.R. Knapp, 2015: Intercomparison of independent calibration techniques applied to the visible channel of the ISCCP B1 data. *J. Atmos. Ocean Tech.*, **32**, 1225-1240, doi:10.1175/JTECH-D-14-00040.1

Inn, E.C.Y., and Y. Tanaka, 1953: Absorption coefficient of ozone in the ultraviolet and visible regions. *J. Opt. Soc. Amer.*, **43**, 870-873.

Intrierie, J., M. Shupe, T. Uttal and B. McCarty, 2002: An annual cycle of Arctic cloud characteristics observed by radar and lidar at SHEBA. *J. Geophys. Res.*, **107**, 8030, doi:10.1029/2000JD000423.

Ivanova, N., O.M. Johannssen, L. Toudal Pedersen and R.T. Tonboe, 2014: Retrieval of Arctic sea ice parameters by satellite passive microwave sensors: Comparison of eleven sea ice concentration algorithms. *IEEE Trans. Geosci. Remote Sens.*, **52**, 7233-7246, doi:10.1109/TGRS.2014.2310136.

Jackson, D.L., D.P. Wylie and J.J. Bates, 2003: The HIRS pathfinder radiance dataset (1979-2001). Presented at 12th Conference on Satellite Meteorology and Oceanography, *Amer. Meteor. Soc.*, Long Beach, CA, 10-13 Feb.

Jensen, E.J., O.B. Toon, S.A. Vay, J. Ovarlez, R. May, T.P. Bui, C.H. Twohy, B.W. Gandrud, R.F. Pueschel and U. Schumann, 2001: Prevalence of ice-supersaturated regions in the upper troposphere: Implications for optically thin ice cloud formation. *J. Geophys. Res.*, **106**, D15, 17,253-17,266.

Jimenez, C., C. Prigent, J. Catherinot and W.B. Rossow, 2012: A comparison of ISCCP land surface temperatures with other satellite and in situ observations. *J. Geophys. Res.*, **117**, D08111, doi:10.1029/2011JD017058, (1-8).

Jin, Y., W.B. Rossow and D.P. Wylie, 1996: Comparison of the climatologies of high-level clouds from HIRS and ISCCP. *J. Climate*, **9**, 2850-2879.

Jin, Y., and W.B. Rossow, 1997: Detection of cirrus overlapping low-level clouds. *J. Geophys. Res.*, **102**, 1727-1737.

Key, J., and R.G. Barry, 1989: Cloud cover analysis with Arctic AVHRR data. 1. Cloud detection. *J. Geophys. Res.*, **94**, 8521-8535.

Kinne, S., D. O'Donnel, P. Stier, S. Kloster, K. Zhang, H. Schmidt, S. Rast, M. Giorgetta, T.F. Eck and B. Stevens, 2013: MAC-v1: A new aerosol climatology for climate studies. *J. Adv. Modelling Earth Sys.*, **5**, 704-740, doi:10.1002/jame.20035.2013.

Knapp, K.R., 2008: Calibration assessment of ISCCP geostationary infrared observations using HIRS. *J. Atmos. Ocean Tech.*, **25**, 143-195, doi:10.1175/2007JTECHA910.1.

Kobayashi, T., 1993: Effects due to cloud geometry on biases in the albedo derived from radiance measurements. *J. Climate*, **6**, 120-128.

Kondragunta, C.R., and A. Gruber, 1994: Diurnal variations of ISCCP cloudiness. *Geophys. Res. Lett.*, **21**, 2015-2018.

Kroon, M., J.F. de Haan, J.P. Veefkind, L. Froidevaux, R. Wang, R. Kivi and J.J. Hakkarainen, 2011: Validation of operational ozone profiles from the Ozone Monitoring Instrument. *J. Geophys. Res.*, **116**, D18305, doi:10.1029/2010JD015100.

Kroon, M., J.P. Veefkind, M. Sneep, R.D. McPeters, P.K. Bhartia and P.F. Levelt, 2008: Comparing OMI-TOMS and OMI-DOAS ozone column data. *J. Geophys. Res.*, **113**, doi:10.1029/2007JD008798.

Lacis, A.A., and V. Oinas, 1991: A description of the correlated k distribution method for modeling nongray gaseous absorption, thermal emission and multiple scattering in vertically inhomogeneous atmospheres. *J. Geophys. Res.*, **96**, D5, 9027-9063.

Lerot, C., M. Van Roozendael, J. van Geffen, J. van Gent, C. Fayt, R. Spurr, G. Lichtenberg and A. von Bargen, 2009: Six years of total column ozone measurements from SCIAMACHY nadir observations. *Atmos. Meas. Techniques*, **2(1)**, 87-98, doi:10.5194/amt-2-87-2009.

Li, J., B.E. Carlson, W.B. Rossow, A.A. Lacis and Y-C. Zhang, 2015: An intercomparison of the spatio-temporal variability of satellite and ground-based cloud datasets using spectral analysis techniques. *J. Climate*, **28**, 5716-5736, doi:10.1175/JCLI-D-14-0537.1.

Liao, X., W.B. Rossow and D. Rind, 1995: Comparison between SAGE II and ISCCP high-level clouds, Part I: Global and zonal mean cloud amounts. *J. Geophys. Res.*, **100**, 1121-1135.

Liao, X., W.B. Rossow, and D. Rind, 1995: Comparison between SAGE II and ISCCP high-level clouds, Part II: Locating cloud tops. *J. Geophys. Res.*, **100**, 1137-1147.

Lin, B., and W.B. Rossow, 1994: Observations of cloud liquid water path over oceans: Optical and microwave remote sensing methods. *J. Geophys. Res.*, **99**, 20,907-20,927.

Lin, B., and W.B. Rossow, 1996: Seasonal variation of liquid and ice water path in nonprecipitating clouds over oceans. *J. Climate*, **9**, 2890-2902.

Liu, X., P.K. Bhartia, K. Chance, L. Froidevaux, R.J.D. Spurr and T.P. Kurosu, 2010: Validation of Ozone Monitoring Instrument ozone profiles and stratospheric ozone columns with Microwave Limb Sounder measurements. *Atmos. Phys. Chem.*, **10(5)**, 2539-2549, doi:10.5194/acp-10-2539-2010.

Loveland, T., J. Brown, D. Ohlen, B. Reed, Z. Zhu, L. Yang and S. Howard, 2009: ISLSCP II IGBP DISCover and SiB land cover, 1992-1993, In F.G. Hall, G. Collatz, B. Meeson, S. Los, E. Brown de Colstoun and D. Landis (Eds.) *ISLSCP Initiative II Collection Data Set*, (available on

line from Oak Ridge National Laboratory Distributed Active Archive Center, Oak Ridge, TN, doi:10.3334/ORNLDAAC/930.

Liu, J., J.A. Curry, C.A. Clayson and M.A. Bourassa, 2011: High-resolution satellite surface latent heat fluxes in North Atlantic hurricanes. *Mon. Wea. Rev.*, **139**, 2735-2747, doi:10.1175/2011MWR3548.1.

Luo, Z., W.B. Rossow, T. Inoue and C.J. Stubenrauch, 2002: Did the eruption of the Mt. Pinatubo volcano affect cirrus properties? *J. Climate*, **15**, 2806-2820.

Ma, Q., and R.H. Tipping, 1991: A far wing line shape theory and its application to the water continuum absorption in the infrared region. I. *J. Chem. Phys*., **95**, 6290-6301, doi:10.1063/1.461549.

Ma, Q., and R.H. Tipping, 1992a: A far wing line shape theory and its application to the water vibrational bands (II). *J. Chem. Phys*., **96**, 8655-8663, doi:10.1063/1.462272.

Ma, Q., and R.H. Tipping, 1992b: A far wing line shape theory and its application to the foreign-broadened water continuum absorption. III. *J. Chem. Phys*., **97**, 818-828, doi:10.1063/1.463184.

Ma, Q., and R.H. Tipping, 1994: The detailed balance requirement and general empirical formalisms for continuum absorption. *J. Quant. Spectrosc. Radiat. Trans.*, **51**, 751-757.

Ma, Q., R.H. Tipping, N.N. Lavrentieva and A.S. Dudaryonok, 2013: Verification of the H_2O linelists with theoretically developed tools. *J. Quant. Spectrosc. Radiat. Trans.*, **130**, 81-99, doi:10.1016/j.jqsrt.2013.07.017.

Mace, G.G., Q. Zhang, M. Vaughan, R. Marchand, G. Stephens, C. Trepte and D. Winker, 2009: A description of hydrometeor layer occurrence statistics derived from the first year of merged CloudSat and CALIPSO data. *J. Geophys. Res.*, **114**, D00A26, doi:10.1029/2007JD009755.

Macke, A., J. Mueller and E. Raschke, 1996: Single scattering properties of atmospheric ice crystals. *J. Atmos. Sci.*, **53**, 2813-2825.

Marchand, R., T. Ackerman, M. Smyth, and W. B. Rossow, 2010: A review of cloud top height and optical depth histograms from MISR, ISCCP, and MODIS. *J. Geophys. Res*., **115**, D16206, doi:10.1029/2009JD013422, (1-25).

Martin, W., B. Cairns and G. Bal, 2014: Adjoint methods for adjusting three-dimensional atmosphere and surface properties to fit multi-angle/multi-pixel polarimetric measurements. *J. Quant. Spectrosc. Radia. Trans.*, **144**, 68-85, doi:10.1016/j.jqsrt.2014.03.030.

Matthews, E., and W.B. Rossow, 1987: Regional and seasonal variations of surface reflectance at 0.6 μm. *J. Climate Appl. Meteor*., **25**, 170-202.

Matricardi, M., and R. Saunders, 1999: Fast radiative transfer model for simulation of infrared atmospheric sounding interferometric radiances. *Appl. Optics*, **38**, 5679-5691, doi:10/1364/AO.38.005679.

Minnis, P., K-N. Liou and Y. Takano, 1993a: Inference of cirrus cloud properties using satellite-observed visible and infrared radiances. Part I: Parameterization of radiance fields. *J. Atmos. Sci.*, **50**, 1279-1304.

Minnis, P., P.W. Heck and D.F. Young, 1993b: Inference of cirrus cloud properties using satellite-observed visible and infrared radiances. Part II: Verification of theoretical cirrus radiative properties. *J. Atmos. Sci.*, **50**, 1305-1322.

Mishchenko, M.I., W.B. Rossow, A. Macke and A.A. Lacis, 1996: Sensitivity of cirrus cloud albedo, bidirectional reflectance, and optical thickness retrieval accuracy to ice-particle shape. *J. Geophys. Res*., **101**, 16,973-16,985.

Mokhov, I.I., and M.E. Schlesinger, 1993: Analysis of global cloudiness. 1. Comparison of ISCCP, Meteor and Nimbus 7 satellite data. *J. Geophys. Res.*, **98**, 12,849-12,868.

Mokhov, I.I., and M.E. Schlesinger, 1994: Analysis of global cloudiness. 2. Comparison of ground-based and satellite-based cloud climatologies. *J. Geophys. Res.*, **99**, 17,045-17,065.

Molling, C.C., A.K. Heidinger, W.C. Straka and X. Wu, 2010: Calibrations for AVHRR channels 1 and 2: Review and path towards consensus. *Int. J. Remote Sens.*, **31**, 6519-6540, doi:10.1080/01431161.2010.496473.

Moncet, J-L., P. Liang, A.E. Lipton, J.F. Galantowicz and C. Prigent, 2011: Discrepancies between MODIS and ISCCP land surface temperature products analyzed with microwave measurements. *J. Geophys. Res.*, **116**, D21105, doi:10.1029/2010JD015432.

Murphy, D.M., and T. Koop, 2005: Review of vapour pressures for ice and supercooled water for atmospheric applications. *Quart. J. Roy. Meteor. Soc.*, **131**, 1539-1565, doi:10.1256/qj.04.94.

Nagaraja Rao, C.R., J. Chen, W.F. Staylor, P. Abel, Y.J. Kaufman, E. Vermote, W.B. Rossow and C. Brest, 1993: Degradation of the visible and near-infrared channels of the Advanced Very High Resolution Radiometer on the NOAA-9 spacecraft: Assessment and recommendations for corrections. NOAA Tech. Rep. NESDIS 70, 25 pp. [Available online at http://docs.lib.noaa.gov/noaa_documents/NESDIS/TR_NESDIS/TR_NESDIS_70.pdf]

Nagaraja Rao, C.R., and J. Chen, 1995: Inter-satellite calibration linkages for the visible and near-infrared channels of the Advanced Very High Resolution Radiometer on NOAA-7, -9 and -11 spacecraft. *Int. J. Remote Sens.*, **16**, 1931-1942, doi:10.1080/01431169508954530.

Neckel, H., and D. Labs, 1984: The solar radiation between 3300 and 12500 A. *Sol. Phys.*, **90**, 205-258, doi:10.1007/BF00173953.

Oinas, V., 2016: "Atmospheric Radiation" in Our Warming Planet: Topics in Climate Change, C. Rosenzweig, D. Rind, A. Lacis and D. Peters (Eds.), World Scientific, Singapore, (in press).

Raschke, E., S. Kinne and P.W. Stackhouse, 2012: GEWEX Radiative Flux Assessment (RFA) Volume 1: Assessment. *WCRP Report 19*, 299 pp.

Reale, A., F. Tilley, M. Ferguson and A. Allegrino, 2008: NOAA operational sounding products for advanced TOVS. *Int. J. Remote Sens.*, **29**, 4615-4651.

Riedi, J., B. Marchant, S. Platnick, B.A. Baum, F. Thieuleux, C. Oudard, F. Parol, J-M. Nicolas and P. Dubuisson, 2010: Cloud thermodynamic phase inferred from merged POLDER and MODIS data. *Atmos. Chem. Phys.*, **10**, 11,851-11,865, doi:10.5194/acp-10-11851-2010.

Robinson, D.A., and A. Frei, 2000: Seasonal variability of northern hemisphere snow extent using visible satellite data. *Professional Geographer*, **51**, 30-314.

Rossow, W.B., and L. Garder, 1984: Selection of a map grid for data analysis and archival. *J. Climate Appl. Meteor*., **23**, 1253-1257.

Rossow, W.B., F. Mosher, E. Kinsella, A. Arking, M. Desbois, E. Harrison, P. Minnis, E. Ruprecht, G. Seze, C. Simmer and E. Smith, 1985: ISCCP cloud algorithm intercomparison. *J. Climate Appl. Meteor*., **24**, 877-903.

Rossow, W.B., A. Wolf and A.A. Lacis, 1987: Geometric dependence of cloud radiation interactions from ISCCP data. *Proceedings of the Beijing International Radiation Symposium*. 26-30 August 1986, Science Press, China and American Meteorological Societies, 446-451.

Rossow, W.B., 1989: Measuring cloud properties from space: A review. *J. Climate*, **2**, 201-213.

Rossow, W.B., C.L. Brest and L.C. Garder, 1989a: Global, seasonal surface variations from satellite radiance measurements. *J. Climate*, **2**, 214-247.

Rossow, W.B., L.C. Garder and A.A. Lacis, 1989b: Global, seasonal cloud variations from satellite radiance measurements. Part I: Sensitivity of analysis. *J. Climate*, **2**, 419-462.

Rossow, W.B., and A.A. Lacis, 1990: Global, seasonal cloud variations from satellite radiance measurements. Part II: Cloud properties and radiative effects. *J. Climate*, **3**, 1204-1253.

Rossow, W.B., and R.A. Schiffer, 1991: ISCCP cloud data products. *Bull. Amer. Meteor. Soc*., **72**, 2-20.

Rossow, W.B., and L.C. Garder, 1993a: Cloud detection using satellite measurements of infrared and visible radiances for ISCCP. *J. Climate*, **6**, 2341-2369.

Rossow, W.B., and L.C. Garder, 1993b: Validation of ISCCP cloud detections. *J. Climate*, **6**, 2370-2393.

Rossow, W.B., A.W. Walker and L.C. Garder, 1993: Comparison of ISCCP and other cloud amounts. *J. Climate*, **6**, 2394-2418.

Rossow, W.B., and B. Cairns, 1995: Monitoring changes of clouds. *Climatic Change*, **31**, 305-347.

Rossow, W.B., 1996: Properties of clouds and cloud systems. Chapter 9, In *Radiation and Water in the Climate System: Remote Measurements*. (E. Raschke, ed.), **NATO ASI Series I, Vol. 45**, Springer-Verlag, Berlin, 193-216.

Rossow, W.B., and R.A. Schiffer, 1999: Advances in understanding clouds from ISCCP. *Bull. Amer. Meteor. Soc*., **80**, 2261-2287.

Rossow, W.B., C. Delo and B. Cairns, 2002: Implications of the observed mesoscale variations of clouds for Earth's radiation budget. *J. Climate*, **15**, 557-585.

Rossow, W.B., and E. Duenas, 2004: The International Satellite Cloud Climatology Project (ISCCP) Web site: An online resource for research. *Bull. Amer. Meteor. Soc.*, **85**, 167-172.

Rossow, W.B., Y-C. Zhang and J-H. Wang, 2005: A statistical model of cloud vertical structure based on reconciling cloud layer amounts inferred from satellites and radiosonde humidity profiles. *J. Climate*, **18**, 3587-3605.

Rossow, W.B. and Y-C. Zhang, 2010: Evaluation of a statistical model of cloud vertical structure using combined CloudSat and Calipso cloud layer profiles. *J. Climate*, **23**, 6641-6653.

Rossow, W.B., and J. Ferrier, 2015: Evaluation of long-term calibrations of the AVHRR visible radiances. *J. Atmos. Ocean Tech.*, **32**, 744-766.

Rothman, L.S., R.R. Gamache, A. Barbe, A. Goldman, J.R. Gille, L.R. Brown, R.A. Toth, J.M Flaud and C. Camy-Peyret, 1983: AFGL atmospheric absorption line parameters compilation: 1982 edition. *Appl. Opt*., **22**, 2247-2256.

Rothman, L.S., A. Barbe, D. Chris Brenner, L.R. Brown, C. Camy-Peyret, M.R. Carleer, K. Chance, C. Clerbaux, V. Dana, V.M. Devi, A. Fayt, J.M. Flaud, R.R. Gamache, A. Goldman, D. Jacquemart, K.W. Jucks, W.J. Lafferty, J-Y. Mandin, S.T. Massie, V. Nemtchinov, D.A. Newnham, A. Perrin, C.P. Rindsland, J. Schroeder, K.M. Smith, M.A.H. Smith, K. Tang, R.A. Toth, J. Vander Auwera, P. Varanassi and K. Yoshino, 2003: The HITRN molecular spectroscopic database: 2000 edition including updates through 2001. *J. Quant. Spectrosc. Radiat. Trans*., **82**, 5-44, doi:10.1016/S0022-4073(3)00146-8.

Saunders, R., M. Matricardi and P. Brunel, 1999: An improved fast radiative transfer model for assimilation of satellite radiance observations. *Quart. J. Roy. Meteor. Soc.*, **125**, 1407-1425.

Saunders, R., P. Rayer, P. Brunel, A. von Engeln, N. Bormann, L. Strow, S. Hannon, S. Heilliette, Xu Lu, F. Miskolczi, Y. Han, G. Mosiello, J-L. Moncet, Gennady Uymin, V. Sherlock and D.S. Turner, 2007: A comparison of radiative transfer models for simulating Atmospheric Infrared Sounder (AIRS) radiances. *J. Geophys. Res.*, **112**, D01S90, doi:10.1029/2006JD007088.

Schiffer, R.A., and W.B. Rossow, 1983: The International Satellite Cloud Climatology Project (ISCCP): The first project of the World Climate Research Programme. *Bull. Amer. Meteor. Soc*., **64**, 779-784.

Schiffer, R.A., and W.B. Rossow, 1985: ISCCP global radiance data set: A new resource for climate research. *Bull. Amer. Meteor. Soc*., **66**, 1498-1505.

Schneider, G., P. Paluzzi and J.P. Oliver, 1989: Systematic error in synoptic sky cover record of the South Pole. *J. Climate*, **2**, 295-302.

Schweiger, A.J., and J.R. Key, 1992: Arctic cloudiness: Comparison of ISCCP-C2 and NIMBUS-7 satellite derived cloud products with surface based cloud climatology. *J. Climate*, **5**, 1514-1527.

Scott, N.A., A. Chedin, R. Armante, J. Francis, C. Stubenrauch, J-P. Charboureau, F. Chevallier, C. Claud and F. Cheruy, 1999: Characteristics of the TOVS Pathfinder Path-B dataset. *Bull. Amer. Meteor. Soc.*, **80**, 2679-2701.

Seze, G., and W.B. Rossow, 1987: Time cumulated visible and infrared histograms used as descriptors of cloud cover. *Adv. Space Res*., **7**, 155-158.

Seze, G., and W.B. Rossow, 1991a: Time-cumulated visible and infrared radiance histograms used as descriptors of surface and cloud variations. *Int. J. Remote Sensing*, **12**, 877-920.

Seze, G., and W.B. Rossow, 1991b: Effects of satellite data resolution on measuring the space/time variations of surfaces and clouds. *Int. J. Remote Sensing*, **12**, 921-952.

Shahroudi, N., and W.B. Rossow, 2014: Using microwave surface emissivities to isolate the signature of snow on different land surface types. *Remote Sensing Environ.*, **152**, doi:10.1061/j.rse.2014.07.008, 638-653.

Shi, L., 2001: Retrieval of atmospheric temperature profiles from AMSU-A measurement using a neural network approach. *J. Atmos. Ocean Tech.*, **18**, 340-347.

Shi, L., J.J. Bates, X. Li, S.M. Uppala and G. Kelly, 2008: Extending the satellite sounding archive back in time: The vertical temperature profile radiometer data. *J. Appl. Remote Sens.*, **2(1)**, 023506, doi:10.1117/1.2889435.

Shi, L., and J.J. Bates, 2011: Three decades of intersatellite-calibrated High-Resolution Infrared Radiation Sounder upper tropospheric water vapor. *J. Geophys. Res.*, **116**, D04108, doi:10.1029/2010JD014847.

Shi, L., J.L. Matthews, S-P. Ho, Q. Yang and J.J. Bates, 2016: Algorithm development of temperature and humidity profile retrievals for long-term HIRS observations. *Remote Sens.*, **8**, 280, (1-17), doi:10.3390/rs8040280.

Smith, A., N. Lott and R. Vose, 2011: The Integrated Surface Database: Recent developments and partnerships. *Bull. Amer. Meteor. Soc.*, **92**, 704-708, doi:10.1175/2011BAMS3015.1.

Stone, T., W.B. Rossow, J. Ferrier and L.M. Hinkelman, 2013: Evaluation of ISCCP geostationary visible channel radiance calibration using lunar techniques. *IEEE Trans. Geosci. Remote Sensing*, **51**, 1255-1266.

Stordal, F., G. Myhre, D.W. Arlander, T. Svendby, E.J.G. Stordal, W.B. Rossow and D.S. Lee, 2005: Is there a trend in cirrus cloud cover due to aircraft traffic?, *Atmos. Chem. Phys.*, **5**, 2155-2162.

Stubenrauch, C.J., W.B. Rossow, F. Cheruy, A. Chedin and N.A Scott, 1999: Clouds as seen by satellite sounders (3I) and imagers (ISCCP). Part I: Evaluation of cloud parameters. *J. Climate*, **12**, 2189-2213.

Stubenrauch, C., W.B. Rossow and S. Kinne, 2012: GEWEX Assessment of Global Cloud Data Sets from Satellites. **WCRP 23/2012**, November, pp. 176.

Stubenrauch, C.J., W.B. Rossow, S. Kinne, S.A. Ackerman, G. Cesana, H. Chepfer, B. Getzewich, L. Di Girolamo, A. Guignard, A. Heidinger, B. Maddux, P. Menzel, P. Minnis, C. Pearl, S. Platnick, C. Poulsen, J. Reidi, S. Sun-Mack, A. Walther, D. Winker, S. Zeng and G. Zhao, 2013: Assessment of global cloud datasets from satellites: Project and database initiated by the GEWEX Radiation Panel. *Bull. Amer. Meteor. Soc.*, **94**, 1031-1049, doi:10.1175/BAMS-D-12-00117.1.

Tipping, R.H., and Q. Ma, 1995: Theory of the water vapor continuum and validations. Atmos. Res., 36, 69-94, doi:10.1016/0169-8095(94)00028-C.

Waliser, D., F. Li, C. Woods, J. Bacmeister, J. Chern, A. Del Genio, J. Jiang, M. Kharitondov, Z. Kuang, H. Meng, P. Minnis, S. Platnick, W.B. Rossow, G. Stephens, S. Sun-Mack, W.K. Tao, A. Tompkins, D. Vane, C. Walker and D. Wu, 2009: Cloud ice: A climate model challenge with signs and expectations of progress. *J. Geophys. Res.*, **114**, D00A21, doi: 10.1029/2008JD010015 (1-27).

Wang, J., and W.B. Rossow, 1995: Determination of cloud vertical structure from upper air observations. *J. Appl. Meteor.*, **34**, 2243-2258.

Wang, J., W.B. Rossow, T. Uttal and M. Rozendaal, 1999: Variability of cloud vertical structure during ASTEX from a combination of rawinsonde, radar, ceilometer and satellite data. *Mon. Wea. Rev.*, **127**, 2484-2502.

Warren, S.G., 1984: Optical constants of ice from the ultraviolet to the microwave. *Appl. Optics*, **23**, 1206-1225.

Warren, S.G., C.J. Hahn, J. London, R.M. Chervin and R.L. Jenne, 1986: Global distribution of total cloud and cloud type amounts over land. NCAR Tech. Note TN-273 + STR/DOE Tech. Rep. ER/60085-HI, 29 pp. plus 200 maps [NTIS number DE87-00-6903].

Warren, S.G., C.J. Hahn, J. London, R.M. Chervin and R.L. Jenne, 1988: Global distribution of total cloud and cloud type amounts over ocean. NCAR Tech. Note TN-317 + STR/DOE Tech. Rep. ER-0406, 42 pp. plus 170 maps [NTIS number DE90-00-3187].

Whitlock, C.H., W.F. Staylor, J.T. Suttles, G. Smith, R. Levin, R. Frouin, C. Gautier, P.M. Teillet, P.N. Slater, Y.J. Kaufman, B.N. Holben, W.B. Rossow, C.L. Brest and S.R. LeCroy, 1990: AVHRR and VISSR satellite instrument calibration results for both cirrus and marine

stratocumulus IFO periods. *FIRE Science Report 1988*. **NASA Conference Publication 3083**, 141-145.

Wielicki, B.A., and L. Parker, 1992: On the determination of cloud cover from satellite sensors: The effect of sensor spatial resolution. *J. Geophys. Res.*, **97**, 12,799-12,823.

Winker, D.M., J. Pelon, J.A. Coakley, S.A. Ackerman, R.J. Charlson, P.R. Calarco, P. Flamont, Q. Fu, R.M. Hoff, C. Kittaka, T.L. Kubar, H. Le Treut, M.P. McCormick, G. Megie, L. Poole, K. Powell, C. Trepte, M.A. Vaughan and B.A. Wielicki, 2010: The CALIPSO mission: A global 3D view of aerosols and clouds. *Bull. Amer. Meteor. Soc.*, **91**, 1211-1229, doi:10.1175/2010BAMS3009.1.

Wu, A., X. Xiong, D.R. Doelling, D. Morstad, D. Angal and R. Bhatt, 2013: Characterization of Terra and Aqua MODIS VIS, NIR, and SWIR spectral bands' calibration stability. *IEEE Trans. Geosci. Remote Sens.*, **51**, 4330-4338, doi:10.1109/TGRS.2012.2226588.

Wylie, D.P., and P-H. Wang, 1997: Comparison of cloud frequency data from the high-resolution infrared radiometer sounder and the Stratospheric Aerosol and Gas Experiment II. *J. Geophys. Res.*, **102**, 29,893-29,900.

Wylie, D.P., and W.P. Menzel, 1999: Eight years of high cloud statistics using HIRS. *J. Climate*, **12**, 170-184.

Xiong, X., and W. Barnes, 2006: An overview of MODIS radiometric calibration and characterization. *Adv. Atmos. Sci.*, **23**, 69-79, doi:10.1007/s00376-006-0008-3.

Xiong, X., J. Sun, W.L. Barnes and V.V. Salomonson, 2007: Multiyear on-orbit calibration and performance of Terra MODIS reflective solar bands. . *IEEE Trans. Geosci. Remote Sens.*, **45**, 879-889, doi:10.1109/TGRS.2006.890567.

Xiong, X., J. Sun, X. Xie, W.L. Barnes and V.V. Salomonson, 2010: Multiyear on-orbit calibration and performance of Aqua MODIS reflective solar bands. . *IEEE Trans. Geosci. Remote Sens.*, **48**, 535-546, doi:10.1109/TGRS.2009.2024307.

Zhang, Y-C., W.B. Rossow, A.A. Lacis, M.I. Mishchenko and V. Oinas, 2004: Calculation of radiative fluxes from the surface to top-of-atmosphere based on ISCCP and other global datasets: Refinements of the radiative transfer model and the input data. *J. Geophys. Res.*, **109**, doi 10.1029/2003JD004457 (1-27 + 1-25).

Zhang, Y-C., W.B. Rossow and P.W. Stackhouse, 2007: Comparison of different global information sources used in surface radiative flux calculation: Radiative properties of the surface. *J. Geophys. Res.*, **112**, D01102, doi: 10.1029/2005JD007008, (1-20).

Zhang, Z., P. Yang, G. Kattawar, J. Riedi, L-C. Labonnote, B.A. Baum, S. Platnick and H-L. Huang, 2009: Influence of ice particle model on satellite ice cloud retrieval: lessons learned from MODIS and POLDER cloud product comparison. *Atmos. Chem. Phys.*, **9**, 7115-7129.

Appendix A.

Acronyms and Abbreviations

Modify the following table to include all acronyms and abbreviations appearing in this document.

Acronym/Abbreviation	Meaning
AERONET	Surface-based aerosol measurement network using multi-wavelength sun photometers
AEROSOL	ISCCP Ancillary Data Product containing global (1.0 degree), monthly values of VIS and IR stratospheric and tropospheric AOD and tropospheric fine fraction
ADD-ON	Addition to ISCCP Operations Guide covering new satellite set-up and radiance calibration procedures
AIRS	Atmospheric Infrared Sounder flown on NASA Aqua satellite
Altocumulus	ISCCP cloud type defined by 440 < PC ≤ 680 mb and TAU < 3.55
Altostratus	ISCCP cloud type defined by 440 < PC ≤ 680 mb and 3.55 ≤ TAU < 22.63
Ancillary OPS Guide	ISCCP Operations Guide for programs producing the Ancillary Data Products from other sources
AOD	Aerosol optical depth
ARSA	Analyzed Radiosoundings Archive v2 (from ARA/ABC(t)/LMD group)
AUX	Intermediate output of ISCCP processing system that combines information from TOPO, SURFACETYPE and REFGEO that is used in the procedure that produces the clear sky composites in the cloud detection algorithm
AVHRR	Advanced Very High Resolution Radiometer
B1U	ISCCP common format for geostationary radiometer images, sampled at 10 km intervals
B1QC	ISCCP quality checking program for B1U-format geostationary and AVHRR radiance data
B3 data	Previous 30-km-sampled version of the ISCCP radiance dataset
B4	Intermediate output from B4PROD subroutine of the ISCCP cloud detection algorithm
B4PLOTS	Graphical output from B4PROD used to monitor data quality
B4PROD	ISCCP processing system subroutine as part of the cloud detection algorithm that conducts spatial radiance contrast tests, re-maps images to common projections and performs temporal radiance contrasts tests

BANDWIDTH	Wavelength integral of IR channel spectral responses for each satellite
BSRN	Baseline Surface Radiation Network under GEWEX
BT	IR (10.5 m wavelength) radiances in energy units (Watts/m^2/sr/m)
BTCLR	IR (10.5 m wavelength) radiances for clear sky in energy units (Watts/m2/sr/mm)
BTOBS	IR (10.5 m wavelength) radiances that are observed in energy units (Watts/m2/sr/mm)
BX	Intermediate output from BXPROD in ISCCP cloud detection algorithm
BXPROD	ISCCP processing system subroutine as part of the cloud detection algorithm that applies preliminary radiance thresholds and writes out intermediate form of pixel-level data
CA	Cloud amount determined from the ratio of the number of cloudy pixels to the total number of pixels in an area (1.0-degree-equivalent equal-area map grid): equivalent to area cover fraction, if instantaneous, or to average cover fraction times frequency of occurrence if time-averaged
CAmarg	Marginal CA, clouds with radiance differences greater than one times TB and/or V but less than two times
CALCOR	ISCCP processing system subroutine that checks normalization of geostationary calibration to the primary afternoon AVHRR by comparing space-time matched values of TS/TC and RS/TAU (the latter converted to cloud reflectance)
Calipso	Cloud-Aerosol Lidar and Infrared Pathfinder Satellite Observation, joint CNES/NASA satellite mission
CERES	Clouds and the Earth's Radiant Energy System, total flux instruments flown on NASA Terra and Aqua satellites
Cirrostatus	ISCCP cloud type defined by PC 440 mb and 3.55 TAU < 22.63
Cirrus	ISCCP cloud type defined by PC 440 mb and TAU < 3.55
CLDRET	Subroutine in ISCCP processing system that returns TC/PC for cloudy sky values of TB
Cloud Mask	Pixel-level flag indicating cloud presence
CloudSat	NASA spaceborne cloud radar mission
CLRSKY	ISCCP processing system subroutine as part of the cloud detection algorithm that estimates the clear sky IR and VIS radiances for every pixel at each time
CMA	China Meteorological Administration
CMC	Canadian Meteorological Centre

CORRAD	ISCCP processing system subroutine that corrects R values for changing sun-earth distance and the effects of ozone absorption and stratospheric aerosol scattering/absorption
Cumulus	ISCCP cloud type defined by PC > 680 mb and TAU < 3.55
C-Version	First version of ISCCP Cloud Products covering 1983-1991
CY	Intermediate output from CYPROD
CYPROD	ISCCP processing system subroutine as part of the cloud detection algorithm that revises the clear sky composites and applies revised radiance thresholds to detect clouds
⊗R	Visible reflectance threshold in final part of ISCCP cloud detection algorithm, scene dependent
⊗™ℜ	IR brightness temperature threshold in preliminary and final part of ISCCP cloud detection algorithm, scene dependent
⊗V	Visible radiance threshold in preliminary part of ISCCP cloud detection algorithm, scene dependent
DX/D1/D2	ISCCP D-Version cloud products, equivalent to H-Version products HXS, HGG and HGH-HGM, respectively
DC	Deep Convective, ISCCP cloud type defined by PC □ 440 mb, TAU □ 22.63
DELn	Parameters used to test relationships of TB statistics in IR clear sky part of the ISCCP cloud detection algorithm (n = 1 – 4).
Delta RS	Calculated uncertainty of RS values based on CA_{marg} and associated properties
Delta TAU	Calculated uncertainty of TAU values based on CA_{marg} and associated properties
Delta TC-PC	Calculated uncertainty of TC-PC values based on CA_{marg} and associated properties
Delta TS	Calculated uncertainty of TS values based on CA_{marg} and associated properties
D-Version	Second version of ISCCP cloud products covering 1983-2009
e_S	Water saturation vapor pressure
EASE Grid	Equal-Area Scalable Earth Grid
ER-2	NASA research aircraft
EROS	Earth Resources Observation and Science Data Center, USGS
ESA	European Space Agency
EUMETSAT	European Organization for the Exploitation of Meteorological Satellites

GAC	Global Area Coverage data format for NOAA polar orbiting radiometer (AVHRR) data
GEWEX	Global Energy and Water Exchanges project of the World Climate Research Program
GISS	NASA Goddard Institute for Space Studies
GLIMS	Global Land Ice Measurements from Space
GMS	Geostationary Meteorological Satellite, first Japanese geostationary weather satellite series
GOES	Geostationary Operational Environmental Satellite (US geostationary weather satellite series)
GSICS	Global Space-based Inter-Calibration System
GOME	Global Ozone Monitoring Experiment, satellite operated by EUMETSAT
GUI	Graphical User Interface
HGG	Main ISCCP H-Version Cloud Product (100 km, 3 hr)
HGH	Monthly-mean-diurnal ISCCP H-Version Cloud Product (100 km, monthly but at eight times of day)
HGM	Monthly-mean ISCCP H-Version Cloud Product (100 km, monthly)
HGS	ISCCP-H Version Cloud Product (100 km, 3 hr) separate by satellite
Himawari	Series of Japanese geostationary meteorological satellites
HIRS	High resolution Infrared Radiometer Sounder, flown on NOAA polar orbiting weather satellites
HIRSPAC	ISCCP processing routine that computes profiles of top-of-atmosphere IR brightness temperatures as a function of satellite view zenith angle from NNHIRS and AEROSOL products
H-Version	High-resolution version of the ISCCP cloud products, covering 1982 to present
HXG	Globally merged Level 2 ISCCP H-Version Cloud Product (10 km, 3 hr)
HXS	Level 2 ISCCP H-Version Cloud Product (10 km, 3 hr), separate by satellite
IASI	Infrared Atmospheric Sounding Interferometer, flown on METOP satellites operated by EUMETSAT
IGBP	International Geosphere Biosphere Project
IMS	Interactive Multisensor Snow and Ice Mapping System, NOAA
INPE	Instituto Nacional de Pesquisas Espaciais, Brazil Institute of Space Research

INTEN	LUT for retrieval of surface reflectance ignoring aerosol effects
INTENn	LUTs for correcting for aerosol effects in retrievals of surface and cloud properties (n = 1 – 3)
IR	“Window” Infrared (≈ 10.5 μm wavelength) radiance
IREMISS	Table of IR (≈ 10.5 μm wavelength) emissivities by surface type
ISCCP	International Satellite Cloud Climatology Project
ISD	Integrated Surface Data, collection of surface weather station reports
JMA	Japan Meteorological Agency
LUT	Look Up Table
μ	Cosine satellite (view) zenith angle
μ_0	Cosine solar zenith angle
MACv.1	Global monthly aerosol product produced from combination of ground-based and satellite observations and an ensemble of transport model results
MLS	Microwave Limb Sounder
MISR	Multi-angle Imaging SpectroRadiometer flown on NASA Terra spacecraft
METEOSAT	European geostationary weather satellite series
METOP	European polar orbiting weather satellite series
MODIS	Moderate Resolution Imaging Spectroradiometer flown on NASA Terra and Aqua spacecraft
MONITOR	ISCCP program for correcting trends in VIS and IR AVHRR calibrations and normalizing them to the reference standard (combined NOAA-9 and NOAA-18)
MTSAT	Second series of Japanese geostationary weather satellites
NASA	National Aeronautical and Space Administration
NCEI	National Centers for Environmental Information (NOAA)
NCLEAR-LT	Number of CLEAR pixels available in each spatial sub-domain over long-time periods used in IR clear sky logic part of the ISCCP cloud detection algorithm
NCLEAR-ST	Number of CLEAR pixels available in each spatial sub-domain over short-time periods used in IR clear sky logic part of the ISCCP cloud detection algorithm
Nimbostratus	ISCCP cloud type defined by 440 < PC ≤ 680 mb and TAU ≥ 22.63
NNHIRS	ISCCP version of new HIRS analysis using a neural network method (100 km, 3 hr)
NOAA	National Oceanic and Atmospheric Administration

NORM	ISCCP program for normalizing geostationary radiometer VIS and IR calibrations to the contemporaneous, primary afternoon AVHRR
NSIDC	National Snow and Ice Data Center
O3	Total ozone column abundance in Dobson units
OMI	Ozone Measuring Instrument, flown on NASA Aura spacecraft
OPS Guide	ISCCP Processing System Operations Guide
OSI-SAF	Ocean Sea Ice – Satellite Application Facility (EUMETSAT)
OTAUHII	LUT for retrieval of ice cloud TAU over open water surfaces
OTAUHIW	LUT for retrieval of liquid water cloud TAU over open water surfaces
OZONE	ISCCP Ancillary product containing global (1.0 degree), daily values of total column ozone abundance
$\backslash_0$	Relative azimuth angle in degrees between satellite view and solar illumination directions (0° is forward scatter direction, 180° is backscatter direction)
P	Atmospheric pressure in millibars
PC	Cloud top pressure in millibars
PCHIP	Piecewise Cubic Hermite Interpolation procedure
PMAX	Pressure at maximum temperature in a profile, which can be PS
PS	Surface pressure in millibars
PT	Tropopause pressure in millibars
PTRANS	Look-up-table used to correct VIS radiances for ozone absorption
Q	Atmospheric specific humidity in g/kg
QA	Atmospheric specific humidity at the surface in g/kg
QAGRD1	LUT that returns RS (and RS0) values from corrected VIS radiances
QC	Quality Checking
QS	Saturation specific humidity in g/kg
QT	Atmospheric specific humidity at the tropopause in g/kg
R	Visible (0.65 m wavelength) reflectance as fraction
RCLR	Final selected clear sky value of R from the VIS clear sky logic part of the ISCCP cloud detection algorithm
REFGEO	ISCCP file containing image projection information for geostationary satellite images to allow determination of latitude-longitude of each image pixel
RH	Atmospheric relative humidity in percent
RHA	Atmospheric relative humidity at the surface in percent

RHMAX	Atmospheric relative humidity at profile-maximum temperature in percent
RHT	Atmospheric relative humidity at the tropopause in percent
RMIN-LT	Minimum R in each sub-domain over long-time periods in the VIS clear sky logic part of the ISCCP cloud detection algorithm
RMIN-ST	Minimum R in each sub-domain over short-time periods in the VIS clear sky logic part of the ISCCP cloud detection algorithm
RMNn	Minimum reflectances from the first stage clear sky composite (n = 1 – 3)
RMODEL	Values of R from the ocean surface reflectance model
RS	Surface visible reflectance as fraction
RS0	Special value of RS retrieved assuming zero tropospheric aerosol
RTM	Radiative Transfer Model
RTTOV	Operational RTM used for analysis of IR sounder data
SAGE	Stratospheric Aerosol and Gas Experiment, NASA
Satellite ID	Unique code number assigned to each satellite
SATHIER	ISCCP processing routine that determines a hierarchy of satellites viewing each location on Earth for each month/year
SAT.PM	ISCCP meta-data file containing information about which satellites are operating in each month/year, the source (format) of the imaging data and the image format characteristics
SATTABLE	Conversion table between TB and BT values
SBUV	Satellite Backscatter Ultraviolet
SCACOR	Subroutine that corrects liquid cloud brightness temperatures for IR scattering effects
SCAICE	Subroutine that corrects ice cloud brightness temperatures for IR scattering effects
SCIAMACHY	Imaging spectrometer (240 – 1700 nm wavelength), operated by ESA
SEAFLUX	GEWEX project to produce global, 3-hourly estimates of ocean surface turbulent fluxes
SHEBA	Surface Heat Budget of the Arctic field experiment in 1998
Shore	Label applied to land pixels close to open water or open water pixels close to land
Sigma	Standard deviation
SMOBA	Stratosphere Monitoring Ozone Blended Analysis, a NOAA combined SBUV and TOVS ozone product

SNOWICE	ISCCP Ancillary Product containing global (1.0 degree), daily values of land snow and sea ice cover fraction
SOLCON	Radiometer "solar constant" used to convert visible radiances to scaled radiances, defined as wavelength integral of the product of the solar spectrum at top-of-atmosphere and the normalized instrument spectral response function
SRFRET	Subroutine in ISCCP processing that returns TS for clear sky TB
SSM/I	Scanning Sensor Microwave/Imager
SSM/IS	Scanning Sensor Microwave/Imager-Sounder
Stratocumulus	ISCCP cloud type defined by PC > 680 mb and 3.55 ? TAU < 22.63
Stratus	ISCCP cloud type defined by PC > 680 mb and TAU ? 22.63
SURFACETYPE	ISCCP Ancillary Product containing surface type classifications (0.25 degree)
SWOOSH	Stratospheric Water and Ozone Satellite Homogenized data set
$\tau_{\sqrt{}}$	IR optical thickness by foreign-broadening part of water vapor continuum absorption
$\tau_{©}$	IR optical thickness by self-broadening part of water vapor continuum absorption
$\tau_{\not\subset}$	IR optical thickness of line absorption by water vapor
T	Atmospheric temperature in Kelvins
TA	Surface air temperature in Kelvins
TAU	Cloud visible optical thickness
TAUCOR	ISCCP processing system subroutine that corrects TC/PC for transmitted IR radiation through optically thin clouds
TAUF2	ISCCP subroutine that returns TAU for corrected VIS radiances over open water
TAUHII	LUT for retrieval of ice cloud TAU over land-ice surfaces when the cloudy scene is brighter than the clear sky
TAUHIW	LUT for retrieval of liquid water cloud TAU over land-ice surfaces when the cloudy scene is brighter than the clear sky
TAULOI	Special LUT for retrieval of ice cloud TAU over snow-ice surfaces when cloudy scene is darker than clear sky
TAULOW	Special LUT for retrieval of liquid water cloud TAU over snow-ice surfaces when cloudy scene is darker than clear sky

TAUVF	ISCCP subroutine that returns TAU for corrected VIS radiances over all surfaces, except open water, when the cloudy scene is brighter than clear sky
TAUVFP	ISCCP subroutine that returns TAU for corrected VIS radiances over snow-ice surfaces when the cloudy scene is darker than clear sky
TAVG-LT	Average TB for pixels labeled CLEAR after space and time tests in spatial sub-domain over long-time periods in the IR clear sky logic part of the ISCCP cloud detection algorithm
TAVG-ST	Average TB for pixels labeled CLEAR after space and time tests in each spatial sub-domain over short-time periods in the IR clear sky logic part of the ISCCP cloud detection algorithm
TB	Infrared (10.5 m wavelength) brightness temperature in Kelvins
TBNN	Intermediate output from HIRSPAC subroutine
TC	Cloud top temperature in Kelvins
TCLR	Final selected clear sky value for TB from the clear sky logic part of the ISCCP cloud detection algorithm
TIROS	Television Infrared Observation Satellite
TMAX	Atmospheric profile-maximum temperature in Kelvins, which can be TS
TMAXn	Maximum TB values in each spatial sub-domains where n indicates the ordinal order (n = 1 – 5) in the IR clear sky logic part of the ISCCP cloud detection algorithm
TMAX-LT	Selected maximum value from TMAXn in each spatial sub-domain for long-time periods in the IR clear sky logic part of the ISCCP cloud detection algorithm
TMAX-ST	Selected maximum value from TMAXn in each spatial sub-domain for long-time periods in the IR clear sky logic part of the ISCCP cloud detection algorithm
TMXn	Maximum TB values from the first stage clear sky composite for each surface type used to adjust the IR clear sky composite (n = 1 – 3)
TN	Infrared (10.5 m wavelength) brightness temperature in Kelvins corrected to nadir view
TOMS	Total Ozone Measuring Satellite
TOPO	ISCCP Ancillary Product containing global mean and standard deviation of topographic height (0.1 and 1.0 degree)
TOPP	Average clear sky values of TB in land-water-mixed sub-domains for pixels of opposite surface type from the target pixel

TOVS	TIROS Operational Vertical Sounder system, flown on NOAA polar orbiting weather satellites comprised of HIRS and either MSU/SSU or AMSU-A/B microwave sounder systems
TS	Surface skin temperature in Kelvins
TSAME	Average clear sky values of TB in land-water-mixed sub-domains for pixels of the same surface type as the target pixel
TT	Tropopause temperature in Kelvins
USGS	United States Geological Service
UTC	Universal Time Convention
UV	Ultraviolet
V	Visible (0.65 m wavelength) scaled radiance as fraction
VIS	Visible (0.65 m wavelength) radiance
VISCOR	ISCCP processing system subroutine that compares geostationary values of land RS to polar orbiter values to correct for effects of broader spectral response functions
WGS84	World Geodetic System
WP	Cloud water path in g/m^2

Appendix B.

Satellite Radiometer Characteristics

Listed below are the satellites and operating agencies that have provided data for the ISCCP products, the VIS and "window" IR spectral responses represented by the peak wavelengths, the instrument "solar constant", SOLCON, which is the wavelength integral of the product of the instrument VIS spectral response (normalized to unity) and the solar spectrum at the top of the atmosphere, and the BANDWIDTH, which is the wavelength interval that is equivalent to the wavelength integral over the spectral response (normalized to unity). Complete information about the spectral responses and the Calibration Coefficients for these satellites can be found by using, https://www.star.nesdis.noaa.gov/smcd/GCC/instrInfo-srf.php

SatName	Operator	Peak IR Wavelength	Bandwidth	Peak VIS Wavelength	Bandwidth	SOLCON
GMS-1	JMA	11.00	10.5 - 13.1	0.60	0.47 - 0.86	113.302
GMS-2	JMA	10.70	10.0 - 13.0	0.60	0.47 - 0.86	114.557
GMS-3	JMA	11.00	10.0 - 12.8	0.62	0.47 - 0.86	119.636
GMS-4	JMA	10.60	10.0 - 12.6	0.59	0.47 - 0.85	123.051
GMS-5	JMA	11.00	10.5 - 11.5	0.72	0.55 - 0.90	178.766
GOES-5	NOAA	11.20	10.5 - 12.6	0.58	0.50 - 0.85	94.564
GOES-6	NOAA	11.20	10.5 - 12.6	0.58	0.55 - 0.75	94.564
GOES-7	NOAA	11.20	10.5 - 12.6	0.65	0.55 - 0.75	106.875
GOES-8	NOAA	10.70	10.2 - 11.2	0.65	0.55 - 0.75	101.245
GOES-9	NOAA	10.70	10.2 - 11.2	0.65	0.55 - 0.75	105.685
GOES-10	NOAA	10.70	10.2 - 11.2	0.65	0.55 - 0.75	111.008
GOES-11	NOAA	10.70	10.2 - 11.2	0.65	0.55 - 0.75	112.425
GOES-12	NOAA	10.70	10.2 - 11.2	0.65	0.55 - 0.75	110.328
GOES-13	NOAA	10.70	10.2 - 11.2	0.65	0.55 - 0.75	82.072
GOES-15	NOAA	10.70	10.2 - 11.2	0.65	0.55 - 0.75	84.985
METEOSAT-2	EUM , ESA	11.50	10.5 - 12.5	0.70	0.50 - 0.90	158.274
METEOSAT-3	EUM , ESA	11.50	10.5 - 12.5	0.70	0.50 - 0.90	190.418
METEOSAT-4	EUM , ESA	11.50	10.5 - 12.5	0.70	0.50 - 0.90	189.122
METEOSAT-5	EUM , ESA	11.50	10.5 - 12.5	0.70	0.50 - 0.90	181.07
METEOSAT-6	EUM , ESA	11.50	10.5 - 12.5	0.70	0.50 - 0.90	179.629
METEOSAT-7	EUM , ESA	11.50	10.5 - 12.5	0.70	0.50 - 0.90	216.88
METEOSAT-8	EUM , ESA	10.80	9.8 - 11.8	0.64	0.56 - 0.71	38.607
METEOSAT-9	EUM , ESA	10.80	9.8 - 11.8	0.64	0.56 - 0.71	38.081
METEOSAT-10	EUM , ESA	10.80	9.8 - 11.8	0.64	0.56 - 0.71	36.896
METOP-2	EUMETSAT	10.80	10.3 - 11.3	0.63	0.58 - 0.68	44.5286

MTSAT-1R	JMA	10.80	10.2 - 12.6	0.60	0.53 - 0.79	118.717
MTSAT-2	JMA	10.80	10.3 - 11.3	0.68	0.55 - 0.80	100.727
NOAA-7	NOAA	10.80	10.3 - 11.3	0.62	0.55 - 0.68	56.688
NOAA-8	NOAA	11.00	10.5 - 11.5	0.62	0.55 - 0.68	56.722
NOAA-9	NOAA	10.80	10.3 - 11.3	0.62	0.55 - 0.68	60.954
NOAA-10	NOAA	11.00	10.5 - 11.5	0.60	0.55 - 0.68	56.92
NOAA-11	NOAA	10.80	10.3 - 11.3	0.60	0.55 - 0.68	58.648
NOAA-12	NOAA	10.80	10.3 - 11.3	0.60	0.55 - 0.68	63.9
NOAA-14	NOAA	10.80	10.3 - 11.3	0.60	0.55 - 0.68	65.464
NOAA-15	NOAA	10.80	10.3 - 11.3	0.63	0.58 - 0.68	42.514
NOAA-16	NOAA	10.80	10.3 - 11.3	0.63	0.58 - 0.68	42.514
NOAA-17	NOAA	10.80	10.3 - 11.3	0.63	0.58 - 0.68	43.365
NOAA-18	NOAA	10.80	10.3 - 11.3	0.63	0.58 - 0.68	42.327

Appendix C. Geophysical Variables in Each Product

All ISCCP H-Version Cloud and Ancillary data products, except HXS, are in NetCDF-4 format. Below is a listing of contents of the Cloud Products in the order in which they appear in nc_dump.

C.1. HXS

The HXS Product is the Level 2 Cloud Product that reports the basic analysis results for each individual satellite image at original sampling intervals (approx. 10-km, 3-hr) and includes more information about how the cloudy-clear decisions was reached, its uncertainty, alternate retrieval information for cloud and surface, and any (up to nine) extra radiances measured by the particular satellite at other wavelengths than the two used by the ISCCP analysis. The purpose of this product is to support development of cloud and other satellite retrieval methods and to study regional variations of clouds at the highest space-time resolution produced by ISCCP.

List of HXS Quantities (per pixel)

Geolocation: Longitude, Latitude

Scene Identification Flags: day/night, land/water, shore, rough topography, glint, snow/ice

Viewing Geometry: Cosine of Satellite Zenith Angle, Cosine of Solar Zenith Angle, Relative Azimuth Angle

Cloud Detection Test Results

Temperature Inversion Flag

Cloud Threshold Results

IR Radiances: IR Radiance, IR Clear Sky Composite Radiance

VIS Radiances: VIS Radiance, VIS Clear Sky Composite Radiance

Additional Channel Radiances

IR (unadjusted) Retrievals: Cloud Top or Surface Skin Temperature, Cloud Top or Surface Pressure, Clear Sky Composite (surface) Temperature, Clear Sky Composite (surface) Pressure

VIS Retrievals (VIS-adjusted): Cloud TAU (liquid) or Surface (visible) Reflectance, Clear Sky Composite (surface visible) Reflectance, Clear Sky Composite (surface visible)

Reflectance with No Aerosol Correction, Cloud Top Temperature (liquid), Cloud Top Pressure (liquid), Ice Cloud TAU, Ice Cloud Top Temperature, Ice Cloud Top Pressure

Quality Flags: IR Clear Sky Logic, VIS Clear Sky Logic, IR Retrieval, VIS retrieval

C.2. HXG

HXG is a globally merged 0.10-degree, 3-hr mapped version of the pixel-level results in HXS that are common to all satellites. Missing data are filled by simple space-time interpolations. The purpose of this product is to support the study of the interaction of clouds and the atmospheric circulation from convective-scale to global-scale. This product can also be used to remove or account for the effects of clouds in other satellite measurement analyses or be combined with other satellite measurements that provide enhanced cloud (or surface) information but at lower time resolution.

List of HXG Quantities (excluding fixed global attributes)

Map Grid Information

Count to Physical Value Conversion Tables: Temperature, Pressure, Visible Reflectance, Cloud Optical Thickness, Cloud Water Path

Scene Identification Flags: day_night, land_water, shore, hightopo, vegetation type, glint, snow_ice

Fill Types: None, Replicate in Longitude, Replicate in Latitude, Interpolate Diurnal

Viewing Geometry: Cosine of Satellite Zenith Angle, Cosine of Solar Zenith Angle, Relative Azimuth Angle

Cloud Detection Test Results

Temperature Inversion Flag

Cloud Mask

IR Radiances: IR Radiance, IR Clear Sky Composite Radiance

VIS Radiances: VIS Radiance, VIS Clear Sky Composite Radiance

IR (unadjusted) Retrievals: Cloud Top or Surface Skin Temperature, Cloud Top or Surface Pressure, Clear Sky Composite (surface) Temperature, Clear Sky Composite (surface) Pressure

VIS Retrievals (VIS-adjusted): Cloud TAU (liquid) or Surface (visible) Reflectance, Clear Sky Composite (surface visible) Reflectance, Clear Sky Composite (surface visible) Reflectance with No Aerosol Correction, Cloud Top Temperature (liquid), Cloud Top Pressure (liquid), Ice Cloud TAU, Ice Cloud Top Temperature, Ice Cloud Top Pressure

Quality Flags: IR Clear Sky Logic, VIS Clear Sky Logic, IR Retrieval, VIS retrieval

Input HXS Files

Satellites Present

Time Coverage: Year, Month, Day, GMT

Spatial Coverage

C.3. HGS

HGS is produced separately for each satellite from the pixel-level HXS results. This product reports the cloud and surface results averaged into a 1.0-degree-equivalent equal-area grid at 3-hr intervals and extends the basic cloud results to an estimate of total cloud cover and the amounts and properties of 18 cloud types defined by top pressure, optical thickness and phase. This product also provides higher-resolution detailed joint distributions of the basic cloud properties (top pressure, optical thickness during daytime, top pressure all day) and provides comprehensive uncertainty estimates for the cloud properties. This product retains more of the geographic coverage from individual satellites that is lost when the globally-merged products are produced by eliminating overlaps. All Ancillary Data Products (except AEROSOL) are also added. This product is intended for regional cloud and surface studies that can use a smaller volume product.

List of Quantities (excluding fixed global attributes)

Array Information: Pressure Intervals, TAU Intervals, Temperature Intervals, Relative Humidity Intervals

Cloud Types Information

Count to Physical Value Conversion Tables: Temperature, Temperature Variance, Pressure, Visible Reflectance, Cloud Optical Thickness, Ozone Abundance, Relative Humidity, Cloud Water Path

Map Grid Information (equal-area, conversion to square, including topography and surface types)

Scene Identification: day-land, day-water, day-coast, night-land, night-water, night-coast

Snow/Ice Cover

Temperature Inversion Flag

Viewing Geometry: cosine of satellite angle, cosine of solar zenith angle, relative azimuth angle

Cloud Amounts: Total Number of Pixels, Number of Cloudy Pixels, Number of IR-Cloudy Pixels, Number of IR-Only-Cloudy Pixels, Number of VIS-Only-Cloudy Pixels, Number of VIS/IR-Marginally-Cloudy Pixels, Number of IR-Marginally-Cloudy Pixels, Number of VIS-Marginally-Cloudy Pixels

Algorithm statistics: Number of Pixels with IR Long-Term Statistics, Ratio Number of IR-Clear Pixels < Clear IR to Number < Clear VIS, Ratio Number of VIS/IR-Clear Pixels > Clear VIS to Number < Clear VIS

PC and IR Cloud Distributions (unadjusted)

PC/TAU and VIS/IR Cloud Type Distributions (VIS-adjusted)

Ice Clouds: Number of Cloudy Pixels for Ice Cloud Types

Mean Cloud Top Pressure for All Cloudy Pixels (VIS-adjusted day, unadjusted night), IR-Cloudy Pixels (unadjusted), IR-Only-Cloudy Pixels (VIS-adjusted), VIS-Only-Cloudy Pixels (VIS-adjusted), IR-Marginally-Cloudy Pixels (unadjusted), VIS-Marginally-Cloudy Pixels (unadjusted), VIS/IR-Marginally-Cloudy Pixels (VIS-adjusted)

Sigma-PC for IR-Cloudy Pixels (unadjusted)

Mean Cloud Top Temperatures for All Cloudy Pixels (VIS-adjusted day, unadjusted night), IR-Cloudy Pixels (unadjusted), IR-Only-Cloudy Pixels (VIS-adjusted), VIS-Only-Cloudy Pixels (VIS-adjusted), IR-Marginally-Cloudy Pixels (unadjusted), VIS-Marginally-Cloudy Pixels (unadjusted), VIS/IR-Marginally-Cloudy Pixels (VIS-adjusted)

Sigma-TC for IR-Cloudy Pixels (unadjusted)

Mean Cloud Tau for All Cloudy Pixels, IR-Cloudy Pixels, IR-Only-Cloudy Pixels, VIS-Only-Cloudy Pixels, IR-Marginally-Cloudy Pixels, VIS-Marginally-Cloudy Pixels, VIS/IR-Marginally-Cloudy Pixels

Sigma-TAU for IR-Cloudy Pixels

Mean Cloud Water Path for All Cloudy Pixels, IR-Cloudy Pixels, IR-Only-Cloudy Pixels, VIS-Only-Cloudy Pixels, IR-Marginally-Cloudy Pixels, VIS-Marginally-Cloudy Pixels, VIS/IR-Marginally-Cloudy Pixels

Sigma-WP for IR-Cloudy Pixels

IR Cloud Type Mean Properties (unadjusted): CA, PC, TC

VIS/IR Cloud Type Mean Properties (VIS-adjusted): CA, PC, TC, TAU, WP

Mean Surface Skin Temperatures for: Clear Sky Composite, All Clear Pixels, IR-Clear Pixels, VIS-Clear Pixels, VIS/IR-Clear Pixels

Sigma-TS for IR-Clear Pixels

Mean Surface Visible Reflectances for: Clear Sky Composite, All Clear Pixels, IR-Clear Pixels, VIS-Clear Pixels, VIS/IR-Clear Pixels

Sigma-RS for IR-Clear Pixels

Mean and Sigma IR Brightness Temperatures for IR-Cloudy Pixels

Mean IR Brightness Temperatures for VIS-Cloudy Pixels, VIS/IR-Cloudy Pixels, IR-Clear Pixels

Sigma-IR Brightness Temperature for IR-Clear Pixels

Mean IR Brightness Temperatures for VIS-Clear Pixels, VIS/IR-Clear Pixels, Clear Sky Composite

Mean VIS Scaled Radiance for VIS/IR-Cloudy Pixels

Sigma-VIS Scaled Radiance for VIS/IR-Cloudy Pixels

Mean VIS Scaled Radiances for IR-Cloudy Pixels, VIS-Cloudy Pixels, VIS/IR-Clear Pixels

Sigma-VIS Scaled Radiance for VIS/IR-Clear Pixels

Mean VIS Scaled Radiances for IR-Clear Pixels, VIS-Clear Pixels, from Clear Sky Composite

Atmospheric Information: Origin Codes, Near-Surface Air Temperature, Temperature Profile, Maximum Temperature, Tropopause Temperature, Surface Pressure, Pressure at Maximum Temperature, Tropopause Pressure, Near-Surface Relative Humidity, Relative Humidity Profile, Relative Humidity at Maximum Temperature, Tropopause Relative Humidity, Ozone Abundance

Input HXS and Ancillary Data Files

Satellite ID

Time Coverage: Year, Month, Day, GMT

Spatial Coverage

C.4. HGG

HGG is the main ISCCP Cloud Product for global cloud-atmosphere-surface studies and is formed by the global merger of HGS (overlapping data are removed to favor the best viewing geometry). The information associated with Marginal Cloud Amounts and Properties can be used to estimate the uncertainties of the main cloud and surface properties related to uncertainty in cloud detection for each location and time. Ancillary quantities are present at all locations and times but results from the analysis of satellite radiances may be missing if a particular image is missing. A filling procedure is applied to reduce the amount of missing cloud and surface information, including an interpolation of daytime-only results over the nighttime interval and into the polar winter.

List of Quantities (excluding fixed global attributes)

Map Grid Information (equal-area, conversion to square, including topography and surface types)

Array Information: Pressure Intervals, TAU Intervals, Temperature Intervals, Relative Humidity Intervals

Cloud Types Information

Count to Physical Value Conversion Tables: Temperature, Temperature Variance, Pressure, Visible Reflectance, Cloud Optical Thickness, Ozone Abundance, Relative Humidity, Cloud Water Path

Satellite ID

Origin Code: not filled, single satellite fill, multi-satellite fill

Fill Information: Number of Missing GMTs, Number of Missing Days, Number of Missing Weeks, Fill Type (None, Estimate-VIS-at-Night, Interpolate-VIS-Overnight, Interpolate-Diurnal, Interpolate-Temporal, Replicate-Longitude, Replicate-Latitude, Interpolate-Weekly)

Scene Identification: day-land, day-water, day-coast, night-land, night-water, night-coast

Snow/Ice Cover

Temperature Inversion Flag

Viewing Geometry: cosine of satellite angle, cosine of solar zenith angle, relative azimuth angle

Cloud Amounts: Total Number of Pixels, Number of Cloudy Pixels, Number of IR-Cloudy Pixels, Number of IR-Only-Cloudy Pixels, Number of VIS-Only-Cloudy Pixels, Number of VIS/IR-Marginally-Cloudy Pixels, Number of IR-Marginally-Cloudy Pixels, Number of VIS-Marginally-Cloudy Pixels

Algorithm statistics: Number of Pixels with IR Long-Term Statistics, Ratio Number of IR-Clear Pixels < Clear IR to Number < Clear VIS, Ratio Number of VIS/IR-Clear Pixels > Clear VIS to Number < Clear VIS

PC and IR Cloud Type Distributions (unadjusted)

PC/TAU and VIS/IR Cloud Type Distributions (VIS-adjusted)

Mean Cloud Top Pressure for All Cloudy Pixels (VIS-adjusted day, unadjusted night), IR-Cloudy Pixels (unadjusted), IR-Only-Cloudy Pixels (VIS-adjusted), VIS-Only-Cloudy Pixels (VIS-adjusted), IR-Marginally-Cloudy Pixels (unadjusted), VIS-Marginally-Cloudy Pixels (unadjusted), VIS/IR-Marginally-Cloudy Pixels (VIS-adjusted)

Sigma-PC for IR-Cloudy Pixels (unadjusted)

Mean Cloud Top Temperatures for All Cloudy Pixels (VIS-adjusted day, unadjusted night), IR-Cloudy Pixels (unadjusted), IR-Only-Cloudy Pixels (VIS-adjusted), VIS-Only-Cloudy Pixels (VIS-adjusted), IR-Marginally-Cloudy Pixels (unadjusted), VIS-Marginally-Cloudy Pixels (unadjusted), VIS/IR-Marginally-Cloudy Pixels (VIS-adjusted)

Sigma-TC for IR-Cloudy Pixels (unadjusted)

Mean Cloud Tau for All Cloudy Pixels, IR-Cloudy Pixels, IR-Only-Cloudy Pixels, VIS-Only-Cloudy Pixels, IR-Marginally-Cloudy Pixels, VIS-Marginally-Cloudy Pixels, VIS/IR-Marginally-Cloudy Pixels

Sigma-TAU for IR-Cloudy Pixels

Mean Cloud Water Path for All Cloudy Pixels, IR-Cloudy Pixels, IR-Only-Cloudy Pixels, VIS-Only-Cloudy Pixels, IR-Marginally-Cloudy Pixels, VIS-Marginally-Cloudy Pixels, VIS/IR-Marginally-Cloudy Pixels

Sigma-WP for IR-Cloudy Pixels

IR Cloud Type Mean Properties (unadjusted): CA, PC, TC

VIS/IR Cloud Type Mean Properties (VIS-adjusted): CA, PC, TC, TAU, WP

Mean Surface Skin Temperatures for: Clear Sky Composite, All Clear Pixels, IR-Clear Pixels, VIS-Clear Pixels, VIS/IR-Clear Pixels

Sigma-TS for IR-Clear Pixels

Mean Surface Visible Reflectances for: Clear Sky Composite, All Clear Pixels, IR-Clear Pixels, VIS-Clear Pixels, VIS/IR-Clear Pixels

Sigma-RS for IR-Clear Pixels

Mean and Sigma IR Brightness Temperatures for IR-Cloudy Pixels

Mean IR Brightness Temperatures for VIS-Cloudy Pixels, VIS/IR-Cloudy Pixels, IR-Clear Pixels

Sigma-IR Brightness Temperature for IR-Clear Pixels

Mean IR Brightness Temperatures for VIS-Clear Pixels, VIS/IR-Clear Pixels, Clear Sky Composite

Mean VIS Scaled Radiance for VIS/IR-Cloudy Pixels

Sigma-VIS Scaled Radiance for VIS/IR-Cloudy Pixels

Mean VIS Scaled Radiances for IR-Cloudy Pixels, VIS-Cloudy Pixels, VIS/IR-Clear Pixels

Sigma-VIS Scaled Radiance for VIS/IR-Clear Pixels

Mean VIS Scaled Radiances for IR-Clear Pixels, VIS-Clear Pixels, from Clear Sky Composite

Atmospheric Information: Origin Codes, Near-Surface Air Temperature, Temperature Profile, Maximum Temperature, Tropopause Temperature, Surface Pressure, Pressure at Maximum Temperature, Tropopause Pressure, Near-Surface Relative Humidity, Relative Humidity Profile, Relative Humidity at Maximum Temperature, Tropopause Relative Humidity, Ozone Abundance

Input HGS Files

Satellite ID

Time Coverage: Year, Month, Day, GMT

Spatial Coverage

C.5. HGH

HGH reports the time-averaged HGG results at eight UTC times of day for each month in the record to allow for the study of the mean diurnal variations of clouds, atmosphere and surface.

List of Quantities (excluding fixed global attributes)

Map Grid Information (equal-area, conversion to square, including topography and surface types)

Array Information: Pressure Intervals, TAU Intervals, Temperature Intervals, Relative Humidity Intervals

Cloud Types Information

Count to Physical Value Conversion Tables: Temperature, Temperature Variance, Pressure, Visible Reflectance, Cloud Optical Thickness, Ozone Abundance, Relative Humidity, Cloud Water Path

Scene Identification: land, water, coast

Number of Observations (HGG cells), Number of Day-Time Observations, Number of Original Cells, Number of Satellite Hierarchy Top-Level Cells

Mean Cloud Amount and Frequency of Occurrence

Mean and Time-Standard Deviation of Cloud Top Pressure

Mean and Time-Standard Deviation of Cloud Top Temperature

Mean and Time-Standard Deviation of Cloud Optical Thickness

Mean and Time-Standard Deviation of Cloud Water Path

Mean IR-Cloud Amount

Mean and Mean Space-Standard Deviation IR-Cloud Top Pressure

Mean and Mean Space-Standard Deviation IR-Cloud Top Temperature

Mean and Mean Space-Standard Deviation IR-Cloud Optical Thickness

Mean and Mean Space-Standard Deviation IR-Cloud Water Path

Mean IR-Only Cloud Amount, Top Pressure, Top Temperature, Optical Thickness, Water Path

Mean VIS-Only Cloud Amount, Top Pressure, Top Temperature, Optical Thickness, Water Path

Mean IR-Marginal Cloud Amount, Top Pressure, Top Temperature, Optical Thickness, Water Path

Mean VIS-Marginal Cloud Amount, Top Pressure, Top Temperature, Optical Thickness, Water Path

Mean VIS/IR-Marginal Cloud Amount, Top Pressure, Top Temperature, Optical Thickness, Water Path

IR Cloud Type Mean Properties (unadjusted): CA, PC, TC

VIS/IR Cloud Type Mean Properties (VIS-adjusted): CA, PC, TC, TAU, WP

Mean Surface Skin Temperatures for: All Clear Pixels, Clear Sky Composite

Mean Surface Visible Reflectances for: All Clear Pixels, Clear Sky Composite

Mean Snow/Ice Cover

Atmospheric Information: Near-Surface Air Temperature, Temperature Profile, Maximum Temperature, Tropopause Temperature, Surface Pressure, Pressure at Maximum Temperature, Tropopause Pressure, Near-Surface Relative Humidity, Relative Humidity Profile, Relative Humidity at Maximum Temperature, Tropopause Relative Humidity, Ozone Abundance

Input HGG Files

Satellite ID

Time Coverage: Year, Month, Day, GMT

Spatial Coverage

C.6. HGM

HGM provides the monthly averages (over the diurnal cycle) of the HGH results. Note that the proper way to average a data record containing a quasi-regular variation, like a diurnal cycle, and a more nearly random variation, like synoptic weather variations, is to first form the average of the regular cycle before averaging over it: hence the HGH product is

produced first, followed by HGM. The purpose of this product is to study longer-term (seasonal to decadal) variations of clouds, atmosphere and surface.

List of Quantities (excluding fixed global attributes)

Map Grid Information (equal-area, conversion to square, including topography and surface types)

Array Information: Pressure Intervals, TAU Intervals, Temperature Intervals, Relative Humidity Intervals

Cloud Types Information

Count to Physical Value Conversion Tables: Temperature, Temperature Variance, Pressure, Visible Reflectance, Cloud Optical Thickness, Ozone Abundance, Relative Humidity, Cloud Water Path

Scene Identification: land, water, coast

Number of Observations (HGH cells), Number of Day-Time Observations, Number of Original Cells, Number of Satellite Hierarchy Top-Level Cells

Mean Cloud Amount, Frequency of Occurrence of Mean Hourly Cloud Amount

Mean and Time-Standard Deviation of Cloud Top Pressure

Mean and Time-Standard Deviation of Cloud Top Temperature

Mean and Time-Standard Deviation of Cloud Optical Thickness

Mean and Time-Standard Deviation of Cloud Water Path

Mean IR-Cloud Amount

Mean and Mean Space-Standard Deviation IR-Cloud Top Pressure

Mean and Mean Space-Standard Deviation IR-Cloud Top Temperature

Mean and Mean Space-Standard Deviation IR-Cloud Optical Thickness

Mean and Mean Space-Standard Deviation IR-Cloud Water Path

Mean IR-Only Cloud Amount, Top Pressure, Top Temperature, Optical Thickness, Water Path

Mean VIS-Only Cloud Amount, Top Pressure, Top Temperature, Optical Thickness, Water Path

Mean IR-Marginal Cloud Amount, Top Pressure, Top Temperature, Optical Thickness, Water Path

Mean VIS-Marginal Cloud Amount, Top Pressure, Top Temperature, Optical Thickness, Water Path

Mean VIS/IR-Marginal Cloud Amount, Top Pressure, Top Temperature, Optical Thickness, Water Path

IR Cloud Type Mean Properties (unadjusted): CA, PC, TC

VIS/IR Cloud Type Mean Properties (VIS-adjusted): CA, PC, TC, TAU, WP

Mean Surface Skin Temperatures for: Clear Sky Composite, All Clear Pixels

Mean Surface Visible Reflectances for: Clear Sky Composite, All Clear Pixels

Mean Snow/Ice Cover

Atmospheric Information: Near-Surface Air Temperature, Temperature Profile, Maximum Temperature, Tropopause Temperature, Surface Pressure, Pressure at Maximum Temperature, Tropopause Pressure, Near-Surface Relative Humidity, Relative Humidity Profile, Relative Humidity at Maximum Temperature, Tropopause Relative Humidity, Ozone Abundance

Input HGH Files

Satellite ID

Time Coverage: Year, Month, Day, GMT

Spatial Coverage

C.7 Count-Conversion Tables

COUNT	Temp	Temp-VAR	Press	Refl	TAU	Ozone	RH	WP
0	160.0	0.000	10.	0.002	0.01	40.	0.1	0.05
1	165.0	0.075	15.	0.004	0.02	50.	0.5	0.10
2	169.0	0.300	20.	0.008	0.04	60.	1.0	0.30
3	172.0	0.600	25.	0.012	0.06	70.	1.5	0.50
4	175.0	0.900	30.	0.016	0.09	80.	2.0	0.80
5	177.8	1.200	35.	0.020	0.11	90.	2.5	1.10
6	180.5	1.500	40.	0.024	0.14	100.	3.0	1.40
7	183.0	1.800	45.	0.028	0.16	110.	3.5	1.60
8	185.5	2.100	50.	0.032	0.19	120.	4.0	1.90
9	187.8	2.400	55.	0.036	0.22	130.	4.5	2.20
10	190.0	2.700	60.	0.040	0.24	140.	5.0	2.40
11	192.0	3.000	65.	0.044	0.27	150.	5.5	2.70
12	194.0	3.300	70.	0.048	0.30	160.	6.0	3.00
13	195.8	3.600	75.	0.052	0.33	170.	6.5	3.30
14	197.5	3.900	80.	0.056	0.37	180.	7.0	3.70
15	199.3	4.200	85.	0.060	0.40	190.	7.5	4.00
16	201.0	4.500	90.	0.064	0.43	200.	8.0	4.30
17	202.8	4.800	95.	0.068	0.46	205.	8.5	4.60
18	204.5	5.100	100.	0.072	0.50	210.	9.0	5.00
19	206.3	5.400	105.	0.076	0.53	215.	9.5	5.30

COUNT	Temp	Temp-VAR	Press	Refl	TAU	Ozone	RH	WP
20	208.0	5.700	110.	0.080	0.57	220.	10.0	5.70
21	209.8	6.000	115.	0.084	0.60	221.	10.5	6.00
22	211.5	6.300	120.	0.088	0.64	222.	11.0	6.40
23	212.8	6.600	125.	0.092	0.68	223.	11.5	6.80
24	214.1	6.900	130.	0.096	0.72	224.	12.0	7.20
25	215.4	7.200	135.	0.100	0.75	225.	12.5	7.50
26	216.7	7.500	140.	0.104	0.79	226.	13.0	7.90
27	218.0	7.800	145.	0.108	0.83	227.	13.5	8.30
28	219.2	8.100	150.	0.112	0.87	228.	14.0	8.70
29	220.5	8.400	155.	0.116	0.92	229.	14.5	9.20
30	221.8	8.700	160.	0.120	0.96	230.	15.0	9.60
31	223.1	9.000	165.	0.124	1.00	231.	15.5	10.00
32	224.4	9.300	170.	0.128	1.04	232.	16.0	10.40
33	225.4	9.600	175.	0.132	1.09	233.	16.5	10.90
34	226.5	9.900	180.	0.136	1.13	234.	17.0	11.30
35	227.5	10.200	185.	0.140	1.18	235.	17.5	11.80
36	228.6	10.500	190.	0.144	1.22	236.	18.0	12.20
37	229.6	10.800	195.	0.148	1.27	237.	18.5	12.70
38	230.6	11.100	200.	0.152	1.32	238.	19.0	13.20
39	231.7	11.400	204.	0.156	1.37	239.	19.5	13.70
40	232.7	11.700	208.	0.160	1.42	240.	20.0	14.20
41	233.8	12.000	212.	0.164	1.47	241.	20.5	14.70
42	234.8	12.300	216.	0.168	1.52	242.	21.0	15.20
43	235.7	12.600	220.	0.172	1.57	243.	21.5	15.70
44	236.6	12.900	224.	0.176	1.62	244.	22.0	16.20
45	237.5	13.200	228.	0.180	1.67	245.	22.5	16.70

COUNT	Temp	Temp-VAR	Press	Refl	TAU	Ozone	RH	WP
46	238.4	13.500	232.	0.184	1.73	246.	23.0	17.30
47	239.3	13.800	236.	0.188	1.78	247.	23.5	17.80
48	240.1	14.100	240.	0.192	1.83	248.	24.0	18.30
49	241.0	14.400	244.	0.196	1.89	249.	24.5	18.90
50	241.9	14.700	248.	0.200	1.95	250.	25.0	19.50
51	242.8	15.000	252.	0.204	2.00	251.	25.5	20.00
52	243.7	15.300	256.	0.208	2.06	252.	26.0	20.60
53	244.5	15.600	260.	0.212	2.12	253.	26.5	21.20
54	245.3	15.900	264.	0.216	2.18	254.	27.0	21.80
55	246.1	16.200	268.	0.220	2.24	255.	27.5	22.40
56	246.9	16.500	272.	0.224	2.30	256.	28.0	23.00
57	247.7	16.800	276.	0.228	2.36	257.	28.5	23.60
58	248.5	17.100	280.	0.232	2.43	258.	29.0	24.30
59	249.3	17.400	284.	0.236	2.49	259.	29.5	24.90
60	250.1	17.700	288.	0.240	2.55	260.	30.0	25.50
61	250.9	18.000	292.	0.244	2.62	261.	30.5	26.20
62	251.7	18.300	296.	0.248	2.69	262.	31.0	26.90
63	252.4	18.600	300.	0.252	2.75	263.	31.5	27.50
64	253.1	18.900	304.	0.256	2.82	264.	32.0	28.20
65	253.9	19.200	308.	0.260	2.89	265.	32.5	28.90
66	254.6	19.500	312.	0.264	2.96	266.	33.0	29.60
67	255.3	19.800	316.	0.268	3.03	267.	33.5	30.30
68	256.0	20.100	320.	0.272	3.10	268.	34.0	31.00
69	256.7	20.400	324.	0.276	3.18	269.	34.5	31.80
70	257.5	20.700	328.	0.280	3.25	270.	35.0	32.50
71	258.2	21.000	332.	0.284	3.32	271.	35.5	33.20

COUNT	Temp	Temp-VAR	Press	Refl	TAU	Ozone	RH	WP
72	258.9	21.300	336.	0.288	3.40	272.	36.0	34.00
73	259.5	21.600	340.	0.292	3.48	273.	36.5	34.80
74	260.2	21.900	344.	0.296	3.55	274.	37.0	35.50
75	260.9	22.200	348.	0.300	3.63	275.	37.5	36.30
76	261.5	22.500	352.	0.304	3.71	276.	38.0	37.10
77	262.1	22.800	356.	0.308	3.79	277.	38.5	37.90
78	262.8	23.100	360.	0.312	3.88	278.	39.0	38.80
79	263.4	23.400	364.	0.316	3.96	279.	39.5	39.20
80	264.1	23.700	368.	0.320	4.04	280.	40.0	40.40
81	264.8	24.000	372.	0.324	4.13	281.	40.5	41.30
82	265.4	24.300	376.	0.328	4.22	282.	41.0	42.20
83	266.0	24.600	380.	0.332	4.30	283.	41.5	43.00
84	266.6	24.900	384.	0.336	4.39	284.	42.0	43.90
85	267.2	25.200	388.	0.340	4.48	285.	42.5	44.80
86	267.8	25.500	392.	0.344	4.57	286.	43.0	45.70
87	268.5	25.800	396.	0.348	4.67	287.	43.5	46.70
88	269.1	26.100	400.	0.352	4.76	288.	44.0	47.60
89	269.7	26.400	404.	0.356	4.85	289.	44.5	48.50
90	270.3	26.700	408.	0.360	4.95	290.	45.0	49.50
91	270.9	27.000	412.	0.364	5.05	291.	45.5	50.50
92	271.5	27.300	416.	0.368	5.15	292.	46.0	51.50
93	272.1	27.600	420.	0.372	5.25	293.	46.5	52.50
94	272.7	27.900	424.	0.376	5.35	294.	47.0	53.50
95	273.2	28.200	428.	0.380	5.45	295.	47.5	54.50
96	273.8	28.500	432.	0.384	5.56	296.	48.0	55.60
97	274.4	28.800	436.	0.388	5.66	297.	48.5	56.60

COUNT	Temp	Temp-VAR	Press	Refl	TAU	Ozone	RH	WP
98	275.0	29.100	440.	0.392	5.77	298.	49.0	57.70
99	275.6	29.400	444.	0.396	5.88	299.	49.5	58.80
100	276.1	29.700	448.	0.400	5.99	300.	50.0	59.90
101	276.7	30.000	452.	0.404	6.11	301.	50.5	61.10
102	277.3	30.300	456.	0.408	6.22	302.	51.0	62.20
103	277.8	30.600	460.	0.412	6.34	303.	51.5	63.40
104	278.4	30.900	464.	0.416	6.45	304.	52.0	64.50
105	278.9	31.200	468.	0.420	6.57	305.	52.5	65.70
106	279.5	31.500	472.	0.424	6.69	306.	53.0	66.90
107	280.0	31.800	476.	0.428	6.82	307.	53.5	68.20
108	280.5	32.100	480.	0.432	6.94	308.	54.0	69.40
109	281.1	32.400	484.	0.436	7.07	309.	54.5	70.70
110	281.6	32.700	488.	0.440	7.20	310.	55.0	72.00
111	282.2	33.000	492.	0.444	7.33	311.	55.5	73.30
112	282.7	33.300	496.	0.448	7.46	312.	56.0	74.60
113	283.2	33.600	500.	0.452	7.59	313.	56.5	75.50
114	283.7	33.900	504.	0.456	7.73	314.	57.0	77.30
115	284.2	34.200	508.	0.460	7.87	315.	57.5	78.70
116	284.7	34.500	512.	0.464	8.01	316.	58.0	80.10
117	285.3	34.800	516.	0.468	8.15	317.	58.5	81.50
118	285.8	35.100	520.	0.472	8.30	318.	59.0	83.00
119	286.3	35.400	524.	0.476	8.44	319.	59.5	84.40
120	286.8	35.700	528.	0.480	8.59	320.	60.0	85.90
121	287.3	36.000	532.	0.484	8.74	321.	60.5	87.40
122	287.8	36.300	536.	0.488	8.90	322.	61.0	89.00
123	288.3	36.600	540.	0.492	9.06	323.	61.5	90.60

COUNT	Temp	Temp-VAR	Press	Refl	TAU	Ozone	RH	WP
124	288.8	36.900	544.	0.496	9.22	324.	62.0	92.20
125	289.3	37.200	548.	0.500	9.38	325.	62.5	93.80
126	289.8	37.500	552.	0.504	9.54	326.	63.0	95.40
127	290.3	37.800	556.	0.508	9.71	327.	63.5	97.10
128	290.7	38.100	560.	0.512	9.88	328.	64.0	98.80
129	291.2	38.400	564.	0.516	10.05	329.	64.5	100.50
130	291.7	38.700	568.	0.520	10.23	330.	65.0	102.30
131	292.2	39.000	572.	0.524	10.41	331.	65.5	104.10
132	292.7	39.300	576.	0.528	10.59	332.	66.0	105.90
133	293.2	39.600	580.	0.532	10.78	333.	66.5	107.80
134	293.6	39.900	584.	0.536	10.97	334.	67.0	109.70
135	294.1	40.200	588.	0.540	11.16	335.	67.5	111.60
136	294.6	40.500	592.	0.544	11.35	336.	68.0	113.50
137	295.0	40.800	596.	0.548	11.55	337.	68.5	115.50
138	295.5	41.100	600.	0.552	11.76	338.	69.0	117.60
139	296.0	41.400	604.	0.556	11.96	339.	69.5	119.60
140	296.5	41.700	608.	0.560	12.17	340.	70.0	121.70
141	296.9	42.000	612.	0.564	12.39	341.	70.5	123.90
142	297.4	42.300	616.	0.568	12.60	342.	71.0	126.00
143	297.9	42.600	620.	0.572	12.83	343.	71.5	128.30
144	298.3	42.900	624.	0.576	13.05	344.	72.0	130.50
145	298.8	43.200	628.	0.580	13.28	345.	72.5	132.80
146	299.2	43.500	632.	0.584	13.52	346.	73.0	135.20
147	299.6	43.800	636.	0.588	13.76	347.	73.5	137.60
148	300.1	44.100	640.	0.592	14.00	348.	74.0	140.00
149	300.5	44.400	644.	0.596	14.25	349.	74.5	142.50

COUNT	Temp	Temp-VAR	Press	Refl	TAU	Ozone	RH	WP
150	301.0	44.700	648.	0.600	14.51	350.	75.0	145.10
151	301.4	45.000	652.	0.604	14.77	351.	75.5	147.70
152	301.9	45.300	656.	0.608	15.03	352.	76.0	150.30
153	302.3	45.600	660.	0.612	15.30	353.	76.5	153.00
154	302.8	45.900	664.	0.616	15.58	354.	77.0	155.80
155	303.2	46.200	668.	0.620	15.86	355.	77.5	158.60
156	303.6	46.500	672.	0.624	16.15	356.	78.0	161.50
157	304.0	46.800	676.	0.628	16.44	357.	78.5	164.40
158	304.5	47.100	680.	0.632	16.74	358.	79.0	167.40
159	304.9	47.400	684.	0.636	17.05	359.	79.5	170.60
160	305.3	47.700	688.	0.640	17.36	360.	80.0	173.60
161	305.8	48.000	692.	0.644	17.69	361.	80.5	176.90
162	306.2	48.300	696.	0.648	18.02	362.	81.0	180.20
163	306.6	48.600	700.	0.652	18.35	363.	81.5	183.50
164	307.0	48.900	704.	0.656	18.70	364.	82.0	187.00
165	307.5	49.200	708.	0.660	19.05	365.	82.5	190.50
166	307.9	49.500	712.	0.664	19.41	366.	83.0	194.10
167	308.3	49.800	716.	0.668	19.78	367.	83.5	197.80
168	308.7	50.100	720.	0.672	20.16	368.	84.0	201.60
169	309.1	50.400	724.	0.676	20.54	369.	84.5	205.40
170	309.6	50.700	728.	0.680	20.94	370.	85.0	209.40
171	310.0	51.000	732.	0.684	21.35	371.	85.5	213.50
172	310.4	51.300	736.	0.688	21.77	372.	86.0	217.70
173	310.8	51.600	740.	0.692	22.20	373.	86.5	222.00
174	311.2	51.900	744.	0.696	22.63	374.	87.0	226.30
175	311.6	52.200	748.	0.700	23.09	375.	87.5	230.90

COUNT	Temp	Temp-VAR	Press	Refl	TAU	Ozone	RH	WP
176	312.0	52.500	752.	0.704	23.55	376.	88.0	235.50
177	312.5	52.800	756.	0.708	24.03	377.	88.5	240.30
178	312.9	53.100	760.	0.712	24.52	378.	89.0	245.20
179	313.3	53.400	764.	0.716	25.02	379.	89.5	250.20
180	313.7	53.700	768.	0.720	25.54	380.	90.0	255.40
181	314.1	54.000	772.	0.724	26.07	381.	90.5	260.70
182	314.5	54.300	776.	0.728	26.62	382.	91.0	266.20
183	314.9	54.600	780.	0.732	27.19	383.	91.5	271.90
184	315.3	54.900	784.	0.736	27.77	384.	92.0	277.70
185	315.7	55.200	788.	0.740	28.37	385.	92.5	283.70
186	316.1	55.500	792.	0.744	28.99	386.	93.0	289.90
187	316.5	55.800	796.	0.748	29.63	387.	93.5	296.30
188	316.8	56.100	800.	0.752	30.29	388.	94.0	302.90
189	317.2	56.400	804.	0.756	30.97	389.	94.5	309.70
190	317.6	56.700	808.	0.760	31.67	390.	95.0	316.70
191	318.0	57.000	812.	0.764	32.40	391.	95.5	324.00
192	318.4	57.300	816.	0.768	33.16	392.	96.0	331.60
193	318.8	57.600	820.	0.772	33.94	393.	96.5	339.40
194	319.2	57.900	824.	0.776	34.74	394.	97.0	347.40
195	319.5	58.200	828.	0.780	35.58	395.	97.5	355.80
196	319.9	58.500	832.	0.784	36.45	396.	98.0	364.50
197	320.3	58.800	836.	0.788	37.35	397.	98.5	373.50
198	320.7	59.100	840.	0.792	38.29	398.	99.0	382.90
199	321.1	59.400	844.	0.796	39.26	399.	99.5	392.60
200	321.4	59.700	848.	0.800	40.26	400.	100.0	402.60
201	321.8	60.000	852.	0.804	41.32	402.	100.5	413.20

COUNT	Temp	Temp-VAR	Press	Refl	TAU	Ozone	RH	WP
202	322.2	60.300	856.	0.808	42.42	404.	101.0	424.20
203	322.6	60.600	860.	0.812	43.57	406.	101.5	435.70
204	323.0	60.900	864.	0.816	44.76	408.	102.0	447.60
205	323.3	61.200	868.	0.820	46.00	410.	102.5	460.00
206	323.7	61.500	872.	0.824	47.31	412.	103.0	473.10
207	324.1	61.800	876.	0.828	48.68	414.	103.5	486.80
208	324.5	62.100	880.	0.832	50.11	416.	104.0	501.10
209	324.9	62.400	884.	0.836	51.60	418.	104.5	516.00
210	325.2	62.700	888.	0.840	53.17	420.	105.0	531.70
211	325.6	63.000	892.	0.844	54.84	423.	105.5	548.40
212	326.0	63.300	896.	0.848	56.59	426.	106.0	565.90
213	326.4	63.600	900.	0.852	58.43	429.	106.5	584.30
214	326.7	63.900	904.	0.856	60.36	432.	107.0	603.60
215	327.1	64.200	908.	0.860	62.40	435.	107.5	624.00
216	327.4	64.500	912.	0.864	64.59	438.	108.0	645.90
217	327.8	64.800	916.	0.868	66.90	441.	108.5	669.00
218	328.2	65.100	920.	0.872	69.36	444.	109.0	693.60
219	328.5	65.400	924.	0.876	71.96	447.	109.5	719.60
220	328.9	65.700	928.	0.880	74.72	450.	110.0	747.20
221	329.2	66.000	932.	0.884	77.73	453.	111.0	777.30
222	329.6	66.300	936.	0.888	80.94	456.	112.0	809.40
223	330.0	66.600	940.	0.892	84.38	459.	113.0	843.80
224	330.3	66.900	944.	0.896	88.06	462.	114.0	880.60
225	330.6	67.200	948.	0.900	92.02	465.	115.0	920.20
226	331.0	67.500	952.	0.904	96.40	468.	116.0	964.00
227	331.4	67.800	956.	0.908	101.01	471.	117.0	1010.10

COUNT	Temp	Temp-VAR	Press	Refl	TAU	Ozone	RH	WP
228	331.7	68.100	960.	0.912	105.51	474.	118.0	1055.10
229	332.1	68.400	964.	0.916	109.87	480.	119.0	1098.70
230	332.4	68.700	968.	0.920	114.33	485.	120.0	1143.30
231	332.8	69.000	972.	0.924	119.59	490.	121.0	1195.90
232	333.1	69.300	976.	0.928	125.92	495.	122.0	1259.20
233	333.5	69.600	980.	0.932	133.66	500.	123.0	1336.60
234	333.8	69.900	984.	0.936	143.12	505.	124.0	1431.20
235	334.1	70.200	988.	0.940	154.65	510.	125.0	1546.50
236	334.5	70.500	992.	0.944	169.56	515.	126.0	1695.60
237	334.9	70.800	996.	0.948	187.49	520.	127.0	1874.90
238	335.2	71.100	1000.	0.952	207.20	525.	128.0	2072.00
239	335.6	71.400	1003.	0.956	228.13	530.	129.0	2277.20
240	335.9	71.700	1006.	0.960	250.44	535.	130.0	2422.40
241	336.3	72.000	1009.	0.964	282.78	540.	131.0	2687.60
242	336.6	72.300	1013.	0.968	323.92	545.	132.0	2892.80
243	336.9	72.600	1016.	0.972	378.65	550.	133.0	3098.00
244	337.3	72.900	1019.	0.976	450.00	555.	134.0	3303.10
245	337.6	73.200	1022.	0.980	-1000.00	560.	135.0	3508.30
246	338.0	73.500	1025.	0.984	-1000.00	565.	136.0	3713.50
247	338.6	73.800	-1000.	0.988	-1000.00	570.	137.0	3918.70
248	339.3	74.100	-1000.	0.992	-1000.00	575.	138.0	4123.90
249	340.0	74.400	-1000.	0.996	-1000.00	580.	139.0	4329.10
250	341.0	74.700	-1000.	1.000	-1000.00	585.	140.0	4534.30
251	342.0	75.000	-1000.	1.030	-1000.00	590.	142.0	4739.50
252	343.0	80.000	-1000.	1.060	-1000.00	595.	144.0	4944.70
253	345.0	85.000	-1000.	1.090	-1000.00	600.	147.0	5149.85

COUNT	Temp	Temp-VAR	Press	Refl	TAU	Ozone	RH	WP
254	350.0	90.000	-1000.	1.120	-1000.00	-1000.	150.0	5355.00
255	-1000.0	-1000.000	-1000.	-1000.000	-1000.00	-1000.	-1000.0	-1000.00

Appendix D. ANCILLARY DATA PRODUCTS

D.1. NNHIRS

Description: NNHIRS is a time varying data product reporting the global variations of the vertical distributions of atmospheric temperature and relative humidity every 3 hours. The basic 1.0-degree product is used in the ISCCP L2 (pixel-level) processing and reported in the L3 (gridded) products.

Format and Contents: The format is NetCDF-4. The product reports global maps every three hours of the vertical profiles from surface to "top" of atmosphere (defined as 10 mb) of the temperature and relative humidity. The temperature and relative humidity are reported at up to nineteen pressure levels, defined by sixteen standard pressures (if present above topography), at the surface (taken to be an estimate of the 2m values), at the tropopause and at the profile-maximum temperature level. The profile-maximum temperature level may either be at the surface or at another pressure level if a near-surface temperature inversion is present. The pressures of the latter three special levels are also reported. Flag values indicate origin codes of the profiles in each map grid cell and the average time of any original measurements. If the particular profile is an original observation, then both the surface skin temperature and the cloud check flags are also reported. Land area fraction is provided. The map grid is the ISCCP 1.0 degree-equivalent equal-area grid. The period covered is 1980 through present.

Table D.1.1. Quantities Reported in NNHIRS Map Grid Cells.

Quantity	Units	Range	Fill Value
UTC Time (Hour) Original Observation	Hours	0–23	255
UTC Time (Minute) Original Observation	Minutes	0–59	255
HIRS Origin Code	N/A	0–43	255
SWOOSH Origin Code	N/A	100-101	N/A
HIRS Surface Skin Temperature	Counts	0-254	255
Most Frequent HIRS Cloud Flag	N/A	0-3	255
Number of Satellites for HIRS interpolation	N/A	1-8	0
HIRS Hour (previous) for time interpolation	N/A	1-143	0
HIRS Hour (next) for time interpolation	N/A	1-143	0
Land Fraction	Percent	0-100	N/A
Near-Surface (2m) Air Temperature	Counts	0-254	255
Temperature at 900 mb	Counts	0-254	255
Temperature at 800 mb	Counts	0-254	255
Temperature at 740 mb	Counts	0-254	255

Temperature at 680 mb	Counts	0-254	255
Temperature at 620 mb	Counts	0-254	255
Temperature at 560 mb	Counts	0-254	255
Temperature at 500 mb	Counts	0-254	255
Temperature at 440 mb	Counts	0-254	255
Temperature at 380 mb	Counts	0-254	255
Temperature at 320 mb	Counts	0-254	255
Temperature at 260 mb	Counts	0-254	255
Temperature at 200 mb	Counts	0-254	255
Temperature at 150 mb	Counts	0-254	255
Temperature at 100 mb	Counts	0-254	255
Temperature at 50 mb	Counts	0-254	255
Temperature at 10 mb	Counts	0-254	255
Maximum Temperature	Counts	0-254	255
Tropopause Temperature	Counts	0-254	255
Surface Pressure	Counts	0-254	255
Pressure at Maximum Temperature	Counts	0-254	255
Pressure at Tropopause	Counts	0-254	255
Relative Humidity Near Surface (2m)	Counts	0-254	255
Relative Humidity at 900 mb	Counts	0-254	255
Relative Humidity at 800 mb	Counts	0-254	255
Relative Humidity at 740 mb	Counts	0-254	255
Relative Humidity at 680 mb	Counts	0-254	255
Relative Humidity at 620 mb	Counts	0-254	255
Relative Humidity at 560 mb	Counts	0-254	255
Relative Humidity at 500 mb	Counts	0-254	255
Relative Humidity at 440 mb	Counts	0-254	255
Relative Humidity at 380 mb	Counts	0-254	255
Relative Humidity at 320 mb	Counts	0-254	255
Relative Humidity at 260 mb	Counts	0-254	255
Relative Humidity at 200 mb	Counts	0-254	255
Relative Humidity at 150 mb	Counts	0-254	255
Relative Humidity at 100 mb	Counts	0-254	255
Relative Humidity at 50 mb	Counts	0-254	255
Relative Humidity at 10 mb	Counts	0-254	255
Relative Humidity at Maximum Temperature	Counts	0-254	255
Relative Humidity at Tropopause	Counts	0-254	255

Table D.1.2. Definition of code and flag values

HIRS Origin Codes	Description
0	Original observations
30	PCA-based Diurnal with daily mean
31	PCA-based Diurnal with daily mean interpolated in ±5-day interval
32	PCA-based Diurnal with 30-day-averaged daily mean
33	PCA-based Diurnal with daily mean from 8-yr climatology (02/2001-01/2009)
40	Daily mean – No PCA
41	Linearly Interpolated in a ±5-day interval
42	30-day-averaged daily mean
43	8-yr Climatology (02/2001-01/2009)

Incoming HIRS Cloud Flags	Description
0	Highly Likely Clear
1	Likely Clear
2	Likely Cloudy
3	No matching PATMOS-x data

UTC Time (Hour, Minute) gives the average of the observation times of all original data in a particular map grid cell if Origin Code = 0. HIRS Surface Skin Temperature is reported from the original HIRS temperature retrievals if Origin Code = 0. Most Frequent HIRS Cloud Flag indicates the likelihood of cloud contamination if Origin Code = 0. Number of Satellites indicates how many different satellites are involved in any average of original values in each map grid cell. Codes 30-33 indicate use of the PCA model of diurnal variation over land that is based on the daily mean, the interpolated daily mean within a ±5-day interval or the 30-day-averaged daily mean. If no daily mean value is available, the climatology of the daily mean is used based on the period from 02/2001 to 01/2009, which was also the basis period for the PCA model. This procedure is used only over land. At pressure levels < 500 mb over land, at all levels over ocean and poleward of 70° latitude at all levels, missing values are filled by linear interpolation in time in a ±5-day interval (Code 41) or filled by the 30-day

mean (Code 42) or the 8-yr climatology (Code 43). The SWOOSH Origin Codes (100, 101) indicate original data or climatological fill.

Input Data Sources: Tropospheric temperature-specific humidity (T-Q) profiles are obtained from a new analysis of the operational HIRS measurements on polar orbiting weather satellites (see Table D.1.4). The radiances have been newly re-calibrated to remove biases between instruments (Shi 2001, Shi *et al.* 2008, Shi and Bates 2011, Shi *et al.* 2016). Unlike previous analysis methods, a cloud algorithm is applied to each HIRS pixel (field-of-view), instead of employing a comparison between HIRS and a microwave sounder, and all clear pixels (17 km size at nadir) are processed to retrieve a T-Q profile instead of selecting the two "warmest" pixels in a larger grid cell (2.5 degrees in the past). Thus, in a region with no clouds, results are obtained at spatial intervals of about 15-20 km. The cloud detection algorithm is patterned after the D-Version ISCCP IR algorithm and applied to HIRS channel 8 at a wavelength near 10 μm (Jackson *et al*. 2003). An additional check for cloud contamination is performed by comparison to coincident and collocated PATMOS-x cloud cover results (Heidinger *et al.* 2014), if available. The T-Q profile retrieval method is a neural network trained by a radiative transfer model, RTTOV Version 9 (Saunders *et al*. 1999, Matricardi and Saunders 1999, *cf.* Saunders *et al.* 2007), to use all wavelengths measured by HIRS. The training is further refined by using GPS-based retrievals of upper-atmosphere T and mid-troposphere Q. This version (Shi *et al.* 2016) is a further development of the method first reported in Shi (2001). Unlike previous retrieval methods, surface skin temperature (using realistic surface emissivities, the ISCCP set IREMISS, see Section 3.3.4, IR RTM) is retrieved as a quantity separate from near-surface air temperature and variable topography is accounted for by training a different neural network for each surface pressure range. Surface pressure is estimated using ISCCP TOPO at 1.0-degree using the relation:

$$PS = 1013.25 - 9.81 \times 1.275 \times Z/100 \text{ mb},$$

where Z is topographic height in meters used as an estimate of geopotential height. All available satellites are analyzed, hence, observations are obtained from two satellites (four samples per day) for most of the time period (Table D.1.3). There are four short periods (1979-1980, 1985, 1997 and 2000) when only one satellite was available (two samples per day) and a 2-year period (2002-2004) when four satellites were available (eight samples per day). The 8-yr period, 02/2001 to 01/2009, had three or four satellites and is used to develop the diurnal temperature variation model over land and the climatology for filling missing observations.

Table D.1.3 Time record of operating polar orbiting satellites providing HIRS data

Satellite	HIRS time record	PATMOS-x time record
M02	12/2/2006-12/31/2014	6/29/2007-12/9/2014

N06	7/13/1979-4/2/1983	6/30/1980-8/19/1981
N07	7/9/1981-1/29/1985	8/24/1981-2/1/1985
N08	4/30/1983-6/1/1984	5/16/1983-10/13/1985
N09	1/1/1985-10/19/1988	2/25/1985-11/6/1988
N10	11/28/1986-8/27/1991	11/17/1987-9/16/1990
N11	10/14/1988-12/30/1994	11/8/1988-8/31/1994
N12	6/1/1991-3/31/1997	9/16/1991-12/14/1998
N14	1/30/1995-7/28/2005	2/9/1995-7/25/2002
N15	10/27/1998-3/30/2005	10/26/1998-12/9/2014
N16	3/1/2001-12/31/2003	3/20/2001-7/19/2006
N17	7/16/2002-3/20/2013	8/24/2002-1/10-2009
N18	X	7/19/2005-12/9/2014
N19	X	4/19/2009-12/9/2014
TIROS-N	X	1/1/1979-1/19/1980

Table D.1.4. Quantities Reported in Original HIRS Profiles (Daily Files)

Quantity	Units	Range	Fill
Cloud Check Flag	N/A	0-3	N/A
UTC Seconds in Day	Seconds	0–86400	N/A
Latitude	Degrees	−90 to 90	N/A
Longitude	Degrees	−180 to 180	N/A
Surface Pressure	Millibars	0-1013	N/A
Surface Skin Temperature	Kelvins	165–345	999
Near-Surface (2m) Air Temperature	Kelvins	165-345	N/A
Temperature at 1000 mb	Kelvins	165-345	999
Temperature at 850 mb	Kelvins	165-345	999
Temperature at 700 mb	Kelvins	165-345	999
Temperature at 600 mb	Kelvins	165-345	999
Temperature at 500 mb	Kelvins	165-345	999
Temperature at 400 mb	Kelvins	165-345	999
Temperature at 300 mb	Kelvins	165-345	999
Temperature at 200 mb	Kelvins	165-345	999
Temperature at 100 mb	Kelvins	165-345	999
Temperature at 50 mb	Kelvins	165-345	999
Specific Humidity Near Surface (2m)	g/kg	0.01-26	N/A
Specific Humidity at 1000 mb	g/kg	0.01-26.6	999

Specific Humidity at 850 mb	g/kg	0-22	999
Specific Humidity at 700 mb	g/kg	0-15	999
Specific Humidity at 600 mb	g/kg	0-11.2	999
Specific Humidity at 500 mb	g/kg	0-7.17	999
Specific Humidity at 400 mb	g/kg	0-3.49	999
Specific Humidity at 300 mb	g/kg	0-1.22	999

Stratospheric specific humidities are obtained from a monthly mean climatology constructed from SAGE II and III measurements from 1984 through 2005 and extended by MLS measurements to current, called the Stratospheric Water and Ozone Satellite Homogenized data set (SWOOSH, Davis and Rosenlof 2016, http://www.esrl.noaa.gov/csd/groups/csd8/swoosh/189401-201312). The values are mapped in a 5-degree latitude by 20-degree longitude map grid. Specific humidity values are reported at 31 pressure levels (Table D.1.5).

Table D.1.5. SWOOSH original pressure levels in millibars.

316.2278	82.54	21.54435	5.623413	1.467799
261.0157	68.1292	17.7827	4.641589	1.211528
215.4435	56.23413	14.67799	3.831187	1
177.8279	46.41589	12.11528	3.162278	
146.7799	38.31187	10	2.610157	
121.1528	31.62278	8.254042	2.154435	
100	26.10157	6.812921	1.778279	

Comparisons to Other Products/Evaluation: Near-surface air temperature (TA) and specific humidities (QA) were compared with the ISD collection of surface weather reports over land (Smith *et al.* 2011) and the SeaFlux determinations over oceans (Clayson *et al.* 2012, Clayson and Bogdanoff 2013). Comparisons of T-Q profiles were made with the ARSA (Analyzed Radiosoundings Archive v2., thanks to ARA/ABC(t)/LMD group for producing and making available the Analyzed RadioSounding Archive (ARSA) database, http://ara.abct.lmd.polytechnique.fr/index.php?page=arsa) collection of radiosondes over land and with the AIRS product globally (V6 L2 , Chahine *et al.* 2006, http://disc.sci.gsfc.nasa.gov/AIRS/documentation/v6_docs). All of these comparisons, except AIRS, were done with the original input HIRS analysis with filters applied (see below). QA over land is the daily minimum value but the 900 mb values of NNHIRS are compared to ARSA since it does not provide surface measurements. The global comparison of NNHIRS with AIRS is done with the final product where filling has been performed.

Processing Steps:

A. Modifications to Original Data: All available profiles of temperature (T) and specific humidity (Q) are collected in monthly histograms in the 1.0-degree ISCCP grid. Simple

additional cloud-clearing procedures were applied to eliminate some remaining cloud contamination in very cloudy locations. Most of the removed profiles are also indicated as probably cloud contaminated by the original cloud check flag. In addition a few unusually hot profiles were discovered so these were also removed. The tests to do this are applied to the near-surface air temperature (TA); the whole T-Q profile is removed if any test fails. For each 1.0-degree grid cell in each month, the 1st and 99th percentile values in the histograms are determined, called TA1 and TA99. All profiles for which either TA < (TA1 □ 3K) or TA > (TA99 + 3K) are discarded. Over oceans the histogram of filtered TA values for each month is then examined to identify the mode value (TAmode) and the value on the larger (hot) side of TAmode with a frequency of occurrence that is half of the mode value, called TA50. Additional profiles are removed if either TA > TAmode + 2 (TA50 □ TAmode) or TA < TAmode □ 2 (TA50 □ TAmode). In some instances, there is no TA50 available on the hot side of the mode, in which case the value with a frequency of occurrence of 70% of the mode on the cold side (TA70) is used and the cold-side test is TA < TAmode □ 3 (TAmode □ TA70). Over land the histogram of filtered TA values for each month is also examined to identify TAmode and TA50. Profiles are removed if TA < TAmode □ 3 (TA50 □ TAmode).

The filtered temperature profiles are averaged over each day and then over all samples of each of the 12 months in the year for the period 02/2001-01/2009 to provide a climatology to be used in the filling procedure. Limited filling in longitude is used to ensure the global completeness of the climatology.

B. Mapping and Vertical Interpolation/Extrapolation: All filtered profiles are labeled as being over land or over water using the 0.25-degree ISCCP land-water mask (TOPO) and mapped into 1.0-degree equal-area global grids at hourly time intervals (centered on the local hour) for each day, where the observation time UTC is converted to local standard time (LST, based on UTC and longitude) to the nearest hour. All profiles falling within a grid cell within one hour are averaged; original quantities in the profiles are averaged separately. If both land and water are present in the grid cell, profiles over each surface type are averaged and then these two are combined weighted by the fractional areal coverage of land and water. If the 1.0-degree grid cell is called land (land fraction > 65%), then at least one profile over land is required otherwise no data are reported. Likewise if the 1.0-degree grid cell is called water (land fraction < 35%), at least one profile over water is required. If the 1.0-degree grid cell is called coast (intermediate land fraction) then at least one profile over land and one over water are required. The available values of the surface specific humidity, QA, are examined for each day to determine the minimum value over land and the average value over ocean; the profile containing the minimum QA over land is replicated to all other hours for that day whereas the whole profile of Q is the daily average at each level over ocean.

Some profiles are missing values near the surface (because of small differences between the original surface pressure used in the HIRS retrieval and the value reported in this product. These are filled by interpolation as part of the re-projection of the profiles from the original NNHIRS standard pressure levels to the ISCCP standard pressure levels. Temperatures are first converted to ISCCP standard count values, which are approximately

linear in radiometer-measured energy, and linearly interpolated in pressure (P). Each monotonic portion of the profile is interpolated separately and then joined smoothly. Specific humidities (Q) are filled by interpolation of log Q with log P. The temperature profile is extrapolated to the 10mb level and the specific humidity profile is extrapolated to the 260 mb level (if necessary). The surface pressure for each profile is adjusted slightly to account for the effects of varying atmospheric temperature using the relation:

$$PS\ (Z) = 1013.25\ [(TA - 6.5 \times Z) / TA]^{5.25}$$

where PS is in millibars, Z in kilometers and TA in Kelvins is the monthly mean near-surface air temperature at each location over land. The profiles are truncated or extended slightly. In mixed land-water grid cells, the surface pressure is the weighted average of the land and water values (where Z = 0 over water). Inland lakes, where topographic information is available in TOPO, are treated as land areas for this purpose. The near-surface temperature and specific humidity values are retained from the original profiles with no adjustment. The tropopause pressure is identified by searching upwards in the temperature profile to the first level where the temperature increases by ≥ 1K, but this location is checked to determine if it represents the absolute minimum temperature of the whole profile. If no minimum is found, then a test for a lapse rate < 0.3 K/km is used to define the tropopause location. If both tests fail to identify a tropopause level, the tropopause pressure is set to 100 mb.

The near-surface temperatures (over land) and specific humidities (over ocean) are slightly adjusted from the original profile values based on systematic differences found in the comparison to the ISD dataset (over land) and the SeaFlux dataset (over ocean). The original NNHIRS values of TA over land exhibited a systematic bias relative to ISD measurements representing overestimates for TA > 300 K and TA < 230 K and underestimates in between (Figure D.1.1).

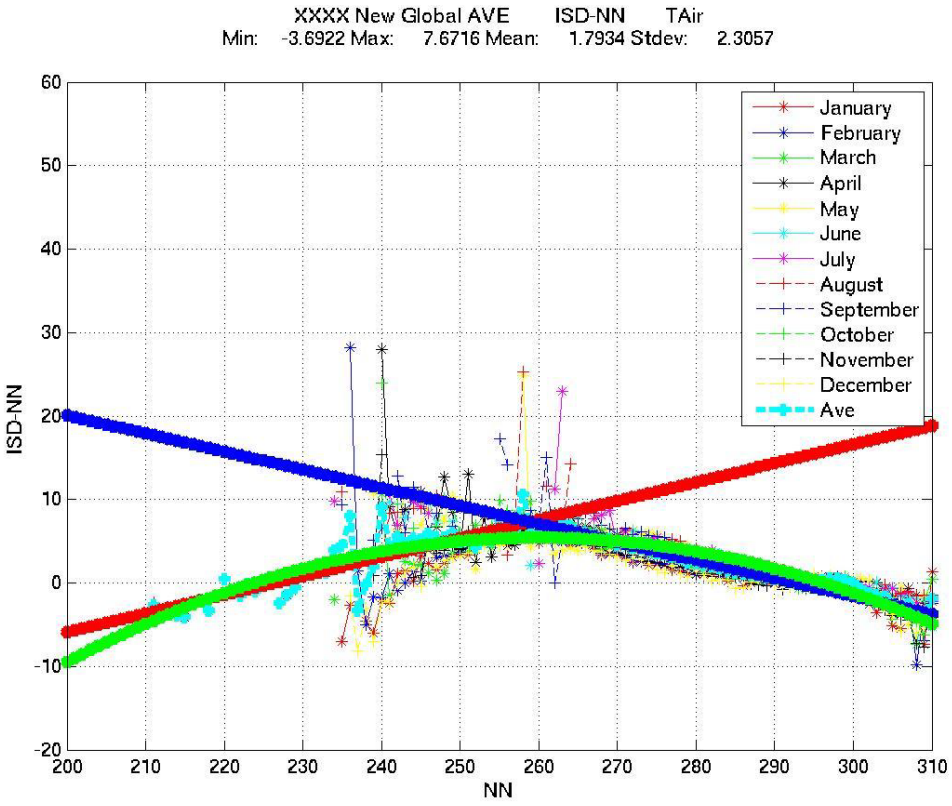

FIGURE D.1.1. Annual Mean TA difference between NNHIRS and ISD as a function of NNHIRS TA

Using the baseline 8-yr climatology period, a three-part fit to the differences as a function of NNHIRS TA was obtained. This fit (illustrated in Figure D.1.1) was done for each month of year to better represent the extremes. The table below gives the fit functions used to adjust the NNHIRS values of TA over land.

Table D.1.6. ISD-based additive adjustments to NNHIRS land TA

Month	Temp <	Formula (Ta+)	Temp between	Formula	Temp >	Formula
Jan.	244	0.3857002519 *ta – 94.5032049617	>244 &<295	-0.0054097694*(ta ^2) +2.9125939259*ta - 388.4916046312	295	-0.1518243949*ta +44.0305015119
Feb.	239	0.2904500663 *ta- 69.8797243893	>239 &<293	-0.0054506843*ta ^2 +2.9003645951*t	293	-0.2036320737*ta +58.8812629801

				a - 381.7292974161		
Mar.	228	0.1929249606 *ta - 44.0568465378	>228 & <294	- 0.0045889045*ta ^2 +2.3972297270*t a - 308.1724536587	295	-0.2166178463*ta +63.1033958409
Apr.	210	0.1324798470 *ta - 27.7097642834	>210 &<299	- 0.0028239784*ta ^2 +1.4352990071*t a - 176.7596947726	299	-0.1807989857*ta +53.7622617563
May	217	0.0981604904 *ta- 18.9647099343	>217 & <296	- 0.0040166274*ta ^2 +2.0625570246*t a - 258.4956821271	296	-0.2415170461*ta +71.1131718104
Jun.	210	0.1640082372 *ta- 33.8080845539	>210 &< 298	- 0.0034019831*ta ^2 +1.7291929471*t a- 213.1600759454	298	- 0.2153255282*ta+63.8890704900
Jul.	207	0.1419663098 *ta - 28.1787714486	>207 & <298	- 0.0031408833*ta ^2 +1.5864432206*t a - 193.6949386353	298	-0.2038138199*ta +60.6835506916
Aug.	204	0.1961498547 *ta- 40.2241299299	>204 &<299	- 0.0033120951*ta ^2 +1.6648981584*t a -201.818862609	299	-0.1871380553*ta +55.8782944215
Sep.	212	0.1708540573 *ta - 34.9000070844	>212 & <295	- 0.0045005593*ta ^2 +2.2801804787*t a -28.0070266930	295	-0.2916077704*ta +85.2141076261
Oct.	209	0.1407779662 *ta – 28.2261622686	>209 & <294	- 0.0038523629*ta ^2 +1.9387707020*t a - 237.0246064576	294	-0.2376603006*ta +69.2794313298

Nov.	228	0.2364392082 *ta - 55.434758346	>228 & <293	-0.0040196954*ta ^2 +2.0959372357*ta - 268.9476735128	293	-0.1976990939*ta +57.2210979996
Dec.	241	0.3266645793 *ta – 79.49309416	>241 & <293	-0.0053380406*ta ^2 +2.8535980471*ta -377.746669059	293	-0.1747278096*ta +50.4574170153

Likewise the NNHIRS values of QA exhibited systematic geographic biases relative to the SeaFlux dataset representing overestimates for 8 g/kg < QA < 14 g/kg and underestimates for QA > 14 g/kg (Figure D.1.2).

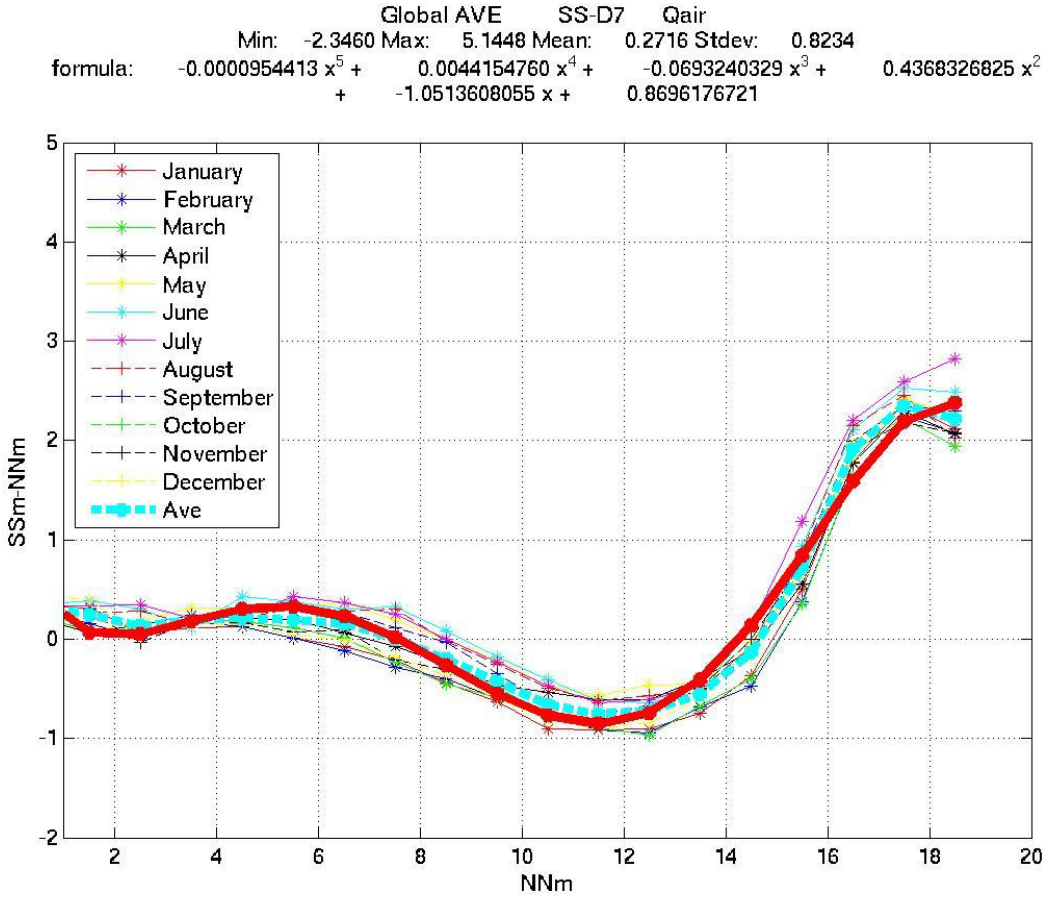

FIGURE D.1.2. Annual Mean QA difference between NNHIRS and SeaFlux as a function of NNHIRS QA

This bias did not exhibit significant seasonal dependence, so the additive adjustment is made with a single empirical curve fit based on the 8-yr climatology period:

$QA = QA + (\square\ 0.0000954413 * QA^5 + 0.0044154760 * QA^4 \square\ 0.0693240329 * QA^3 + 0.4368326825* QA^2 \square\ 1.0513608055 * QA + 0.8696176721)$

The SWOOSH monthly mean stratospheric Q profiles are re-mapped to the ISCCP 1.0-degree equal area grid by replicating values from the original lower resolution grid and then interpolated to the NNHIRS standard pressure levels by log Q versus log P. A monthly climatology based on the whole original dataset is produced.

C. Filling Method: When four satellites are operating, the original observations cover about 6-34% (19% average) of the earth for each 3-hr interval during the day. The more usual situation is that observations are available from two satellites. To achieve the goal of adequate diurnal resolution and to compensate for the inhomogeneous time-of-day sampling over the whole time record, the temperature values from the 8-yr period (02/2001-01/2009) with three-to-four satellite coverage (six to eight samples per day) were fit by an analysis of the diurnal variations for each month of the year at each geographic location at each pressure level. The analysis has two steps. First, the monthly mean diurnal anomalies (deviations from the average over all times of day for each satellite separately) at local hour intervals are combined for all satellites and fit with a cubic spline (unless the temperature range is < 2 K or > 5 K over ocean or > 40 K over land, in which case a Piecewise Cubic Hermite Interpolation, PCHIP, method is used). As part of the evaluation of the fits, the standard deviation of the monthly-hour average values for each grid cell and each month of the year are used to discard the one value farthest from the daily mean if it is more than two standard deviations from the mean and if its removal reduces the standard deviation by more than 20%. Second, PCA is performed on the hourly anomalies from the daily mean temperature for each grid cell at each pressure level over the globe and the whole period 02/2001-01/2009. The final diurnal variation model uses only the first three PCs to smooth out the variations, which explains about 55% of the variance over oceans (where this procedure is not used) and about 94% over land (*cf*. Aires et al 2002). The rms differences between the 3-term and the all-term PCA representations were found to increase as the diurnal amplitude decreases so the PCA model was restricted to locations where the diurnal range is ε 2 K: over all land areas at pressure levels ε 500 mb. Generally diurnal variations over ocean and in the upper atmosphere were smaller than this cutoff. The PCA model is also used to determine bias corrections for determining the daily mean temperatures from a limited diurnal sample.

Time filling: Daily mean T profiles are determined for all days that have at least one daytime and one nighttime sample; the PCA-based bias corrections are applied to correct for the specific time-of-day samples available. The Q profiles are retained only for days with an existing daily mean T profile. Monthly averages of these T and Q profiles are also calculated.

For a 2-satellite period, over land for a 3 hour time period, there is on average 10% original data, so the T profile filling procedure starts with the daily mean value for each location (an average of about 45% of the cases). If a daily mean value is not available on a particular

day, the daily mean is obtained by interpolating from nearby daily mean values in a ±5-day interval (about 27% of the cases). If the interpolation fails because data are not available, the monthly averaged daily mean value is used (about 25% of the cases); if there is no monthly mean, then the climatology for the appropriate month is used (< 2% of the cases). The PCA model is then applied to the daily mean T profiles from the surface up to the 500 mb level. Values aloft are filled through linear interpolation in time (24 hours +/-5 days), if data are not available then daily mean or climatology mean is used. Over ocean there is about 3% original data, 64% is filled through linear interpolation between the closest available times regardless of time of day (over an interval +/- 5 days), 21% is filled by the monthly mean, and 11% by the climatological mean.

Humidity values for all hours on days with a daily mean T profile are already filled with the daily minimum value over land and the daily average over ocean. If the daily mean T profile is missing, the Q profile is replaced by linear interpolation of daily minimum (mean) values over a ±5-day interval; if this interpolation fails, the monthly mean daily minimum Q profile is used. If the monthly mean Q profile is missing, the climatology from 02/2001-01/2009 of daily minimum (mean) Q values for the appropriate month is used.

The available stratospheric specific humidities are much sparser in the earliest years of the SWOOSH record; these are filled using a climatology based on the SWOOSH record from 2005-2014. The resulting monthly mean maps in 1° by 1° equivalent equal-area grid are replicated to each local hour of each day.

D. Reconciliation: The monthly mean stratospheric specific humidity values from SWOOSH were compared at the overlapping NNHIRS pressure levels (316 versus 320 and 261 versus 260 mb for SWOOSH and NNHIRS, respectively). In addition distributions of the differences in specific humidity between different pairs of pressure levels were examined to find those that showed (almost entirely) positive differences between an NNHIRS value at a higher pressure (only NNHIRS levels that actually report non-zero values are used in this comparison) and the SWOOSH values at a lower pressure. The NNHIRS values at 260 mb or 320 mb (almost) always exceed those in the stratosphere at 100 mb. Since the documentation of the stratospheric product recommends using humidity values for pressures ≤ 100 mb, the two water vapor profiles were joined by interpolating log Q versus log P between the 100 mb level and the last level with non-zero values in the NNHIRS product, generally the 320 mb level (see example in Figure D.1.3).

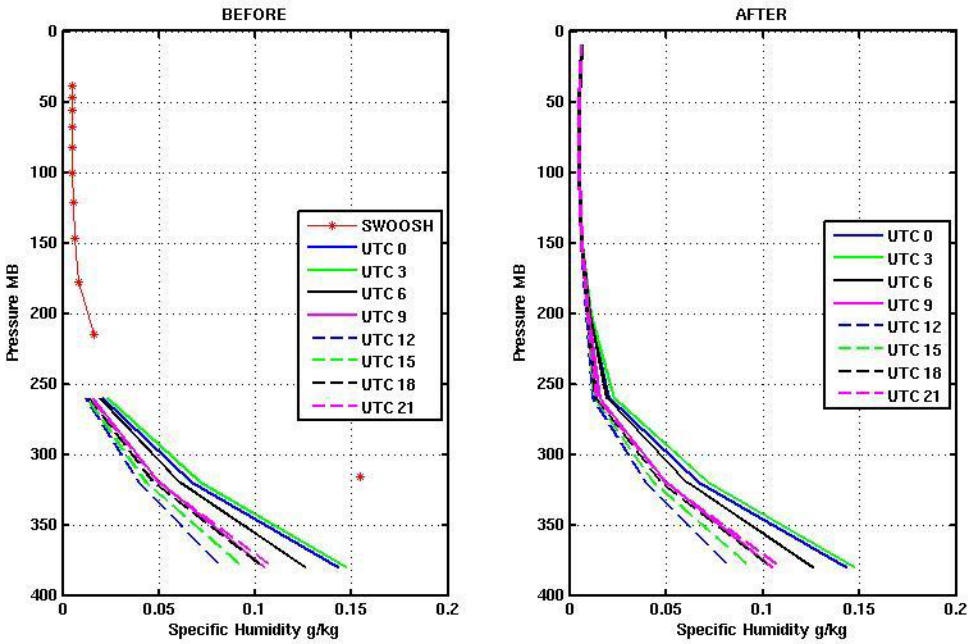

Figure D.1.3 Example of reconciliation of HIRS and SWOOSH vertical humidity profiles

E. Merging: The SWOOSH profiles are merged with NNHIRS for each 1-hour local time for each 1.0-degree grid cell. In this fashion, the synoptic variations in the troposphere are weakly reflected into the lower atmosphere below the 100 mb level by the interpolation procedure.

F. Final Modifications: The profiles of T and Q were also compared with results from AIRS over ocean and the ARSA collection of radiosondes over land; no significant systematic differences were found that were larger than the uncertainties of both products.

To preserve precision over the whole range of specific humidity values, Q, they are converted to relative humidity, RH = Q/QS at each location and local hour using the hourly temperature values in formulae for e_s from Murphy and Koop (2005):

$$e_{s,l} = e_0 \exp [(\langle \square 1) e_6 + d_2 (T_0 \square T) / TT_0 + d_3 \ln (T/T_0) + d_4 (T \square T_0)],$$

where $e_{s,l}$ is the saturation vapor pressure over liquid water for $T \geq T_0$, $T_0 = 273.15$ K, $e_0 = \exp (e_1 + e_6) = 6.091888$ mb, $\langle = \tanh [e_5 (T \square 218.8 \text{ K})]$, $d_i = (e_i + \langle e_{i+5})$ and the values of e_i are:

$e_1 = 6.564725$

$e_2 = \square 6763.22 \supseteq$

$e_3 = \square 4.21$

$e_4 = 0.000367 \text{ K}^{-1}$

$e_5 = 0.0415 \text{ K}^{-1}$

$e_6 = \square 0.1525967$

$$e_7 = \square 1331.22 \supseteq$$
$$e_8 = \square 9.44523$$
$$e_9 = 0.014025\ K^{-1}$$

and

$$e_{s,i} = B \exp [b_1 (T_0 \square T) / T_0T + b_2 \ln (T/T_0) + b_3 (T \square T_0)]$$

where $e_{s,i}$ is the saturation vapor pressure over ice for $T < T_0$, $b_0 = 9.550426$, $b_1 = \square 5723.265$ K, $b_2 = 3.53068$, $b_3 = \square 0.00728332\ K^{\square 1}$ and

$$B = (10^5) \exp [b_0 + b_1/T_0 + b_2 \ln (T_0) + b_3T_0] = 6.111536 \text{ mb}$$

The vapor pressures are converted to saturation specific humidity using

$$QS = 0.622\ e_s / (P \square 0.378\ e_s)$$

Thus RH is determined with respect to liquid phase at and above freezing temperature (273.15 K) and with respect to ice phase below freezing. If the NNHIRS value of RH = Q/QS < 0.5% at any temperature, it is reset to 0.5%. If RH > 110% at T ε 273.15 K, then it is re-set to 110%. If RH > 150% at T < 273.15 K, it is reset to 150%. The larger upper limit at lower temperatures is consistent with upper air humidity measurements indicating very large vapor supersaturations are required to initiate ice condensation (Jensen *et al.* 2001).

The now globally complete profiles of T and RH at 1-hr intervals in local time are finally reduced to a 3-hr UTC version by taking the hourly value closest to the center of the 3-hr time window based on the longitude of each grid cell. This approach produces a better-behaved diurnal temperature cycle over land but can mean that some original observations are dropped. However, the values reported are based on all the original observations through the daily mean value.

D.2. OZONE

Description: OZONE is a time varying data product reporting the daily variations of the global distribution of total column ozone abundance. The basic 1.0 degree version is used in the ISCCP L2 (pixel-level) processing and reported in the L3 (gridded) products.

Format and Contents: The format is NetCDF-4. The product reports daily global maps of total column ozone abundance in Dobson units along with flags that indicate the source of each value, either directly from one of the products or produced by one of the filling procedures. The map grid is the ISCCP 1.0 degree-equivalent equal-area map. The period covered is 1979 through present.

Table D.2.1. Quantities Reported in OZONE Map Grid Cells.

Quantity	Units	Range	Fill Value
Total ozone abundance	Dobson	0 to 1000	N/A

Origin Code	N/A	100 to 500	N/A

Code Value	Origin
100	Original TOMS
105	Space-filled TOMS
111-177	Time-filled TOMS (up to 7 day interval), dates used are encoded
200	Original OMI
205	Space-filled OMI
211-277	Time-filled OMI (up to 7 day interval), dates used are encoded
300	Time-filled SMOBA (up to 7 day interval), dates used are encoded
311-377	Original SMOBA
400	Original TOVS
500	TOMS Monthly Climatology

Input Data Sources: The primary input data sources are the NASA TOMS for 11/1978 – 11/1994 and 7/1996 – 12/2005 (documentation at http://ntrs.nasa.gov/search.jsp?R=19960022782, data at http://disc.sci.gsfc.nasa.gov/acdisc/TOMS/tomsl3_dataset.gd.html) and OMI for 10/2004 to current (Liu *et al.* 2010, Kroon *et al.* 2011, http://eospso.gsfc.nasa.gov/eos_homepage/for_scientists/atbd/docs/OMI/ATBD-OMI-O3.pdf) satellite products, which are based on UV measurements and mapped on a 1.25 degree or 1.0 degree longitude, respectively, by 1.0 latitude grid. These products report ozone column abundance in daily composites of measurements accumulated from multiple orbits over each day but do not always provide spatially complete coverage of the sunlit portion of Earth (these two products provide better coverage than other available products). Secondary sources are the daily 2.5 degree equal-angle grid TOVS ozone product for 12/1980 – 4/2005, which is based on infrared measurements and thus available to fill in ozone abundances for the wintertime polar regions, and the daily 2.5 degree equal-angle NOAA SMOBA product for 3/1997 to current, which is a merger of SBUV measurements with TOVS (http://www/cpc.ncep.noaa/products/stratosphere/SMOBA/smoba_doc.shtml). The available datasets merged for each time period to produce this product are illustrated in the Figure D.2.1.

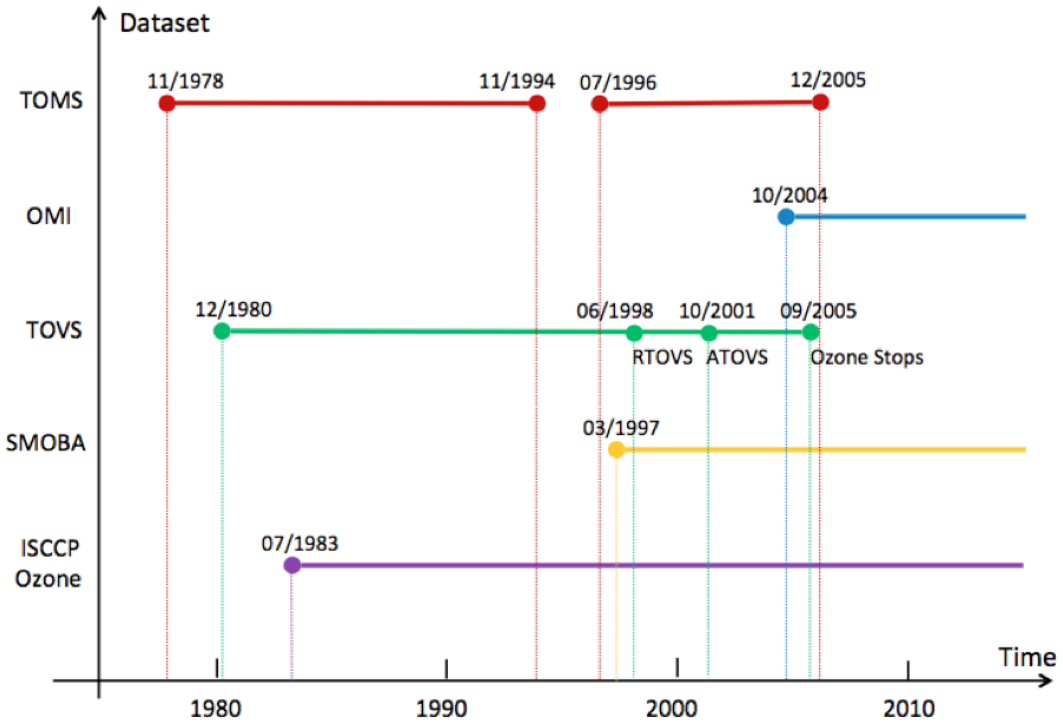

Figure D.2.1 Time record of ozone datasets used

Comparisons to Other Products/Evaluation: The TOMS, OMI, TOVS and SMOBA products were compared to ozone products from GOME for 7/1995 – 6/2003 (at http://www.ospo.noaa.gov/Products/atmosphere/gome/gome-A.html)

and SCIAMACHY for 8/2002 to current (Lerot *et al.* 2009, http://www.sciamachy.org/products/index.php?species=O3).

Processing Steps:

A. Modifications to Original: The TOMS, OMI, TOVS and SMOBA products are each re-mapped into the ISCCP 1.0 degree-equivalent-equal-area grid. In the case of 1.0 degree grids, the equal-area version is produced by averaging. In the case of the lower resolution products, values are replicated at finer intervals by a nearest neighbor re-sampling approach.

B. Filling Methods:

Some spatial and temporal gaps in each product are filled by linear interpolation; the limit on spatial gaps is approximately 1000 km and the limit on temporal gaps is 14 days. Larger gaps are filled by alternate data (see below). The majority of the spatial gaps are between orbit swaths, representing for about 17% of the data for OMI after 10/2004, when the analysis swath width was reduced. This statistic is exaggerated because of the removal of

spuriously large values of ozone abundance at the edges of each swath (most noticeable at lower latitudes where the abundance is lowest). The OMI product was edited by removing 2 degrees longitude of data near the swath edges before spatial interpolation was performed. TOMS and TOVS generally do not have small spatial gaps nor does SMOBA, which is a merged product. Temporal gaps were more common at the beginning of the TOMS record in 1980 (about 9%) and during 1993-94 (about 24%), but generally the gaps filled by time interpolation represent only about 1-2% of the data. For OMI, temporal interpolation was used only < 1% of the time before 2006 but about 4% of the time afterwards. The SMOBA also had some time periods with missing data, representing about 5% of the data in 1997-2005 but much less than 1% before and after. Overall, the amount of missing data filled is generally less than 10-15% except for March 1993 thru November 1994 and July 1996 thru February 1997.

C. Reconciliation: There is about 1 year of overlap between TOMS and OMI; comparison of daily global distributions from these two datasets indicated rms differences < 15 Dobson units, indicating excellent quantitative agreement to within < 5% (*cf.* Kroon *et al.* 2008). Likewise regressions were performed for TOVS versus TOMS and SMOBA versus TOMS. These results indicated more significant differences between TOVS or SMOBA and TOMS that are both regionally and seasonally dependent The results of an analysis of linear regressions performed by latitude zone and month-of-year were used to normalize the TOVS and SMOBA products to TOMS–OMI, where the normalization coefficients vary with latitude zone (30 degree latitude intervals) and month: all available overlapping data were used (see Table D.2.2). However, even this approach had to be limited because of "unusual" values occurring in the datasets, too small sample sizes or very small variation ranges, all of which affected the regression results. Thus, the following constraints were applied: (1) only daily values that differ from TOMS by less than two standard deviations of the monthly mean difference are retained for each latitude zone (these data are not removed from the product, only from the regression analysis), (2) if a zone has < 80% data that meets the first constraint, the values from that zone-month are discarded, (3) if more than four of the zones have been discarded in a month, the whole month is discarded, (4) if the total number of values available in a month is too small (<60%), that month is discarded, (5) if the range of differences in ozone abundance in a zone-month is too small (< 30 Dobson) as often happens at low latitudes, no regression is performed. The regression results (Table D.2.2) are used to normalize TOVS and SMOBA to TOMS with two exceptions. If the range of differences is too small (< 30 Dobson), then TOVS or SMOBA are simply corrected for the mean difference. Likewise only a bias correction is applied in the polar regions (60° to the pole). All of the datasets exhibited very different values of minimum and maximum ozone abundance as follows: TOMS (73, 949), OMI (84, 906), TOVS (24, 515) and SMOBA (3, 608). Based on the shape of the ozone abundance values, limits of 50 and 600 were imposed, which affected < 0.01% of the data.

D. Merging and Derivation of Additional Quantities: The combined TOMS-OMI product (overlapping OMI data are used to fill any gaps in the TOMS data) is merged with the normalized TOVS–SMOBA (Table D.2.2), where space-time filling has not been able to fill the gap: TOVS is used before October 2005, SMOBA after. The majority of the merger serves to fill in the winter polar regions that the UV instruments do not measure. If all of the above

filling and merging procedures fail to produce a value, then a monthly climatology of ozone abundance, based on the whole TOMS record, is used. The product reports for each map grid cell a code value that indicates the source of that ozone abundance values (Table D.2.1).

Table D.2.2. Regression Coefficients of various other ozone datasets against TOMS.

Regional Monthly Regression between TOMS and SMOBA (1997-2010)

(TOMS = A*SMOBA + B)

Region	Mon	Corr.	Linear Regression Slope (A)	Intercept (B)	Diff of Mean (toms-smoba)	Max_diff -Min_diff
90S – 60S	Jan	0.9216	1.1127	-44.6856	-10.8871	19.8467
	Feb	0.9301	1.0661	-28.4334	-9.1887	24.5348
	Mar	0.8206	1.1457	-52.1449	-9.9629	41.2533
	Apr	0.7722	1.4212	-134.8573	-11.5327	35.6392
	May	0	0	0	-11.4181	111.5733
	Jun	0	0	0	-14.5448	28.5485
	Jul	0	0	0	-22.9871	50.3125
	Aug	0	0	0	-32.838	64.6414
	Sep	0.9858	1.0028	-22.8455	-22.1933	50.3892
	Oct	0.9895	0.9755	-14.5627	-20.973	60.6859
	Nov	0.9811	0.9959	-17.1458	-18.3295	49.2954
	Dec	0.9554	1.1176	-49.3677	-14.1308	22.7761
60S – 30S	Jan	0.992	0.9615	7.5101	-3.5592	13.3784
	Feb	0.9899	0.9701	5.4034	-2.9864	14.3085
	Mar	0.9858	1.0073	-5.09	-3.0709	14.473
	Apr	0.9888	0.999	-1.9848	-2.2536	14.0497
	May	0.9861	0.9522	12.7865	-0.8774	18.287
	Jun	0.9503	0.8456	45.2729	-0.8329	32.9128
	Jul	0.9545	0.9068	28.768	-0.1785	31.4134
	Aug	0.9477	0.9383	19.6223	-0.3566	32.6711
	Sep	0.9698	0.9877	3.3748	-0.7369	41.2949
	Oct	0.9772	0.9761	5.7953	-2.2419	39.6011
	Nov	0.9798	0.9088	26.0141	-3.3816	24.5378
	Dec	0.9886	0.8967	26.9481	-3.4648	16.3291

30S – 0	Jan	0.9613	0.9324	15.1787	-2.3551	23.1108
	Feb	0.9381	0.938	13.7779	-2.2267	23.574
	Mar	0.9241	1.0194	-8.2321	-3.1937	24.0297
	Apr	0.9112	1.0371	-12.9502	-3.303	21.2001
	May	0.9154	1.0961	-28.1546	-3.2599	20.2805
	Jun	0.9303	1.0522	-16.4347	-2.8558	22.6405
	Jul	0.9448	1.0843	-24.3162	-2.0417	25.9176
	Aug	0.9559	1.1341	-37.4159	-1.3044	28.9219
	Sep	0.9752	1.1217	-33.9755	-0.3492	28.1756
	Oct	0.983	1.071	-19.7529	-0.1262	26.4619
	Nov	0.9837	1.0283	-8.4117	-0.7757	25.7504
	Dec	0.9793	0.9919	0.5102	-1.2097	23.2306
0 – 30N	Jan	0.9301	0.742	60.6389	-4.7272	34.948
	Feb	0.9425	0.7516	59.3361	-4.7942	34.4579
	Mar	0.9637	0.8065	46.7641	-5.3709	29.0697
	Apr	0.9766	0.8581	33.6546	-6.1543	28.3267
	May	0.9818	0.9029	21.1114	-6.469	25.4918
	Jun	0.9784	0.8899	24.6983	-6.5304	21.5388
	Jul	0.9732	0.8772	28.6501	-6.1314	20.2682
	Aug	0.9554	0.8643	32.657	-5.3268	21.6373
	Sep	0.9022	0.8383	40.8361	-3.9715	19.7941
	Oct	0.8745	0.8333	41.2363	-3.4556	22.5856
	Nov	0.8815	0.8299	40.3806	-3.8407	27.9284
	Dec	0.9261	0.804	45.5175	-3.6274	28.003
30N – 60N	Jan	0.9836	1.0345	-22.3082	-10.4241	47.0497
	Feb	0.9894	1.0102	-18.3572	-14.6406	37.0935
	Mar	0.9907	0.9902	-10.8642	-14.5308	35.0459
	Apr	0.9894	0.9815	-6.1097	-12.9598	29.6014
	May	0.9891	1.0171	-16.7685	-10.6511	27.7939
	Jun	0.9846	1.0424	-22.9367	-8.5007	30.5156
	Jul	0.9756	1.0211	-14.2672	-7.4484	24.1598
	Aug	0.9655	1.0667	-26.8767	-6.2111	24.7789
	Sep	0.9507	1.0502	-20.3286	-5.3242	23.5873
	Oct	0.9748	0.9745	1.2659	-6.2365	25.1634
	Nov	0.9799	0.9678	2.0151	-7.7148	32.7857

	Dec	0.9788	1.0189	-13.3415	-7.5242	45.7164
60N – 90N	Jan	0	0	0	15.0824	102.2868
	Feb	0	0	0	0.4008	154.8595
	Mar	0.9661	0.8444	54.992	-9.8681	42.3171
	Apr	0.9717	0.9151	19.5606	-16.4352	24.518
	May	0.9299	0.8107	59.4174	-16.5365	18.8943
	Jun	0.7149	0.7234	87.5264	-11.7944	19.6357
	Jul	0.9007	1.0817	-36.1379	-9.3955	22.0323
	Aug	0.8962	1.1932	-66.2355	-7.2013	27.4162
	Sep	0.8885	1.1041	-36.4344	-5.7035	32.8075
	Oct	0.9425	0.9114	21.131	-5.2752	73.7992
	Nov	0	0	0	-4.8946	40.0747
	Dec	0	0	0	2.59	80.8787

Regional Monthly Regression TOMS vs. TOVS (1983-2005)

(TOMS = A*TOVS + B)

Region	Mon	Corr.	Linear Regression Slope (A)	Intercept (B)	Diff of Mean (toms-tovs)	Max_diff - Min_diff
90S – 60S	Jan	0.9023	1.5185	-183.5631	-20.2495	31.3223
	Feb	0.8078	1.1685	-77.1404	-24.0767	39.898
	Mar	0.8931	1.6159	-214.6254	-24.1823	41.4943
	Apr	0.9327	1.6644	-226.7324	-22.6842	37.8113
	May	0	0	0	-20.6952	110.2693
	Jun	0	0	0	-18.3075	42.5652
	Jul	0	0	0	-26.9919	44.0858
	Aug	0	0	0	-55.8364	94.9988
	Sep	0.9262	1.838	-310.235	-60.1217	151.6803
	Oct	0.8207	1.7398	-279.7153	-48.3499	201.2857
	Nov	0.4484	0.9272	-10.2542	-32.6647	159.2206
	Dec	0.3685	0.4664	155.2471	-20.7715	62.6803
60S – 30S	Jan	0.9566	0.809	49.8796	-6.2129	31.1981
	Feb	0.9284	0.6715	89.998	-4.3439	33.7649
	Mar	0.9222	0.6492	93.1308	-6.6203	29.3043
	Apr	0.9488	0.7625	60.1396	-8.1645	29.4515

	May	0.9548	0.7939	53.5111	-7.5764	27.2077
	Jun	0.9553	0.7621	63.8806	-11.0845	28.2126
	Jul	0.9198	0.7576	68.5201	-9.8985	37.5982
	Aug	0.8915	0.9027	21.5993	-11.2194	49.7932
	Sep	0.9217	1.0377	-20.6835	-6.7391	65.3113
	Oct	0.9299	1.0153	-10.0505	-4.2772	73.0788
	Nov	0.9339	0.9144	21.1615	-6.4163	36.3671
	Dec	0.9537	0.7916	55.5128	-8.4237	26.344
30S – 0	Jan	0.8779	0.8362	42.6106	0.2287	30.2354
	Feb	0.8602	0.8422	42.2028	1.86	28.7725
	Mar	0.8211	0.7271	72.6972	3.3351	30.8471
	Apr	0.7561	0.6429	93.4631	2.3473	35.9284
	May	0.7439	0.6817	81.739	0.4571	40.6477
	Jun	0.8546	0.8153	45.7529	-2.3048	36.9481
	Jul	0.9162	0.9316	16.0561	-2.1332	34.3216
	Aug	0.9443	0.928	20.6654	1.1046	36.1446
	Sep	0.9563	0.9186	27.865	5.6516	36.0831
	Oct	0.9589	0.9185	30.297	7.5549	34.0628
	Nov	0.9526	0.9338	21.5068	3.192	33.7296
	Dec	0.9302	0.9283	19.3004	1.1179	29.9964
0 – 30N	Jan	0.7838	0.5764	99.1897	-11.2533	51.6078
	Feb	0.8211	0.7042	70.1276	-7.0279	45.6884
	Mar	0.8487	0.7648	61.8216	-0.3921	46.7758
	Apr	0.8313	0.8154	54.5864	4.8898	51.9495
	May	0.8164	0.7707	68.5909	6.2388	59.6903
	Jun	0.7947	0.6596	99.05	5.7988	56.0603
	Jul	0.7921	0.6277	108.422	6.06	48.5928
	Aug	0.703	0.5206	137.4642	8.3788	44.4299
	Sep	0.572	0.3058	193.033	7.8335	47.0946
	Oct	0.529	0.2551	199.8707	4.7865	50.8242
	Nov	0.5248	0.2819	182.2138	-4.9897	51.4279
	Dec	0.6895	0.4651	128.8716	-9.9765	49.5997
30N – 60N	Jan	0.96	1.2207	-82.3186	-6.7137	99.6332
	Feb	0.9741	1.0502	-27.2057	-7.7175	68.2241
	Mar	0.9758	1.0484	-20.8648	-1.191	61.1932

	Apr	0.9754	0.9436	18.9566	-0.8877	49.7782
	May	0.9562	0.9188	28.8596	0.9965	48.1556
	Jun	0.945	0.8737	43.9806	2.2854	50.3387
	Jul	0.9034	0.788	69.0061	1.1473	51.0113
	Aug	0.8565	0.6619	104.591	2.1693	46.6742
	Sep	0.8871	0.6477	102.5498	-2.4279	40.5269
	Oct	0.9256	0.8888	26.4369	-6.4438	41.888
	Nov	0.9688	1.069	-33.2072	-12.2824	41.1636
	Dec	0.9671	1.2084	-75.1626	-8.7845	72.5862
60N – 90N	Jan	0	0	0	19.7148	144.1113
	Feb	0	0	0	10.8071	161.2818
	Mar	0.8684	1.4883	-199.1265	8.9276	67.6899
	Apr	0.8421	1.1721	-78.1186	-3.0807	43.4997
	May	0.5734	0.7164	102.7381	-8.5993	39.2982
	Jun	0.5593	0.5989	131.5788	-14.6019	32.107
	Jul	0.7673	1.2762	-113.7592	-20.567	34.9845
	Aug	0.5837	1.3733	-147.2648	-24.7427	41.5716
	Sep	0.7398	1.3724	-142.0375	-23.7945	33.7119
	Oct	0.9341	1.9212	-308.2379	-18.9993	49.5389
	Nov	0	0	0	-16.9296	57.387
	Dec	0	0	0	-2.706	203.0887

D.3 AEROSOL

Description: AEROSOL is a time varying data product reporting monthly average global distributions of aerosol optical properties from 1979 to present. The aerosol properties reported are optical depth at 0.65 μm and 10.5 μm wavelengths, together with the fine fraction for tropospheric aerosols, and the zonal monthly mean optical depths at the same wavelengths for stratospheric aerosols. The basic 1.0 degree-equivalent-equal-area version used in the ISCCP L2 (pixel-level) processing but is not reported in any of the other ISCCP products.

Format and Contents: The format is NetCDF-4. The product reports global monthly mean maps on a 1 degree equal-area grid of tropospheric and stratospheric aerosol optical depths at 0.65 μm and 10.5 μm wavelengths and the fine fraction of the tropospheric aerosols (stratospheric aerosols are assumed to have fine fraction = 100%). Some missing fine fraction information in the southern oceans was filled by a constant minimum value, indicated by a flag value. After 2000, the stratospheric optical depths are assumed to be the same as those in 2000. The period covered is 1979 to present.

Table D.3.1. Quantities reported in AEROSOL Map Grid Cells.

Quantity Reported in Map Grid Cell	Units	Range	Fill Value
Tropospheric Aerosol VIS Flag	N/A	0 to 1	N/A
Tropospheric Optical Depth at 0.65 μm	N/A	0 to 1.2	N/A
Tropospheric Fine Fraction	N/A	0 to 1	N/A
StratosphericAerosolVIS Flag	N/A	0 to 2	N/A
Stratospheric Optical Depth at 0.65 μm	N/A	0 to 1.2	N/A
Tropospheric Aerosol IR Flag	N/A	0 to 1	N/A
Tropospheric Optical Depth at 10.5 μm	N/A	0 to 1.2	N/A
StratosphericAerosolIR Flag	N/A	0 to 2	N/A
Stratospheric Optical Depth at 10.5 μm	N/A	0 to 1.2	N/A

Input Data Sources: The tropospheric monthly mean, aerosol optical depth, single scattering albedo and asymmetry parameter at 0.55 μm and 10 μm are obtained from a reconstruction, called MAC-v1, that merges direct observations, both surface-based from AERONET and satellite products from MODIS and MISR, with the median results from an ensemble of emission-transport models (Kinne *et al*. 2013). These global data are mapped in a 1.0 degree equal-angle grid and cover the period 1980 through 2013. The stratosphere zonal monthly mean, wavelength-dependent aerosol optical depths are based on SAGE II and III, are reported at 1 degree latitude intervals, and cover the period 1976 through 1999 (although only data since 1980 were obtained).

Comparisons to Other Products/Evaluation: This aerosol product was tested against two other reconstructions, one used in the GISS climate model and one compiled by the CERES project, by using them to calculate surface downwelling shortwave fluxes and comparing these fluxes to those measurement by the BSRN set of surface sites. The flux comparison statistics were improved using the MAC-v1 aerosol optical depths by a small amount, both a decrease in the rms differences and a decrease in systematic latitude-dependent differences.

Processing Steps:

A. Modifications to Original: By assigning fixed optical properties (particle size distribution, shape, single scattering albedo) of sulfuric acid to fine aerosols and mineral dust properties to coarse aerosols in a wavelength-resolving radiative transfer model that calculates radiances, the original tropospheric aerosols optical properties are matched by adjusting the fine fraction (i.e., a mixture of fine and coarse aerosols) and shifted to new reference wavelengths (from 0.55 to 0.65 μm and from 10 to 10.5 μm). For the stratospheric aerosols, which are composed solely of sulfuric acid, only the wavelength shift is calculated. The resulting tropospheric aerosol properties are re-mapped from 1.0 degree equal-angle grid to 1.0 degree-equivalent-equal-area grid at monthly time intervals from 1979 – 2013. The stratospheric zonal mean values are replicated to all longitudes in each 1.0 degree zone.

B. Filling Methods: Some values of the anthropogenic contribution to the aerosol properties are missing in a few months in areas over the southern oceans. These values are set to a default minimum value. Missing months/years in the record are filled by replicating the nearest available data; this procedure was applied to both the troposphere and stratosphere for 1979 but only to the stratospheric aerosols after 2000 so far. As the volcanic aerosol decays, the AOD in the stratosphere falls below detectable limits, so minimum values for the visible and infrared values (0.0005 and 0.00005, respectively) are set whenever the reported AOD is smaller. All values for 2000 and beyond are the minimum values.

Flag Codes

VIS Troposphere: 0 = original, 1 = replicated from same month in 1980 backwards or 2013 forwards

IR Troposphere: 0 = obtained from VIS Troposphere and location-month-dependent spectral ratio, 1 = replicated from same month in 1980 backwards and 2013 forwards

VIS Stratosphere: 0 = original with 5.00E-04 minimum, 1 = replicated from same month in 1980 backwards and 2000 forwards

IR Stratosphere: 0 = original with 5.00E-05 minimum, 1 = replicated from same month in 1980 backwards and 2000 forwards

C. Reconciliation: None required.

D. Merging and Derivation of Additional Quantities: The tropospheric and stratospheric aerosol parameters are combined and an adjusted fine fraction determined to represent variations of tropospheric aerosol optical properties.

D.4. SNOWICE

Description: SNOWICE is a time varying data product reporting the daily variations of snow and sea ice cover fraction over the whole globe. The basic 0.25-degree product is used in the ISCCP L2 (pixel-level) processing (each pixel at 0.1 degree intervals that falls within a 0.25-degree cell reports the same information) and a 1.0 degree version is reported in the L3 (gridded) products. All versions are produced directly from the basic 0.25 degree product.

Format and Contents: The format is NetCDF-4. The product reports daily snow cover as an area fraction and sea ice concentration, both taken to represent the absolute area fraction within a map grid cell. In addition, the fractions of the map grid cell covered by permanent glaciers on land and permanent ice shelves on water are reported from SURFACETYPE. The land fraction is reported from TOPO. The sum of the (fixed) glacier fraction and snow cover fraction is ≤ land fraction. Likewise the sum of permanent ice shelf fraction and sea ice fraction is ≤ (1 − land fraction). Also reported are snow and sea ice margin zones: for map grid cells with land but no snow or permanent glacier, the distance to the nearest snow-

glacier-covered land up to 115 km is reported. For map grid cells with water but no sea ice or permanent ice shelf, the distance to the nearest sea ice or ice shelf up to 115 km is reported. Source and quality flags are also provided. The period covered is 1979 to present.

Table D.4.1. Quantities Reported in SNOWICE Map Grid Cells.

Quantity	Units	Range	Fill Value
Land area fraction	Percent	0 to 100	-9999
Snow cover fraction	Percent	0 to 100	-9999
Permanent Glacier cover fraction	Percent	0 to 100	-9999
Distance to snow-glacier for open land	Meters	0 to 1115000	-9999
Sea Ice cover fraction	Percent	0 to 100	-9999
Permanent Ice Shelf cover fraction	Percent	0 to 100	-9999
Distance to sea ice-shelf for open water	Meters	0 to 1115000	-9999
Sea Ice Status Flags*	N/A	0 to 204	-9999

Output Sea Ice Status Flags*

Flag	0.25 degree meaning	1.0° meaning	Valid Range	Fill value
1	% input status flag=0	% input pixels w/Flag 1	0-100	-9999
2	% input status flag=1-2	% input pixels w/Flag 2	0-100	-9999
3	% input status flag=10-14	% input pixels w/Flag 3	0-100	-9999
4	% input status flag=100-102	% input pixels w/Flag 4	0-100	-9999
5	Fill type (201 – 204)	% of 1.0° map filled	0-204	-9999

The quantity marked by an asterisk refers to five flags, four of which report information from the original data product (see Input Data Source description below) and the last of which has a different meaning in the basic 0.25 degree version, where it indicates the method used to fill missing values (see Filling Method below) but in lower resolution versions, it indicates the percentage of the grid cell filled.

Input Data Sources: Snow cover information, available only for the northern hemisphere, is obtained from two NOAA products (*cf.* Robinson and Frei 2000, Brown and Robinson 2011), the Northern Hemisphere EASE-Grid Weekly Snow Cover and Sea Ice Extent, Version3 (Armstrong and Brodzik 2002), covering the period 1966 – 2007, obtained from:

http://nsidc.org/data/nside-0046.html and the NOAA NSIDC IMS Daily Northern Hemisphere Snow and Ice Analysis at 24 km Resolution (Helfrich *et al.* 2012, there is also a 4-km resolution version available), covering the period 1997 to present (obtained from http://nsidc.org/data/noaa/g02156_ims_snow_ice_analysis). The newer version of the weekly snow cover product is reported on a 25 km equal-area grid (the EASE grid), representing the re-mapping of the older NOAA operational product originally reported in a polar stereo projection with an effective spatial interval of 2.0 degree. This product is derived from the manual interpretation of visible-band imagery from weather satellites. The daily snow cover product is the current operational product produced on 24 km polar stereo grid. The IMS product is produced from a combined analysis of visible-band and microwave imagery. Polar land surfaces that are not illuminated by sunlight and all of Greenland are set to 100% snow cover. These products report a binary snow cover at the original grid intervals.

The global sea ice concentrations come from two datasets (obtained from http://osisaf.met.no/p/ice, technical documents available). The two products are called the OSI-SAF Global Sea Ice Concentration Reprocessing Dataset, covering 1978 through 2009, and the SSM/I Sea Ice Concentration Maps, covering 2005 to present. Both products report sea ice concentrations in 10 km polar stereo grids and are based on analysis of satellite microwave measurements but with slightly different algorithms.

In the original sea ice concentration product, there are quantities that give the fraction of original satellite pixels with the following status flags: 0 = nominal sea ice concentration, 10-14 = nominal value changed (coastal correction, climatological maximum constraint applied in area, climatological maximum applied out of area, gap filled), and 100-102 = missing value (land present, missing satellite pixel, unclassified) and 1-2 = nominal value questionable because of too high surface temperature (> 10° C) or because of "lake". The temperature consideration was removed from the input data after September 2009. During processing to the 0.25 degree version, this last flag is changed to also report any pixel where the near-surface air temperature is greater than 278 K (> 5° C). In these cases the ice concentration is reset to 0. The monthly mean near-surface air temperature is from an 8-yr climatology (February 2001 – January 2009) based on the NNHIRS atmospheric product. Another change is to label as suspicious any ice concentration values that are < 70% over more than 30° of longitude at latitudes > 85° N. These pixels were flagged "missing" and later filled.

See the description of SURFACETYPE (Appendix D.6) which provides information about permanent glaciers and ice shelves that is added to the SNOWICE product.

Comparisons to Other Products/Evaluation: Comparison of the weekly and daily snow cover products in their overlapping period shows good agreement for weekly results and very little actual day-to-day variation in the daily product (< 3% of locations show a change of cover during a week). The snow cover product has been compared with the MODIS snow cover product, another simple microwave-based product (NSIDC), the Canadian surface measurements of snow depth (CMC) and a new microwave-based analysis by Shahroudi and Rossow (2014) for the overlapping periods. The disagreement ranges from < 10% for MODIS to slightly more than 20% for NSIDC.

The OSI-SAF sea ice product has been compared to the NOAA operational product, as well as earlier versions of other products produced at NSIDC (*cf*. Ivanova *et al.* 2014). The older microwave-based products show spurious open water in the interior of the Arctic sea ice from surface melt ponds. The newer products show only small differences in the location of ice edge. The frequency of mismatches is < 1%. One systematic difference is that the OSI-SAF land-water mask seems to shift the coastline out to sea, possibly to avoid side-lobe contamination.

Processing Steps:

A. Modifications to Original: The weekly snow cover product for 1979 through 1996 is replicated to daily intervals and re-mapped to the ISCCP 0.25 degree-equivalent-equal-area grid using a nearest neighbor re-sampling approach. The daily snow cover product for 1997 onwards is also re-mapped in the same fashion to the ISCCP 25 km grid. For this grid, the snow cover is either 0 or 100%. The land masks are reconciled by eliminating any snow report for map grid cells with land fraction = 0%; all other values are retained but re-scaled so that snow fraction is ≤ land fraction. The daily OSI-SAF sea ice product for 1979 through 2009 is re-mapped to the ISCCP 0.25 degree-equivalent-equal-area grid using a nearest neighbor re-sampling approach; the daily SSM/I sea ice product for 2010 onwards is also mapped to the ISCCP 25 km grid. The land masks are reconciled by eliminating sea ice reports for any map grid with a land fraction = 100%; all other values are retained but re-scaled so that sea ice fraction ≤ (1 − land fraction). Some ice pixels (north of 85° latitude) were found to contain bad data. These pixels were filled with climatology as explained below.

B. Filling Method: No filling of the snow product was required but some minor spatial filling by linear interpolation was required for the re-mapped sea ice product. Also there were some time periods missing from the sea ice product that were filled by linear time interpolation at each location. In the basic 0.25 degree version, the sea ice fill flag has the following values:

201 original data
202 Temporal interpolation
203 Climatology fill using the monthly mean from up to 2 years before and after
204 Climatology fill using the monthly mean for the same month based on the whole record

The monthly mean climatology is based on the whole sea ice dataset available at this time (1979-2013). There were some instances of missing data or bad data (ice fraction less than 70%) north of 85 degrees latitude. These values were filled via replication in latitude with values from the most northern latitude band containing valid data. For the 1.0 degree version, the “fill” flag is replaced by a report of the percentage of 0.25 degree grid cells with filled values that were used to produce the 1.0 degree version.

C. Reconciliation: The snow cover fraction is reconciled to the land mask from TOPO and the (fixed) permanent glacier fraction (if primary) added from SURFACETYPE (see Appendix D.6) such that the sum of the permanent glacier and snow cover fractions is ≤ land fraction. If the sum exceeds the land fraction, the snow cover fraction is reduced until the sum

equals land fraction. After this step the snow cover fraction may no longer be binary (0 or 100%). Likewise the sea ice cover fraction is reconciled to the land mask from TOPO and the (fixed) permanent ice shelf fraction (if primary) added from SURFACETYPE (see Appendix D.6) such that the sum of the permanent ice shelf and sea ice fractions is ≤ (1 – land fraction). If the sum exceeds the water fraction, the sea ice fraction is reduced until the sum equals the water fraction.

D. Merging and Derivation of Additional Quantities: The re-gridded snow cover and sea ice cover fractions are merged with the permanent glacier and permanent ice shelf fractions and reconciled as described above. Then snow or sea ice margin zones are determined as follows: for map grid cells with land but no snow or permanent glacier, the distance to the nearest snow-glacier-covered land up to 115 km is reported and for map grid cells with water but no sea ice or permanent ice shelf, the distance to the nearest sea ice-covered or ice shelf-covered water up to 115 km is reported. Lower resolution versions are produced from the basic 0.25 degree-equivalent-equal-area version by area averaging.

D.5. TOPO

Description: TOPO is a fixed data product providing a land-water mask together with topographic height information over land. A 0.1 degree-equivalent-equal-area ("10-km") version is used in processing ISCCP L2 (pixel-level) and is reported in the two ISCCP L2 products for each pixel present; some information from a 1.0 degree-equivalent-equal-area version is also used in the cloud analysis. A 1.0 degree-equivalent-equal-area version is reported in the ISCCP L3 (gridded) products. All versions are constructed directly from the same 0.1 degree basic product.

Format and Contents: The format is NetCDF-4. The product reports land fraction in percent, "shore" distance in km, the mean and standard deviation of topographic height in meters (only land points included in the statistics in mixed land-water grid cells). Shore distance is the distance to the center of the nearest land-dominated (land fraction >65%) or mixed land-water (coast) grid cell if the map grid cell is water-dominated (land fraction < 35%) or to the nearest water-dominated or coast grid cell if the map grid cell is land-dominated. The distance is 0 km for coast map grid cells.

Quantities	Units	Range	Fill Value
Land fraction	Percent	0 to 100	32767
Mean topographic height above mean sea level	Meters	-405 to 6626	32767
Standard deviation of topographic height	Meters	0 to 1351	32767
Distance to land for all water cells	Kilometers	0 to 11500	32767
Distance to water for all land cells	Kilometers	0 to 11500	32767

Input Data Sources: One land-water mask is from the USGS Global Land 1-KM AVHRR Project (obtained from the USGS EROS data center at http://edc2.usgs.gov/1KM/land_sea_mask.php), compiled from the World Vector Shoreline

data set for ocean boundaries and the Digital Chart of the World for the large inland lakes, estuaries and rivers. These sources were rasterized to 1-km grid cells, where the type is assigned based on dominant area coverage. The original mapping is a Lambert Azimuthal Equal Area projection.

The global digital elevation model used to provide land topographic heights is GTOPO30 (obtained from the USGS EROS data center at http://lta.cr.usgs.gov/GTOPO30). Topographic height in meters above mean sea level is reported at intervals of 30-arc seconds (0.008333 degrees) referenced to WGS84. Ocean areas have been masked to a "no data" value of −9999, hence this product also provides a land-water mask. The Digital Elevation Model is compiled from eight sources. Complete documentation can be found at http://eros.usgs.gov/#/Find_Data/Products_and_Data_Available/gtopo30_info and

http://eros.usgs.gov/#/Find_Data/Products_and_Data_Available/gtopo30/README The original product mapping is the Interrupted Goode Homolosine projection broken up into smaller tiles for convenience.

Comparisons to Other Products/Evaluation: GTOPO30 was compared to ETOPO2v2 (obtained at https://www.ngdc.noaa.gov/mgg/global/global.html). ETOPO2v2 is lower resolution than GTOPO30 but includes bathymetry for oceans and large lakes. Ignoring the differences for inland lakes, the main differences (less than ± 200 m) appear over high terrain, where resolution effects would be expected. However, there are larger differences up to 500 m over Greenland, both high and low, as well as along the southern boundary of the Himalayas. GTOPO30 was selected for use because it is a global digital elevation model at smaller spatial intervals and makes a clear distinction between continents and oceans. The land-water masks in the GTOPO30 product was compared to the 1-KM AVHRR Project product; differences were reconciled as discussed below.

Processing Steps:

A. Modifications to Original: The 1-KM AVHRR Project product was re-mapped into the ISCCP-style equal-area grid at the same effective resolution (0.01 degree-equivalent-equal-area) using a nearest neighbor re-sampling approach and inspected for any flaws (missing values) produced by this step (none found). The GTOPO30 data were re-mapped to the same 0.01 degree-equivalent-equal-area grid. In this step, the land fraction and (mean) topographic height are calculated.

B. Filling Methods: None required.

C. Reconciliation: The two land-water masks are reconciled in the ISCCP 1 km grid in favor of the GTOPO30 land fraction as follows:

	AVHRR 1-KM value	0	100
GTOPO30 value			
0		0	0

> 0 but < 100	GTOPO value	GTOPO value
100	0	100

The replacement of the GTOPO30 land fraction in the interior of continents when the 1-KM AVHRR reports all water is necessary to identify large lakes but the GTOPO30 topographic information is retained for these locations so they can be distinguished from open ocean locations which have no topographic information. Inspection of differences in the land mask at high latitudes suggested that the AVHRR land mask includes permanent ice shelves as part of the land, whereas GTOPO30 does not (also confirmed by ETOPO2v2). Thus an ice shelf fraction is determined for all locations poleward of 60 degrees where the AVHRR land fraction = 100% but GTOPO30 gives < 100%: in this case the ice shelf fraction is given by 100 – GTOPO30 land fraction and land fraction is set to 0%. This result is added to the SURFACETYPE product as ice shelf cover (see Appendix D.6).

D. Merging and Derivation of Additional Quantities: The GTOPO30 dataset at 1-km, after the modifications to reconcile with the AVHRR Project land-water mask, is used to produce all other versions of the ISCCP TOPO product on equal-area map grids, equivalent to 0.1, 0.25, 0.50, 1.0, 2.0 and 2.5 degrees at the equator. All lower resolution values of land fraction, mean topographic height and standard deviation of topographic height are calculated directly from the 1-km product. In each mapping, an additional quantity, called "shore", is determined as follows. First, each map grid cell is classified as water (land fraction < 35%), land (land fraction > 65%) or coast (intermediate land fractions). Then for grid cells classified as water, the distance from the center of the grid cell to the center of the nearest grid cell classified as either land or coast, up to 115 km, is determined. For grid cells classified as land, the distance to the center of the nearest grid cell classified as either water or coast is determined. For grid cells classified as coast, the shore distance is set to zero.

D.6. SURFACETYPE

Description: SURFACETYPE is a fixed data product that characterizes the Earth's surface at each map location as water or permanent ice shelf or as land in terms of vegetation type or permanent glaciers. The basic 0.25-degree-equivalent-equal-area version is used in processing ISCCP L2 (pixel-level) and is reported in the two ISCCP L2 products (each pixel at 0.1 degree intervals, falling within the same 0.25 degree map grid reports the same information). A 1.0 degree-equivalent-equal-area version is reported in the ISCCP L3 (gridded) products. All versions are produced from the basic 0.25-degree version.

Format and Contents: The format is NetCDF-4. The product reports the top three surface types in terms of fractional area coverage of each map grid cell: the sum of all land types is ≤ the land fraction.

Quantity	Units	Range	Fill Value
Land fraction	Percent	0 to 100	255
Primary type code	N/A	0 to 18	255
Primary type cover fraction	Percent	0 to 100	255

Secondary type code	N/A	0 to 18	255
Secondary type cover fraction	Percent	0 to 100	255
Tertiary type code	N/A	0 to 18	255
Tertiary type cover fraction	Percent	0 to 100	255

Table D.6.2. Surface type code definitions.

Surface Type Code	Description
0	Water
1	Evergreen Needleleaf Forest
2	Evergreen Broadleaf Forest
3	Deciduous Needleleaf Forest
4	Deciduous Broadleaf Forest
5	Mixed Forest
6	Closed Shrubland
7	Open Shrubland
8	Woody Savanna
9	Savanna
10	Grassland
11	Permanent Wetland
12	Cropland
13	Urban and Built-up
14	Cropland/Natural Vegetation Mosaic
15	Permanent Snow and Ice (Glaciers)
16	Barren or Sparsely Vegetated
17	Unclassified
18	Permanent Ice Shelf

Input Data Sources: The primary land vegetation classification is the IGBP-DISC data product (Loveland *et al.* 2009) obtained from the USGS EROS data center at

http://daac.ornl.gov/ISLSCP_II/guides/edc_landcover_xdeg.html. This product provides the fractional area coverage in a 0.25 degree equal-angle mapping for the first 17 types listed above. The unclassified type typically represents small islands. If the fractional coverage by Type 0 is > 50%, the IGBP-DISC product discards any land surface information and reports only Type 0 as present. Information about glacier coverage is provided by the GLIMS data product (Armstrong *et al.* 2005, obtained from http://www.glims.org), which is in the form of the coordinates of the each glacier's edge at an approximate spatial resolution of 0.2-0.3 km. The permanent ice shelf product, reporting ice shelf fraction

poleward of 60 degrees latitude, is derived at 1-km during the processing of the TOPO data product (see Appendix D.5).

Processing Steps:

A. Modifications to Original: IGBP 0.25 degree-equivalent-equal-angle data is remapped to 0.25 degree ISCCP-equal-area, fractions for all types present are calculated as averages of the original values. The GLIMS "glacier shapes" are used to determine areal coverage that is projected into 0.25 degree-equivalent-equal-area map grid. The ice shelf product is first re-mapped to a 0.1 degree-equivalent equal-area grid by averaging and then all fractions < 98% are discarded. The result is then re-mapped to 0.25 degree equal-area.

B. Filling Methods: None required

C. Reconciliation: The Ice Shelf product at 0.25 degree-equivalent-equal-area is added to the IGBP-DISC product, reported as Type 18. If the GLIMS fractional coverage minus Ice Shelf fraction is > Type 15 fraction from IGBP-DISC, the Type 15 fraction is replaced by the GLIMS value. If water (Type 0) is in the top three (or is the only type), its coverage fraction is revised to agree with the TOPO land fraction. Any other original type fractions from IGBP-DISC are then re-scaled so that the sum of all non-water types is ≤ land fraction (the < condition can arise since very small amounts of some land types are dropped because they do not make it into the top three). The SURFACETYPE product is then reduced to the top three fractional coverage types: less than 5% of the 0.25 degree map grid cells contain more than one surface type and less than 0.03% of the grid cells contain two types with identical fractional coverage. In the latter case the higher type number is taken as dominant over the other type.

D. Merging and Derivation of Additional Quantities: Ice Shelf fraction is added as Type 18 to the original surface types in IGBP-DISC. When GLIMS minus Ice Shelf is greater than IGBP-DISC Type 15 fraction, the latter value is replaced by the GLIMS value. Lower resolution versions of the basic 0.25 degree version are produced by averaging to other equal-area grids.

Appendix E. ISCCP OPERATIONS GUIDE

See CDRP-MAN-0876 Cloud Properties - ISCCP Operations Guide (01B-29)

Appendix F. ISCCP Calibration Add-On Document

See CDRP-MAN-0877 Cloud Properties - ISCCP Calibration Monitoring (01B-29)